Acoustics and Manufacture of Caribbean Steelpans

Soren Eldred Maloney

Wolfson College

December 2010

This dissertation is submitted for the degree of Doctor of Philosophy

University of Cambridge
Department of Engineering

To my Grandparents, Aunt Dovie and Valerie-Ann

Preface

This dissertation is the result of my own work and includes nothing which is the outcome of work done in collaboration except where specifically indicated herein. No part of this dissertation has been or is currently being submitted for any other qualification at this or any other university.

The work herein was conducted solely at the Cambridge University Engineering Department from April 2006 to December 2010 and was funded by the University of Trinidad and Tobago.

This dissertation is 64994 words in length and contains 105 figures and 37 tables, which is within the limits set by the Degree Committee for Engineering.

Soren Eldred Maloney
Cambridge, December 2010

Abstract

The Caribbean steelpan is a pitched percussion instrument that originated in Trinidad and Tobago during the Second World War. Despite several research initiatives to improve the making of this relatively new instrument, several areas remain unaddressed. This thesis presents new approaches to help improve the making of the instrument. These approaches are situated in the production, vibration and material aspect of the steelpan.

A novel sheet forming technology termed Incremental Sheet Forming (ISF) is applied to the production of miniature steelpan dishes. The thickness distribution in the wall of the ISF dishes is compared to the wall thickness distribution in a traditionally formed steelpan dish and a wheeled dish. Unlike traditional forming and wheeling, ISF produces stretching in only a portion of the walls of the formed dishes. Multi-pass ISF is used to extend the stretched zone but this extension is minimal. A break even analysis is also applied to investigate the fiscal viability of ISF application to the production of miniature and full size steelpan dishes. The application of ISF to steelpan making is found to be commercially profitable but could be jeopardised by the tuning stage of the steelpan making process.

A preliminary study on the effect of impact on tone stability is conducted on a pair of notes on a full size steelpan and detuning is found more likely to occur by repeated impact of the note at its centre. Mode confinement in test-pans is also investigated. ISF is used to produce miniature test-pans with test-notes that are geometrically identical to notes on full size pans. It is possible to confine modes by varying the curvature of the bowl surrounding the test-note. The number of localised modes in the test-note increases as the radius of curvature of the surrounding bowl increases. The natural frequency of the first confined mode in the test-notes is sensitive to material springback in ISF and the mechanism of confinement appears to be due to the change in geometry that occurs between the flat test-note region and the bowl wall. This control of mode confinement may find use in future efforts to completely or partially automate the steelpan making process.

Material damping and mechanical properties in low-carbon steel used to produce steelpans are researched. Damping and mechanical properties are extracted from low-carbon steel that is subjected to identical stages to the steelpan production process. Material damping trends suggest that an annealing temperature between 300°C and 400°C would be appropriate for the heat treatment of steelpans. Air-cooled and water-quenched low-carbon specimens exhibit comparable damping trends. Hardness increases in cold formed low-carbon specimens is attributed to strain hardening and not strain ageing. Investigation of damping trends and mechanical properties in ultra-low bake-hardenable and interstitial-free steels reveals that a wider range of low-carbon steels may be suitable for steelpan making.

Acknowledgements

Table of Contents

List of Figures

List of Tables

Chapter 1   Introduction

1.1 The Steelpan: An Introduction

Bans on the people of the islands of Trinidad and Tobago to express themselves musically lead to the genesis of a new percussion instrument: the **Caribbean steel drum**. Drum refers to the oil containers or barrels from which the instrument is fabricated but the instrument is commonly referred to as the **steelpan** or **pan**. Throughout this dissertation the name steel drum, steelpan or pan will be used interchangeably when referring to the instrument. A brief introduction of the instrument is necessary before delving into the problems to which this work is intended to provide answers.

1.2 A concise history

There is a consensus that the steelpan first emerged on the musical scene towards the end of World War II. One researcher said in 2000:

> *"Its life so far, a mere 60 years, is a dot in the world of music."* [1]

This relatively new percussion instrument has its roots in the drumming traditions of two major ethnic groups in Trinidad and Tobago; West Africans and East Indians [2]. A summary of the history of the steelpan is given in Figure 1.1. For the reader with more interest a comprehensive history can be obtained in references [2-7].

1.3 The steelpan family and musical ranges

Each steelpan consists of two regions namely the playing surface on which the note regions are located and the side commonly referred to as the skirt (see Figure 1.2). In music, note refers to the sign used in musical notation or to the pitch of a sound. In this work, the word '*note*' with respect to the steelpan will not only be used to denote sound or pitch but will also be used when referring to the physical space or region associated with or allocated to a note on the pan surface.

The present playing range of a steel band orchestra extends from G1 to G6 on the musical scale, approximately five octaves, with overlaps between each pan type as shown in Table 1.1 [8]. Table 1.1 also shows some steelpan types and the number of drums used to create each set.

1

African skin drums: Banned in 1883 as this was considered as a tool to incite revolt.
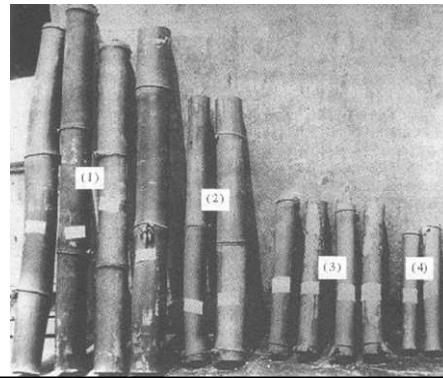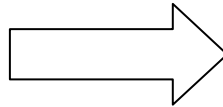
Tamboo Bamboo bands emerged to replace skin drums but were also eventually banned sometime between 1930 and 1935 due to clashes among rival groups.
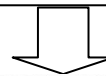
The expanding oil industry and the American Naval bases in Trinidad during WWII provided an abundance of used oil drums which provided a new raw material for experimenting.

Between 1935 and 1938 new instruments took the form of buckets, biscuit pans, paint tins, grease barrels and wooden boxes.
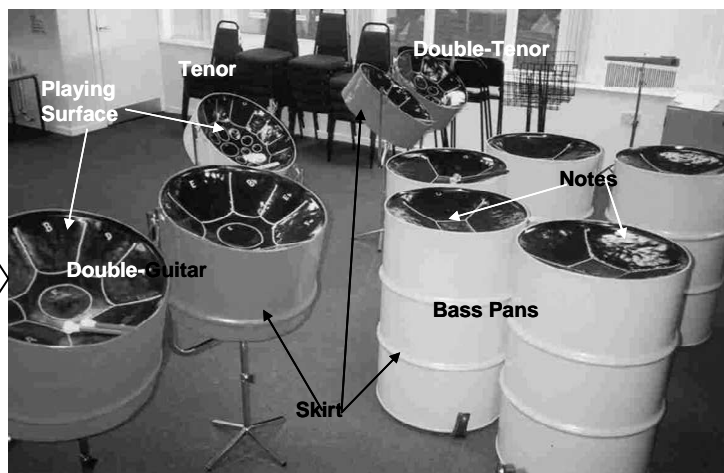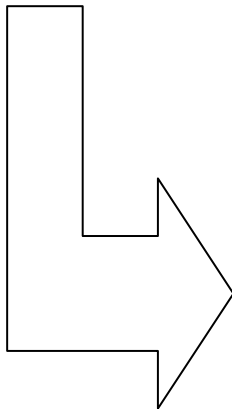
1945 saw a new instrument in the form of the steelpan which today has grown into a family of instruments.

Figure 1.1: Evolution of the steelpan [4,9]

Pan Type	Number of Drums	Bowl Depth (mm)	Skirt or Side Length (mm)	Musical Range	Frequency (Hz)
Tenor (Soprano)	1	200	140	C4 – F6	262 - 1397
Double Tenor (Alto)	2	180 - 195	240	F3 – C6	175 - 1047
Double Second	2	160 - 165	215	F$^{\#}$3 – B5	185 - 988
Guitar Pan	2	140	460	D3 – F4	147 - 349
Cello Pan	3 or 4	130 - 160	450	B2 – B^{b}4	123 - 466
Quadrophonic Pan	4	150	280	B2 – B^{b}5	123 - 932
Bass Pan	4, 6 or 9	90 - 100	620	G2 – D4 (4)	98 – 294
			to entire drum side	A1 – D3 (6)	55 – 147
				A1 – B3 (9)	55 - 247

Table 1.1: Typical steelpan dimensions and associated musical range [8,10]
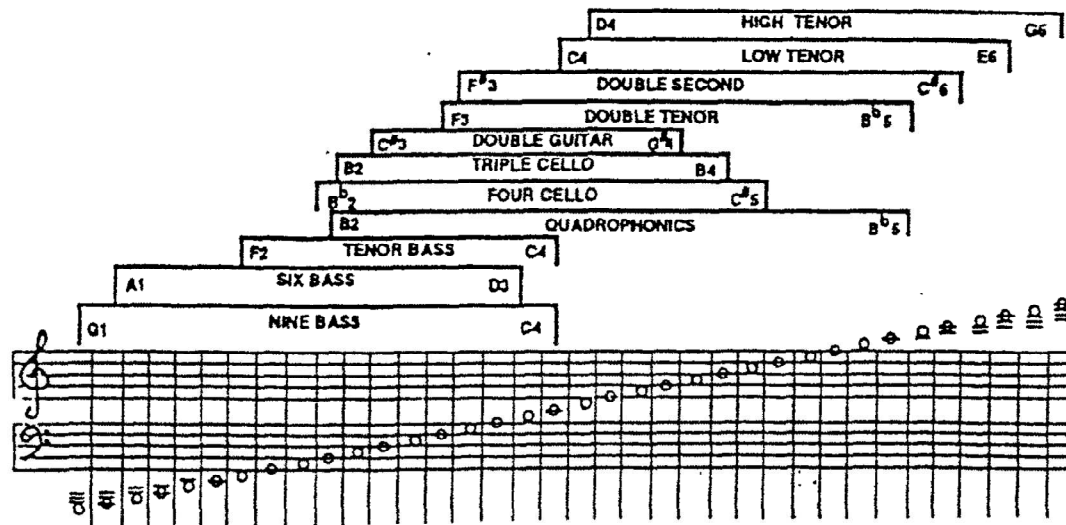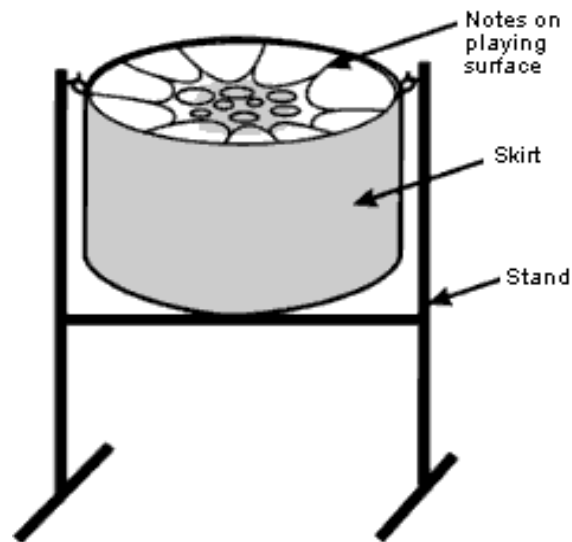
Figure 1.2: Regions of a steelpan [11]

1.4 Traditional steelpan crafting

Steelpans are today still largely produced by traditional handcrafting which begins by dishing the top of a tight-head oil barrel. The following stages are described below (see also Figure 1.3):

1. *Sinking or dishing*: This involves stretching the drum head with a sledge hammer to create an evenly dished surface. Instead of using an oil drum, some pan makers use a metal disc or blank which they form into the pan head (Figure 1.4).
2. *Creation of note regions*: This is where the pan maker divides the dished surface into sections that will be used for placement of the various notes.
3. *Grooving*: This is the process in which each note region is defined by a boundary that consists of a continuous line of punch marks on its perimeter.
4. *Cutting the drum*: The side of the drum is cut to length in accordance with the steelpan type under production. Bass pans usually retain the entire side of the drum.
5. *Firing*: This is typically done by placing the drum upside down on a wooden or kerosene-fired heat source for several minutes so as to remove any paint or oil on the surface. The firing or heat treatment of the drum is also believed to provide strain relief in the drum head to facilitate further cold-working during tuning.
6. *Tuning*: This is where a few modes in each note region are tuned (making adjustments to the shape of the note region by hammer peening) until the desired frequencies (fundamental and harmonics) on the musical scale are achieved. Steelpans are tuned to the Western twelve tone equal temperament scale in which the reference or standard pitch is 440Hz or A440.
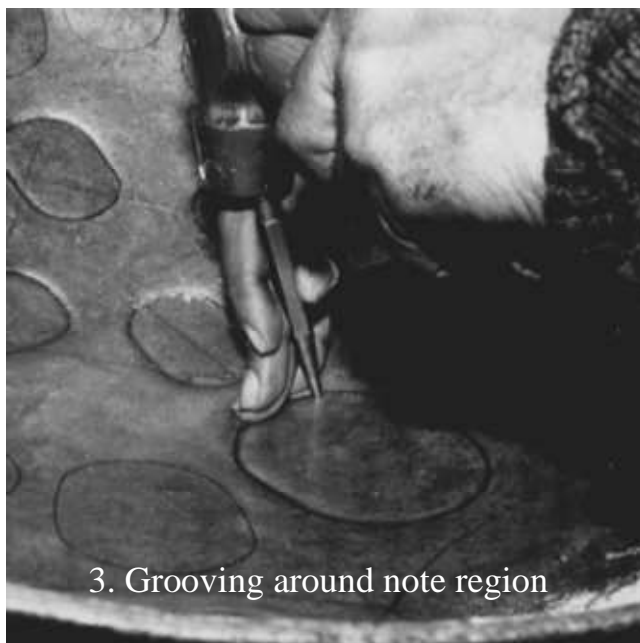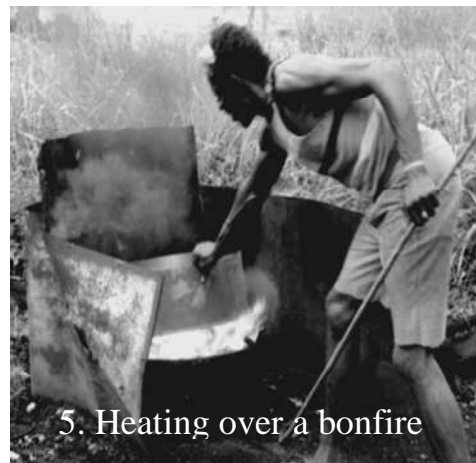
Figure 1.3 : Traditional steelpan fabrication [10]

(a)

Tight head oil drum

Sinking or dishing

Dish or bowl also known as pan head

Cutting of drum side

Pan head with skirt

(b)

Blank

Sinking or dishing

Dish or bowl also known as pan head

Skirt or side

Joining

Pan head with skirt attached
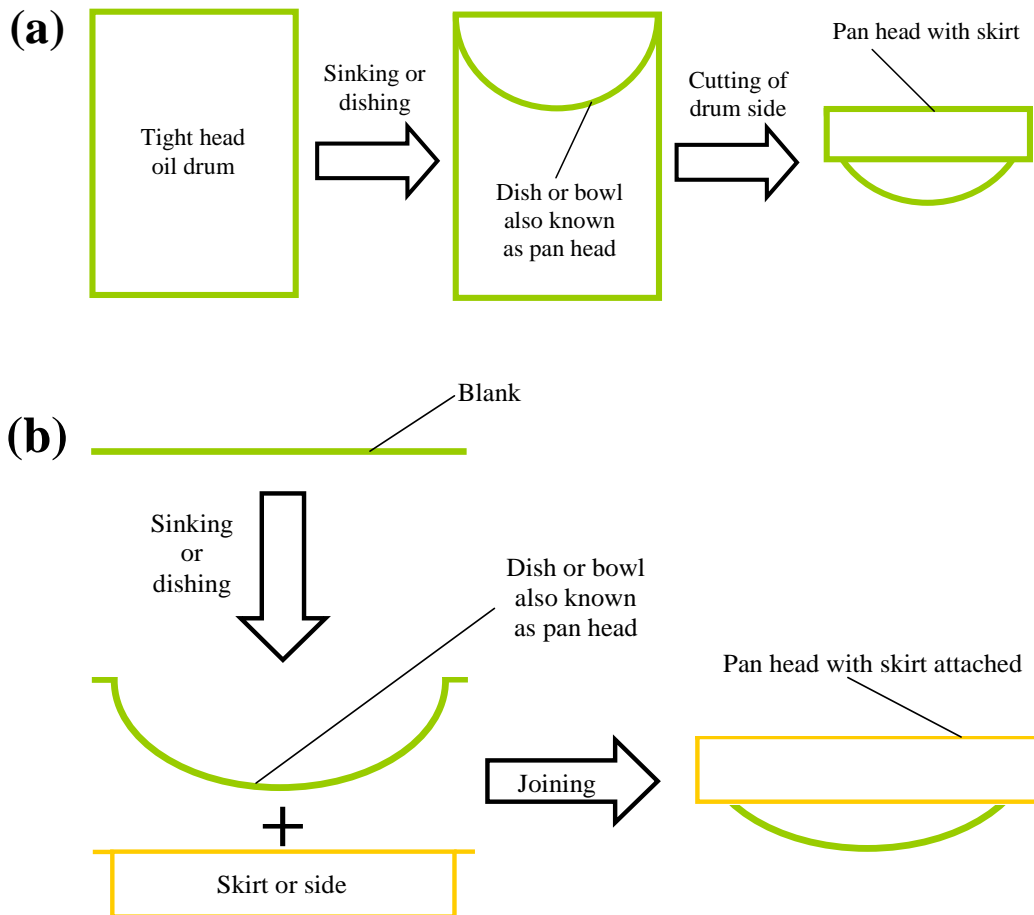
Figure 1.4: Pan dishing: **(a)** using tight-head oil drum and **(b)** using a sheet metal blank

1.5 Note placement and standardization

The note arrangement or note pattern refers to the placement of notes on the pan-dish surface. There has been some movement to standardize [1,12] the choice and the placement of notes on pan surfaces. This work is not concerned with the standardization of note arrangement on pan surfaces. Figure 1.5a, b and c shows three note arrangements that are found on soprano pans. Figure 1.5a shows an arrangement which is based on the circle of 4ths and 5ths, hence the name 4ths and 5ths tenor pan. In this arrangement adjacent notes in the anti-clockwise direction have their fundamental frequencies in the ratio of a musical 5th (3:2) and adjacent notes in the clockwise direction have their fundamental frequencies in the ratio of a musical 4th (4:3). In this pan the notes are arranged in three rings, referred to as the outer, middle and inner ring. The fundamental frequencies of the notes on the middle ring are the octave frequencies of the notes on the outer ring, and the same relationship exists between the notes on the inner and middle rings.

The Ellie Manette or Invader soprano pan (Figure 1.5b) is also arranged in a series of rings. However, adjacent notes on each ring are either a semitone or whole tone apart, with some adjacent notes having their fundamental frequencies in the ratio of a musical fourth or fifth. The Aubrapan (Figure 1.5c) named after its inventor Aubrey Bryan has adjacent notes that have a whole tone difference in tone. Several other layouts of the soprano pan are in circulation but the 4ths and 5ths soprano pan continue to be the predominant and preferred note pattern. A 4ths and 5ths soprano pan and an Aubrapan were used for some of the experiments in this work.
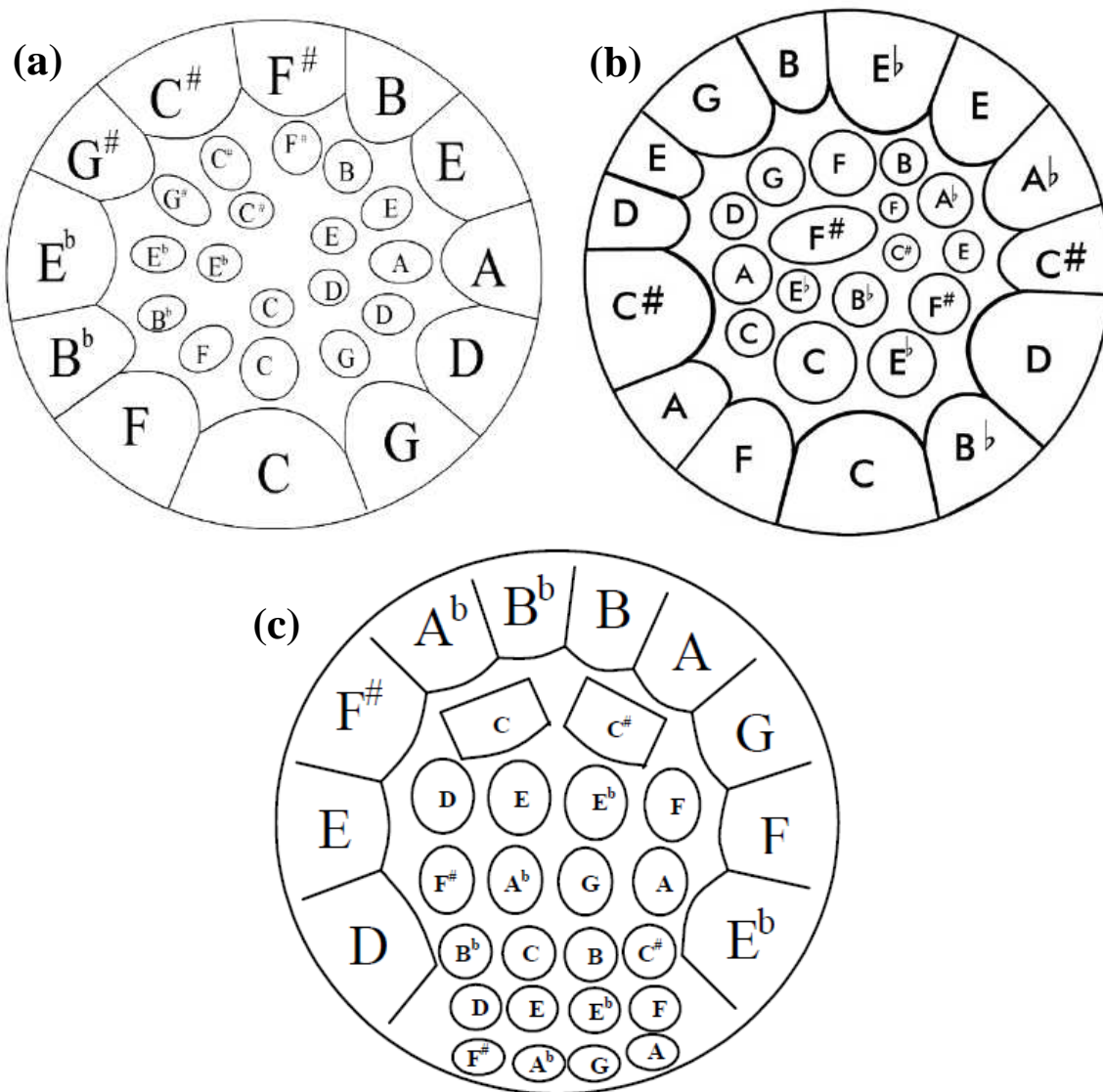
Figure 1.5: (a) 4ths and 5ths soprano pan; (b) Ellie Mannette Invader or Desporadoes soprano pan; (c) The Aubrapan

1.6 Motivation

The manufacture of the steelpan is summarized in Figure 1.6. From this it is apparent that the study of the steelpan is multidisciplinary, bringing together the disciplines of manufacturing technology,

materials science and vibration and acoustics. This work will concentrate on problems that are positioned in each of these respective disciplines.
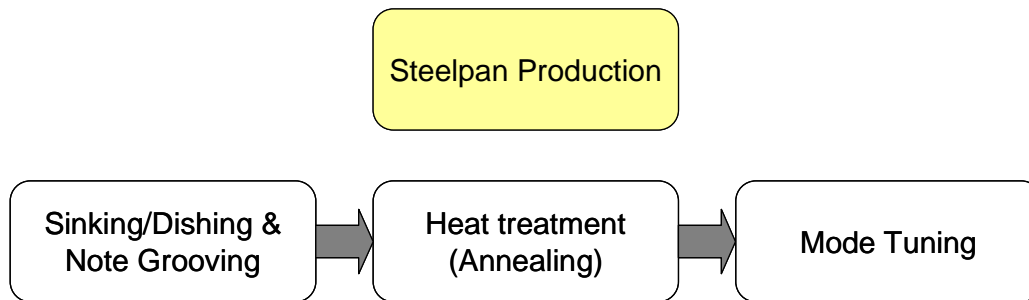
Figure 1.6: Summary of steelpan production

1.6.1   Steelpan dish production

As mentioned previously, steelpans are still largely produced in a traditional manner which entails dishing the top of a tight-head oil barrel with the use of heavy hammers. This process is highly skill dependent, dexterous and does not allow for repeatability. It is considered a public nuisance and there is a significant amount of material wastage due to drum splitting. The process subjects pan builders to: (1) noise induced hearing loss due to the high noise levels (~100db) [13] generated and (2) occupational diseases associated with prolonged exposure to the hand-arm vibrations experienced during sinking. For these reasons, pan builders have long called for a mechanized alternative. Over the past four decades several sheet metal forming technologies have been employed for producing steelpan dishes and these include conventional spinning, hydroforming, and deep-drawing. Some of these technologies are still currently used while some have been abandoned in preference for a currently popular pneumatic assisted sinking which employs a hammer-head attached to the end of a reciprocating piston. This process is identical to sinking by hand and introduces the same problems previously mentioned.

A novel sheet metal forming technology, termed single point incremental forming (SPIF) was applied to steelpan production in this work. This sheet metal forming technique was selected owing to its relative quietness and its ease of control through computer software which allows for improved repeatability of products. Unlike spinning, hydroforming and deep-drawing, incremental sheet forming does not require dedicated tooling (moulds or dies) thereby making it highly flexible and relatively cheaper. The study took the form of a pilot project which looks at the feasibility of using SPIF for the manufacture of mini-pan dishes which are typically 300mm in diameter and 45-50mm deep. A custom built incremental sheet forming machine at the Cambridge University Engineering Department was used to produce the mini-pan heads.

1.6.2   Mode confinement

Steelpan makers generally tune two or three modes in each outer note of a tenor pan and one in the middle and inner note regions. The fundamental mode in each note is: (1) tuned to a frequency on the musical scale and (2) the frequencies of the overtones are coaxed into an approximate harmonic relationship with the fundamental or into musical ratios that are accepted as pleasing to the human ear. In an effort to better understand the vibrational behaviour of steelpan notes, several models have been proposed by various researchers. Some models attempt to explain how manipulation of structural geometry [14,15] can achieve modal tuning while another model explains modal tuning by manipulation of boundary condition parameters [16]. However, neither of these models account or explain the capability of some tuners who manage to tune as many as four modes in the outer notes of tenor pans. One such tuner in Germany [17] claims that he is able to tune four modes in the outer modes and two modes in the middle notes of his tenor pans. Therefore, another aspect of this work will entail an investigation of mode confinement phenomenon.

1.6.3   Steelpan detuning

Part of this work involves a preliminary investigation of detuning of steelpan notes subject to impact forces comparable to that of normal steelpan playing. Like any other musical instrument, a steelpan is expected to need retuning at several stages during its lifetime. The aim in this preliminary work is not to eliminate detuning but to set out recommendations for further investigations which may assist in revealing solutions towards enhancing the stability of the tuned frequencies of steelpan notes.

1.6.4   The effect of manufacturing regime on vibration damping

The manufacture of steelpans involves several stages which include cold forming during the dishing of the pan head followed by heat treatment (annealing) and surface peening during tuning (see Figure 1.6) and surface coating (either painting or chrome plating). Previous studies [18,19] have concentrated on the effect of the manufacturing regime on the surface hardness of the pan head in an effort to establish the optimum parameters at which the steelpan must be heated in order to achieve an appropriate level of surface hardness that will facilitate effective tuning. Although a previous study by Ferreyra [20] also acknowledged a change in material damping properties after heat treatment there was no effort to correlate material damping and hardness properties.

Part of this work will focus on the effect of the manufacturing regime on material damping in steelpans in an attempt to identify damping mechanisms along with the optimum conditions required for achieving the appropriate level of material damping necessary for the production of superior quality steelpans.

1.7 Dissertation Outline

A background of the relevant literature in the respective engineering disciplines in combination with a review on previous work on the steelpan is done in Chapter 2 to emphasize the main gaps in the present knowledge and to outline the scope of the current work. Chapter 3 involved the production of miniature steelpan dishes using incremental sheet forming (ISF) and a financial analysis was conducted to determine the feasibility of using ISF for the production of full size pan dishes. Chapters 4 and 5 were vibration studies on full size and test steelpans respectively. Chapter 4 involved the study of modes of vibration and detuning of steelpan notes while Chapter 5 focused on mode confinement in test pans. The effect of the steelpan manufacturing regime on material damping is investigated in Chapter 6, leading to the summary and recommendations for further research in Chapter 7.

Chapter 2   Background

2.1 Steelpan dish production

2.1.1   Traditional crafting

The traditional crafting of steelpans is still largely a hand made process which begins by dishing the top of a tight-head steel drum with a sledgehammer or a heavy metal ball (see Figure 2.1). This process is still largely used internationally and many pan makers still believe that pan dishes formed in any other manner would be inferior to pans entirely made by hand. In spite of this, several problems associated with the traditional approach to sinking have lead pan builders to search for a mechanised approach to dishing. Some of these problems range from high noise intensity levels [13] associated with manual drum sinking which sometimes proves to be a public nuisance, material wastage due to splitting of the drums during the sinking process and problems experienced by pan builders which include noise induced hearing loss and exposure to hand-arm vibrations (HAV). Some pan builders take many months or years to master the art of sinking without tearing the drum surface and the problems of noise induced hearing loss and HAV present a direct threat to the already depleting population of skilled pan makers.

Figure 2.1: Traditional sinking of steelpan dish; **Left:** dishing a tight-head drum with a sledgehammer [21]; **Middle:** dishing a blank which is held in a jig; **Right:** dishing with a heavy steel ball [22]

An important characteristic of dishing a tight-head drum is the resulting thickness distribution in the dish. Since the drum head is fixed at the ends, the dish is formed by stretching which creates a thickness distribution that varies roughly from 10% reduction close to the rim to as much as 50% in

the dish base [19]. This distribution of thickness may or may not be crucial to the acoustics of the instrument.

To address the problems associated with traditional sinking several mechanised sheet metal forming alternatives have been attempted. Some are currently in use while some have been abandoned (see Figure 2.2). These processes include pneumatic hammering, spinning, hydroforming and deep-drawing. The benefits and drawbacks of each of these processes will be discussed. A relatively novel technology, incremental sheet forming (ISF) will also be presented as a promising alternative for the mechanisation of the steelpan dishing process.
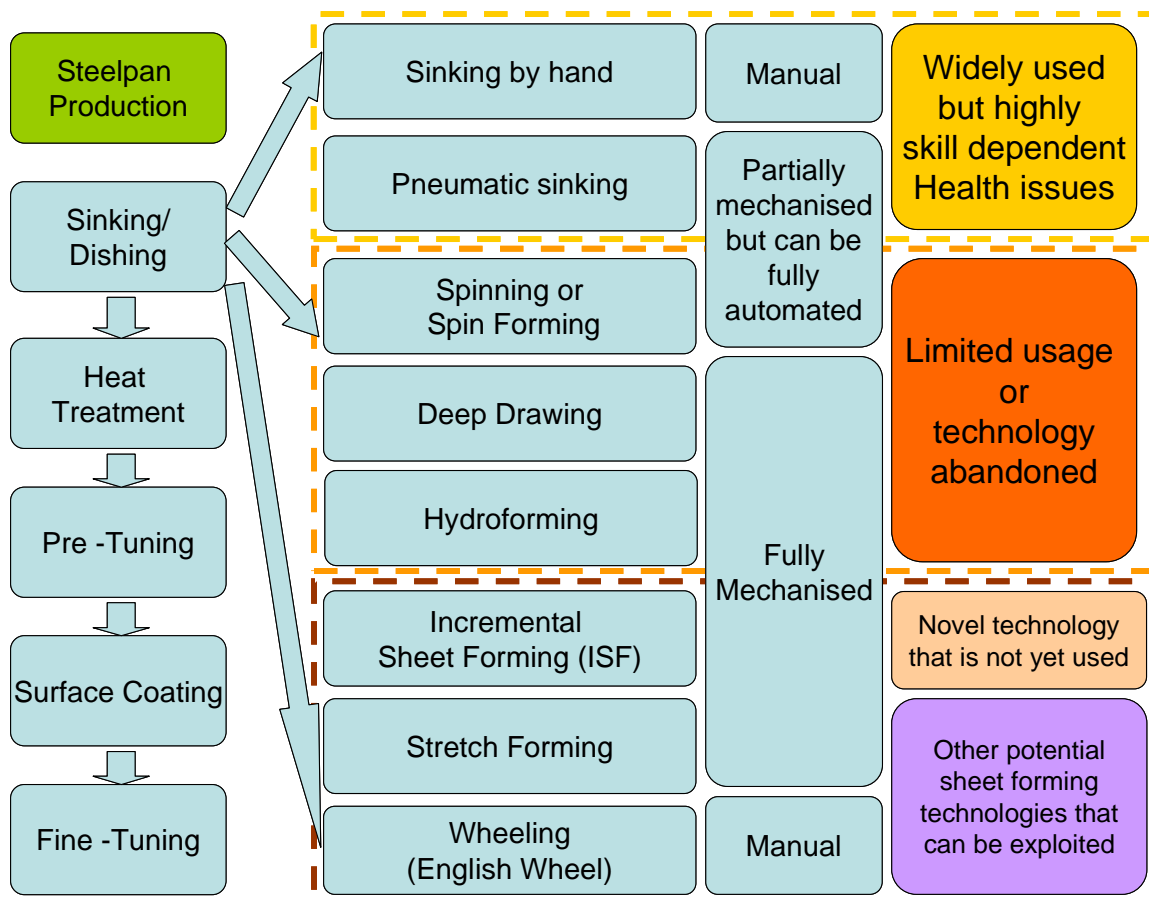
Figure 2.2: Steelpan dishing operations

2.1.2 Pneumatic and Robotic assisted dishing

Today *pneumatic dishing* or *pneumatic hammering* has become popular among pan builders and it is considered the de facto method for sinking that is largely replacing hammering by hand. The hammering force required for dishing is provided by a reciprocating piston in a chamber (see Figure 2.3). This method has become very attractive owing to its relatively low cost and relatively high speed. A soprano pan with an average depth of 210mm can be sunk in 20-30 minutes once the

process is mastered [23]. Some pan builders are also using this process to shape the note regions on the pan dish. Pneumatic hammering is less energy demanding when compared with traditional handcrafting but the use of this technology requires just as much skill on the part of the pan maker as careful control of the hammer movement and impact force are required in order to achieve the appropriate depth without splitting the dish surface. Pneumatic hammering, like traditional sinking also exposes the pan builder to noise induced hearing loss (Noise levels ~100dB) [13] and problems connected with hand-arm vibrations (HAV). HAV will soon be discussed.
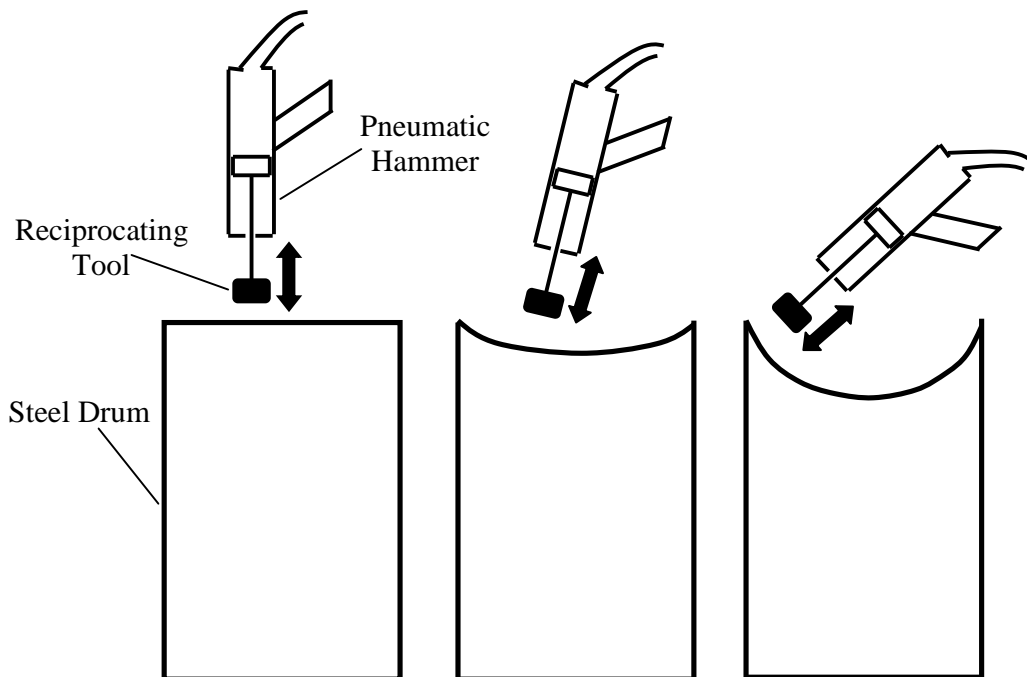
Figure 2.3: Schematic of pneumatic hammering

Like hammering by hand, high material wastage due to material splitting usually occurs before the operator is able to become comfortable and master the process. The final pan dish should also appear axisymmetric to be aesthetically pleasing and achieving this is also skill dependent. Neither traditional handcrafting nor pneumatic sinking provides means of ensuring dimensional repeatability. One possible way of improving shape repeatability would be to form the blank into a die cavity but several cavities would be needed as pans vary in depth (see Table 1.1).

There is also a movement to use a hammering tool attached to a CNC controlled industrial robotic arm. This would eliminate the skill dependency associated with hand and pneumatic hammering in addition to significantly reducing exposure to hand vibrations. However, this option is very expensive and would still be noisy. Nevertheless, researchers in Finland [24] and Germany [25] have explored the use of sheet forming with a hammering tool held by a robotic arm but accurate

forming was difficult owing to insufficient rigidity of the robotic arms [26]. Figure 2.4 shows sheet forming using an industrial robot.
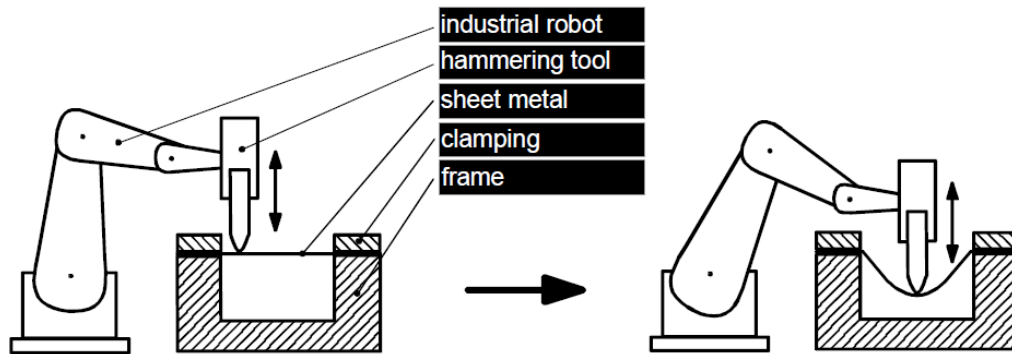
Figure 2.4: Incremental hammering using an industrial robotic arm [25]

2.1.3 Conventional spinning

Spinning or *conventional spin forming* has also been successfully used to manufacture pan dishes. Spinning involves the progressive shaping of a rotating metal blank over a rotating mandrel which is in the shape of the part to be formed (Figure 2.5). Parts to be formed are typically axisymmetric [27]. Steelpans vary in depth and it is obvious that a mandrel will have to be created for each pan type. Spinning also allows pan builders to experiment with pans of various sizes in contrast to using standard drums with fixed diameters. The process is capable of forming diameters ranging from 3mm to 10m and thicknesses from 0.4mm to 25mm [28]. An additional step is also introduced for the production of the completed instrument whereby the dish is attached to a skirt. A major advantage of spinning is that it uses simple and inexpensive tooling and the process involves localised deformation as the tool is applied locally to the workpiece [29]. This means that larger forming limits can be achieved with considerably lower forming forces and machine power as compared to conventional press forming.

Spinning unlike traditional handcrafting and pneumatic hammering makes it possible to produce pans with a relatively good degree of consistency (shape repeatability) since the same mandrel is used repeatedly. However, manual spinning can also be physically challenging and requires dexterity as control of the process is highly dependent on the competence of the operator [29,30].

The spinning technology was initially exploited by A.G. Major, a metal spinning company in Croydon, England. A.G. Major began by spinning miniature pans in 1973 [31]. Almost one decade later spinning was also used by the Metal Industries Company Limited (MIC) in Trinidad to produce full size soprano pan dishes [32]. A typical soprano pan dish was spun in approximately 15 minutes [32]. These spin formed dishes were sold to pan tuners. MIC had a large cadre of highly

skilled machinists and was able to produce high quality spin formed pan dishes for almost a decade before the technology was sold to a steelpan factory, Panland Ltd formerly known as Trinidad and Tobago Instruments Ltd (TTIL) [32]. In spite of this activity, there is no technical publication on the use of spinning for the dishing of steelpans. However, there is a brief account on spin formed dishes at MIC in a pan tuning manual by Kronman [10].

Panland was also able to successfully manufacture pan dishes using spinning but the company recently abandoned this technology in favour of pneumatic hammering [33]. Panland reported that on some occasions spinning produced high quality dishes with uniform thickness distribution while on other occasions the process produced pan dishes which were either too thick in the middle or too thick at the base. In some instances the dishes fractured during the spinning operation. Rohner and Schärer [34] also applied conventional spinning to pan production but abandoned the technology in preference for deep drawing after experiencing identical problems as Panland. It is also likely that A.G. Miller spinners discontinued the production of spin formed mini-pans due to similar problems experienced by Panland.

Spinning is defined as a rotational forming process for the creation of axisymmetric shapes in which there is no change in the wall thickness [19,20,25].The problem of uneven thickness distribution experienced by Panland may be a consequence of over-spinning or under-spinning [28]. These are conditions in which too great or too small tool forming forces result in an uneven distribution of thickness in the finished shape. The problems reported may be attributed to poor technique rather than process. Observation of the operator's spinning technique could have provided some useful information which may have helped to unearth the fundamental reasons for these problems.

Up until the abandonment of the spinning technology by Panland, all spinning of pan dishes was done manually and it is also likely that no studies were conducted in an attempt to capture the best practices which resulted in high quality pans. One manner in which this could have been done is with the use of programmable numerical control (PNC) which uses playback technology [28]. Here, the pan dish is spun manually by an experienced operator while his motion/tool path is recorded and played back to form subsequent pan dishes. Playback technology capitalises on both the operator skill and the repeatability given by the computer for faster and improved quality production. Spinning can also be automated with the use of computer numerical control (CNC) and numerical control (NC) programs.
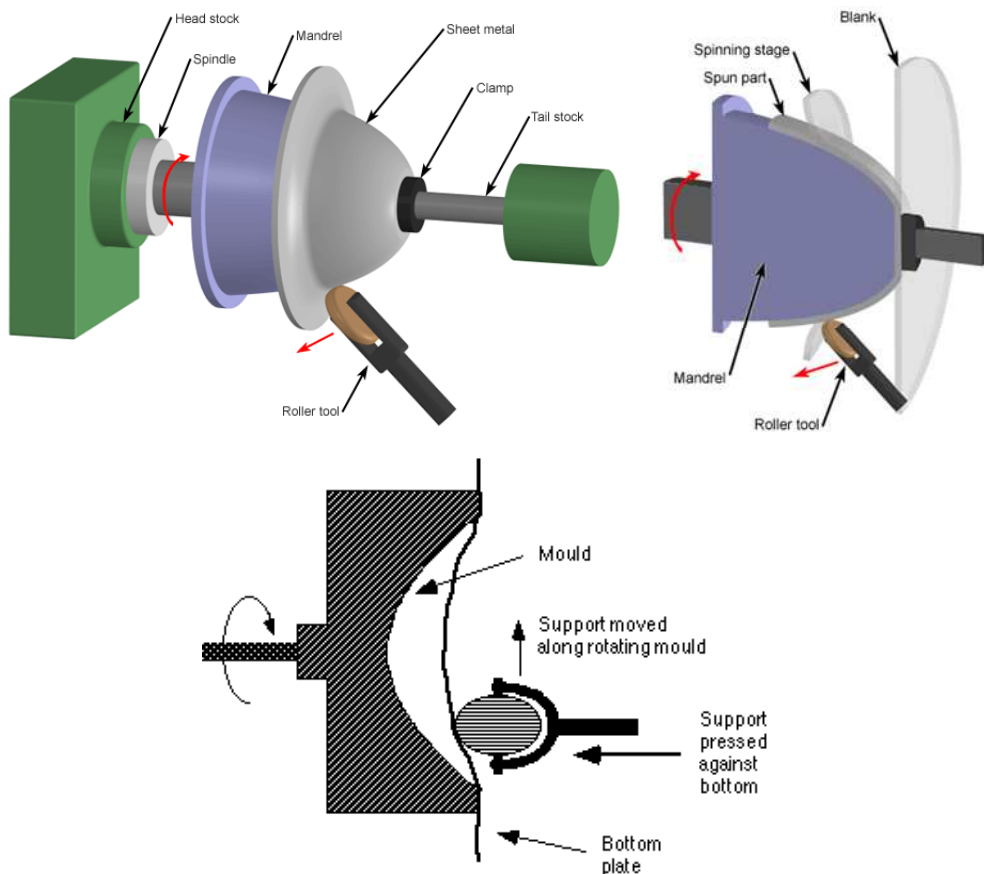
Figure 2.5: Schematic of conventional spinning of a steelpan dish using; **Top:** a convex mandrel [35] and **Bottom:** concave mandrel [10]

2.1.4   Problems associated with the use of vibrating hand tools

Manual sinking and pneumatic hammering are equally problematic as they each expose the craftsman to the risk of developing problems associated with hand-arm vibrations. Hand-arm vibration (HAV) is vibration transmitted from work processes into the hands and arms of workers [36,37]. Frequent and long-continued exposure to hand-arm vibration can lead to the development of a constellation of conditions known as hand-arm vibration syndrome (HAVS) [26,28-31]. HAVS affects the vascular, nervous and musculoskeletal systems and some of the signs and symptoms associated with HAVS include Raynaud's disease or the phenomenon also known as vibration induced white fingers (VWF) or dead hand where the finger tips blanch intermittently particularly in cold and wet conditions. In extreme cases permanent damage or gangrene is the end result; tingling and numbness in the fingers; cold intolerance and loss of muscle control and grip strength. These signs and symptoms typically occur with jobs in which there is frequent use of vibrating tools and equipment [36,37]. While some of the symptoms can be the result of other medical conditions, Raynaud's phenomenon is generally considered to be occupational and it is common among air hammer users [38,39].

Many pan builders employ workers who are solely dedicated to dishing the pan surface. Some of these workers can spend up to 8 hours a day or more on dishing. The latency interval for the onset of HAVS symptoms can vary but most symptoms can appear within one or two years and most of the effects are exacerbated with continued exposure to HAV [38,40]. The effects of HAVS after prolonged exposure to hand-arm vibrations are irreversible and in the majority of cases cannot be dispelled by medication or surgery [40]. Permanent disability is usually an end result. Raynaud's phenomenon will inevitably result in loss of work time during blanching attacks and an employer may eventually incur employee litigation for disability claims if the employer is deemed to be negligent in his duty of care towards his employee. Many workers who operate vibrating tools are most times ignorant of the risks involved and it is a legal requirement and the responsibility of the employer to protect employees by assessing and controlling the risks from vibrating equipment. Self employed pan builders should also be made aware of the risks involved in the use of vibrating tools. There is a large body of guidance which is available to assist employers and users of vibrating tools in this regard [36,37].

Several measures have been taken to damp vibrations in vibrating tools and these include the use of gloves and rubber pads [41]. Some users of the pneumatic hammers complain that the use of gloves makes use of the tool uncomfortable and interferes with accurate control. The Health and Safety Executive (HSE) [37] has recommended that employers shorten the number of hours in which employees are in contact with vibrating equipment but some argue that this only postpones the onset of HAVS [41]. The best way to avoid the problems highlighted above is to completely mechanise or automate the dishing process. Attention will now be given to technologies in which the dishing process is completely mechanised.

2.1.5 Hydroforming and deep-drawing

Sheet *hydroforming* and *deep-drawing* are other sheet metal forming technologies that are being used for the production of pan dishes. Sheet hydroforming is subdivided into sheet hydroforming with a punch (SHF-P) [42] or sheet hydroforming with a die (SHF-D) [43], depending on whether a male or female tool is being used to form the part. Forming pressure in hydroforming is provided in conjunction with a fluid medium. Unlike hydroforming, deep-drawing requires the manufacture of both punch and die. While both technologies can be used to form the completed pan dish in a single operation, the main drawback is the relatively high costs in comparison to pneumatic hammering and spinning.

The time savings achieved by these processes are phenomenal as a pan dish can be formed in a few seconds. However, a large volume of pans would need to be created in order to recoup capital and

tooling costs. The first record of the use of hydroforming for steelpan dishes was in the mid 1970's in a collaborative project between the Caribbean Industrial Research Institute (CARIRI) and SAAB automakers in Sweden. Some 200 hydroformed tenor pan dishes were produced and given to professional tuners who reported on their experiences in using these dishes. One of the problems experienced by the team was poor thickness distribution in the dish. It was not specified what poor thickness distribution meant but it is likely that the thickness distribution obtained in these hydroformed dishes was not comparable to the thickness distribution in hammer formed pan dishes. However, the project was eventually abandoned due to lack of funding [44].

Nevertheless, Withmyre and Price [45] and Schärer *et al*. [46] have also recently successfully manufactured pan dishes using hydroforming and deep-drawing respectively. Withmyre and Price determined the average shape and dimensions of the top of the playing surface of several D^1-tenor pans. The topographic information obtained from this survey were compiled and used to generate a CNC tool path which was used to machine a male punch which was integrated into a hydroforming press.

Unlike Withmyre and Price, Schärer and his team designed a drawing punch which they claimed was suitable for all pan types. Both groups produced pan dishes of similar dimensions with dishes having an average diameter of 600mm and depth of 210mm using low-carbon steel sheets of various thicknesses. Both groups also claim to have attained uniform thickness distribution in formed dishes. This claim is reasonable as in hydroforming and deep drawing, stretching is reduced which results in almost uniform wall thickness and relatively small material thin-out [47,48]. Murr *et al*. [49] were able to successfully tune uniform thickness stainless steel pans produced by the hydroforming process patented by Withmyre and Price [45]. This means that the thickness distribution obtained via stretching as in manual and pneumatic hammering may not be crucial to pan tuning.

Hydroforming and deep-drawing are completely mechanised processes and the problems associated with noise induced hearing loss and HAV are tremendously reduced. These processes also deliver superior geometrical accuracy, tolerance, and repeatability, but poor flexibility as dedicated tools will be required for each pan type. To make these processes viable, a large volume of pan dishes need to be produced but the steelpan is still currently a low-volume product.

---

[1] This is a pan in which the lowest frequency note is D4.
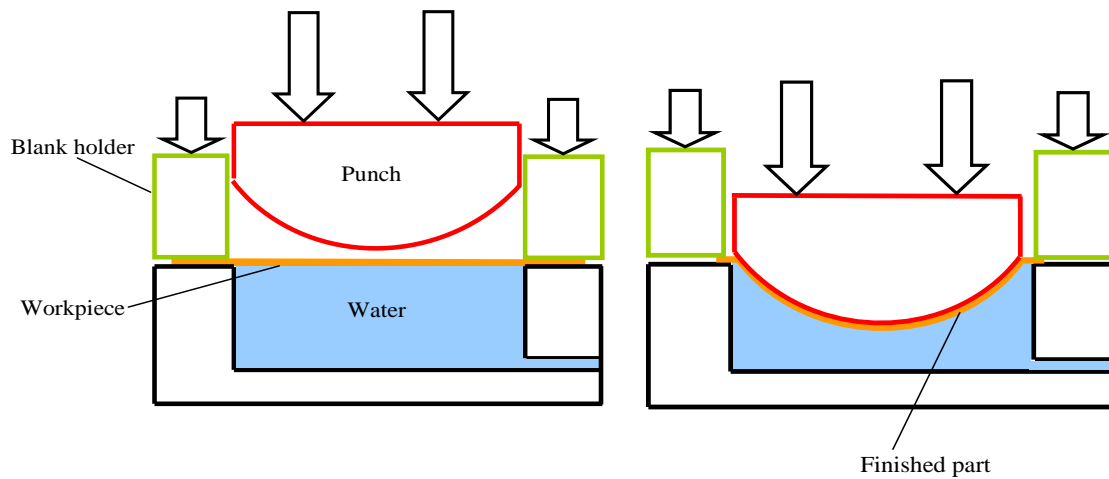
Figure 2.6: Hydroforming of steelpan dish
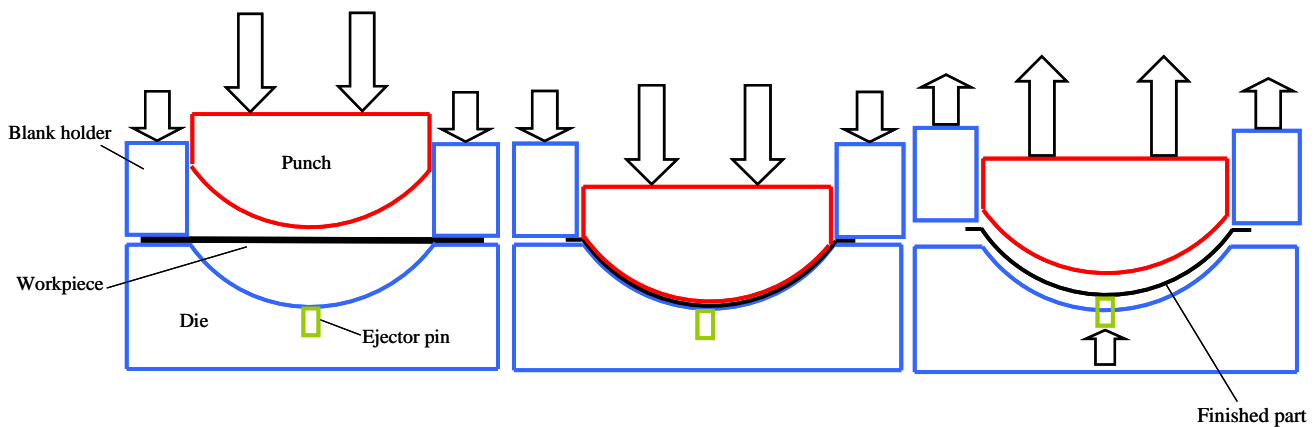
Figure 2.7: Schematic of deep-drawing a pan dish

2.1.6 Incremental sheet forming

A novel technology which can be exploited for the production of steelpan dishes is *incremental sheet forming* (ISF). Incremental sheet forming refers to a constellation of forming processes in which sheet metal is formed by the computer controlled movement of a small tool or punch which causes localised plastic deformation when in contact with the sheet [50,51]. The completed shape depends on the programmed tool path and on any supports or tools which may be on the reverse side of the sheet [52]. Figure 2.8 shows three typical configurations which are commonly used in incremental sheet forming. These figures illustrate the versatility of ISF but most geometries can be easily achieved with single point incremental forming (SPIF).

19
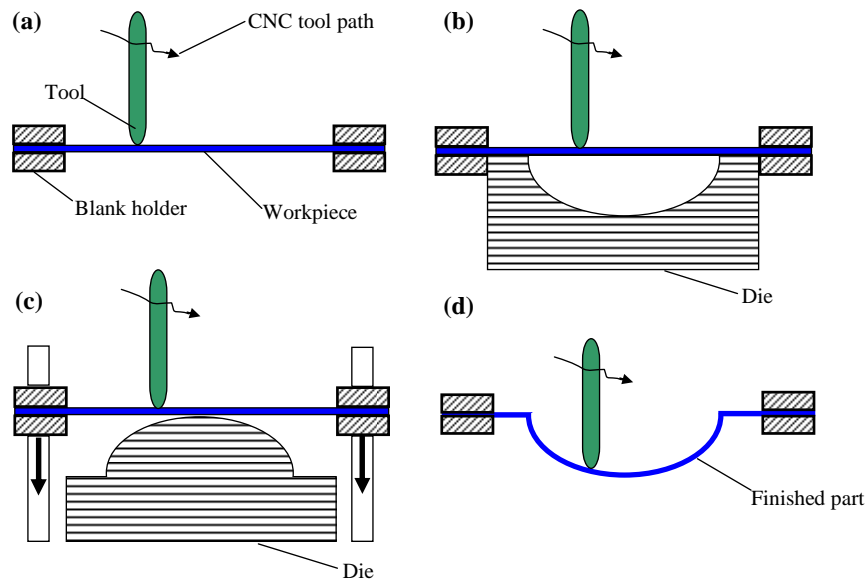
Figure 2.8: Three configurations of the incremental sheet forming process[53]; **(a)** Single point incremental sheet forming; **(b)** Incremental sheet forming with negative die; **(c)** Incremental sheet forming with positive die and **(d)** Completed part using (a) and (b)

The benefits provided by this technology make it highly attractive for the production of steelpan dishes. Firstly, the operation is very quiet [54] and the operator is not in contact with the equipment during forming so exposure to high noise levels and hand-arm vibrations is tremendously reduced. Secondly, if SPIF is used for dishing, no dedicated forming dies would be required as in the case of spinning, hydroforming and deep-drawing. Although dedicated machines [26] have been manufactured only for ISF, some researchers have been able to retrofit three axis CNC machines for ISF use [47,48]. These modified CNC machines are fitted with an open top worktable which enables access to the reverse side of the sheet during forming and instead of using a cutting tool, the CNC machine incorporates a custom made non-cutting, hemispherical or ball tip tool whose tip is usually designed to rotate freely. Figure 2.9 shows a schematic of a CNC machine system for single point incremental forming. However, CNC machines are not designed to withstand high spindle loads [26] and this is generally avoided by limiting blank thickness to 1mm to avoid bearing damage [50]. Custom made ISF machines will be generally designed to accommodate higher bearing loads and can therefore accommodate blanks of greater thickness. However, a machine with a 1mm blank range is sufficient for dish production as most steelpans are constructed from sheet of thickness 1.0-1.2 mm.
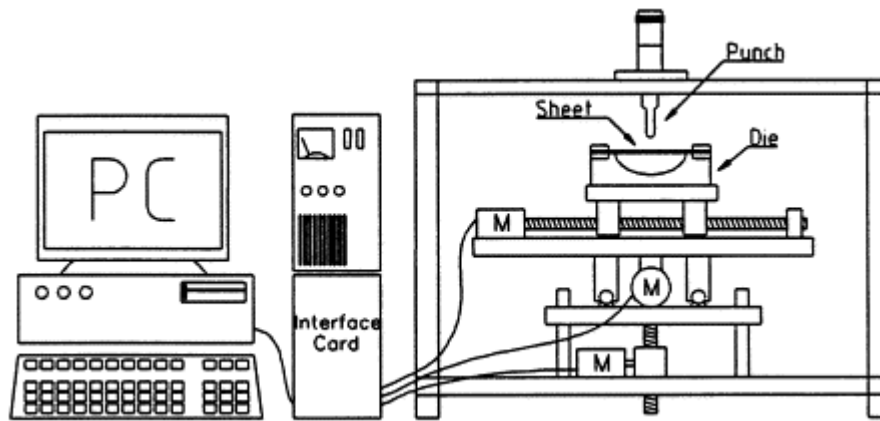
Figure 2.9: Schematic diagram of the CNC incremental sheet forming system [55]

Another attractive feature of CNC ISF is its high flexibility such that in order to manufacture or modify a product all that is required is a modification of the part program on the computer [50,51,54,56]. Different steelpan dishes would only require a simple change in the part program in contrast with spinning, hydroforming and deep-drawing which require dedicated dies for each dish type. While being highly flexible, one drawback of ISF is that is a very slow process which is only likely to be economical for batch sizes less than or equal to 100 parts [52]. Although ISF presents a trade-off between flexibility and high volume production, its slowness may not be a drawback as the steelpan is largely a low volume product.

Another drawback of incremental sheet forming is poor accuracy [56-58] of the finished part such that there are geometrical deviations between the designed and manufactured product. This is largely in part due to bending near the inner edge of the clamping plate (see Figure 2.10) and material spring back [56,58,59] after the punch load is removed from the blank. Poor accuracy is also compounded by distortions in the geometry after unclamping and trimming. In some instances a "pillow" effect (Figure 2.10) [56,58] is observed in the base of some finished products. These are some of the defects that will be inevitably encountered if ISF is to be used for steelpan dishing.
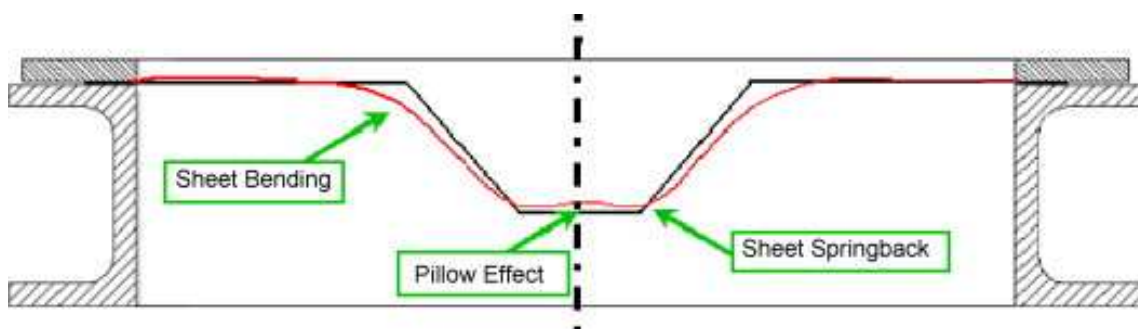
Figure 2.10: Geometrical errors of the single point incremental sheet forming process [56]

Several techniques are being used to detect error in ISF and some include the use of co-ordinate measuring machine (CMM) systems and online control with laser cameras or laser scanning equipment [56]. There is also consistent effort by several researchers to reduce or eliminate the effects contributing to poor accuracy. In some instances a flexible support is placed on the reverse side of the blank in an effort to reduce springback [52,60] or a counter pressure is provided by using pressurised water (similar to hydroforming) in a sealed system [56]. This helps to reduce springback, is relatively cheap to implement but is only effective provided that the fluid pressure is properly controlled. Tool path optimisation [56,58,61] multi-pass forming [51,59] and over bending [56,58] where more deformation is applied during the forming regime are other techniques that are currently being explored as avenues to improve geometrical accuracy in incremental sheet formed objects.

The steelpan dish is a relatively simple geometry and small deviations in accuracy can be tolerated as there are still final adjustments to be made to the dish during tuning. Geometrical inaccuracy may be more apparent in the production of dishes for full size pans whose diameters are typically to the order of 600mm. These larger dishes may experience a greater degree of material springback and elastic deflection since the working area is significantly larger and the stiffness at the centre of the blank will be lower than that of a blank that is used to create a mini souvenir pan whose diameter is usually less than 300mm. In this work ISF has only been used to produce mini-pan dishes. Trimming of the clamping area will also result in distortion of the dish but the subsequent attachment of the skirt (see Figure 1.4b) should provide sufficient stiffness to counteract this problem.

Moreover, higher forming limits i.e. formability can be achieved through ISF than conventional pressing as the material is deformed locally by a small tool [56]. This may provide an opportunity to explore the idea of extending the current depth of most dish types thereby creating a larger dish surface which can accommodate more notes or simply allow for more spacing between adjacent notes.

Formability of the material in ISF is affected by the punch diameter and the vertical step size i.e. feed rate between contours. A larger diameter tool reduces the formability as a much larger area is in contact with the surface [56]. Several researchers recommend a 10mm ball head tool for forming operations [60,62]. A slower feed rate or small steps between contours improves formability and surface finish but has the drawback of increasing production time [19,43,50]. Formability is also enhanced by using multiple passes or stages instead of a single pass tool path. Cerro *et al.* [51] found that objects formed using multiple passes were less likely to fracture since the deformation in

each stage is reduced thereby decreasing the strain hardening effects in the material. In most cases a lubricant [19,43,48] in the form of grease is used for good surface quality and it is also recommended that the clamping frame be the same shape as the product [60]. This means that the blank used for the steelpan dish should be held in place by a circular clamp.

2.1.7   Stretch forming and Wheeling

Stretch forming and *wheeling* (English wheel) are other sheet metal forming technologies that can be exploited for pan dishing. Stretch forming, see Figure 2.11, is the forming of a sheet blank with a rigid punch whereby the blank is rigidly clamped between a pair of hydraulically actuated gripping jaws located on opposite ends [63]. Gripping jaws can be stationary as in simple stretch forming (Figure 2.11a) or moveable as in flexible stretch forming (Figure 2.11b).
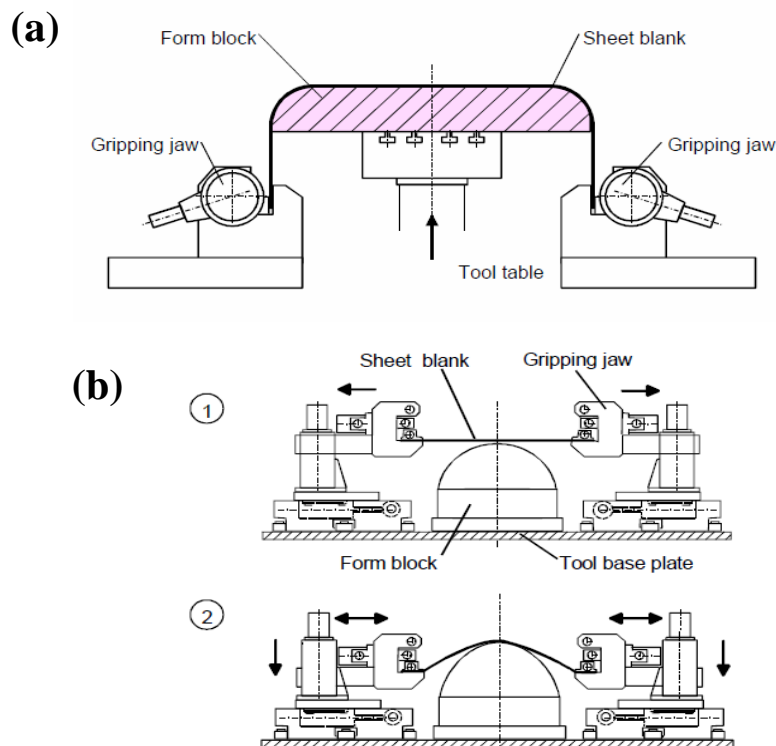
Figure 2.11: Stretch forming: (a) Simple stretch forming and (b) Flexible stretch forming [64]

In stretch forming a single punch is used and various pan dishes may be created by simply varying the depth of the draw of the punch into the blank surface. This makes the process highly flexible thereby eliminating the need for several punches for each pan type as in hydroforming, deep drawing and spinning. It is apparent that stretch forming offers an alternative that is highly flexible, skill independent, quiet but may be expensive to implement.

Wheeling unlike stretch forming is completely manual and the sheet metal is formed by repeated passing between two rollers of different radii. This is done on a machine referred to as the English wheel (see Figure 2.12) which resembles the letter "C" and has rolling wheels situated at the ends of the "C". The distance between the center of the rollers and the vertical arm of the "C", known as the throat is the depth that determines the size of the sheet that can be formed in the machine [65].
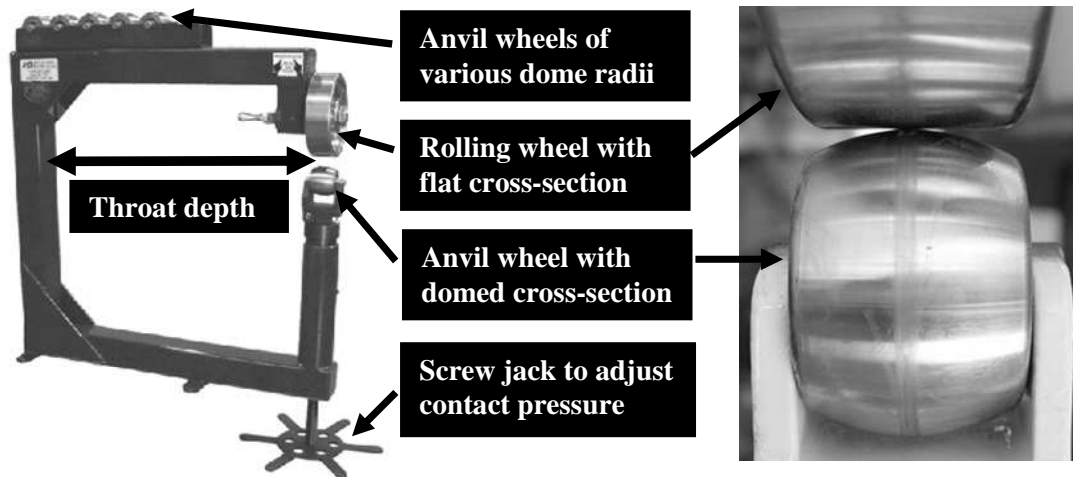
Figure 2.12: The English wheel [66,67]

As the material thins during wheeling, the gap between the rollers is adjusted so that the appropriate contact pressure is maintained to allow forming to progress smoothly. The lower or anvil wheels are changed accordingly until the desired shape is achieved.

The English wheel is portable, the process is quiet, the surface finish obtained is much smoother as compared to hand sinking and pneumatic hammering and the equipment is relatively cheap. However, this process is tiring and highly skill dependent and there is no guarantee of shape repeatability. It would also be difficult to form large size pan dishes on the English wheel but the process may be better suited to forming mini-pan dishes which have small diameters and are relatively shallow.

2.1.8   Summary of steelpan dish production

The technologies currently used for steelpan dishing have been discussed. **Table 2.1** summarises these technologies. Hand and pneumatic sinking although very cheap exposes pan builders to huge levels of noise and vibration which is a direct threat to their health and longevity as steelpan craftsmen. Hydroforming and deep-drawing, while relatively quiet, skill independent and fast are inflexible, require significant capital outlay and large volumes of dishes would be required to break even on investment. The spinning technology is also very attractive provided that it can be fully

automated. Further research on the application of this technology for steelpan dishing is recommended.

A novel technology, ISF, contains attractive features which makes it a good candidate for mechanisation of steelpan dishing. ISF significantly reduces exposure to high noise and vibration levels, does not require dedicated tooling; is flexible and relatively cheap. Its slowness and poor accuracy are not major drawbacks since the steelpan is still largely a low volume product and the dish would require further adjustment during the tuning process. In this work, the process of ISF will therefore be applied to steelpan dishing.

Table 2.1: Comparison of steelpan dishing technologies

TECHNOLOGY	Capital Cost (£)	Time to make one pan†	Skill Level	Health Risks	Flexibility	Accuracy	Thickness Distribution	Material Wastage	Volume
					FEATURE				
Hand Sinking	100-200	4 hours	High	High	Good	Poor	Material is stretched	High	Low
Pneumatic Sinking	500 - 1500	20 to 30 minutes	High	High	Good	Poor	Material is stretched	High	Low
Manual Spinning	1500 - 3000	15 – 20 minutes	High	Medium	Poor	Moderate	Uniform	High	Low
Hydroforming	[a](20 – 35) k	1 – 1.5 minutes	Low	Low	Poor	Excellent	Uniform	Low	High
Deep Drawing	[b](20 – 35) k	10 – 30 seconds	Low	Low	Poor	Excellent	Uniform	Low	High
Incremental Sheet Forming (ISF)	**(10 – 15) k ‡**	**5 hours**	**Low**	**Low**	**High**	**Poor**	**Based on sine law[54]**	**Low**	**Low**

NOTES:

† Times based on sinking a soprano pan to a depth of 200mm.

‡ Cost based on building a stand alone ISF machine [26] but could be reduced if a CNC milling machine is retrofitted.

a and b: These are costs for 250 ton presses [68]. The costs of the press tools are not included.

2.2 Materials and vibration damping in steelpans

The standard governing the design and production of oil drums, specifies steel sheet with carbon content which does not exceed 0.15%C [69-71]. Within the last decade, several studies have also explored the feasibility of manufacturing pans from different metals. These studies made use of the metal alloys alpha brass (70%Cu/30%Zn) [72], 304 stainless steel [49] and aluminum 6061 (T0 and T6 heat treatable grades) [73]. These metals were chosen primarily because of their high formability as they are among the most ductile in their respective alloy classes (see Table 2.2). Unlike carbon steels which require a surface coating to provide protection against corrosion, these metal alloys intrinsically offer exceptional corrosion resistance. The use of aluminum provides the opportunity for light weight pans which can be hard coated and coloured through the anodizing process. However, the alternative of using these metal alloys for pan making required subtle changes to the traditional pan production process (see **Table 2.3**).

Research [18,19] on the pan was initially focused on identifying the optimum process conditions required to achieve appropriate levels of hardness, to facilitate tuning. This was done by measuring the material hardness after cold deformation (sinking/dishing) and heat treatment (stress relief annealing). While the hardness of the pan head is crucial for tunability, another important property that has not been considered is the effect of the pan production process on material damping. There is no record in the literature of any study that deals with the effect of the production process on material damping in steelpans. However, there are several studies which consider each process individually. This section of the review will draw on these works in an effort to forecast the effect of each production stage, including surface coating, on material damping in the steelpan. A comparison will also be made with the use of low-carbon steel and other metal alloys as raw materials in the pan production process.

2.2.1 Vibration damping: material and non material damping

Damping is an important property in many musical instruments, for instance in high quality bells and wind chimes a low damping capacity is preferred. Damping is generally understood to be the extraction or dissipation of energy from a vibrating system, usually by sound radiation and the conversion of this energy to heat [74,75]. There are two types of damping, namely: material and non material damping or external (system or structural) damping. Material damping also referred to as internal friction, has been attributed to several mechanisms which are inherent to the material [76-78]. Non-material or external damping usually comes from joints and attachments and includes interfacial micro slipping, air pumping, rattling of loose joints, acoustic radiation or deliberately applied damping treatments [75,76,78]. The interest herein is primarily with material damping.

2.2.2   Material damping mechanisms

The internal mechanisms which contribute to internal friction in metals may be a consequence of the creation of imperfections such as point defects, atomic diffusion, vacancy migration or the interaction between impurity atoms or precipitates with imperfections such as dislocations [79-83]. Since internal friction is sensitive to these mechanisms it is apparent that any process, be it external or internal, that affects these mechanisms will have a direct impact on material damping. Several studies have shown that plastic deformation (cold forming), heat treatment, grain size and chemical composition affects the internal friction in metals [79,81,83-90]. Figure 2.13 shows a wide loss factor range for steels, Cu and Al alloys, for very narrow ranges of Young's modulus. These ranges are likely to be for these metals in their manufactured state, prior to any processing. If this is the case, then it may be possible to expand or contract these ranges by manipulating the internal friction using various manufacturing regimes. The effect of cold deformation, heat treatment and surface coating on internal friction will be discussed shortly.
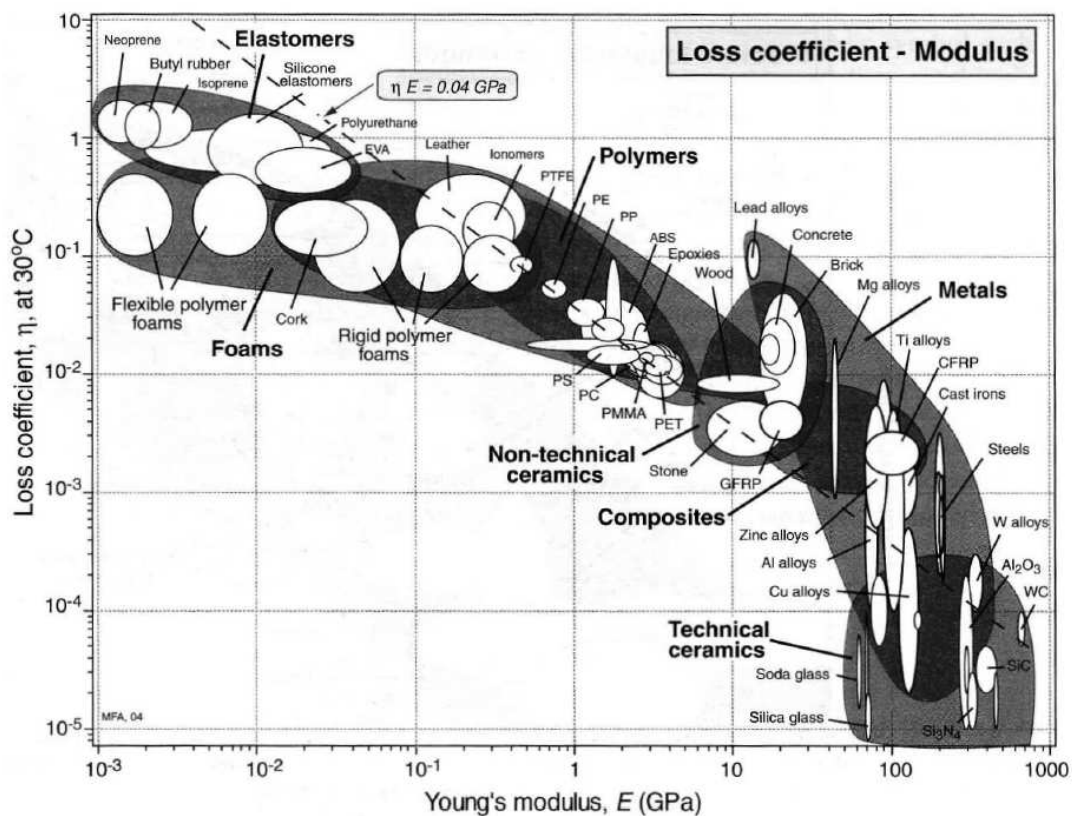
Figure 2.13: Variation of damping for different materials [91]

Table 2.2: Comparison of Low Carbon steel with other materials used for steelpan manufacture [92]										
Pan head material	Young's Modulus (E) GPa	Density (ρ) kg/m^3	Poisson's ratio (v)	Sound Velocity (c_L) ms^{-1} $(E/\rho)^{1/2}$	Work/strain hardening coefficient (n)	Tensile Strength (MPa)	Yield Strength (MPa)	Elongation (%)	Vickers Hardness [49](VHN)[a]	Material price (£/kg)[b]
(0.06% Carbon) – SAE 1006	200	7870	0.28	5040	0.26	HR -295 CD - 330	HR -165 CD - 285	HR – 30 CD - 20	118	1.6
α-Brass (70% Cu/30% Zn) – C26000	110	8530	0.30	3590	0.50	A – 338 CW - 524	A – 117 CW - 434	A – 57 CW – 8	116	5.6
304 Stainless Steel (0.08% C max, 19% Cr max) – AISI 304	193	7900	0.30	4943	0.53	A - 586	A - 241	A - 55	196	4.0
316L Stainless Steel (0.03%C max, 18% Cr max) – AISI 316	193	8000	0.30	4910	0.52	A – 586 CD - 620	A – 241 CD - 415	A – 55 CD - 45	196	4.0
6061 Aluminium†	69	2700	0.33	5055	< 0.20	T0 - 124 T6/T6511 - 310	T0: 55 T6/T6511: 276	T0 - 25 T6/T6511 - 12	122	2.9

NOTES:
HR – Hot Rolled; CD – Cold Drawn; A – Annealed; CW – Cold Worked
T0 – Annealed to obtain lower strength temper
T6/T6511 – Solution heat treated and artificially aged
† Yield strength for 6061 Aluminium is taken at 0.2% proof stress
c_L – Longitudinal sound velocity
a – Micro indentation hardness prior to cold deformation
b – Estimates obtained from Cambridge University Engineering Stores

Team	Traditional pan making	Schärer and Rohner [93]	Murr *et al.* [41,64,65]			Kronman [10]
Material	Low carbon steel (0.03 to 0.06 wt%)	Carbon steel (Fe PO1 and Fe PO4 grades)	*α*-brass (70%Cu/30%Zn)	Aluminum 6061 (T0 and T6 grades)	Stainless Steel (304)	Stainless steel (grade not stated)
PRODUCTION STAGES						
Step 1 (sinking or dishing)	By hand or pneumatic hammer – pan head sunk to final depth	Deep drawing – pan dish created to final depth	Pneumatic hammer – pan head sunk to an intermediate depth		Hydroforming process by Withmyre and Price – notes zones already incorporated into die. Pan dish created to final depth	By hand – drum head sunk to final depth
Step 2	Heat treatment, usually over a bonfire or propane torch	Skirt attached to pan head	Intermittent annealing - 288°C for 1 hour and air cooling	Intermittent annealing - 208°C for 45 minutes and air cooling	Vacuum annealed at 1061°C for 1 hour before rapid quenching in nitrogen gas	Cutting of drum side
Step 3	Cutting of side and marking of note zones	Gas nitriding for 7 to 12 hours at 500°C	Pneumatic hammer – pan head sunk to final depth		Skirt attached to pan head	Heat treatment over bonfire
Step 4	Pre-tuning	Marking of notes zones	Skirt attached to pan head		Tuning	Cutting of drum side
Step 5	Surface coating (spray or bake painting/ chrome plating)	Tuning	Marking of note zones			Marking of note zones
Step 6	Fine Tuning		Tuning			Tuning

Table 2.3: Production process for pans manufactured from different materials

2.2.3   Cold deformation and heat treatment effects on material damping

- **Cold deformation**

It is well established that internal friction is expected to increase with cold forming and the same outcome is expected for the pan material after dishing. The primary reason for the increase in material damping with plastic deformation has been attributed to an increase in dislocation density and the creation of point defects during deformation [74,75,79,86]. Zener [89] assumed that the increase in internal friction was a consequence of the residual stresses produced by inhomogeneous cold working. Residual stress variation is brought on in part by dislocation pile-ups at grain boundaries and obstacles [48].

Additionally, plastic deformation at room temperature also brings about a decrease in the elastic modulus of the material and this was shown by Nowick [83], Hikata *et al.* [94] and Granato *et al.* [87]. However, the Young's modulus and internal friction were shown to relax (i.e. recover) provided plastic strain is very small (0.4 – 4%) [83,87]. The increase in material damping and decrease in elastic modulus resulting from room temperature deformation and subsequent rapid recovery is known as the Köster effect [83]. The dishing process for pans heads can result in deformations which are to the order of 50 percent strain [19], much larger than the range in which the Köster effect is observed. Since, the deformations experienced by the pan head material in this case are extremely large, the relaxation as observed in the Köster effect may not be significant to enable a complete recovery of the internal friction and Young's modulus. Hence, the pan head material may display a permanently decreased Young's modulus after dishing.

- **Heat treatment**

Heat treatment (annealing) is expected to have the reverse effect on internal friction in cold formed pan heads. For instance, Zener [89,95] discussed the variation of internal friction with the annealing temperature of cold worked metal specimens (see Figure 2.14). Zener [89] attributed the initial decrease in internal friction which occurred below the recrystallisation temperature to the relaxation of internal stresses, while the rise in internal friction beyond the recrystallisation temperature was attributed to an increase in grain size. No noticeable change in hardness was detected but the Young's moduli increased by approximately 5 percent. The decrease in Young's modulus as a consequence of the Köster effect in cold forming may be offset by the increase in Young's modulus that will be brought on by annealing, so there may be a very small or no apparent change in the elastic modulus after the annealing of previously cold rolled pan heads. This decrease in internal friction with annealing has also been explained in terms of dislocation/point defect (vacancies and interstitials) interactions. Nowick [83] attributed the recovery of internal friction to a rearrangement

31

of dislocations to more stable positions while Granato *et al.*[87] and Cottrell and Bilby [96] credited the recovery to the migration of solute atoms to dislocations and the subsequent anchoring of these dislocations by strain ageing.
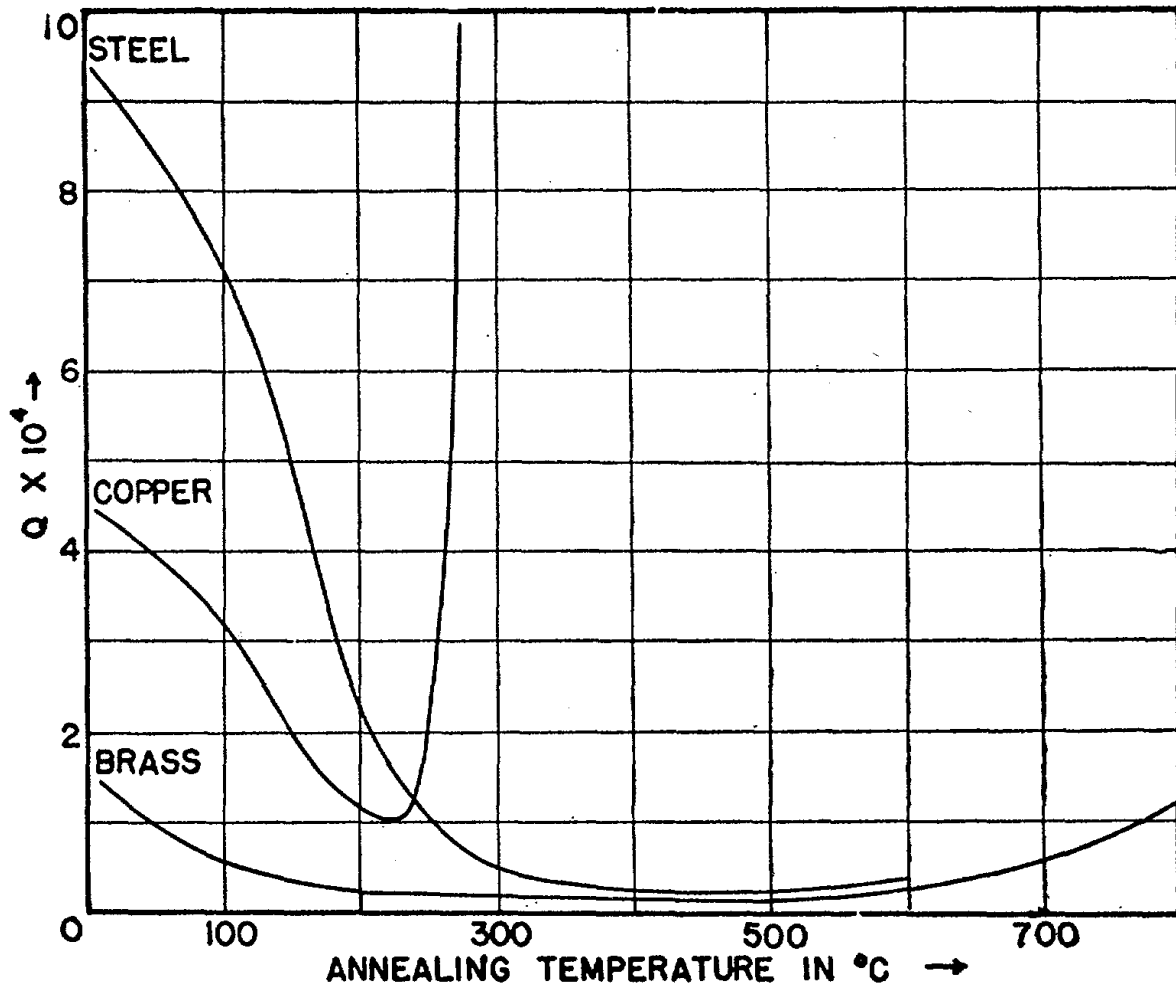
Figure 2.14: Effect of annealing temperature on cold worked specimens [89] with Q on the *y*-axis refers to the inverse of Quality factor in the author's notation

Strain ageing results in the pinning of dislocations which would have the effect of decreasing internal friction as pinning impedes dislocation translation and vibration. However, the dislocation density is also decreased during heat treatment, which means that dislocation-dislocation interaction is also decreased. This will have the effect of decreasing internal friction. It is possible that the latter effect will outweigh the former thereby resulting in an overall decrease in internal friction. It is also important to note that there may be other mechanisms that may contribute to the recovery of internal friction.

2.2.4   Carbon content on damping

Baik *et al.* [85] and Potekhin and Potekhin [88] studied the effect of varying carbon content on the damping properties in carbon steels. Baik *et al.* [85] investigated damping in solution treated and quenched Fe-17%Mn alloy in which carbon content was varied from 0.02wt% and 0.28wt%. while Potekhin and Potekhin [88] considered damping in annealed ferritic steels having 0.002%C and 0.06% carbon. In both studies, damping was found to increase with increasing carbon content. Baik *et al.* attributed this increase to the increased pinning of austenite-martensite grain boundaries by interstitial carbon atoms while Potekhin and Potekhin attributed the increase in damping to the increased levels of iron carbide as carbon content increased.

2.2.5   Surface coating on damping

Steelpans are chrome plated, spray painted or bake painted to provide protection against corrosion. Gas nitriding which has been applied by Schärer and Rohner [93], mainly to improve surface hardness, also improves corrosion resistance. These surface layers can also be considered as surface damping treatments which will inevitably result in an increase in the system damping [78]. There are two categories of surface damping treatments. The first is referred to as unconstrained, free-layer or extensional damping and the second is known as constrained-layer or shear damping. This work mainly involves free-layer damping since the pan is mainly coated with a layer of Nickel. Since chrome-plating is commonly used on steelpans, manipulation of the system loss factor would be mainly through the manipulation of the thickness ratio.

2.2.6   Pan material: low carbon steel vs. metal alloys

Plain carbon steels are usually classified into four main groups namely [97,98]: 1) 'dead-mild' or low-carbon steels containing up to 0.15%C, 2) mild steel which usually contain between 0.10-0.30%C, 3) medium-carbon steel (0.30-0.60%C) and 4) high carbon and tool steels containing 0.60-1.5%C. This work is primarily concerned with group one since this is the material specified [70,71] for use in the manufacture of steel barrels/drums of which steelpans are predominantly crafted. Before considering the use of metal alloys, the factors which influence the formability and heat treatment of low-carbon steels will be discussed.

2.2.7   Mechanical properties and formability of low-carbon steels

- **Carbon content on formability**

It is well established that carbon content affects the mechanical properties of plain carbon steels. For instance, consider Figure 2.15a. As carbon content increases; tensile strength, yield strength and hardness increases, whereas percentage elongation, percentage reduction in area and Izod energy decreases as carbon content increases(see Figure 2.15b). The increase in strength at the expense of ductility is mainly due to the formation of carbide particles in the ferrite matrix as carbon content is increased [99]. Although having low tensile strength $\leq$ 350MPa (see Figure 2.15a), the high percentage elongation (good stretch formability) and good impact resistance of low-carbon steels indicate why this group of plain carbon steels has always been well suited for steelpan production. Practice has shown that severe springback is likely to occur for low-carbon steels with yield strengths above 240MPa, while low-carbon steel sheets, with yield strengths below 140MPa [99], are less likely to develop sufficient strength and hardness after deformation.
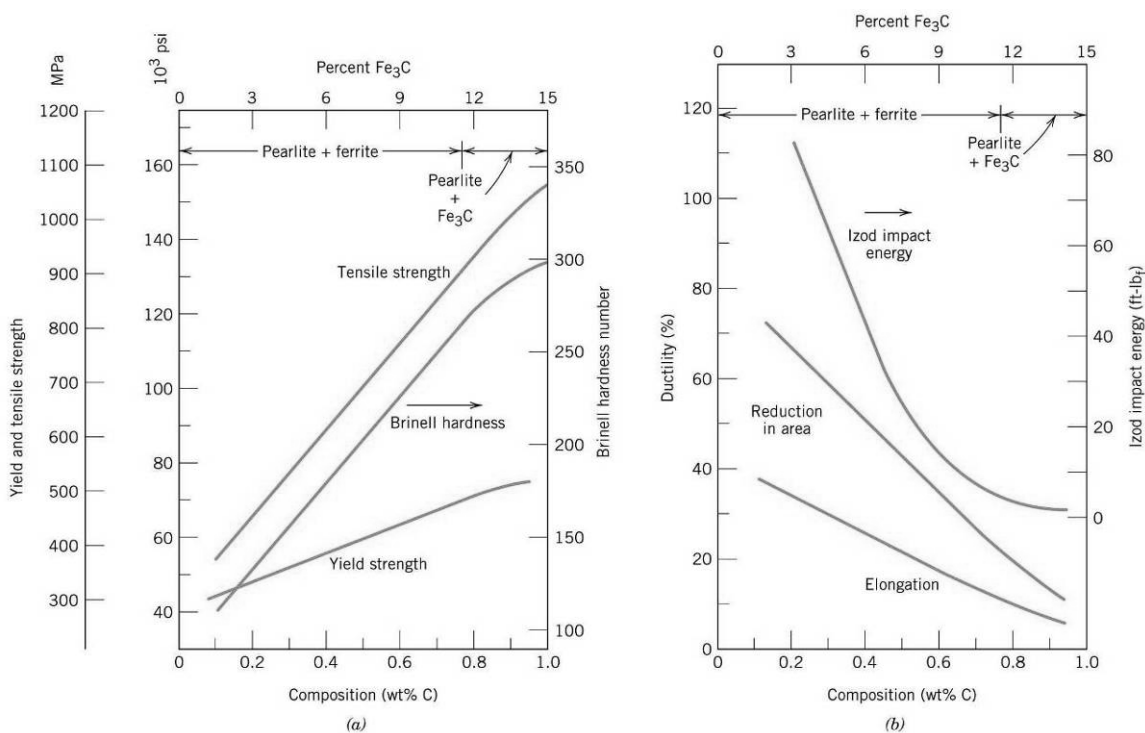
Figure 2.15: *(a)*Yield strength, tensile strength and Brinell hardness versus carbon concentration for plain carbon steels having microstructures consisting of fine pearlite. *(b)* Ductility (%EL and %RA) and Izod impact energy versus carbon concentration for plain carbon steels having microstructures consisting of fine pearlite. [100]

There are other parameters which are used as indicators of forming behaviour. These include the strain hardening exponent or work hardening coefficient '*n*', the strain rate sensitivity '*m',* the plastic strain ratio '*r*', the normal plastic anisotropy '*r$_m$*' and the planar anisotropy '*Δr*' [48]. The

strain hardening exponent or work hardening coefficient '*n*' represents the gradient of the log-log plot of true stress versus true strain for a tensile test. Good stretch formability or stretch-ability and work hardening ability is indicated by high values of *n* [101]. Although most cold formable steel grades have *n* values between 0.20 and 0.25 [99,101], the strain hardening exponent is also influenced by carbon content [102]. Figure 2.16 shows the progressive decrease and plateauing of the *n* value as carbon content is increased for steel strips which were continuously annealed.

The other parameters which are defined as follows:

$$m = \frac{\partial \ln \sigma}{\partial \ln \dot{\varepsilon}} ; \tag{2.1}$$

$$r = \frac{\varepsilon_w}{\varepsilon_t} ; \tag{2.2}$$

$$r_m = \frac{r_0 + 2r_{45} + r_{90}}{4} \tag{2.3}$$

and

$$\Delta r = \frac{r_0 + r_{90} - 2r_{45}}{2} \tag{2.4}$$

where σ and $\dot{\varepsilon}$ are the flow stress and strain rate respectively; ε_w and ε_t are the strains in the width and thickness directions respectively and r_0, r_{90} and r_{45} are the plane strain ratios measured in the directions parallel, transverse and at 45° to rolling respectively [48]. Since *r* is sensitive to crystallographic orientations, r_m is conventionally used as a measure of plastic anisotropy. The strain rate sensitivity and plastic anisotropy are also used as measures of the resistance of low-carbon steel to thinning [99,103] during forming operations .
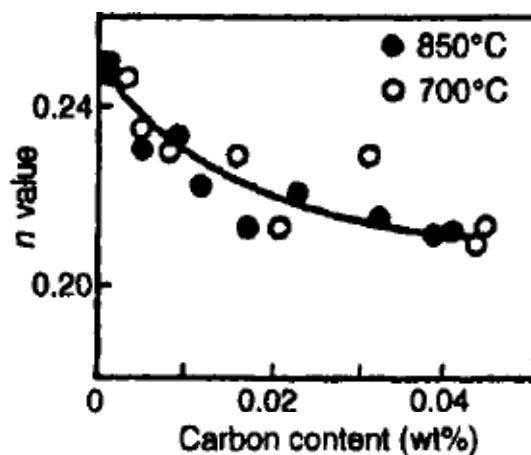
Figure 2.16: Variation of strain hardening exponent with carbon content for aluminum killed steel, continuously annealed at 700 and 850°C [102].

- **Residual elements and inclusions on formability**

Residual elements and intentionally added elements which together usually total <1% [99] in low-carbon steel also affect the formability of low-carbon steels. Most elements in large amounts will affect the formability of low-carbon steels by acting as solid solution strengtheners or obstacles to dislocation movement. This increases the material strength at the expense of its ductility. Elements such as P and S, if present in large concentrations can decrease ductility and toughness. These elements are known to embrittle steels by their segregation to grain boundaries [99,104]. This condition is avoided by usually having no more than 0.035 and 0.040% of P and S [99] respectively in low-carbon steels. Ni and Ti which are strong nitride and carbide formers reduce the levels of interstitial C and N in steel so that the yield point effect and discontinuous yielding are mitigated. Al [48,99] is also a strong nitride former and like Ti and Ni [99,101,105] , it is known to aid the development of crystallographic orientations [99] that improves resistance to thinning in low-carbon steel sheets.

Iron carbides and other non-metallic inclusions such as sulphides, silicates and nitrides affect formability [99]. These increase the strength of the material by impeding dislocation movement. The presence of large amounts of inclusions also encourages crack formation and growth, making the likelihood of failure imminent during forming operations [99].

- **Steelmaking process on formability**

The steelmaking process also influences the formability of low-carbon steels. Low-carbon steels are either rimmed or aluminium-killed. The main difference between these steels is that in Al-killed steels, Al, and sometimes small amounts of Si, are added to the ingot to suppress the out-gassing or bubbling action that is associated with non-deoxidized or rimmed steels. The effervescing action associated with rimmed steels produces an ingot that is rich in iron on the outer layer and rich in carbon and other residual elements at the core [104,105]. This surface-to-center segregation is not found in aluminium killed steels. In contrast, there is a uniform composition of elements across Al-killed ingots. Unlike rimmed steels which have a pure outer iron layer, Al-killed steels tend to have a greater degree of surface imperfections which encourage crack growth during forming [99,104] .

Besides being used as an oxidizing agent, Al is also a strong nitride former. It combines with nitrogen to form aluminium nitride thereby improving the strain ageing resistance of the sheet. Research has shown that the addition of Al also promotes the formation of crystallographic textures that allow Al-killed steels to be better suited to deep drawing in which a high-resistance to thinning is crucial [99]. Rimmed steels are found to be better applied to stretch forming operations [99]. Rimmed steels which are highly susceptible to strain ageing are usually temper rolled by straining ~

1% to suppress the yield point effect and Lüder bands (see Figure 6.29) formation during forming [106]. However, there is a latency period before the return of strain ageing in storage. Nowadays the continuous casting process is largely replacing the ingot casting process and as a consequence most low-carbon steels are aluminium-killed [104,105]. Additionally, low-carbon steel sheets are being produced with even lower concentrations of particle inclusions and residual elements through the process of vacuum degassing, in which elements such as Ni and Ti are added to suppress interstitial C and N to concentrations <0.005% [99,104,105]. The resultant sheet product is referred to as interstitial free (IF) since very low amounts of C and N are left in solid solution. Interstitial free steels are therefore highly resistant to strain ageing, and perform exceptionally in deep drawing applications.

- **Microstructure on formability**

The grain size of steel sheets will inevitably affect formability characteristics. The well known Hall-Petch equation shows the dependency of yield strength on grain size [27,48]. Small or fine grain steels are usually stronger and less formable. This is a consequence of the large number of grain boundaries encountered by dislocations during deformation.

- **Embrittlement of low-carbon steels**

There are several forms of embrittlement which occur in low-carbon steels namely: blue brittleness, quench embrittlement (quench ageing) [107] and strain-age embrittlement (strain ageing) [98,107,108]. All of these forms of embrittlement result in an increase in strength and hardness and a decrease in toughness and formability. Blue-brittleness acquires its name from the bluish colour that steels adopt when heated in the vicinity of 300°C [107]. This is not observed for Al-killed and IF steels and it is believed that blue-brittleness is due to the diffusion of interstitial atoms. Quench aging occurs when steels are heated to slightly below the lower critical temperature (A_1 or 723°C) and subsequently quenched. However, steels heated below 560°C are not susceptible to quench ageing [107].

Strain ageing generally occurs in steels that are not Al-killed or interstitial free. Strain age embrittlement refers to the return of the yield point effect after cold deformation. This can occur at room temperature after an extended period but can be accelerated by elevated temperatures i.e. on heat treatment. Strain ageing is also dependent on the degree of prior deformation and interstitial atom concentration [98,108]. Strain ageing impairs formability as it results in discontinuous yielding which is manifested by the appearance of Lüder's bands on the sheet surface during

forming. The phenomenon of strain ageing is explained by the affinity of interstitial atoms, such as C and N, for dislocations in low-carbon steels [48,108].

- **Heat treatment and hardenability of low-carbon steels**

Carbon content also affects the hardenability of plain carbon steels [27,98]. Hardenability is referred to as the ability of steel to form martensite (an extremely hard crystal structure) when quenched from its austenitic range. Plain carbon steels containing < 0.30%C [98] do not harden appreciably when heat treated. This can be illustrated with the comparison of the time-temperature-transformation or TTT diagrams for a steel having eutectoid composition (0.8%C) and a hypo-eutectoid steel (<0.8%C). TTT diagrams indicate the relationship between the rate of cooling and the structure that will be produced when austenite is cooled to any intermediate transformation temperature.
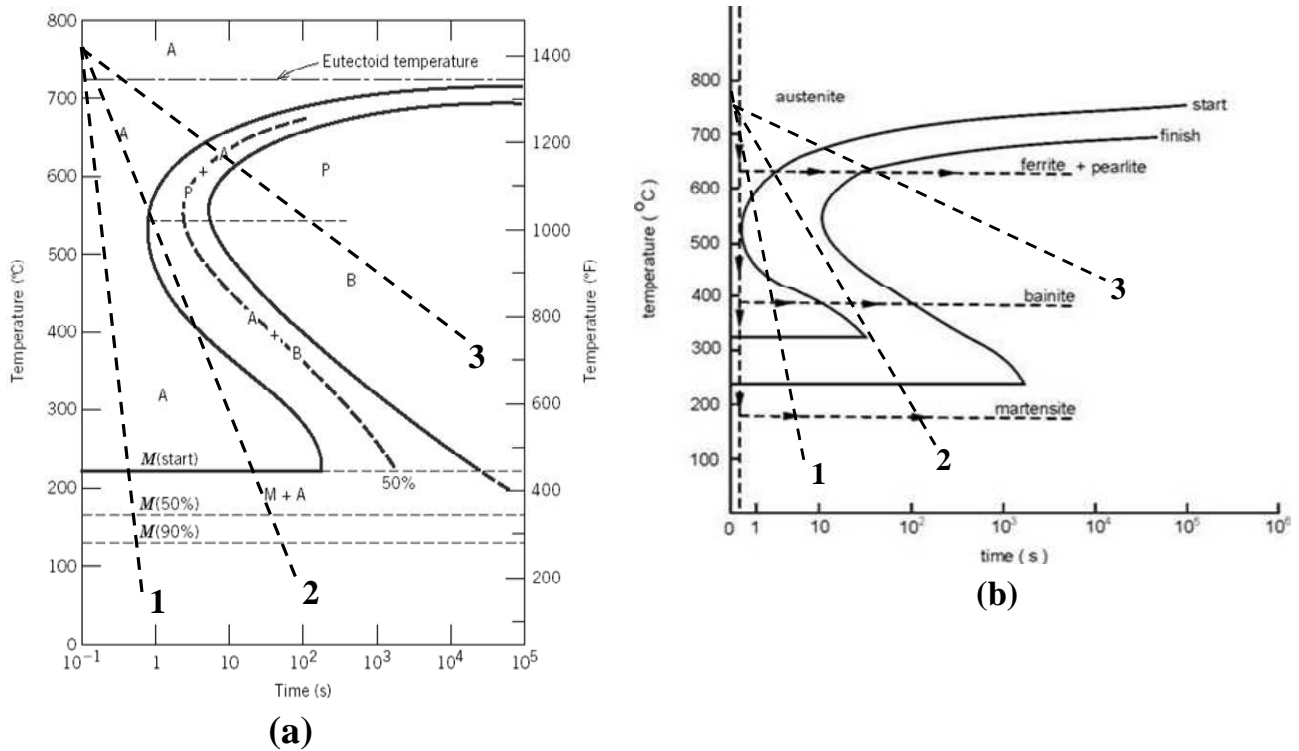
Figure 2.17: TTT curves for (a) [100] eutectoid steel (0.8%C) and (b) [109] hypoeutectoid steel (<0.8%C); Superimposed lines 1, 2 and 3 represent continuous cooling rates, where line 3-normalized or air cooling, 2-oil quenching and 1-water quenching; In (a) A represents austenite, B represents bainite, F represents ferrite, M represents martensite and P represents pearlite. Note: TTT diagrams are used herein, however it is more accurate to use continuous cooling transformation (CCT) phase diagrams in the heat treatment of steel under these circumstances.

In order to produce an entirely martensitic structure, the steel must be quenched at a rate such that the line or curve representing its cooling rate must pass clear of the *'knee or nose'* of the transformation-begin curve in the vicinity of 550°C (see Figure 2.17a and b). The line representing

the rate of water quenching (Line 1) in Figure 2.17a does not cut into the 'knee or nose' and the steel is transformed into martensite embedded in austenite [109]. Slower rates of cooling as represented by lines 2 (Oil quenching) and 3 (Air or furnace cooling) will result in final structures which will be combinations of martensite with pearlite or bainite [98]. For steels containing less or more than the eutectoid composition, the 'nose' of the TTT curve is shifted to the left (see Figure 2.17b). Therefore, the fastest rate of cooling will inevitably intercept the 'nose' of the TTT curve making it impossible to achieve a completely martensitic microstructure. The final structure will be a combination of martensite together with soft ferrite (Figure 2.17b). This is why low-carbon steels do not harden sufficiently on heat treatment. Figure 2.18 shows the effect of carbon content on hardness of plain carbon martensitic steels.
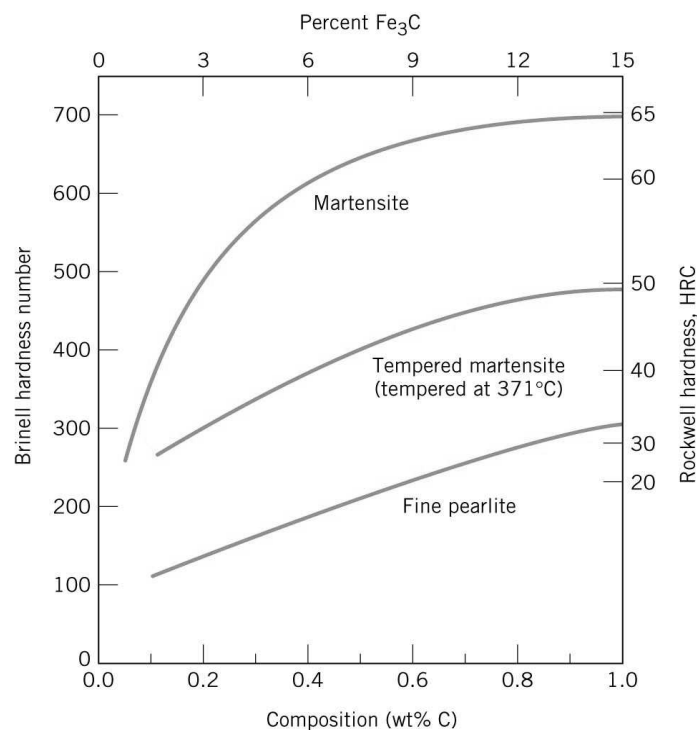
Figure 2.18: Hardness as a function of carbon concentration for plain carbon martensitic, tempered martensitic [tempered at 371°C] and pearlitic steels [100]

One way in which the hardenability of steels can be improved is by the addition of alloying elements such as manganese, chromium or molybdenum. Alloying has the effect of shifting the nose of the TTT diagram further right, therefore making it easier to attain wholly martensitic steels on water quenching [98]. However, the use of low-carbon alloy steels may be an alternative that most pan makers would be unable to afford.

The ability to form martensite in steels is also dependent on section thickness. To ensure that quenched sections of carbon steel produce a uniformly martensitic structure throughout, 'ruling

sections' or maximum section thicknesses have been specified for a wide range of steel compositions and quench treatments [98]. In any case, the section thickness of cold formed pan heads is usually in the range of 0.45 to 1.20mm, so any quenching treatment should result in a material that has the same surface and interior hardness.

- **Implications of low-carbon steel usage on pan making**

The above discussion highlights the importance of the history i.e. the steelmaking process, the effect of micro-constituents, inclusions and microstructure on the formability of low-carbon steels. However, obtaining some of this information may be difficult, particularly the steelmaking history. It becomes increasingly difficult if the steel drums used are not produced locally or if the steel drums and the steel sheets are produced in different countries.

The history of the material may help to unearth some of the problems pan makers experience, particularly during the forming of the pan head. For instance, some drums may be produced from steel sheet in which there is a high inclusion content, making them highly susceptible to fracture during forming. In addition, some drums may be produced from steels that are either Al-killed or interstitial free. Such steels are resistant to strain ageing. Since most low-carbon steels do not form sufficient martensite for hardenability, most low-carbon steels usually benefit from the ability to achieve an increase in strength through strain ageing.

A measure of control over the material history may be achieved if pan-makers (1) purchase steel sheet directly from mills or (2) order virgin steel containers/drums directly from drum manufacturers. There is currently one such arrangement in operation in Trinidad, but it is uncertain whether the history of each batch of steel sheet used for producing these drums are known since the raw material is imported. The next section will compare the use of metal alloys with low carbon steels for pan production.

2.2.8 Cold deformation effects on formability in pans: low carbon steel vs. metal alloys

Sinking/dishing which involves cold deformation is the initial step of the pan making process. Several cold forming technologies applied to pan making were discussed in the section on steelpan dish production. **Table 2.3** summarises some of these techniques as applied in various studies. The study of cold deformation with regards to steelpan production was pioneered by a research group at the University of Texas at El Paso, United States [18-20,110]. The main initiative of their study was to identify the optimum conditions that produced a pan dish that was sufficiently hard to enable effective tuning. Cold deformed samples having thickness reduction from 10% to 50% were taken from steels having carbon content ranging between 0.01 and 0.1 wt% carbon [13,106-108]. These

samples were extracted from cold-rolled sheets or taken from sunken steel drum lids. These specimens were heated at temperatures ranging from 177°C to 1000°C for times ranging from 1 to 10 minutes and were either cooled in air or quenched in water.

As expected, cold deformation resulted in an increase in hardness. This can be attributed to the work hardening of the material as dislocation density increased during the cold forming process. The El Paso group observed that drum heads with carbon contents beyond 0.06 wt% C usually failed during the dishing operation while drum heads with less than 0.02 wt% C could not achieve appropriate hardness levels for tuning even after heat treatment. The El Paso team also identified that the requisite hardness increase in the cold formed drum heads was also due in part to the phenomenon of strain ageing.

Since strain ageing was identified as the cause of embrittlement in these steels, it is possible that the sheet material was produced from steel that was susceptible to strain ageing i.e. a rimmed steel. Strain ageing may also explain why steels with carbon contents beyond 0.06%C failed during sinking, primarily due to the Lüder's band formation which comes with discontinuous yielding. Substantial strain ageing is observable in steels with carbon levels as low as 0.002 wt% C and at temperatures between 20°C and 150°C [108]. The work of the El Paso group does not state the concentrations of N present in the steels used. Although the results of the El Paso group imply that the effects of nitrogen are minor since the concentration of N is unlisted, it is well known that nitrogen levels as low as 0.001wt% can have severe effects on strain ageing [108]. Failure of pan dishes during hand sinking can also be due to poor forming technique. Failure may also be attributed to the presence of small cracks on the drum head which may be introduced during stamping of labels or due to high inclusion content.

The ability of the 0.02wt%C steel to harden sufficiently was due to its inability to produce sufficient martensite on quenching. Although, this might have been a rimmed steel, the effects of strain ageing was probably also insufficient to achieve any useful strength.

It is obvious that the sinking stage of metal alloy pans would require a different approach to the traditional manufacture of pans and this is shown in **Table 2.3** which compares the pan production stages for pans constructed from different materials. Murr *et al*. [41,64,65] and Kronman [10] pioneered the use of metal alloys for pan production while Schärer and Rohner [93] turned to gas nitriding of steel as an alternative way of achieving the requisite hardness in steelpan heads that enable effective tuning. Unlike low-carbon steels the hardness of the metal alloys used by Murr *et al*. [41,64,65] and Kronman [10] are generally controlled by plastic deformation and heat treatment for the exception of aluminum 6061 which is age hardenable.

Dishing of low-carbon steelpans is performed with relative ease owing to a strain hardening exponent which is almost half that of alpha brass, 304 and 316L stainless steels. These high strain/work hardening coefficients exhibited by *α* brass and 304 stainless steel (see Table 2.2) meant that these materials work hardened rapidly and required intermittent annealing in order to complete the dishing process.

- **Heat treatment effects on formability in pans**

The intermittent annealing of alpha-brass, stainless steel and aluminium would most likely be necessary in the formation of pan heads to be used for high frequency pans (soprano pans) which have the deepest dishes. In the case of the 304 stainless steel, annealing treatment was applied subsequent to hydroforming in order to facilitate tuning whereas for the aluminium pan head, heat treatment was applied as 6061 Al in the T6 condition is embrittled by cold working. This high strain hardening exponent of stainless steel in conjunction with high material springback also explains why Kronman [10] experienced great difficulty in dishing a stainless steel drum head.

In an effort to control the formability and hardness of the metal alloys during the sinking operation, there is the risk of over annealing i.e. heating at the annealing temperature for too long. Alpha-brass and 304 and 316L stainless steels are softened by annealing and quenching/cooling treatment. If the pan head material is over annealed, the remaining plastic deformation required to complete the sinking process may not be sufficient to achieve the hardness required to allow effective tuning of the pan surface. The 304 stainless steel pan heads produced by the El Paso group were annealed after dishing. This may be a better approach to control surface hardness before tuning provided that pan heads can be dished without any intermittent annealing. In this way completed dishes can be heated at the recommended annealing temperatures for different times to ascertain the optimum temperature/time combination that would produce the appropriate range of surface hardness for tuning. Pans may be distributed to different tuners so that a temperature/time/tuning map can be established. This approach was not taken by the El Paso group when considering the metal alloys and it is therefore suggested for further study.

Kronman [10], unlike Murr *et al*. [49] created his drum head by traditional sinking with a sledge hammer. The pan head was subsequently heated over a bonfire which clearly demonstrates that Kronman was probably unaware of the implications of heating stainless steel in this manner. Although the grade of stainless steel is not stated in this work, it may be assumed that the drum was made from an austenitic stainless steel such as 304, 316 and 316L grades. These grades are non-hardenable by heat treatment. They are usually annealed by heating to 1010°C -1120°C followed by rapid quenching. A bonfire will not attain such high temperatures, thus heating in this way would be ineffective. This may also explain the difficulty experienced by Kronman in tuning this pan.

- **Surface treatment effects on formability and hardness in pans**

Another method used to manipulate the surface hardness of pan heads is gas nitriding. This process was used by Schärer and Rohner [93] to harden the surface of deep drawn pan heads prior to tuning. Gas nitriding is a case hardening thermo-chemical process in which nitrogen is introduced into the surface of steel. The steel is kept in contact with a nitrogenous gas, usually ammonia and held at an appropriate temperature, typically in the range of 500°C to 575°C for several hours [111]. Other benefits of nitriding include improved corrosion resistance, increased wear resistance and prolonged fatigue life [111]. Very high surface hardness [111] can be achieved through gas nitriding and the yield strength of the steel is also increased as a result of strain aging due to the introduction and diffusion of interstitial nitrogen [102,108]. However the application of this process is expensive and control of surface hardness may be difficult.

2.2.9   Material influence on steelpan design

Another implication of using metal alloys for pan production is the effect of the material properties on the acoustics of the note. For instance, if a note were to be modelled as a circular clamped plate, its fundamental frequency can be expressed as [112]:

$$f_{0,0} = \frac{0.467t}{r^2}\sqrt{\frac{E}{\rho\left(1-\upsilon^2\right)}} \qquad\qquad \textbf{2.5}$$

where t is the thickness of the note metal, r is the radius of the note up to the clamping boundary, ρ is the density of the note metal, E is its Young's modulus and υ is Poisson's ratio. The above formulae can be reduced to:

$$f_{0,0} = \frac{0.467t}{r^2}c_L \qquad\qquad \textbf{2.6}$$

where c_L represents the longitudinal sound velocity which is given by the expression $\sqrt{E/\rho\left(1-\upsilon^2\right)}$. Consider Table 2.2 which compares the values of c_L for different pan materials. The values of c_L for low-carbon steel, the stainless steels and 6061 aluminium are identical which implies that the geometry note areas in pans of these materials can be comparable, provided uniform thickness. However, in the case of α-brass for which c_L is lower, note sizes may need to be approximately 20% smaller. However, this is an oversimplification as notes are generally slightly arched. Adjusting the note height by arching as discussed in the section on the vibration and acoustics of the pan is another way of manipulating the normal mode frequencies of notes. Therefore, notes in metal alloys

pans can probably be of comparable area as other geometrical parameters may be used, during tuning, to compensate for differences in material properties.

2.2.10 Drawbacks in the use of metal alloys

In spite of the attractive benefits of using metal alloys for pans, there are a number of drawbacks which will for a considerable period continue to impede their large scale application. Unlike low-carbon steel, tight-head, oil drums which usually come cheap and in some instances free, the venture of using metal alloys as an alternative material for pan production will not come cheap. The high cost of these metal alloys in comparison to low-carbon steel (see Table 2.2) is enough to deter pan builders from using metal alloys. The use of metal alloys will also require changes to the traditional forming and tuning techniques. This is also costly and will take considerable time and effort to master.

Another drawback, particularly with stainless steel, is the problem of sensitisation. This is a phenomenon which usually occurs during the solution treatment of stainless steels (Heating to 1010-1120°C and cooling rapidly). If the stainless steel is not cooled rapidly, particularly between 500°C and 850°C, there is the risk of sensitisation which refers to the precipitation of chromium carbides. This depletes the steel of chromium thereby undermining its corrosion protection capability [102,108].

Unlike the production of low-carbon steelpans where a wood fuelled or propane gas fire is sufficient for providing heat, the temperature range for the solution annealing of stainless steel will require the use of a large (big enough to contain the pan head) specialised furnace and appropriate cooling equipment to facilitate effective heat treatment and rapid cooling to prevent sensitisation. The resulting higher energy consumption and sophisticated furnace and cooling equipment equate to higher costs which again discourages pan builders from the metal alloy alternative. This is likewise for the process of nitriding which will also require the procurement of sophisticated, computer controlled batch furnaces, which are capable of controlling the process parameters to avoid nitrided surfaces from becoming oversaturated with nitrogen. Oversaturation leads to brittle patches on the surface of nitrided products. Large stocks of ammonia gas will also be required.

2.2.11 Summary

Although a review of the use of metal alloys as alternative materials for pan production was made, the material of choice continues to be low-carbon steel. Although its poor corrosion properties and heavy weight are significant disadvantages to its usage, its low cost, high availability, ease of forming and ease of recycling, continue to see low-carbon steel as the de-facto material for pan

making. Although alpha-brass, stainless steel and Al offer attractive benefits, pan makers would remain hesitant to change as the current production and tuning techniques have also evolved around the several decades of using of low-carbon steel.

In spite there being no single study that considers the effects of the manufacturing regime on the material damping properties in pans, the relevant studies consulted were able to provide a forecast of what is expected in practice. It is expected that material damping would increase on cold deformation, followed by a decrease on heat treatment and another increase which accompanies surface coating. This work will investigate these claims with the use of a low-carbon steel that is specified for the manufacture of tight-head oil drums.

2.3 Acoustics and Vibrations in Steelpans

2.3.1 Steelpan Note Models

The steelpan like the timpani or kettledrum [113], Indian drums (thabla and mrdanga) [114-116], orchestral crotales [117], xylophone [118-123], marimba [120,121,123-125], Western church bells [126-130] and the hang [131,132] is a pitched percussion instrument in which there are two distinctive features. Firstly, the first mode in each steelpan note is tuned to have a dominant fundamental tone and secondly, some of the natural frequencies of the higher modes are coaxed or tuned into a harmonic relationship with the fundamental. For instance in a soprano pan the first two or three modes of each outer note are tuned into a harmonic relationship while only one or two modes are tuned in the middle and inner notes. This has been clearly demonstrated by the numerous mode studies conducted on steelpans [15,123,133-143] with two of the earliest mode studies by Dennis [144] and Barlow *et al.* [143] using Chladni analysis and holographic interferometry respectively.

However, several researchers have moved a step further by attempting to develop models that characterize the modal tuning of steelpan notes and the approach followed by researchers in this regard can be divided into two categories. The first looks at the use of structural geometry manipulation to achieve modal tuning while the other looks at boundary conditioning as a technique for mode tuning in steelpans. Before considering previous proposed models, a brief consideration of basic vibrations of plates and shells may provide some insight into mode tuning of pans. Some steelpan notes resemble rectangular or elliptical plates while others resemble circular plates. If a note were to be modelled as a clamped circular plate and using equation 2.5 the fundamental frequency could be expressed as [145]:

$$f_{0,0} = A\left(\frac{t}{r^2}\right) = \pi A\left(\frac{t}{S}\right)$$

2.7

where t is the note thickness, r is the note radius up to the clamping boundary, ρ is the density of the material, v is the Poisson's ratio, and $A = 0.47(E/\rho(1-v^2))^{1/2}$ (a constant for an isotropic material). The equation above can be further manipulated such that $S = \pi At/f$. This shows that the fundamental frequency can be altered by manipulating the note area, S. However, the other partials do not naturally assume a harmonic relationship and adjustment of other parameters are needed to achieve modal tuning. In the case of the rectangular and elliptical plate, another parameter or '*degree of freedom*' becomes available for the manipulation of mode frequencies. If the note is modelled as a clamped elliptical plate the fundamental frequency is given by [112]:

$$f \approx \left(\frac{Bt}{a^2}\right)\sqrt{1 + \frac{2}{3}\left(\frac{a}{b}\right)^2 + \left(\frac{a}{b}\right)^4}$$

2.8

where, $B = 0.291(E/\rho(1-v^2))^{1/2}$, t is the thickness and a/b is the aspect ratio of the ellipse, where a and b are the major and minor axes lengths of the ellipse. For a fixed area, the modes of the plate could be altered by manipulation of the aspect ratio. Another degree of freedom that is available to the tuner to enable the coaxing of the mode frequencies into an approximate harmonic relationship is that of arching. According to Soedel [146], the natural frequencies of any cap shell can be computed by:

$$f_{shell} = f_{plate} + \frac{E}{\rho(2\pi R)^2}$$

2.9

where R is the radius of curvature. Soedel has demonstrated that this formula applies to spherical caps of any shape of boundary and not only to circular shapes. Therefore, the area of the note could be used to allow the tuner to approximate the fundamental mode frequency of the plate to a frequency on the musical scale while the aspect ratio and arching are used to achieve mode tuning between the first and second mode frequencies.

- **Mode tuning by structural geometry manipulation**

Prominent to the effort of modelling the vibration behaviour of pans are the primarily analytical works of Achong [147-153] which models the steelpan as a system of interacting and non-interacting mode-localised vibrators through the use of complex mathematical expressions that

describe their vibration behaviour. In Achong [151] the steelpan note is modelled as a spherical cap shell in which the effects of compressive and thermal stresses (introduced during the deformation and heat treatment stages), material and geometrical properties are considered. Ferreyra *et al.* [20] recommended that the model given by Achong [151] be revised to account for the effects of metallurgical alterations produced during severe deformation and annealing.

Rossing *et al.* [15]; Rossing and Hansen [138]; and Dennis [144] used either analytical or a combination of analytical and experimental approaches towards modelling steelpan notes. Rossing *et al.* [15] in an effort to determine if there is a single surface topography for which the normal mode frequencies of a steelpan note fall into a harmonic relationship modelled steelpan notes as shallow rectangular shells and used physical measurements taken from steel drums to execute a computer program of their model. They discovered that there was no single surface topography that satisfied a harmonic relationship among the first few modes. Rossing and Hansen [138] examined the relationship between the longest dimension '*L*' of notes and their fundamental frequency '*f*' and took measurements from various pans ranging from tenor to bass. They concluded that the relationship between the longest dimension and the fundamental frequency can be represented by a scaling law: $L=Kf^{3/2}$ where K is a constant. The constant K may depend on the specific conditions of the pans measured and is not necessarily representative of all pans. Dennis [144] simply compared the measured fundamental frequencies of tenor pan notes to the theoretical fundamental frequencies of simply supported and clamped rectangular and circular plates.

The relationship provided by Rossing and Hansen [138] implies that each frequency on steelpans is associated with a particular length. However, a consideration of basic plate and shell vibration indicates that mode tuning cannot be achieved through manipulation of a single geometrical parameter. Although the material properties of the steelpans used by Rossing and Hansen [138] may not have varied, the scaling law would have fallen apart when considering pans made from different metals. The modal frequencies of plates and shells are also dependent on the speed of sound which is a function of the material's physical properties [123,145,154,155]. The discrepancy between measured and calculated frequencies in the Dennis [144] investigation may be attributed to two reasons: Firstly, steelpan notes are slightly arched and boundary conditions may not be entirely simply supported or clamped.

Gay [156] and Bridge [14] have applied the finite element method to examine the vibration behaviour of bass and tenor pans respectively. Gay examined the effects of skirt lengths and rolling

hoops[2] on the frequencies and mode shapes of tenor bass pans while Bridge focused on the effect of geometrical parameters (aspect ratio, thickness and arching) on the modal frequencies of tenor pan notes modelled as elliptical shells. Gay discovered that the skirt vibrations overlapped with the musical range of the notes on the bass pan head and this was generally responsible for skirt-note mode coupling. Gay also found the degree of skirt-note coupling was dependent on the skirt length and hoop location. The findings of this could be useful in pan design particularly in determining the optimum skirt length for each pan type. However, the skirt-note mode coupling may also be affected by the stiffness of the connection between the skirt and the pan dish. The findings of Bridge [14] agreed closely with basic plate and shell theory and her findings showed that the first two modes of elliptically shaped notes could be tuned into a harmonic relationship by manipulation of the aspect ratio and arching.

This harmonic tuning between the first two modes of pan notes is shown in Figure 2.19a. The higher modes are not integer multiples of the fundamental but are sometimes multiples of consonant frequency intervals. For instance, the 3rd and 4th mode frequencies of the D_5 note in Figure 2.19a are approximately multiples of a major third i.e. 2(5/4) and 3(5/4) respectively. In this regard, mode tuning could also mean the tuning of mode frequencies to have frequency ratios that are multiples of consonant musical intervals. In the models discussed, constant thickness throughout the note and symmetry of the note are assumed whereas pan dishes are predominantly formed by stretching and notes are not symmetrical. Departure from symmetry might be another degree of freedom that is used to achieve mode tuning. Barlow *et al.* [143] recommended that finite elements be used to determine how the first few modes are affected by manipulating the shape of the note in a selected small region. The effect of both departure from symmetry and varying thickness in the notes may add further insight into mode tuning in pans.

- **Mode tuning by boundary conditioning**

In order to investigate the effects of boundary conditions on the modal tuning of steelpans Muthukumaran *et al.* [16] developed an analytical model to investigate boundary conditioning as a technique for structural tuning in rectangular plates. They were able to demonstrate that the natural frequencies of the plate can be altered by manipulation of rotational and translational stiffness coefficients at the boundaries. However, Muthukumaran and his team also recognised that structural tuning of modes by boundary conditioning was by itself insufficient to achieve overtone tuning in steelpans and that other parameters such as the material properties and structural geometry are necessary in order to better describe the vibration behaviour of the steelpan.

---

[2] Rolling hoops are created on oil drums/barrels to provide improved stiffness. Most barrels contain two or three hoops along their sides.

It is useful to mention that Dennis [144] observed that the vibration in steelpan notes were mainly confined to the slightly raised portions and attributed this confinement to manipulation of the edge condition during tuning. This observation was proven true by the holographic images of modes obtained from the works of Barlow *et al.* [143]; Rossing and Hansen [139] and Rossing *et al.* [140]. Figure 2.19b illustrates mode confinement in a soprano pan. Note that the vibrational motion of the note is confined or localised to its designated region.
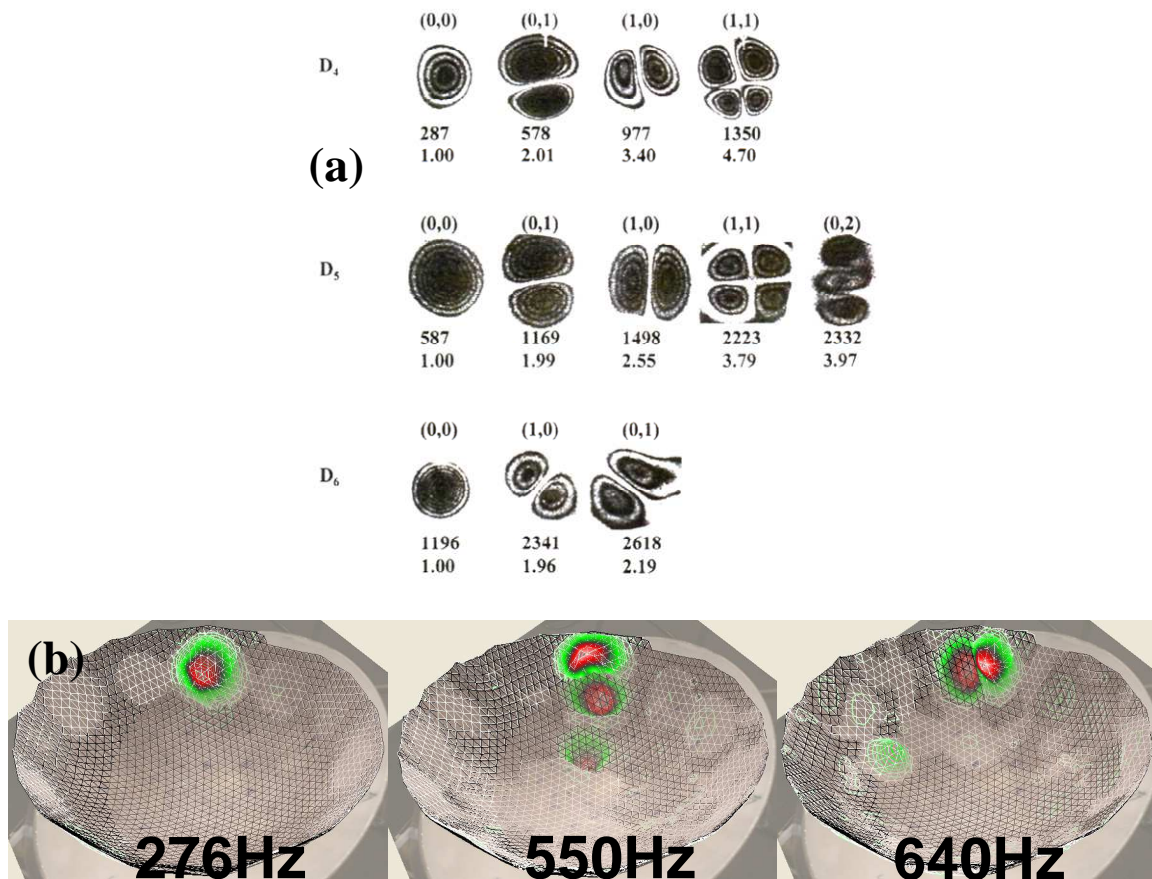
Figure 2.19: (a) Holographic interferograms of several modes in the D4, D5 and D6 note areas of a soprano pan [140]; **(b)** First three modes for C4# in a tenor pan. Note mode confinement to individual region

A similar phenomenon is seen in an instrument known as the musical saw. Mode confinement or localisation may be explained by an analogy with the musical saw pictured in Figure 2.20a. The musical saw resembles a typical carpenter's saw or a made-for-music saw which is usually longer and without teeth and no handle. The player sits, clutching the handle of the broad part of the saw between his legs and holds the far end with one hand (see Figure 2.20a). The blade is flexed into a shallow S-shaped curve and played by bowing or tapping the edge of the blade.

A study of the musical saw by Scott and Woodhouse [157] was particularly concerned with the mechanism of the confinement and the nature of the confined mode or modes of vibration in the musical saw. Their analysis considered two scenarios in a one-dimensional, rectangular strip of uniform thickness. The first objective was to look at the vibration-transmission properties of the strip with constant curvature, which they modeled as the section of a cylindrical shell, and the second objective was to investigate the effect of slowly varying curvature on the confinement phenomenon. Their findings revealed that: 1) it is possible to confine modes to the vicinity of the inflection by a process of total internal reflection from points of critical curvature; 2) these confined modes are unaffected by the boundary conditions at the end of the strip which meant that damping would be governed solely by internal dissipation in the material and radiation damping; 3) increasing curvature leads to the confinement of higher modes.
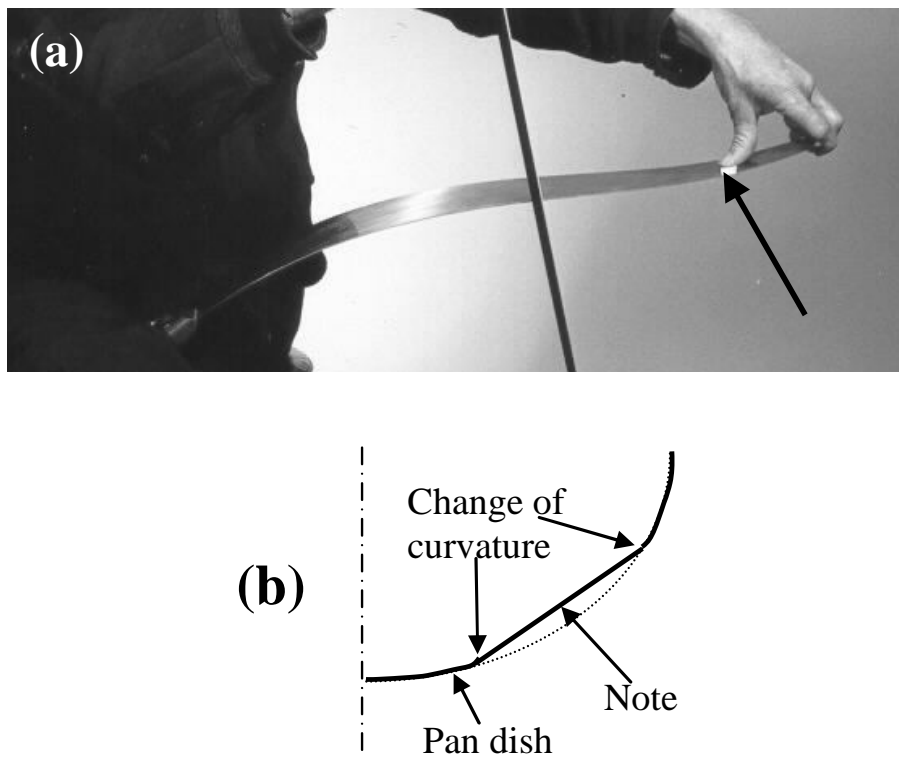
Figure 2.20: (a) The Musical Saw: A standard playing position with an arrow indicating the bowing point at which there is zero curvature as the curve reverses direction [158] and **(b)** Typical profile of pan note showing curvature change at note boundary

Examination of the cross-sectional profiles of steelpan notes bears resemblance to that of the musical saw (see Figure 2.20b). Although boundary conditioning alone may be insufficient to achieve mode tuning it may give some insight into why some tuners claim to be able to tune more than the average number of modes [17] while some usually tune no more than three in the outer

notes or two in the inner notes of tenor pans. Part of this work will look at mode confinement in steelpans in an effort to explain why some tuners are able to tune more than the average number of modes.

Chapter 3   Production studies: Forming of mini-pan dishes

3.1 Introduction

This chapter presents the findings of the application of single point incremental sheet forming (ISF) to the production of miniature pans. The production of mini-pans was pursued for four reasons: Firstly, to demonstrate by means of a pilot study, the feasibility of applying ISF to steelpan dish forming; secondly, the current forming methods are either very expensive or pose several health hazards to the limited pool of pan makers and thirdly because the ISF machine at the CUED is designed to form sheet metal with a maximum dimension of 360mm x 360mm[3]. Fourthly: with several annual carnivals [159] worldwide featuring the steelpan in locations such as Trinidad and Tobago, Brazil, London, Miami, New York and Toronto Caribana, the use of ISF for the creation of mini-pans presents a strong entrepreneurial opportunity. A section of this chapter is therefore dedicated to a break-even analysis of the application of ISF to mini-pan production, to determine the profitability. This pilot study also provides an economic basis for applying incremental sheet forming to the production of full size steelpans.

In the work ISF was identified as an attractive novel technology for the production of steelpan dishes when compared to other sheet metal forming technologies that are currently used for steelpan dishing. The major benefits of using ISF for steelpan dishing were identified in Chapter 2.

While the slow speed [51] of the ISF process is highlighted as a drawback, this is offset by the fact that steelpans are a low volume product. The focus of this work was primarily on the areas in which ISF could be better adapted to steelpan dishing and included:

1. Geometrical deviation obtained between the desired product and the manufactured product as a consequence of material springback. This problem was addressed with the incorporation of a backing plate in the forming set-up. The use of a backing plate was identified as a means of controlling geometrical deviations in incremental sheet formed products [52,60].

2. A thickness distribution in which a small region of the material is stretched and other regions remain at almost the original thickness of the blank [55]. This

---

[3] Full size pans are typically 570mm and above in diameter

inhomogeneous thickness distribution was found to particularly occur in ISF products which were formed using a single tool pass [55]. Multiple pass forming [55,160,161] method was identified as a possible way of improving the thickness distribution in the walls of ISF products. The thickness distribution in traditionally formed steelpan dishes is one in which the material is stretched and reduces in thickness from the rim to the base. In a typical soprano pan dish, there is a thickness reduction which varies from 10% near the rim to 50% [19] at the base of the dish. Although there is no evidence to support whether or not such a reduction in thickness is better suited for tuning, steel pan tuning appears to be conducive to drums which are stretched from the rim to the base.

Another initiative that was considered in this work is as follows:

3. The use of ISF for the production of dishes from 304 austenitic grade stainless steel sheet. The high work hardening characteristic of stainless steel makes it very difficult to form by using conventional sheet forming methods. Hence, this work took advantage of the local-forming [56] characteristics of ISF in the forming of stainless steel.

This chapter begins by outlining the mini-pan production process followed by the introduction of incremental sheet forming and its usage in the mini-pan production process. The findings of the use of ISF for mini-pan dish production is presented for the following investigations: (1) production of mild steel mini-pan dishes with and without a backing plate; (2) production of mini-pans using 304 stainless steel sheet; (3) comparison of thickness distribution in dishes formed conventionally with ISF and by wheeling (see Chapter 2); (4) multi-pass [55,160,161] forming for thickness distribution improvement in the dish wall and (5) a break even analysis on the potential profitability of applying ISF to mini-pan and full size pan production.

3.2 Mini-pans: An overview of the production process

Figure 3.1 and Figure 3.2 gives an overview of the stages involved in the mini-pan production process. This process is identical to the traditional manufacturing of steelpans but in this case the only difference is that ISF was used to form mini-pan dishes.

Mini-pan Production Process

Sheet Forming

1.   Extract blank for mini-pan
2.   Extract strip for mini-pan side
3.   Forming of mini-pan using ISF
4.   Water jet cutting of mini-pan dish from blank
5.   Rolling of strip for mini-pan side

Joining

Join mini-pan dish to skirt
using TIG welding

Heat treatment

Annealing of mini-pan dish

Pre-Tuning

Surface coating

Fine-Tuning
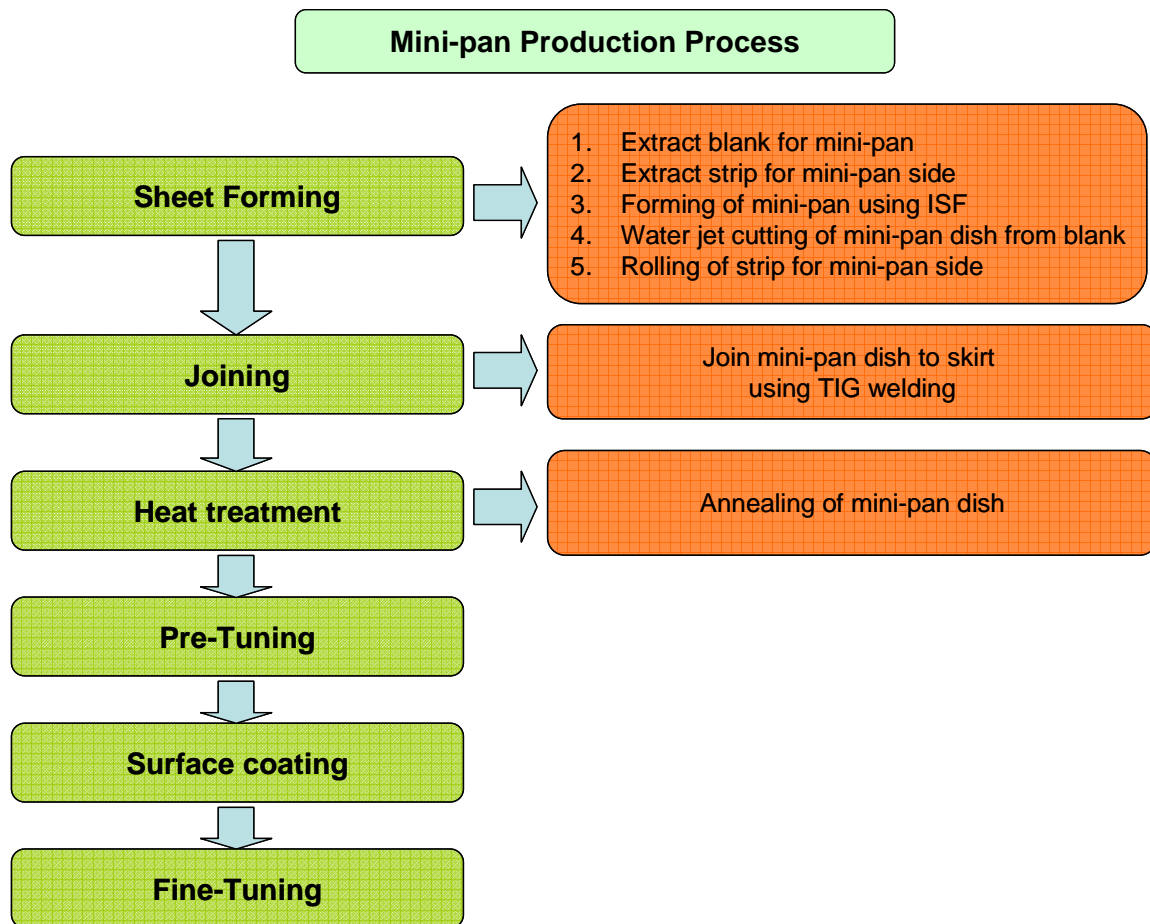
Figure 3.1: Overview of mini-pan production process with ISF used for dishing

The production of a mini-pan began by cutting the blank to the required size (360mm x 360mm) with the use of a guillotine. The sheet was subsequently clamped securely in the ISF machine and lubricated with bearing grease (Figure 3.2b) before forming. There was a tendency of the sheet to bulge upwards after clamping in the frame of the machine. In addition to material springback, this bulging may contribute to deviations from the desired geometry. To eliminate this effect, clamping bolts were fastened by moving from bolt to bolt and tightening each by a small amount until all the bolts were tightened sufficiently to secure the sheet firmly.

Upon removal from the machine, the dish was cleaned before being extracted from the blank using a water-jet cutting machine. The extracted dish was then TIG (Tungsten Inert Gas) welded to a rolled strip which formed the skirt or side (Figure 3.2g). The surface of the mini-pan dish was then annealed with an oxy-acetylene flame (Figure 3.2h) to provide some stress-relief before being tuned. The mini-pans created in this work were not coated.
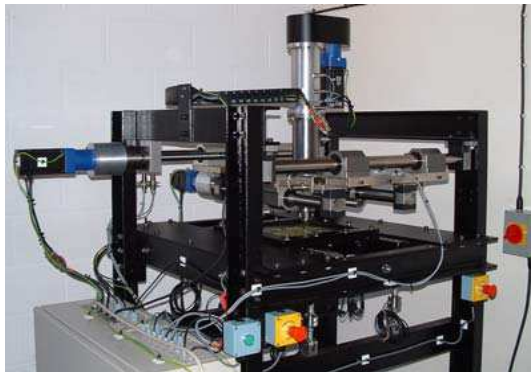
(a) ISF machine at CUED [54]

(b) Lubricated sheet-blank clamped in ISF machine

(c) Mini-pan dish being formed

(d) Mini-pan dish with flange

(e) Extracted mini-pan dish

(f) Rolled strip for mini-pan side

(g) Joining of mini-pan dish to side

(h) Annealing of mini-pan dish surface

Figure 3.2: Mini-pan production process

The sequence of the mini-pan production steps shown in Figure 3.2 may vary depending on the material being used to form the mini-pan dish. This will become more apparent later on when the use of 304 stainless steel sheet was considered. Although complete mini-pans were produced in this work, the emphasis herein was placed on the forming of the mini-pan dish.

3.3 Incremental sheet forming: The process

Incremental sheet forming was used to produce mini-pan dishes and other structures that were used in other sections of this dissertation. The tool path used to create the minipan dishes in this work was adapted from a tool path written by Dr. Kathryn Jackson. The tool path was written to allow forming to occur in one direction using incremental steps. Forming began with the tool moving downwards and making contact with the sheet in the *x-y* plane. The tool then moved to complete an entire circular contour in 8 segments. On the completion of each segment the tool stopped and moved downwards. Subsequent contours were formed in the same manner with the tool completing successive contours in 8 segments and so on.

Figure 3.2a shows the CUED custom built ISF machine used in this work. A highly polished spherical tool of radius 7.5mm was used to construct all the structures used in these investigations. The design of the CUED ISF machine requires the material to be cut into sheets of dimensions 360mm x 360mm or 150mm x 150mm. In this work the larger size sheet was used.

The sheet to be formed was held in place by clamping between a pair of blank holders. On clamping the effective forming area of the sheet is reduced to 300mm x 300mm. All structures were produced from sheet that was less than 1mm thick. Although further research is being conducted to increase the initial wall angle of incremental sheet formed products, ISF on the machine in Figure 3.2a is currently limited to forming conic shapes with a maximum wall angle of 67.5° [26]. For the dishes formed, the radius of the vertical circle R_v was manipulated by varying the initial wall angle α (Figure 3.3). The relationship between the vertical radius, the initial horizontal diameter of the bowl, *D* and the wall angle is given by the equation:

$$R_v = \frac{(D/2)}{\sin \alpha} \qquad\qquad\qquad \textbf{3.1}$$

Using the geometry in Figure 3.3 the bowl depth *h* can be written as:

$$h = R_v(1 - \cos \alpha) \qquad\qquad\qquad \textbf{3.2}$$
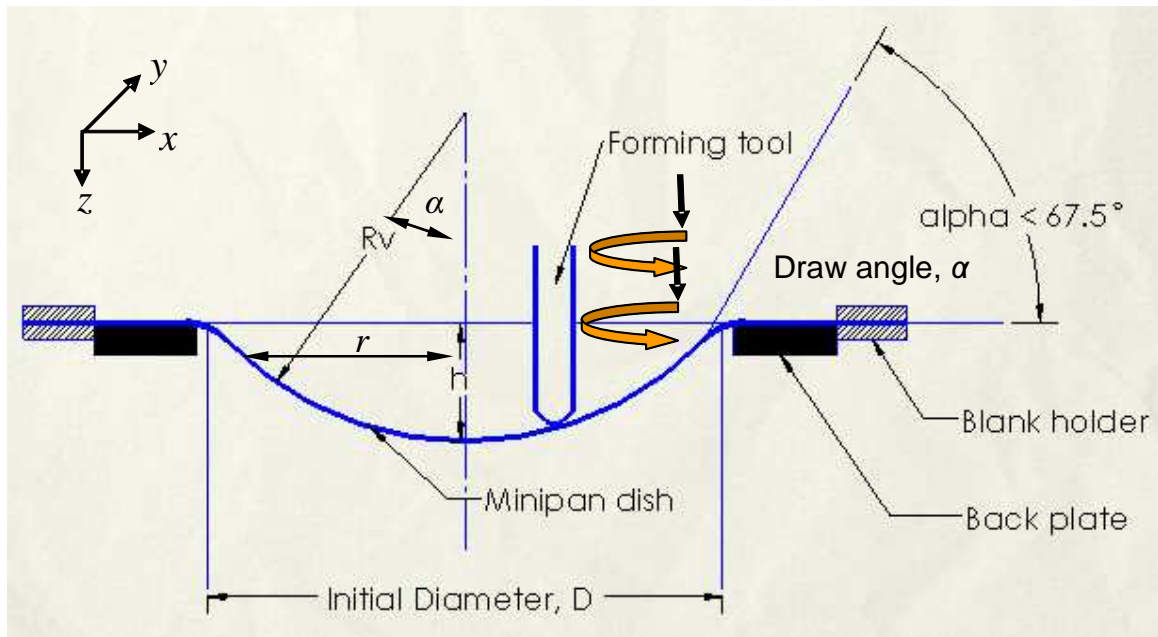
Figure 3.3: ISF of mini-pan: initial wall angle (alpha) is limited to 67.5°

Using equations 3.1 and 3.2, the relationship between the initial diameter *D*, and the bowl depth *h* is given by:

$$h = \frac{D(1 - \cos\alpha)}{2\sin\alpha}$$

3.3

Since, one of the interests of this work is in extending ISF to the production of full size pans it would be useful to produce a chart which displays the relationship between the bowl geometry parameters. From the relationship above the draw angle *α* could be expressed as:

$$\alpha = \arccos\left[\frac{D^2 - 4h^2}{D^2 + 4h^2}\right]$$

3.4

This relationship can be used to calculate the required draw angle to produce drums with a desired diameter and depth. It could also be used to display the limitations of the machine and the ISF process. Figure 3.4 shows a chart that can be used to guide the incremental sheet forming of full size steelpan dishes.
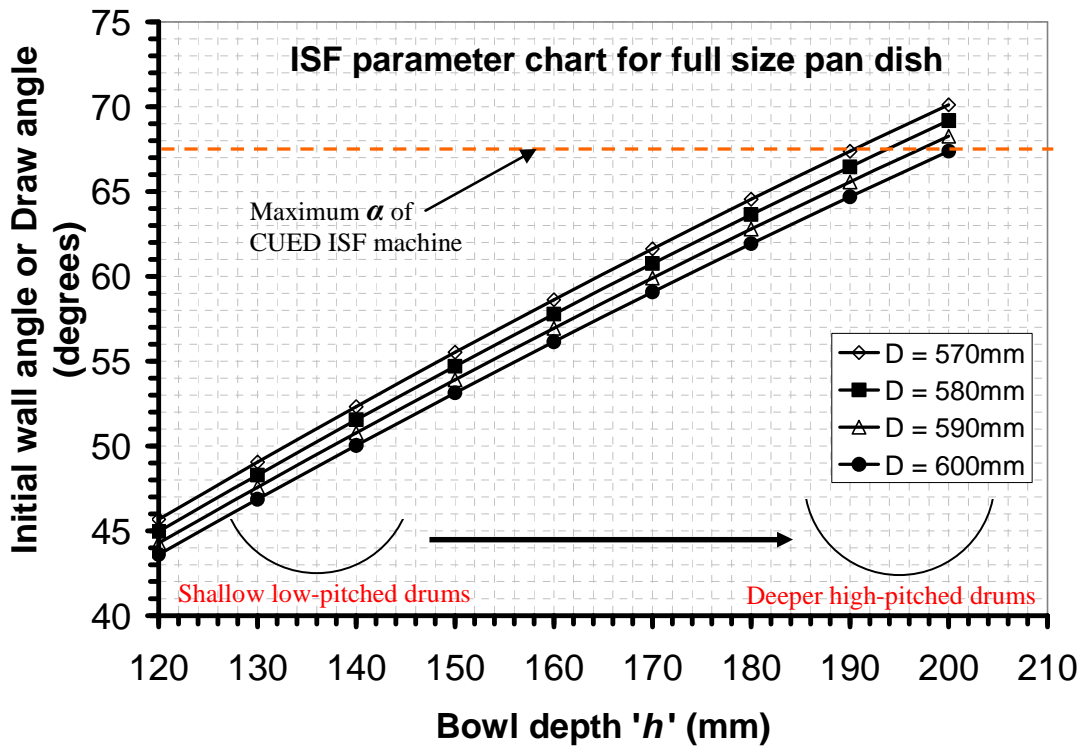
Figure 3.4: ISF design chart for full size pan dishes

3.4 Mini-pan dish production with mild steel sheet

A pair of dishes was created to investigate the effect of forming with and without the incorporation of a back-plate into the forming rig. These dishes were produced from 0.86mm mild steel plate of grade BS 1449-1.8:1991. The initial diameter of all the dishes formed was 244mm. The forming tool feed rates on the *x, y* axes were set to 40mm/s and a *z* axis acceleration of 20mm/s^2 as tool moves between contours. A dish was formed in 37 minutes. The dishes had initial wall angles of 50° and were formed in a single pass. One bowl in the pair was formed with the backing plate incorporated on the underside of the sheet (Figure 3.3) while the other was formed without the use of the backing plate. The backing plate was designed to make allowance for the tool radius of 7.5mm, hence the diameter of 260mm (Figure 3.5). The average profile of each dish was measured using an OMICRON CMM (Coordinate Measuring Machine). Three profiles were measured for each dish and an average taken. With the center of the bowl set as the origin, a profile was taken to be a measurement from the center of the dish to the rim. Two profiles were measured along the positive and negative *x* axes and one along the positive *y* axis (taking the axes to be parallel to the plane of the page).
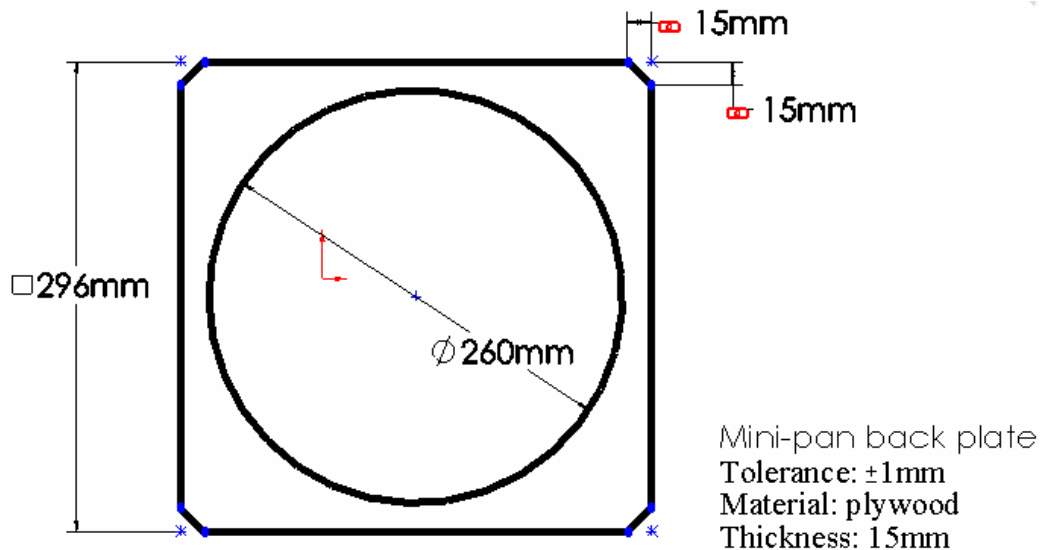
Figure 3.5: Backing-plate

3.5 Mini-pan production with 304 stainless steel sheet

One pair of mini-pan dishes was produced from 304 stainless steel sheet. One dish was formed with the backing plate incorporated on the underside of the sheet and the other was formed without a backing plate. Initially 0.90mm sheet was used and forming was found to be difficult. During the forming of the dish, without the backing plate, the machine began to vibrate excessively. This excessive vibration resulted in tool slippage on the sheet surface which resulted in a shape that deviated significantly from the programmed shape. In order to complete the forming of this dish and to reduce the unwanted vibrations, the forming tool feed rates on each axis were reduced to quarter (i.e. x and y axis feed rates = 10mm/s; z axis acceleration rate = 5mm/s^2) of those used in the forming of the mild steel mini-pan dishes. This resulted in a fourfold increase (148 minutes) in production time. This dish was not used in this work. The subsequent pair of stainless steel mini-pan dishes was formed from 0.70mm thick 304 stainless steel sheet with initial wall angles of 50°. When forming the 0.70mm stainless steel dishes the spindle speeds were set to half of those used for the forming of the mild steel dishes (i.e. x and y axis feed rates = 20mm/s; z axis acceleration = 10mm/s^2). This resulted in a two fold (74 minutes) increase in the production time. The dishes were produced using the same backing plate used for the production of the mild steel dishes in the previous section and the profile of each stainless steel dish was also measured in the same manner. These dishes were also created by forming with a single tool pass.

3.6 Mini-pan dish production on the English Wheel

The English wheel was used to produce a mini-pan dish from 0.86mm thick mild steel sheet of dimensions 360mm x 360mm. This dish was formed by the repeated passing of the sheet between

different pairs of wheels on the English wheel. Figure 3.6 illustrates the manner in which the material is moved between the rollers to achieve dishing. One wheel in the pair of rollers (i.e. the lower or anvil wheel) on the English wheel is changeable (see Figure 3.6). The forming of the dish began by using the anvil wheel with the 'lowest crown' and as the sheet was progressively formed into a dish, the anvil wheels where changed in order of increasing crown height. This increased the depth of the dish being formed. As the material became thinner, contact pressure between the rollers and the sheet was maintained by making adjustments to the screw jack. The dish formed on the English wheel was cut in half so that the thickness variation in its wall could be compared to the wall thickness variation in a (1) conventionally made (i.e. hand sunk) Aubrapan and (2) incremental sheet formed mild steel and stainless steel bowls formed without a backing-plate. The Aubrapan and the ISF bowls were also cut into halves and wall thickness was measured using a ball-end metric micrometer (Figure 3.11).

(a) Top view   **(b)** Side view
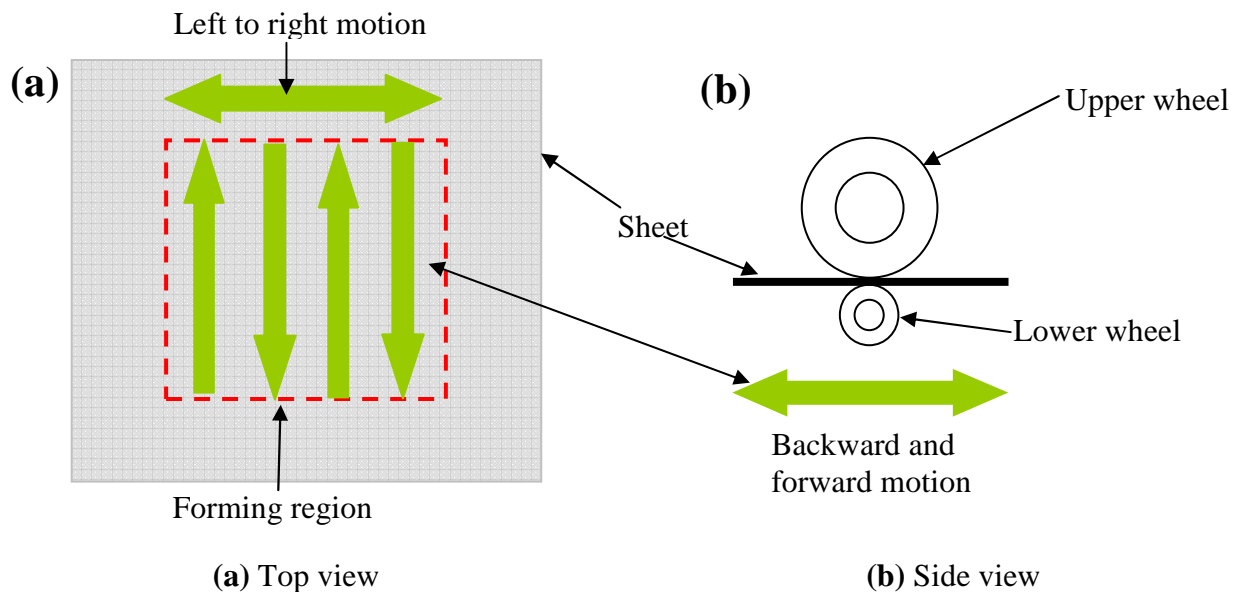
Figure 3.6: Dishing with the English wheel: Forming begins with the rollers situated in the middle of the sheet. The dish is formed by pushing the sheet forwards and backwards between the rollers while simultaneously moving the sheet from side to side. The rollers are kept inside the forming area which is highlighted with the dashed lines. After a number of side to side movements the sheet is rotated through 90° and forming continues in the same manner.
.

3.7 Mini-pan dish production: Multi-pass forming for improvement of thickness distribution in dish wall

Multiple-pass forming [55] was identified as a solution to obtaining a more uniform thickness distribution in the dish wall of minipans. Multi-pass forming is incremental sheet forming where products are formed using multiple tool passes (see Figure 3.7). Two dishes were manufactured using multi-pass forming. The first was formed using a double pass method in which the first shape was an intermediate dish with an initial wall angle of 25° and the final shape was a dish with an

initial angle of 50°. The second dish was formed in three passes with intermediate bowls having initial wall angles of 20° and 35°, followed by the final dish which had an initial wall angle of 50° (see Figure 3.7). These bowls were also formed using 360mm x 360mm x 0.86mm mild steel sheet with x and y axis forming tool feed rates = 40mm/s and a z axis acceleration = 20mm/s^2. These bowls took 74 and 111 minutes to produce respectively and were made without the use of a backing plate. These dishes were subsequently cut into halves and the wall thicknesses measured.
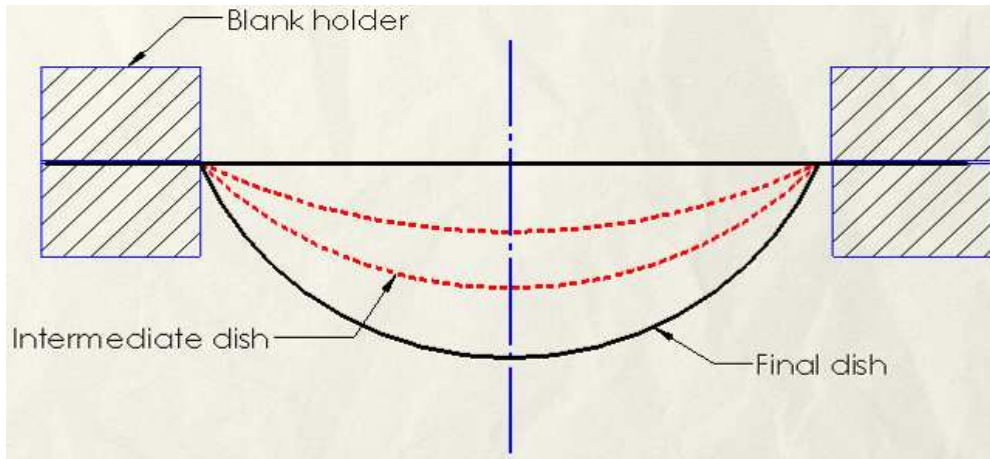
Figure 3.7: Illustration of multi-pass forming using a triple pass method in ISF

3.8 Results

3.8.1   Mild steel mini-pan dish production with and without back-plate

Figure 3.8a shows the profiles of mild steel mini-pan bowls formed with and without a backing plate. It was expected that a set-up that did not include a backing plate would generate dishes that are less deep than dishes formed with the use of a backing plate. Figure 3.8b shows good agreement between the ideal or desired geometry and actual geometry of both dishes. Less than 1.0mm and 1.5mm deviations were observed throughout the bowl with backing plate and dish without back plate respectively. Larger deviations in geometry were observed for both dishes beyond 110mm, closer to the rim, where deviations between 2mm and 6mm were observed (Figure 3.8b).

(a)

(b)

Dimple or Pillow
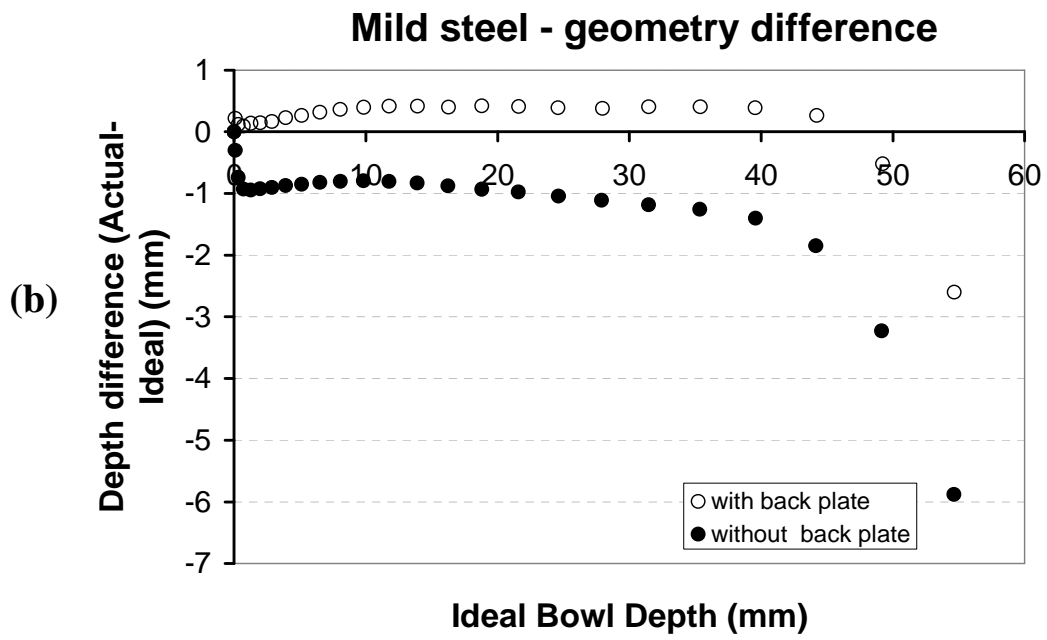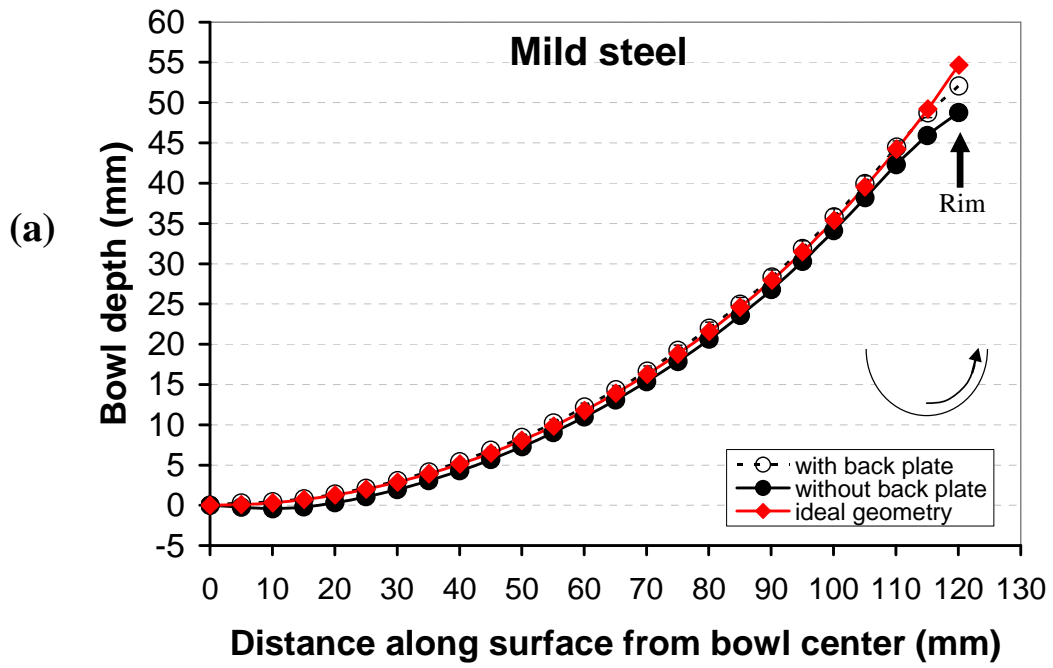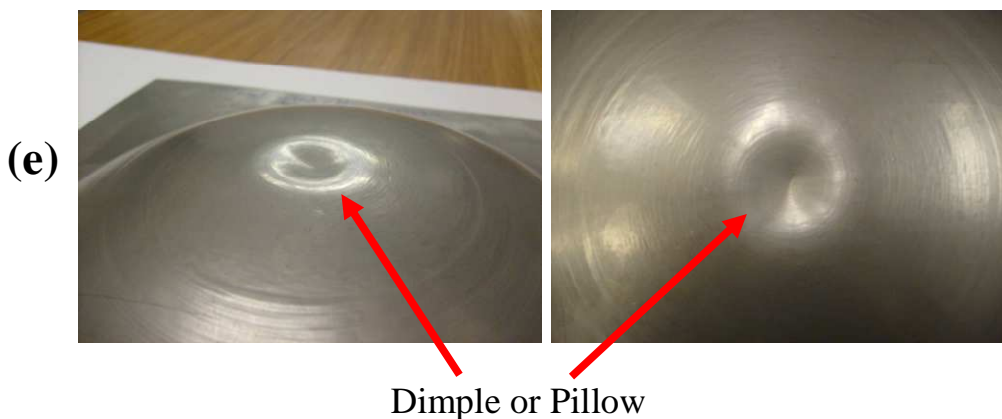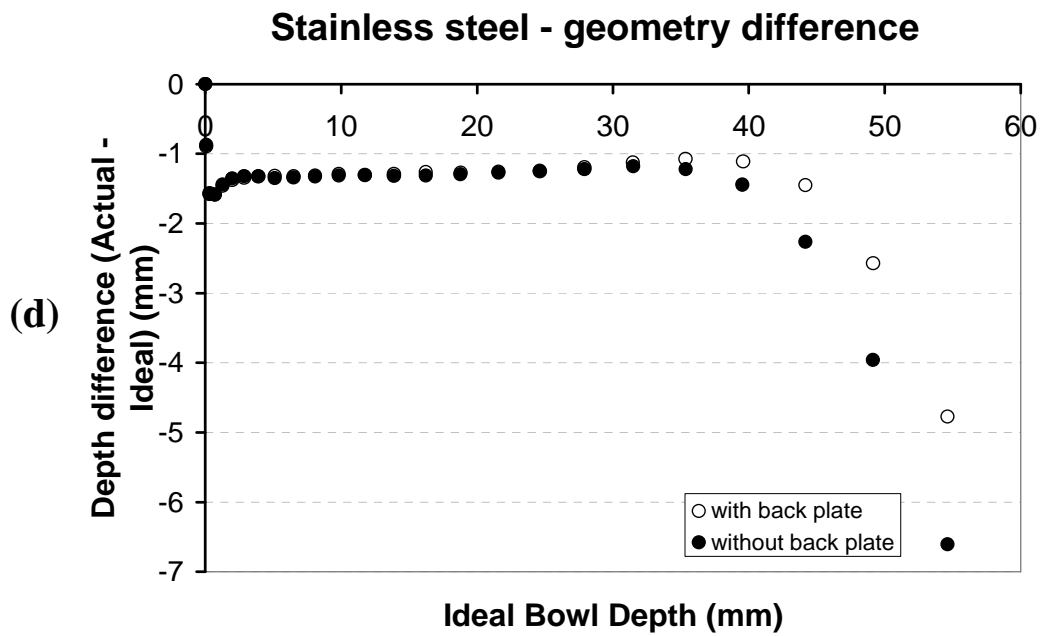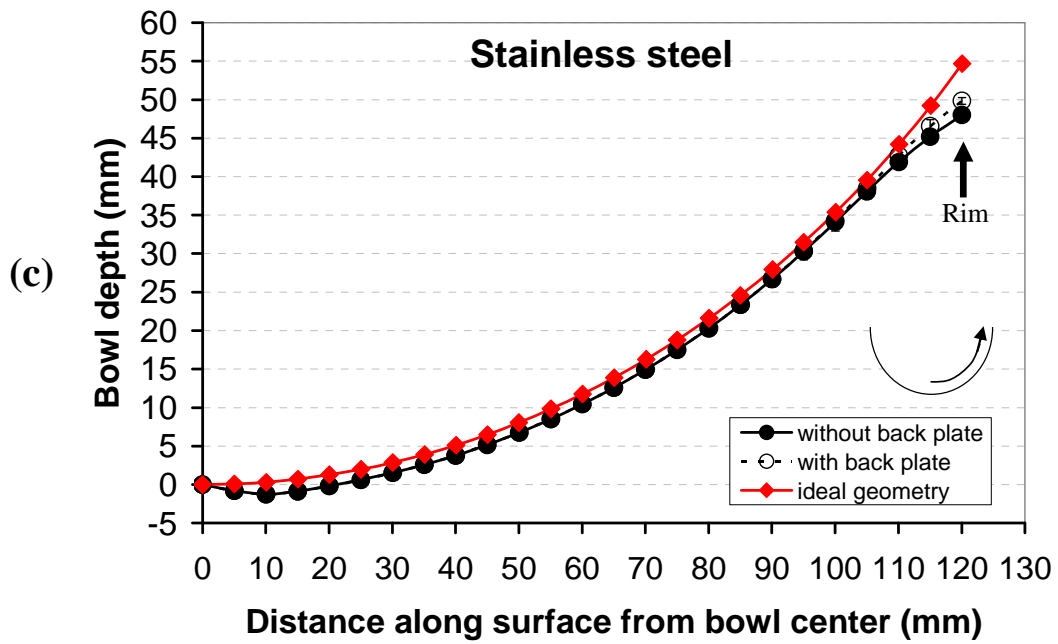
Figure 3.8: (a and b) Mild steel 50° bowl profiles and bowl depth difference respectively; (c and d) 304 stainless steel 50° bowl profiles and bowl depth difference respectively; (e) Pillowing effect in 304 stainless steel mini-pan bowls

3.8.2   304 stainless steel mini-pan dish production with and without back-plate

Figure 3.8c shows the profiles of 304 stainless steel bowls formed with and without the backing-plate. The geometrical profiles of both stainless steel dishes formed with and without the use of a backing-plate also display good agreement with the ideal or desired geometry. The geometry deviations in both bowls are comparable with differences in geometry not exceeding more than 1.5mm (Figure 3.8d). However, larger deviations from the ideal were displayed beyond 110mm, closer to the rim, in which deviations between 2mm and 7mm are observed (Figure 3.8d). A similar trend is seen in the mild steel bowls. Compare the geometrical deviations in the mild steel bowls with those seen in the 304 stainless steel bowls (see Figure 3.8b and Figure 3.8d).

3.8.3   Pillowing

Another feature of the manufactured bowls is shown in Figure 3.8e and this feature was manifested in the initially negative bowl depth (see Figure 3.8a and c). When measuring the bowl profiles, the origin co-ordinates were taken to be the center of the base of the bowls. This rising or arching of the base of the finished bowls is described as the pillow effect. This was observed after the removal of the forming load. Pillowing was found to be more distinct in the stainless steel bowls (compare Figure 3.9a with Figure 3.9b).

3.8.4   Extraction of dish from flange

Although the profiles of the dishes were not measured after water-cutting, some deviation from the desired geometry was expected. Figure 3.9 compares the appearance of the mild steel and stainless steel mini-pan bowls after extraction from the flange. The mild steel dish in Figure 3.9a retained its shape while the stainless steel bowl became severely distorted and folded on itself (Figure 3.9b).

The heavy distortion which resulted on the removal of the stainless steel mini-pan dish from its flange made it apparent that annealing would have to be performed before extracting the stainless steel mini-pan dish from its flange. To investigate this, a pair of stainless steel bowls was formed, without the use of a backing-plate. One bowl was annealed before extracting from the flange while the other was extracted without prior annealing. Both bowls were formed using 360mm x 360mm x 0.70mm 304 stainless steel sheet. The initial diameter and wall angle of these bowls were 160mm and 50° respectively.
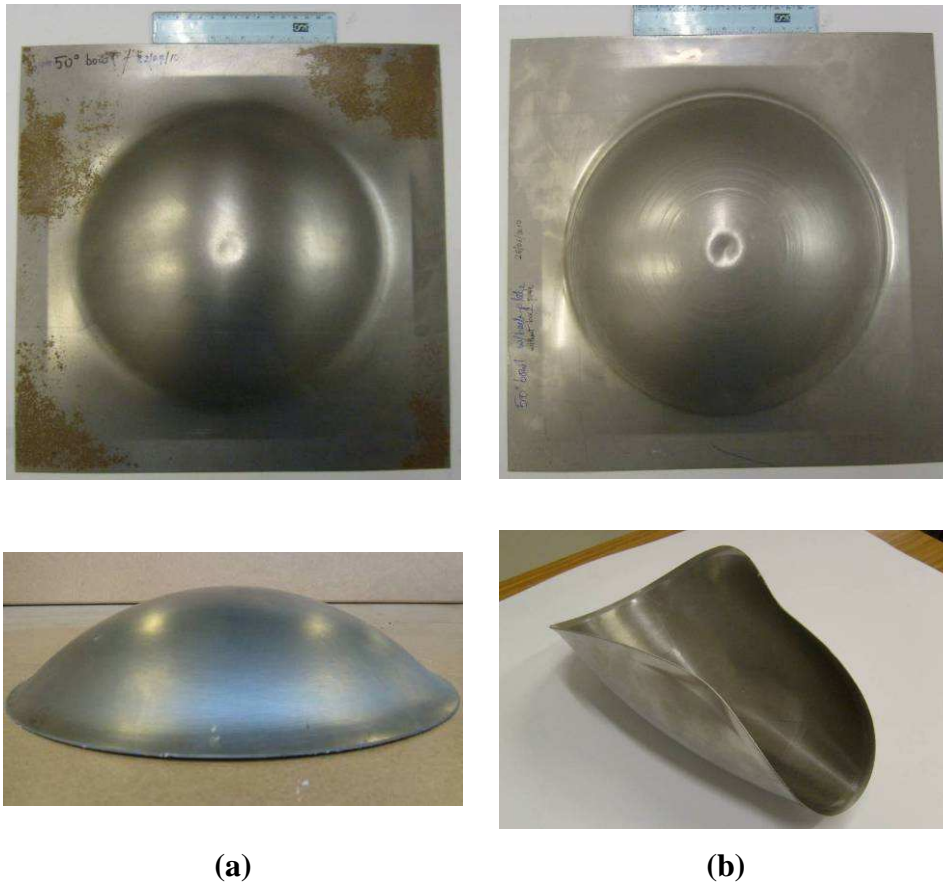
(a)   **(b)**

Figure 3.9: Bowls formed with back plate: (a) Mild steel bowl before and after removal of flange; (b) 304 stainless steel before and after removal of flange

After forming, the flange area of the bowl to be annealed was reduced to 200mm x 200mm to enable accommodation in the furnace. The furnace dimensions are 182mm x 125mm with a diagonal length of 220mm. The furnace was heated to 1050°C before introducing the bowl to be annealed. After inserting the bowl, the furnace temperature was raised to 1080°C and the bowl was held at this temperature for 15 minutes followed by water quenching. Water quenching was done by removing the heated bowl and inserting into a large basin of water. The bowl was held firmly at the flange while stirring vigorously in a swirling manner. This annealed bowl was extracted from the flange using a water-jet cutting machine.

Figure 3.10 illustrates the difference of annealing before extracting the dish. The bowl extracted before annealing was also heavily deformed (see Figure 3.10b-c) as seen earlier with the mini-pan bowls in Figure 3.9b. However, the bowl that was annealed prior to extracting from its flange retained the desired shape (Figure 3.10d-e).
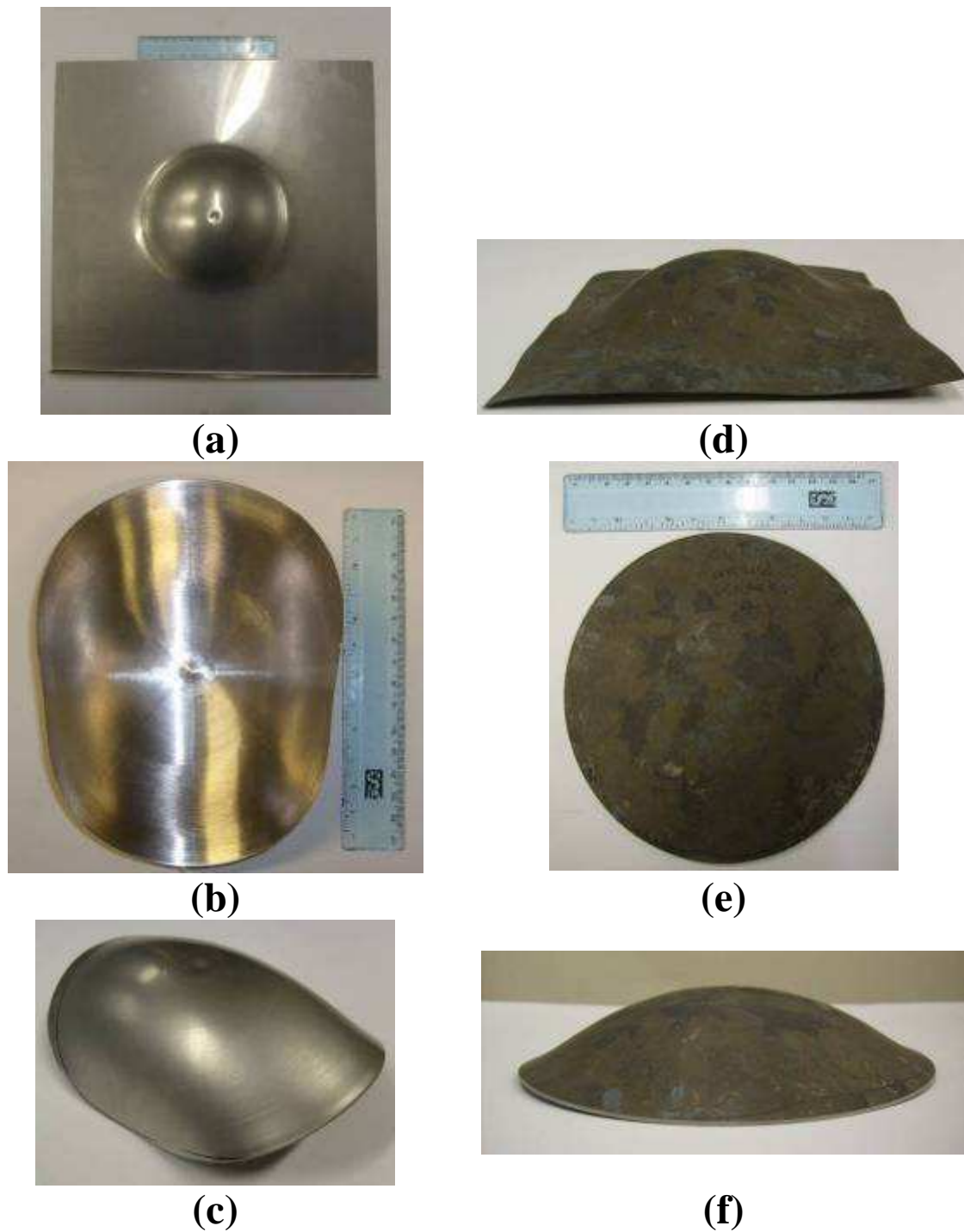
Figure 3.10: ISF and heat treatment of 304 stainless steel bowls: (a)-(c) production and extraction of bowl without prior annealing; note heavy distortion in (c) after extraction; (d)-(f) Annealing or solution treatment of bowl before extraction; note retaining of shape in (f). The black appearance of the bowl in (d)-(f) is due to surface scaling i.e. the oxide film formed on the surface due to the elevated temperature treatment.
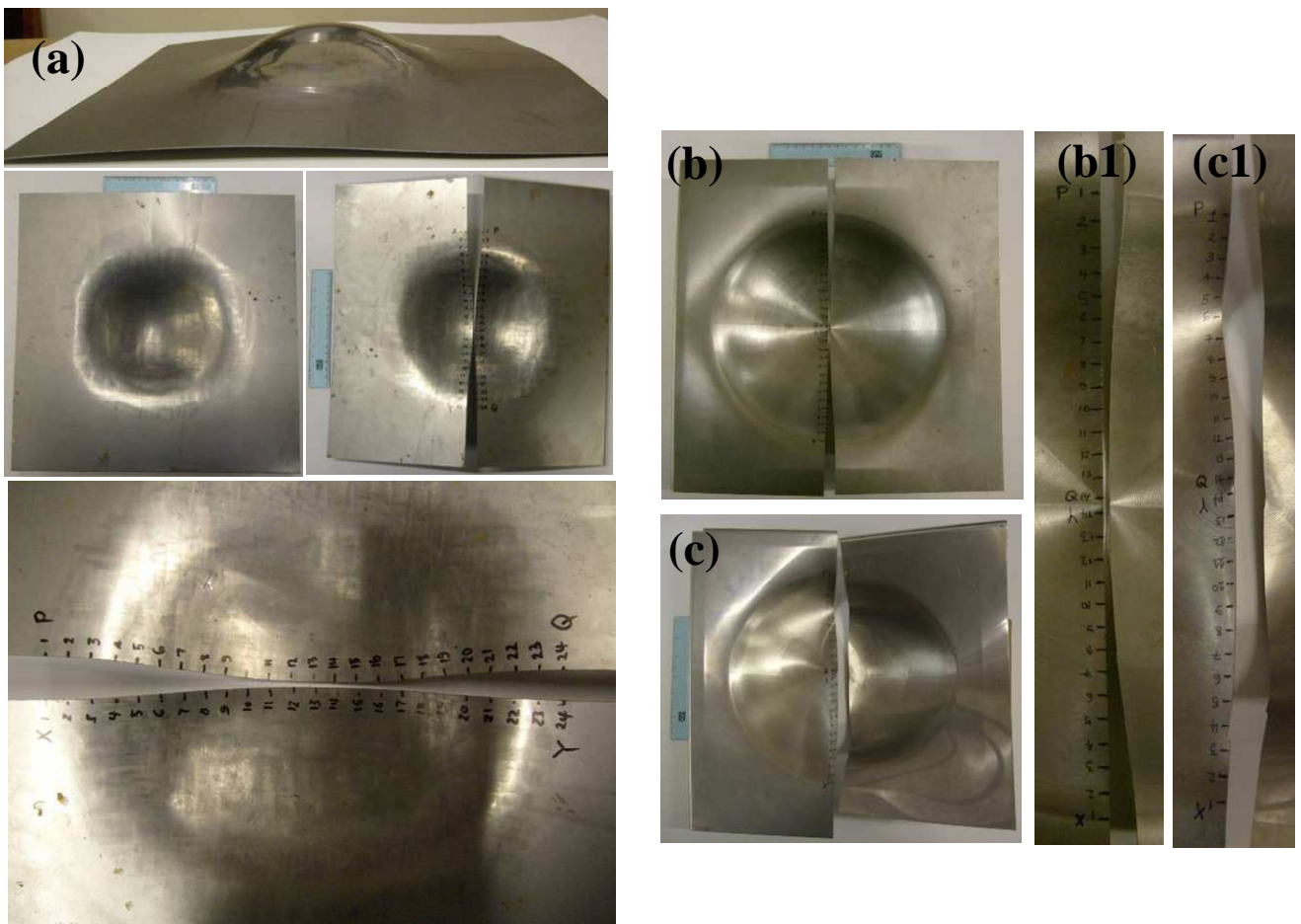
(a) Wheeled dish

ISF dishes: (b) mild steel and (c) stainless steel;
(b1) and (c1) zoom-in of cuts in (b) and (c)

(d) Hand sunk dish (Aubrapan)

Figure 3.11: Middle section cuts for dish-wall thickness measurement: Note the points P to Q and X to Y on the surfaces of the measured specimens

3.8.5 Wall thickness comparison in a conventional, wheeled dish and single and multi-pass ISF dishes

There are four points to note for the thickness variation across these dishes:

- The first is the comparable thickness reduction seen in the hand sunk (Aubrapan) and wheeled dish walls (see Figure 3.12a and b). The wall thickness in these dishes decreases in an approximately linear manner from the rim of the dish to near the base with the Aubrapan achieving a 47% thickness reduction and the wheeled dish a 20% thickness reduction. The Aubrapan is a full size steelpan with an initial diameter of 570mm and depth of approximately 200mm while the wheeled dish has an initial diameter of 180mm and a depth of 37mm.

- Secondly, the wall thickness in both mild and stainless steel ISF dishes does not show a trend in which the thickness decreases continually from the rim to the base (Figure 3.12c). Only a minor portion of the bowls are stretched for approximately the first 30mm along the bowl wall after which the thickness begins to increase until the value of the thickness at the base is similar to the original thickness of the blank.

- Double pass and triple pass forming caused a minimal extension of the stretched zone but resulted in a thickness distribution that was closer to traditional distribution as indicated by marginally thinner side walls than the bowl formed with a single tool pass (see Figure 3.12c)

- The maximum thickness reduction obtained in the ISF bowls can be approximated by the sine law of thickness reduction which is given by $t_{wall} = t_{blank}sin\alpha$ [54]. This is highlighted by the straight lines parallel to the x axis in Figure 3.12c. However small over stretching was observed in the double and triple pass bowl walls (Figure 3.12c). The sine-law of thickness is therefore better suited at predicting the final wall thickness in shells with conical walls. The reversion to original thickness in Figure 3.12c suggests that bending is the mechanism of deformation beyond the stretched zone.

(a)

(b)

(c)
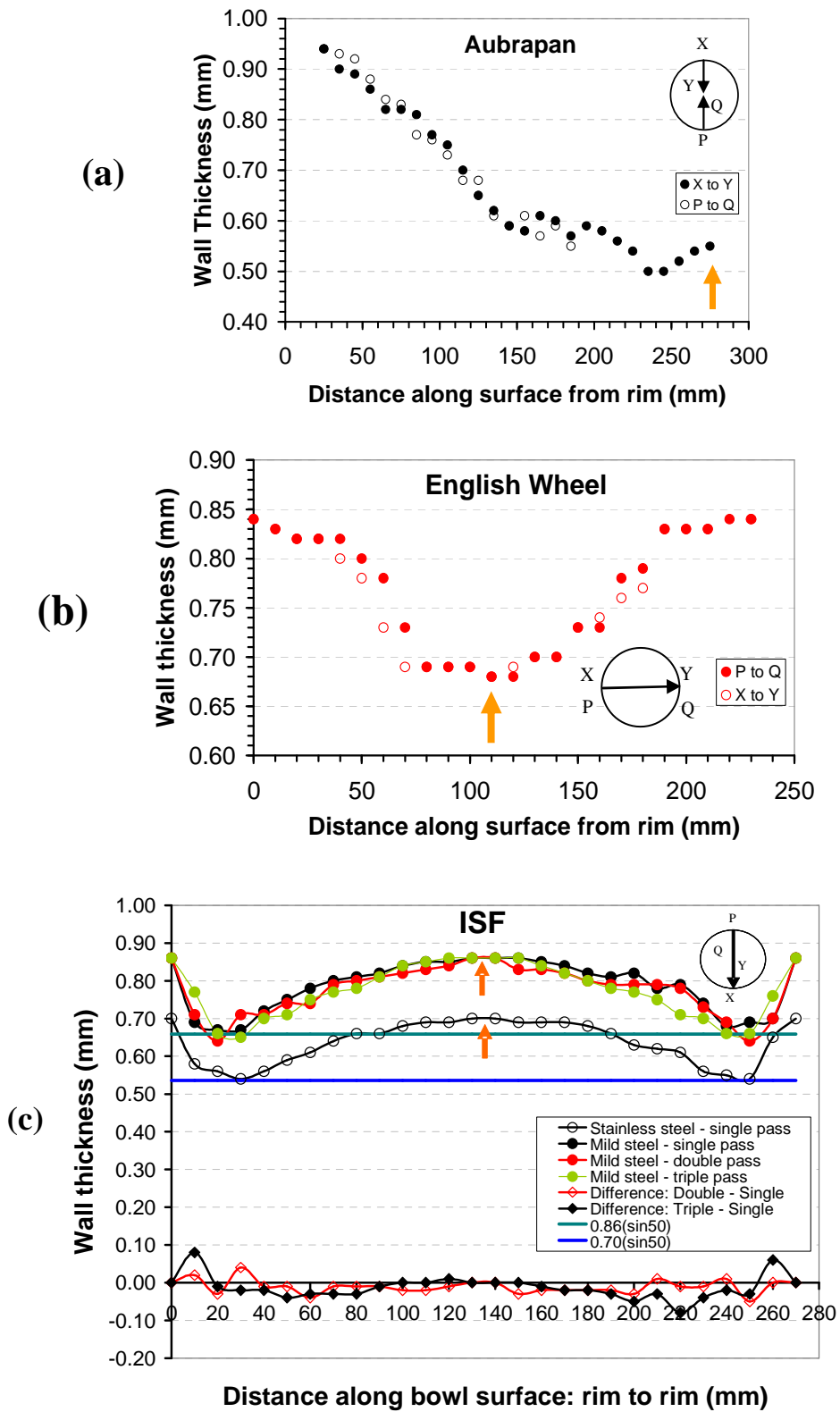
Figure 3.12: Wall thickness in dishes made by (a) hand sinking (Aubrapan) (see **Figure 3.11**d); (b) wheeling (see **Figure 3.11**a) and (c) incremental sheet forming using a single pass (see **Figure 3.11** b and c). In (a) thickness measurements started at 25mm from Aubrapan rim. In (b) thickness measurements started at 70mm from plate edge or flange. In (c) thickness measurements started at bowl rim. Note: Aubrapan diameter = 570mm; diameter of wheeled dish = 180mm and ISF bowl diameters = 244mm. **Note: Orange arrows indicate centre of pan dishes**

3.9 Break-Even Analysis: Profitability of ISF minipan dishes and extrapolation to full-size pan production

The first step in promoting a novel technology for application is demonstrating that it could conduct the desired functions better and possibly cheaper than current technology. Secondly, entrepreneurs, investors, lending agencies, managers or any stakeholder would be interested in whether investing in the new technology would be a profitable venture. In this work, the break even analysis (BEA) was used to investigate the profitability of applying ISF to the production of minipans and full size tenor pans.
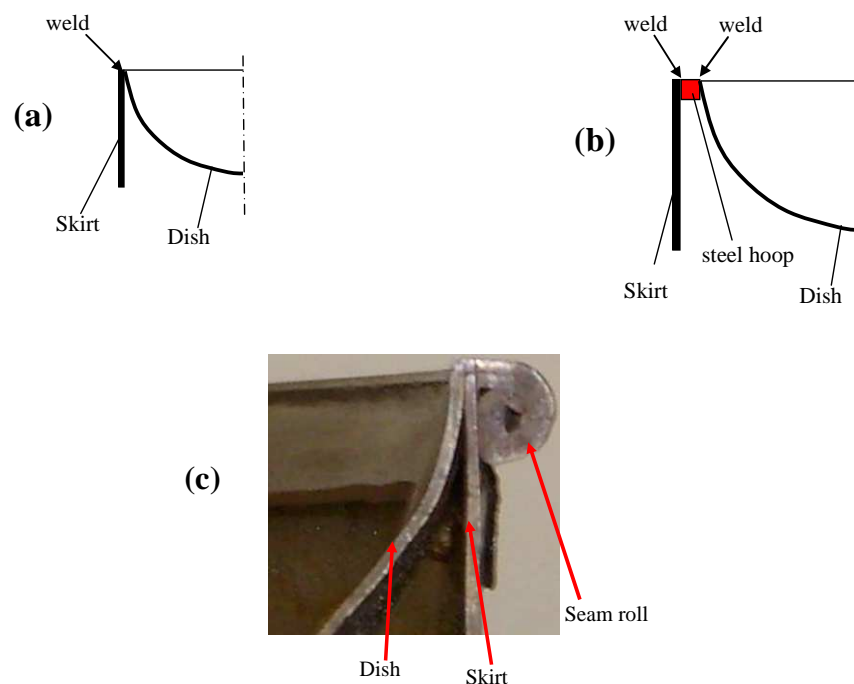
Figure 3.13: Joining methods in pans: (a) Minipan – dish is welded directly to skirt; (b) Full size pans: Dish and skirt are connected by a rigid mild steel hoop; (c) Seam roll of flanged edges in steel drum used to craft the Aubrapan

In each case the production of a single item was considered. The first case considered the 244mm diameter minipan while the second case investigated the 570mm diameter soprano pan[4]. The production process stages for the soprano pan are identical to those shown for the minipan in Figure 3.1. However, there is one additional detail in the joining stage. For the minipan, the skirt was attached directly to the dish (Figure 3.13a). In constructing the soprano pan a solid mild steel hoop (of cross-section 1mm x 1mm) would be used. The dish would be welded to the inside of the hoop while the skirt is welded to the outside of the hoop (see Figure 3.13b). The use of the hoop is a

---

[4] The blank size used to create this dish would be 640mm x 640mm and the skirt will be 170mm long. Only two full size soprano pans could be constructed from 2000mm x 1000mm mild steel sheet.

patented [162] process and was used in this work only for conducting a BEA. However, another way of joining the skirt to the dish involves the seam rolling of the flanged edges of the dish and side. In this method, the bowl and the side require flanging before forming the seam rolled joint. The option of seam rolling versus welding of the joint will be discussed later on.

In extending the BEA to full size pans, values of the initial wall angle and the forming time were required. The initial wall angle for soprano pan with $D = 570$mm and $h = 190$mm could be obtained directly from Figure 3.4. This was calculated to be $67.4°$. The estimated time to form the full size soprano pan dish was calculated in the following manner:

- It is assumed that a tool path identical to the one used to create the minipan dish would be used to create the soprano pan dish

- An expression that could be used to estimate the length of the soprano dish tool path was produced

- Determine the average forming speed of the CUED ISF machine by using the length of the tool path and the forming time for the 244mm diameter mild steel minipan dish when the machine is operating at its fastest (i.e. when x and y axis forming tool feed rates = 40mm/s and a z axis acceleration = 20mm/s^2)

- Use the average forming speed obtained and the length of the soprano pan tool path to estimate the forming time for the soprano pan dish

Using equation 3.3 the depth of the 244mm minipan with draw angle of $50°$ was found to be 56.89mm. The tool path is written so that the forming tool moves downward by 1mm between each contour or lap which means that this dish would be formed with 58 contours. The length of each lap or contour can be written as $2\pi r_n$ where r is the radius (see Figure 3.3) of a contour and $n = 0, 1, 2,$ 3 to 57. When $n = 0$, $h = 0$ and so on. The length of a contour using equation 3.3 can be also written as:

$$2\pi r_n = 2\pi \left[2R_v h_n - h_n^2\right]^{1/2} \qquad\qquad\qquad \textbf{3.5}$$

Therefore the total distance moved by the tool during the forming of a bowl can be expressed as:

$$2\pi \sum_{n=0}^{n=h} \left[2R_v h_n - h_n^2\right]^{1/2} + D/2 + h \qquad\qquad\qquad \textbf{3.6}$$

Using equation 3.6 the estimated time it would take to complete a 570mm diameter tenor pan bowl was calculated (Table 3.1).

Table 3.1: Estimated forming time for soprano pan			
244mm diameter, 57mm deep minipan		**570mm diameter, 190mm deep soprano pan**	
Tool path length (mm)	30896	Tool path length (mm)	246850
Time taken (min)	37[¥]	Average forming speed (mm/min)	835
Average forming speed (mm/min)	835[†]	Time taken to form full size pan (min)	296 (4.93hrs)
Note: ¥ This time was measured during the forming of the minipan dish † Average forming speed found for minipan was used to estimate forming time for full size soprano pan			

These BEA investigations began by assuming an investor in the ISF technology would acquire all the necessary equipment and factory space that would facilitate the production of the pans. The analysis also considered all the stages (see Figure 3.2) that contributed to the production of a minipan and a full size soprano pan. While dish forming may be an integral stage in the pan forming process, the BEA considered all the stages so as to unveil any problems that may be overlooked if only the forming stage was considered. The application of the BEA required several assumptions to be made. The following assumptions [163-165] were made in this work:

- All the minipans/full size pans produced will be sold i.e. no inventory will be kept

- Single product scenario in which only minipans/full size soprano pans are considered

- The total cost and revenues generated are linear

- Fixed and variable cost per minipan or full size soprano pan remain constant

In order to conduct the BEA, the fixed costs and variable costs associated with the production of each pan were calculated. **Table 3.2** gives the fixed costs and Table 3.11 and Table 3.12 gives the variable costs associated with the minipan and full size pan respectively. For the production of full size soprano pans, it was assumed that a CNC machine could be purchased and retrofitted for the same cost as the purpose built ISF machine. Therefore **Table 3.2** would remain unchanged and the fixed costs associated with producing a unit soprano pan would be identical to that of a minipan. Table 3.3 to **Table 3.8** lists the variables used to calculate the variable cost associated with the production of both pans (see Table 3.11 and Table 3.12). The BEA was used to determine the number of each pan type required to break-even on investment when different selling prices/unit are applied. The number of break even units can be calculated from the formula below [163] and a graphical illustration of the break even units along with the potential profits for the minipan and soprano pan is shown in Figure 3.14 a and b.

$$n = \frac{F}{(S - V)}$$

3.7

where,

n = break-even number

F = total fixed costs

S = sales price per minipan

V = variable cost per minipan

The break even analysis for both minipan and full size soprano pans indicated the following:

- Joining (welding), heat treatment and tuning are the most expensive stages of the minipan and full size pan making processes (see **Table 3.11**and **Table 3.12**).

- Minipans and full size tenor pans could be produced and sold at a competitive price with a production process which involves the use of ISF. Consider some current market values of pans as follows:

    1. Panyard, Inc. (USA) Jumbie-Jam minipan on amazon.co.uk - £199.99 [166]
    2. New Castle drum centre, high and low soprano pans: £777.00 and £872.00 respectively [167]
    3. Panyard, Inc. (USA) lead soprano pans: $4195.00 - $4995 (£2630.50 - £3132.10) [168]
    4. E.C.S Steel drums (Germany) soprano pans: €1455.12- €2187.93 (£1208.03 - £1816.40) [169]

Table 3.2: Fixed costs for minipan and full size soprano pan*								
EQUIPMENT	**Initial Cost (£)**	**Life (Yrs)**	**Annual Depreciation Rate† (£/year)**	**SALVAGE VALUE AT THE END OF EACH YEAR**				
				Yr1	**Yr2**	**Yr3**	**Yr4**	**Yr5**
ISF Machine and accessories [26]	15000.00	15	1000.00	14000.00	13000.00	12000.00	11000.00	10000.00
Computer	750.00	5	150.00	600.00	450.00	300.00	150.00	0.00
Sheet metal guillotine [170]	1821.25	8	227.66	1593.59	1365.94	1138.28	910.63	682.97
Manual slip roll [171]	1051.63	10	105.16	946.47	841.30	736.14	630.98	525.82
AC/DC TIG Welding Plant [172]	1678.46	8	209.81	1468.65	1258.85	1049.04	839.23	629.42
Water Jet Cutter ¥ [173]	(80000.00)	15	(5333.33)	74666.67	69333.33	64000.00	58666.67	53333.33
Infrared thermometer [174]	171.58	8	21.45	150.13	128.69	107.24	85.79	64.34
Oxyacetylene gas blow torch [175]	229.05	8	28.63	200.42	171.79	143.16	114.53	85.89
Bench grinder with sander [176]	46.98	8	5.87	41.11	35.24	29.36	23.49	17.62
Miniature Angle grinder [177]	62.25	5	12.45	49.80	37.35	24.90	12.45	0.00
TOTAL CAPITAL EQUIPMENT COST	**20811.20**							
MAINTENANCE, SHELTER AND INSURANCE								
Equipment Maintenance p.a. @ 2.5% of initial cost for first 5 years ‡			520.28					
Insurance Premium p.a. (@ 3% of initial equipment cost for first 5 years) ‡			624.34					
Shelter (Rental of Business Space, paid monthly at 3% of initial equipment cost) x 12 ‡			7492.03					
FIXED COSTS per annum (without water-jet)			**15731.01**					
MONTHLY FIXED COST (without water-jet)			**1310.92**					

NOTES:

* For the production of full size soprano pans, it is assumed that a CNC machine could be purchased and retrofitted for the same cost as the purpose built ISF machine. Therefore the fixed cost of producing a full size soprano pan would be identical to that of producing a minipan.

† Depreciation calculation: The salvage value is taken to be zero at the end of the life of the equipment. Therefore the Annual Depreciation Rate [178] was calculated as follows:
Annual Depreciation Rate = (Initial Cost/Life of Equipment).

‡ It is standard practice to estimate Equipment Maintenance, Insurance and Shelter each at 2-3% of the Initial Capital Cost for the first 5 years

¥ It is assumed that the investor will initially pay for access to a water-jet cutter owing to its high cost. The cost of this equipment was therefore not used in this work. This aspect of the production would be subcontracted.

Table 3.3: Minipan production times for each stage	
Item	**Time (Minutes)**
Time to guillotine sheet into pieces for 8 minipans/8	20/8 (2.5)
ISF forming time for mini-pan dish	37
Total ISF time (including times for lubricating, set-up, removal and cleaning product surface)	45
Water jet cutting to remove finished mini-pan dish from flange (including set-up and removal time)	11.2 (10 minutes set-up time and 1.2 minutes cutting time)
Deburring of cut edges of mini-pan dish	2
Deburring of strip to be formed into skirt	2
Rolling of side	5
Attachment of bowl to side (including time for positioning, tack-up, welding and cleaning)	30 (10 minutes for tacking and 20 minutes for welding i.e. arc time†)
Heat treatment of mini-pan dish surface	10
NOTES:	
†Argon gas only runs during arc time, therefore in these calculations only the 20 minutes of welding are used in the calculation and the 10 minutes for set-up are ignored as the arc time during tacking is short	

Table 3.4: Full size tenor pan production times for each stage	
Item	**Time (Minutes)**
Time to guillotine sheet into pieces for 2 soprano pans	10/2 (5)
ISF forming time for soprano dish	296
Total ISF time (including times for lubricating, set-up, removal and cleaning product surface)	326 (30 minutes added for set-up time since larger blank holders would be required)
Water jet cutting to remove finished soprano dish from flange (including set-up and removal time)	12.62 (10 minutes set-up time and 2.62 minutes cutting time)
Deburring of cut edges of soprano dish	2
Deburring of strip to be formed into skirt	2
Rolling of hoop	5
Rolling of side	5
Attachment of bowl to hoop and side to hoop (including time for positioning, tack-up, welding and cleaning)	90 (30 minutes for tacking and 60 minutes for welding i.e. arc time†)
Heat treatment of soprano dish surface	15
NOTES:	
†Argon gas only runs during arc time, therefore in these calculations only the 60 minutes of welding are used in the calculation and the 30 minutes for set-up are ignored as the arc time during tacking is short	

Table 3.5: Equipment Specification, Flow and feed rates	
Equipment Power Usage	
Item	**Power (kW)**
ISF Machine	2.25 [26]
Computer	1.0
TIG Welding Plant	33.13 [172]
Bench grinder with sander	0.24 [176]
Miniature angle grinder	0.84 [177]
Industrial electricity rate	9.22pence/kWh[179]
Flow and feed rates	
Item	**Rate**
Argon gas flow rate	8 L/s
Propane gas flow rate	-
Acetylene gas flow rate	0.084 L/s
Oxygen gas flow rate	0.092 L/s
NOTES: Feed and flow rates were obtained from the CUED machine shop	

Table 3.6: Material Costs	
Item	**Value**
2000mm x 1000mm x 1mm black mild steel sheet, £/sheet	32.90
10mm solid square mild steel rod, £/kg	1.80
TIG filler rod cost(£/kg)	11.85
Argon gas cost (99.95% purity) £/L	0.117
Propane gas cost (£/L)	0.35
Oxygen gas cost (£/L)	0.20
Acetylene gas cost (£/L)	0.50
NOTES: Values in this table were obtained from the CUED purchasing stores or office	

Table 3.7: Minipan geometry and consumption calculations	
Item	**Value**
Diameter of minipan D_m (mm)	244
Length of minipan skirt L_m (mm)	100
Length to be welded = $\pi D_m + L_m$ (mm)	866.5
Length of electrode consumed for minipan L_e (m)	1.733†
Diameter (d) of TIG welding filler rod (mm)	1.0
Density (ρ) of TIG welding filler rod (kg/m^3)	7833.4
Mass of electrode consumed =$(\pi d^2/4)$ x L_e x ρ (kg)	0.0107
NOTES: † Rule of thumb: Each 500mm of weld consumes 1000mm of 1mm diameter electrode	

Table 3.8: Soprano pan geometry and consumption calculations	
Item	**Value**
Inner Diameter of soprano pan D_i (mm)	570
Outer Diameter of construction which includes 10mm square mild steel hoop D_o (mm)	590
Length of skirt L_s (mm)	170
Length of square rod used for hoop = $\pi (D_i + D_o)2$	1822
Length to be welded = $\pi (D_i + D_o) + L_s$ (mm)	3814
Length of electrode consumed for minipan L_e (m)	7.628†
Diameter (d) of TIG welding filler rod (mm)	1.0
Density (ρ) of TIG welding filler rod (kg/m^3)	7833.4
Mass of electrode consumed = $(\pi d^2/4)$ x L_e x ρ (kg)	0.0469
NOTES: † Rule of thumb: Each 500mm of weld consumes 1000mm of 1mm diameter electrode	

Table 3.9: Number of mini-pans required to break even per month (see Figure 3.14a)				
Fixed cost, 'F' (£)	1310.92	1310.92	1310.92	1310.92	1310.92
Variable cost, 'V' per unit (£)	124.68	124.68	124.68	124.68	124.68
Selling cost, 'S' per unit (£)	150.00	175.00	200.00	225.00	250.00
Break even units (n)	52	27	18	14	11

Table 3.10: Number of full size soprano pans required to break even per month (see Figure 3.14b)				
Fixed cost, 'F' (£)	1310.92	1310.92	1310.92	1310.92	1310.92
Variable cost, 'V' per unit (£)	461.85	461.85	461.85	461.85	461.85
Selling cost, 'S' per unit (£)	600.00	650.00	700.00	750.00	800.00
Break even units (n)	10	7	6	5	4
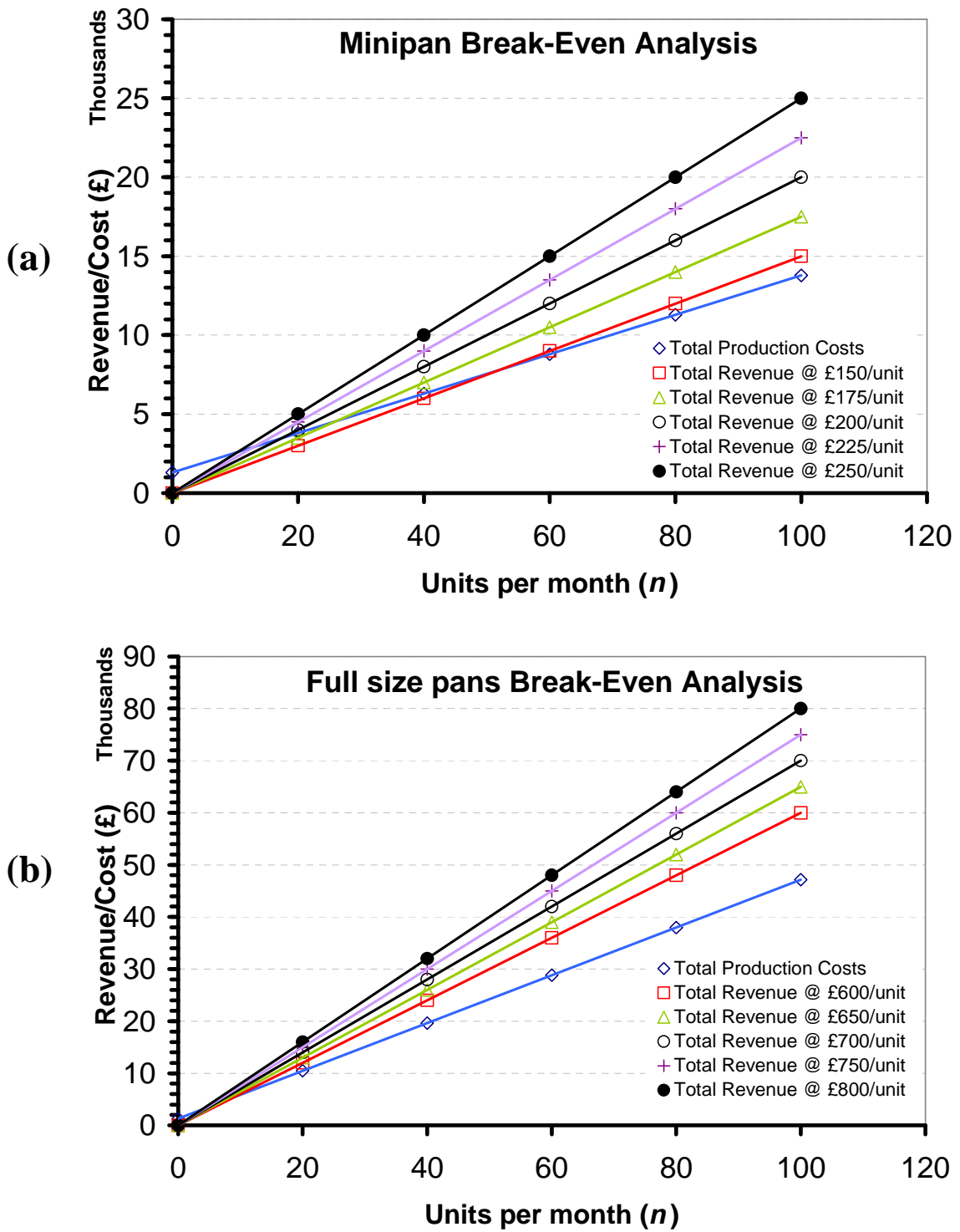
Figure 3.14: (a) Break-Even Analysis of mini-pan production with ISF; **(b)** Break-Even Analysis of full size soprano pan with ISF

Table 3.11: Minipan variable costs			
Item	**Description/Comments**	**Formula**	**Cost (£)**
Material Cost	Eight minipans to be produced from a 2000mm x 1000mm x 1mm black mild steel sheet	Cost of one sheet/8 = (32.90/8)	4.11
Incremental Sheet forming	Energy cost - Here, only the forming time is used in the calculation. Set-up and removal times are accounted for in the labour cost	Forming time(hrs) x(ISF Machine rating (kW)+Computer rating (kW)) x Average industrial electricity cost(£/kWhr) = (37/60 x 3.25 x 0.0922)	0.18
Water jet cutting [180] *	This is subcontracted	Negotiated with machine shop	4.00
Deburring water-cut edge of minipan dish	Energy cost here only: Time for energy consumption and labour time are identical	Deburring time (hrs) x Belt grinder machine rating(kW) x Average industrial electricity cost(£/kWhr) = (2/60 x 0.24 x 0.0922)	0.00074
Deburring of strip to be formed into minipan skirt	Energy cost here only: Time for energy consumption and labour time are identical	Deburring time (hrs) x Belt grinder machine rating(kW) x Average industrial electricity cost(£/kWhr) = (2/60 x 0.24 x 0.0922)	0.00074
Rolling side	See labour cost. Also this machine is manual and uses no mains power	See labour cost	-
Welding/Joining	TIG welding - energy and consumables consumption (electrode and shielding gas) i.e. Energy cost +Filler metal cost + Shielding gas cost. Note that the welding time used here is the arc-time i.e. the average length of time the arc was maintained during a weld. Set-up times are not included. Set-up times are accounted for in the labour cost	[Arc time(hrs) x Machine rating (kW) x Average industrial electricity cost(£/kWhr)] = (20/60 x 33.13 x 0.0922) + [Mass of electrode used (kg) x electrode cost(£/kg)] = (0.0107 x 11.85) +[Argon flow rate(L/s) x welding time(s) x argon gas cost(£/L)] = (8 x 20 x 0.117)	19.86
Heat treatment	Consumables cost: Only annealing time is used here.	Acetylene flow rate(L/s) x Annealing time(s) x Acetylene gas cost(£/L) = (0.084 x 10 x 60 x 0.50) + Oxygen flow rate (L/s) x Annealing time(s) x Oxygen gas cost (£/L) = (0.092 x 10 x 60 x 0.20)	36.24
Tuning	Pre-tuning before coating and fine tuning after coating is completed	Negotiated with pan maker (£/minipan)	35.00
Coating	This is subcontracted	Negotiated with paint shop(£/minipan)	3.00
Labour	Labour cost only uses time taken to guillotine, supervision of ISF, joining, heat treatment and water jet cutting as tuning and coating are assumed to be outsourced.	Hourly rate (£/hr) x (guillotine +rolling + ISF + deburring + joining+ heat treatment)(hr) = 11.60 x [(2.5 + 5 + 45 + 4 +30 + 10)/60]	18.66
SUB TOTAL			**121.05**
Miscellaneous supplies and Packaging	bearing grease, cleaning paper, mallet material, ethanol for cleaning surface of minipan dish after ISF etc (3% of cost to produce a minipan)	0.03 x cost to produce a minipan = 0.03 x SUBTOTAL	3.63
TOTAL VARIABLE COST			**124.68**
NOTES: *The cost of subcontracting the water jet cutting operation was estimated from [180] which estimated the hourly operating cost at £12/hour for a single head cutting machine.			

Table 3.12: Full size tenor pan variable costs			
Item	**Description/Comments**	**Formula**	**Cost (£)**
Material Cost	Two soprano pans to be produced from a 2000mm x 1000mm x 1mm black mild steel sheet + 1822mm of 1mm square solid hoop material	Cost of one sheet/2 + mass of hoop material (kg) x cost (£/kg) $=(32.90/2 + 0.01^2$ x 1.822 x 7800 x 1.8) = 16.45 + 2.55	19.00
Incremental Sheet forming	Energy cost - Here, only the forming time is used in the calculation. Set-up and removal times are accounted for in the labour cost	Forming time(hrs) x(ISF Machine rating (kW)+Computer rating (kW)) x Average industrial electricity cost(£/kWhr) = (296/60 x 3.25 x 0.0922)	1.47
Water jet cutting [180]*	This is subcontracted	Negotiated with a machine shop (£/soprano dish)	7.00
Deburring water-cut edge of soprano dish	Energy cost here only: Time for energy consumption and labour time are identical	Deburring time (hrs) x Belt grinder machine rating(kW) x Average industrial electricity cost(£/kWhr) = (2/60 x 0.24 x 0.0922)	0.00074
Deburring of strip to be formed into soprano skirt	Energy cost here only: Time for energy consumption and labour time are identical	Deburring time (hrs) x Belt grinder machine rating(kW) x Average industrial electricity cost(£/kWhr) = (2/60 x 0.24 x 0.0922)	0.00074
Rolling side and solid hoop	See labour cost. Also this machine is manual and uses no mains power	See labour cost	-
Welding/Joining	TIG welding - energy and consumables consumption (electrode and shielding gas) i.e. Energy cost +Filler metal cost + Shielding gas cost. Note that the welding time used here is the arc-time i.e. the average length of time the arc was maintained during a weld. Set-up times are not included. Set-up times are accounted for in the labour cost	[Arc time(hrs) x Machine rating (kW) x Average industrial electricity cost(£/kWhr)] = (60/60 x 33.13 x 0.0922) + [Mass of electrode used (kg) x electrode cost(£/kg)] = (0.0469x 11.85) +[Argon flow rate(L/s) x welding time(s) x argon gas cost(£/L)] = (8 x 60 x 0.117)	59.76
Heat treatment	Consumables cost: Only annealing time is used here.	Acetylene flow rate(L/s) x Annealing time(s) x Acetylene gas cost(£/L) = (0.084 x 15 x 60 x 0.50) + Oxygen flow rate (L/s) x Annealing time(s) x Oxygen gas cost (£/L) = (0.092 x 15 x 60 x 0.20)	54.36
Tuning	Pre-tuning before coating and fine tuning after coating is completed	Negotiated with pan maker (£/minipan)	200.00
Coating	This is subcontracted	Negotiated with paint shop(£/minipan)	20.00
Labour	Labour cost only uses time taken to guillotine, supervision of ISF, joining, heat treatment and water jet cutting as tuning and coating are assumed to be outsourced.	Hourly rate (£/hr) x (guillotine +rolling + ISF + deburring + joining+ heat treatment)(hr) = 11.60 x [(5 + 10 + 326 + 4 +90 + 15)/60]	86.81
SUB TOTAL			**448.40**
Miscellaneous supplies and Packaging	bearing grease, cleaning paper, mallet material, ethanol for cleaning surface of minipan dish after ISF etc (3% of cost to produce a minipan)	0.03 x cost to produce a minipan = 0.03 x SUBTOTAL	13.45
TOTAL VARIABLE COST			**461.85**
NOTES: *The cost of subcontracting the water jet cutting operation was estimated from [180] which estimated the hourly operating cost at £12/hour for a single head cutting machine.			

3.10 DISCUSSION

3.10.1 Thickness distribution and springback in ISF dishes

While there are numerous benefits that would come with applying ISF to steelpan dish production, the major elements surrounding its suitability to pan dishing are material springback and thickness distribution in the formed bowls. It has been long established that steel drums are predominantly produced from bowls in which the sheet metal is either stretched, or, until recently, produced from sheet metal in which the thickness is constant for the most part of the wall of the completed bowl as in spinning, deep drawing and hydroforming. As regards the thickness distribution in ISF, the bowls created by single and multiple pass forming in this work had a thickness distribution in which stretching occurred in a small region of the bowl, closer to the rim, after which thickening occurred until the material reverted to its original thickness. The maximum possible thickness reduction obtained in the stretched portion of the single, double and triple pass bowl walls showed good agreement with the sine law of shear forming. Since the length of the region in which stretching occurs in the single pass and multi-pass bowls are comparable, there may be no need to produce pan dishes in multiple passes as there is minimal extension of the stretched zone. Producing pan dishes in multiple passes will only result in an insubstantial distribution in the wall thickness in addition to an unnecessary increase in production time and variable cost of production.

Steelpans have long been crafted from dishes that were produced by stretching and there is no documented evidence to suggest that steelpans should be made solely from stretched or constant thickness domes, although personal communication has indicated a preference and a strong bias for stretched dishes probably because this has been proven to work best. To answer the question of whether the thickness distribution in ISF is suitable, completed dishes formed in three ways: traditionally, by ISF and a method which maintains constant thickness, could be passed to tuners and their experiences documented when tuning each pan. The tuners would not have prior knowledge of the manner in which the domes were made.

While wheeling was not a highlight in this work, the exercise was conducted in order to examine the thickness variation in its walls. Firstly, the reduction in thickness in the bowl wall resembled that of a traditionally dished pan. This feature may make the process an ideal candidate for pan dishing. However, wheeling is entirely a craft process which requires sufficient time and patience to master. Furthermore, there are some limitations of using the English wheel which primarily include the size of the sheet that the operator can physically manage in the machine. Wheeling may be practically applied to minipans which are about 300mm wide and 30-40mm deep but may be more difficult for forming full size dishes which can be 600mm wide and 200mm deep.

The main cause for the geometrical deviations manifested in the ISF bowls was springback. Springback results in a deviation in shape when the forming tool is removed from the surface of the formed part [101]. One type of springback is a consequence of the bending [56,161] of the bowl between the rim and the flange. Figure 3.8 b and d shows that the maximum deviations experienced in the mild steel and stainless steel bowls were in this region. Previous work has shown that a solution to mitigating this problem requires the use of a backing plate [52,60] in the forming arrangement. In this work, a backing plate which provided a rigid support near the rim of the bowls was used and springback in this region of the bowls was minimized (Figure 3.8 b and d). The geometrical deviations manifested in most part of the bowls formed with and without a backing plate were mostly in good agreement with the ideal geometry with deviations of no more than 2mm. However, it is not certain what the level of deviation would be when production is scaled up to produce full size pans but deviations may be greater than those observed in the forming of minipan dishes. One way to predict the level of deviation would be to conduct finite element simulations on the incremental sheet forming of full size dishes formed with and without a back plate.
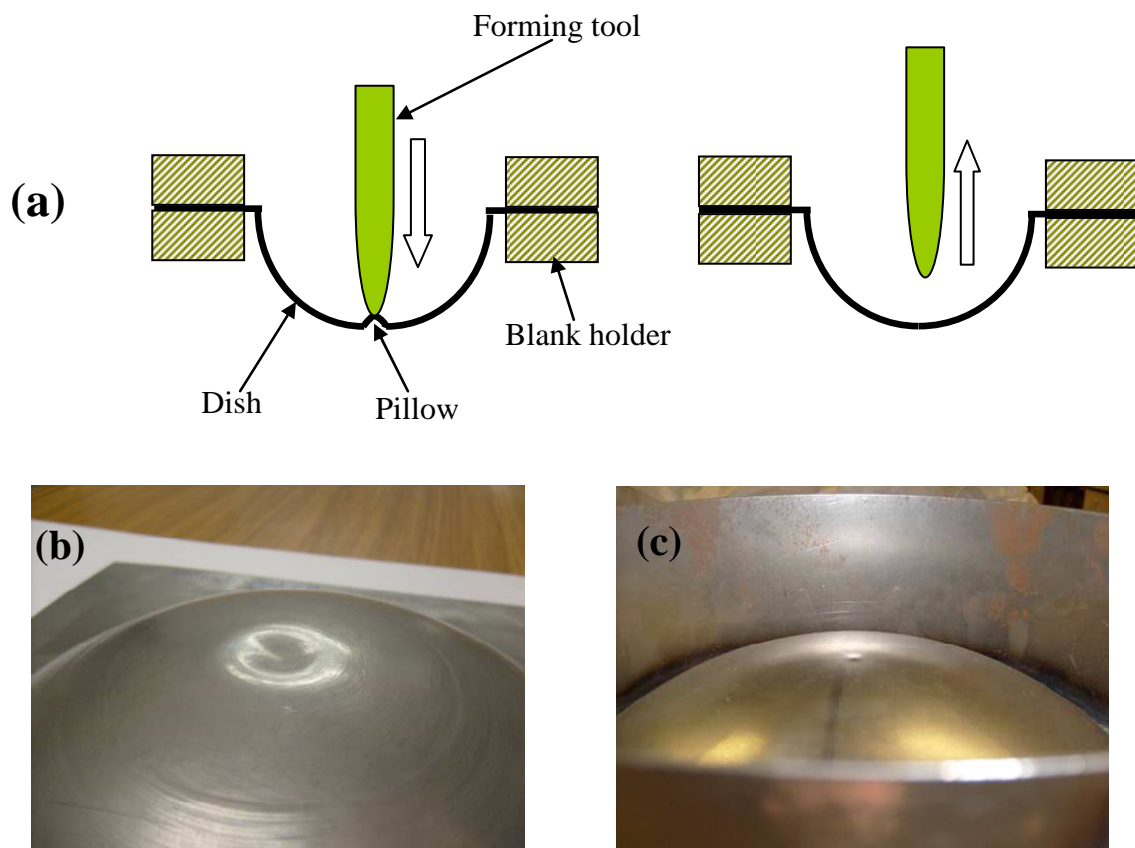
Figure 3.15: Pillowing can be reduced with by pushing the forming tool onto the pillow after completion of the dish; (b) Dish with pillow; (c) Dish with reduced pillow

Another form of springback manifested in the dishes created was the presence of '*pillow*'(Figure 3.15b) at the base of the dish on completion of the forming process. For the production of pans, the

appearance of this pillow would be considered unaesthetic and one manner of dealing with this problem is illustrated in Figure 3.15a. After the forming of the dish, the forming tool could be used to suppress the appearance of the pillow (see Figure 3.15 b and c).

3.10.2 Forming with 304 stainless steel

Stainless steel of the 300 series, particularly 304 and 316/316L grades are considered to be exceptional material candidates for the production of steelpans owing to their high formability (see Table 2.2) and good corrosion protection capability. However, these steels have proven to be somewhat of a problem due to their rapid work hardening characteristic. The work hardening coefficient of these austenitic stainless steel grades is almost double that of mild steel (Table 2.2). During forming, stainless steel sheet work hardens rapidly making further forming increasingly difficult. Unlike the mild steel dishes, the stainless steel dishes produced in this work were heavily distorted after trimming of the flange area. The high work hardening of the material probably contributed to the development of high residual stresses. However, it was possible to demonstrate that the high residual stresses and by extension the severe distortion could be minimized by solution treatment annealing the stainless steel bowls before trimming (see Figure 3.10).

Annealing of the 304 stainless steel bowls created in this work took place at 1080°C without a controlled nitrogen atmosphere to reduce surface scaling. Therefore the stainless steel bowls annealed in this work were heavily scaled (see Figure 3.10). Maintaining a controlled atmosphere in addition to acquiring a furnace large enough to accommodate a full size pan is very expensive. However, in this work, attempts were made to identify cheaper alternatives to mitigate the problem of surface scaling in annealed stainless steel bowls. The first alternative involved the use of a compound, III-tri-chloro-ethane which was painted onto the surface of the dish before placing in the furnace. This alternative was abandoned after discovering that the coating released hazardous fumes when heated beyond 580°C. The CUED furnace vents were also not fitted to allow fumes to escape outside the building. Continuing with this venture would have resulted in the release of hazardous fumes within the lab. The other alternative involved the removal of the scale after annealing the dish. The intention was to clean the scaled surface with a sand blast or glass bead blast although a glass bead blast may give a smoother surface finish. It was not possible to conduct this alternative as the blasting machines at the CUED were decommissioned for maintenance and relocation. This alternative is therefore recommended for future work.

Another important element that is recommended for further work is the measurement of tool forces during the forming of materials to be used for pan making. This could be done by measuring the forces on the tool for various materials, tool feeds and speeds blank thickness as well as tool radius

to blank thickness ratios. This information would be vital in selecting a CNC machine that could be retrofitted for pan dish forming.

3.10.3 Break even analysis

The BEA was applied in this work as it is suitable to industries which are not subject to a fast change in technology in addition to being suitable for single product scenarios [165]. In this work it was applied to the production of two entities, one in each instance: minipans and full size soprano pans. The steelpan industry tends to also be sluggish in its transition to new technology [44,45,181]. It is also reasonable to assume that if ISF is adopted, at some stage, it could become the de-facto dishing used by a number of pan makers among which there is a consensus for the full automation of the manufacture of the instrument. While the BEA can provide useful information that could be used in decision making for a new venture there are some elements that could severely undermine its credibility. These elements are related to the fact that production costs are not static due to influence by external factors on which the manufacturer has no control. Once these elements are monitored and the respective costs adjusted to reflect the variation, the BEA would continue to be useful. This is also the principal reason why the BEA was not applied for a period greater than a year.

The cost of the ISF machine listed in Table 3.2 is for a custom built machine that was manufactured at the CUED solely for the purpose of sheet forming. A pan maker may consider purchasing a used or new CNC milling machine which would be adapted for ISF use. This alternative may be cheaper and maintenance costs may also be lower as CNC machines are widely produced and parts and accessories could be easily and cheaply acquired. The Amino Corporation in Japan is currently the only commercial manufacturer of purpose built ISF machines which would undoubtedly cost several tens of thousands of pounds. The retrofit CNC alternative could result in a reduction in the fixed cost and by extension the total production cost associated with the production of a minipan or soprano pan. The machine need not be solely for ISF but could also be adapted to perform other operations when not being used for ISF.

In this work, the pan maker using ISF, was assumed to be solely producing minipans or full size soprano pans. In reality, pan makers produce a range of pans and thus the fixed costs would be shared among each product group. For instance, if a pan maker produced four pan types in addition to one type of minipan, then the fixed cost for producing the minipans would become total fixed cost/5.

There are also elements which affect the variable costs. One of the most obvious elements is the price of steel which due to fluctuation in demand and availability would influence the final cost of the minipan. Any changes in the price of steel would be manifested in the price of steel sheet and the price of the welding electrodes. The BEA would need to be adjusted to account for this. Additionally, changes in energy prices (electricity and welding gases); increases in the national minimum wage; value added tax (VAT) adjustments by the government; inflation and the availability of good tuners would also affect the break even calculation.

3.10.4 Realistic minipan production

The welding/joining and tuning stages in conjunction with labour costs were identified as the elements adding the most value to the minipan and soprano pan. Tuning has manifested itself as a '*rate determining step*' or '*bottle-neck*' in the production of the instrument. In order to understand the effect of this single stage on the overall production, the number of bowls of each pan type that could be produced monthly by ISF and the number of bowls that could be realistically tuned in the same time period must be considered. The CUED ISF machine, at its fastest feed rates for mild steel, takes an average of 45 minutes and approximately 5.5 hours to form a 244mm minipan and a full size 570mm soprano pan dish respectively, inclusive of set-up time.

A business week or work week is typically 5 days from Monday to Friday with each work day operating between the hours of 9am and 5pm. If an hour is excluded for breaks each day, then the work day would be 7 hours. A calendar month will usually have 22 working days and assuming an operating efficiency of 90%, then in a calendar month the ISF machine at its fastest rate can produce approximately 185 minipan bowls or 25 full size soprano pans (see Table 3.13). It is also assumed that a pan tuner would be able to completely tune (pre tune and fine tune) an average of 2 minipans or 0.75 soprano pans per day. In a calendar month, a single tuner can provide either 44 tuned minipans or 17 tuned soprano pans (Table 3.13).

The speed of the ISF machine only becomes crucial if more than 185 minipans or 25 soprano pans are required monthly, which may be unlikely. However, if this occurs the work day and/or work week may be extended to increase the production of bowls but the problem still remains on the realistic number of minipans that could be tuned. There is currently a handful of highly skilled tuners in the UK and they are not centrally located, some being hundreds of miles apart. Even if it becomes possible to have (a) permanent tuner(s) located at the pan production site, the reality is, a single tuner can only tune a limited number of pans per month. The only recourse to meet an increasing demand for pans would be to solicit the services from additional tuners of which there is a limited pool. It is easy to foresee the calamity that can result due to problems with sourcing tuners

in addition to accounting for times when tuners would be unavailable. It is unrealistic to assume that an individual will work without any sort of interruption (bereavement, vacation, illness, retirement etc.).

Table 3.13: Realistic production of pans using ISF		
Item	**Minipan**	**Full size soprano pan**
Diameter (mm)	244	570
Total production time (mins)	45	326
ISF production at fastest rate (pans/month)	185	25
Realistic tuning rate (pans/day)	2	0.75
Realistic pans per working calendar month (22 days)	44	17
Minimum price for profit (£) see Table 3.9 and Table 3.10	175.00	600.00

In this light, if it is assumed that there is a single reliable tuner the estimated number of both pan types that could be produced and the minimum selling price for profit realization is summarized in Table 3.13. The analysis above indicates that a pan production process which applies ISF could be viable. However, the exercise also reinforced that the heart of the pan production process is tuning. This is the stage that creates a '*bottle-neck*' in the overall pan production process since it is highly susceptible to impairment and undermining owing to the small pool of skilled tuners. It is also apparent that the speed of ISF only becomes an issue if there is a demand beyond which the machine can realistically produce at its fastest rate. The fact is, tuning remains the core of the pan making process and efforts to improve other stages of the process while overlooking tuning would be futile. This therefore builds the case for research into partial or full automation of the tuning stage of steelpans. Many may argue that this may be unnecessary as steel drums remain a low volume entity. However, from the perspective of a pan factory, the limited availability and uncertain reliability of tuners will continue to be a challenge as long as manual tuning remains the only option for tuning pans.

3.10.5 Areas for cost reduction

Apart from tuning, welding was identified as one of the costly steps in the pan production process. Unlike heat treatment which is inevitable, the pan maker has the option of using another method of joining the dish to the skirt. This option is illustrated in Figure 3.13c where the flanged edges of the dish and the side are rolled together to form a seamed joint. If the pan maker decides to use this method of joining, it is assumed that a rotary flanging and seaming machine could be purchased for a total cost not exceeding £15000. It is also assumed that no maintenance would be required in the

first year. Table 3.14 shows the payback period in recouping the capital outlay for the flanging and seaming machines if either minipans or full size pans are produced. This alternative appears attractive as the payback periods are short.

Table 3.14: Payback period: seam rolling versus welding		
Item	Minipan	Full size soprano pan
Estimated total cost of rotary flanging and seaming machines (£)	15000.00	15000.00
Costs associated with using welding to join dish to skirt (£)		
Material (£)†	0.00	2.55
Welding/Joining (£)†	19.86	59.76
Labour(£)†	5.80	17.40
Total Savings per pan (£)	25.66	79.71
Realistic pans per calendar month (22 days)¥	44	17
Savings per month: Realistic pans per month x savings per pan (£)/month	1129.04	1355.07
Payback period (months)		
Estimated machine cost/Savings per month (months)	14	12
Notes: † Values taken from Table 3.11 and Table 3.12 ¥ Values taken from Table 3.13		

3.10.6 Pneumatic hammer versus ISF

Pneumatic assisted sinking still remains one of the most popular ways of dishing steel pans primarily because of its low cost and the energy for sinking is provided mechanically and not by the arms of the pan maker. Although the cost of a pneumatic gun and compressor would be about 1/10 to ½ of the cost of an ISF machine, the benefits of implementing an ISF machine cannot merely be assessed in terms of cost. For instance, sinking a soprano pan, the deepest pan in the pan family, with a pneumatic hammer takes approximately 4 to 6[5] hours compared with 5 hours for ISF. Pneumatic hammering also subjects the user to high noise and vibration levels. Forming on the ISF machine allows the pan maker to attend to other jobs nearby while the dish is being formed. This is impossible with pneumatic forming. The ISF machine can be programmed to work within the forming limits [54] of the material so that fracture and consequent wastage is avoided. In pneumatic assisted sinking, preventing material fracture is highly dependent on the skill of the pan sinker. However, a pneumatic hammer may be kept to complement the ISF machine in periods when there is down time for maintenance or machine break down.

---

[5] This time estimate includes stoppage time for resting.

3.11 Conclusions

- Material springback in ISF dishes formed could be mitigated by the use of a backing plate. However, the effect of a backing plate was more effective in minimizing the springback which occurred in the region nearest the rim of the bowls. Springback in most part of all the dishes measured did not exceed 2mm.

- The 304 stainless steel dishes were successfully formed using ISF but required slower feed rates during forming and solution treatment annealing in order to minimise distortion on trimming.

- The reduction in thickness by the incremental sheet forming of mild steel and 304 stainless steel bowls occurred in a small portion of the walls of the minipan dishes, closer to the rim, unlike the thickness reductions observed in traditionally formed and wheeled dishes in which there was stretching throughout most part of the walls of these dishes.

- Multi-pass forming (double and triple) resulted in minimal extension of the stretched zone in ISF minipans, therefore only a single pass may be necessary when forming pan dishes.

- The maximum thickness reduction obtained in the ISF bowls agreed closely with the sine law of thickness reduction. However, the reduction in thickness in the ISF bowls may or may not be suitable for pan tuning and therefore further investigation is recommended.

- The break even analysis indicated that minipans and full size tenor pans could be profitably and competitively produced by pan making processes which applies ISF for pan dishing. However, the overall profitability of the pan making process could be jeopardised by the tuning stage.

Chapter 4 Vibration studies I: Full size steelpans

4.1 Introduction

This chapter presents the findings of two preliminary investigations. A pair of 4ths and 5ths soprano steelpans, one paint-coated and the other chrome-plated, was provided by pan maker Aubrey Bryan for use in this work. The first investigation was a mode study of the pans in which natural frequencies, modal damping and mode shapes were extracted. Mode frequencies and damping were extracted from the paint-coated pan while the chrome plated pan was used primarily for the extraction of mode shapes which was provided courtesy of Polytec Ltd. The second investigation was a detuning experiment in which a pair of notes on the paint-coated pan was subjected to repeated hammer impacts in an effort to determine tone stability i.e. the ease with which the fundamental mode frequencies in these notes could be detuned.

4.2 Modal Testing: Basic theory and assumptions

Since modal testing will be used on several occasions throughout this work it is appropriate to introduce and describe it at this stage so as to avoid unnecessary repetition throughout the dissertation.

Modal testing is the process of extracting modal parameters (natural frequencies, mode shapes and material damping) from measured vibration data so as to describe the dynamic behaviour of a structure. However, before conducting a modal test four assumptions are made about the test structure:

1. It is assumed that the behaviour of the test structure is linear. The response of the mechanical system to external excitation forces acting simultaneously follows the principle of superposition.
2. The test structure's dynamic behaviour and the entire measurement set-up system is time invariant.
3. The test structure is observable in that measured outputs yield sufficient information to construct a reliable mathematical model.
4. Finally, the structure honours Maxwell's reciprocity principle. This means that the measurement and excitation point are exchangeable.

The mathematical foundation and the test procedure(s) for conducting modal testing is documented in texts such as Ewins [182]; Heylen *et al.* [183], He and Fu [184] and Maia *et al.* [185]. A structure's dynamic behaviour can be described using a spatial model in which the physical characteristics of the structure are represented in terms of its mass, stiffness and damping properties. These characteristics can be described by linear second order differential equations:

$$[M]\{\ddot{x}\}+[C]\{\dot{x}\}+[K]\{x\}=\{f\} \tag{4.1}$$
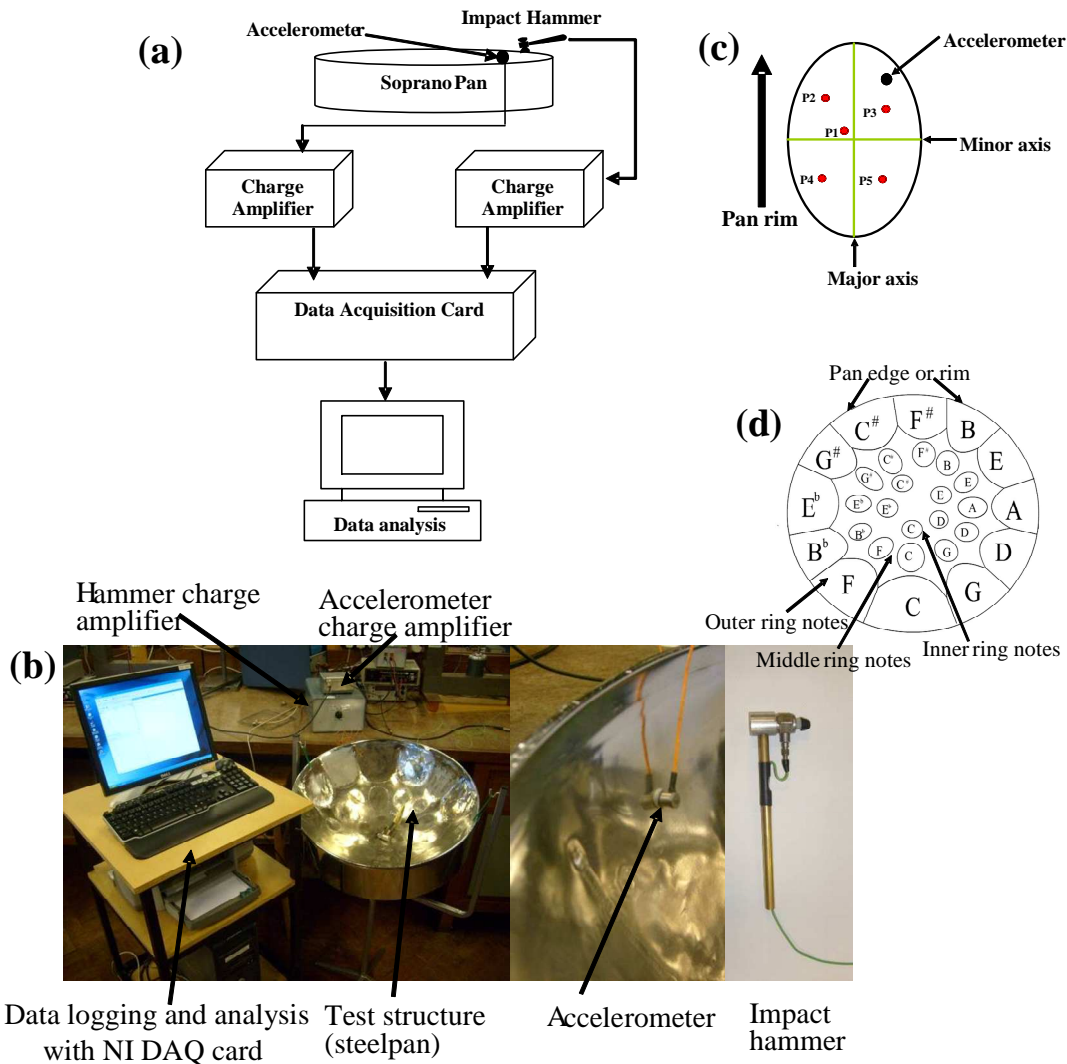
Figure 4.1: **(a)** and **(b)** Experimental arrangement and apparatus; **(c)** impact points used in modal tests and **(d)** note pattern of soprano pan used in modal tests

where *x* and *f* are the time varying displacement and external applied force vectors. *M* is the mass or inertia matrix, *C* is the viscous damping matrix and *K* is the stiffness matrix. The modal model is defined by a set of natural frequencies with associated damping factors and ratios and corresponding vibration mode shapes. The modal model is fully described by a matrix of frequency

response functions, $H(\omega)$, which are obtained by calculating the ratio of the response $\ddot{X}(\omega)$ to the input signal $F(\omega)$ in the frequency domain.

Since an accelerometer was used in the impact tests the response measured was acceleration and therefore the transfer function is referred to as an accelerance transfer function and is given as:

$$A(\omega) = \frac{\ddot{X}(\omega)}{F(\omega)}$$

                                                                                                      4.2

In subsequent chapters of this thesis a scanning laser vibrometer was used to measure the velocity response. The transfer function would be a mobility transfer function $H(\omega)$ and is expressed as:

$$H(\omega) = \frac{\dot{X}(\omega)}{F(\omega)}$$

                                                                                                      4.3

4.3 Extraction of mode frequencies and damping

Impact modal testing was used to extract the important mode frequencies, damping and mode shapes from the notes of a soprano steelpan. The experimental arrangement is shown in Figure 4.1a and b comprised of a paint coated soprano pan (not the one shown here); an instrumented impact hammer, a small lightweight (1.5g) accelerometer; charge amplifiers and a data logging computer provided with software for modal analysis. The note pattern of the soprano pan used is shown in Figure 4.1d. Impact modal testing was conducted only on the notes on the outer and middle rings. The notes on the inner ring were damaged and were therefore not used.

Vibration response was measured by the lightweight accelerometer which was attached to the surface of the note using a thin layer of beeswax. Both signals from the hammer and accelerometer were buffered by suitable charge amplifiers before being fed through a data card to the PC. Data logging was typically done for a time long enough to capture the decaying response of the test structure. The sampling frequency and logging time were 5 kHz and 2s respectively. These signals (Figure 4.2a and b) were also checked to insure that there were no leakage or clipping and truncated or clipped signals were discarded. Both signals are transformed to the frequency domain using an FFT. This Fourier transformation is a dedicated algorithm to determine the spectral content of the digitized time signal

The frequency response function (FRF) for each input/output measurement was calculated and averaged for 5 trials. Taking several trials allowed for the coherence function to be calculated, which is an indication of the quality of the measured FRF. The coherence function $\gamma^2(\omega)$ at each frequency point is defined as:

$$\gamma^2(\omega) \equiv \frac{\left|S_{xy}(\omega)\right|^2}{S_{xx}(\omega)S_{yy}(\omega)}$$

4.4

where S_{xy} denotes the cross-correlation between the input and the output while S_{xx} and S_{yy} respectively denote the auto-correlation functions of the input and output signals. Coherence gives a measure of the linearity between the input and the output: values close to unity on a linear scale (or zero on the log scale) indicate adequate linearity (see Figure 4.2c)..
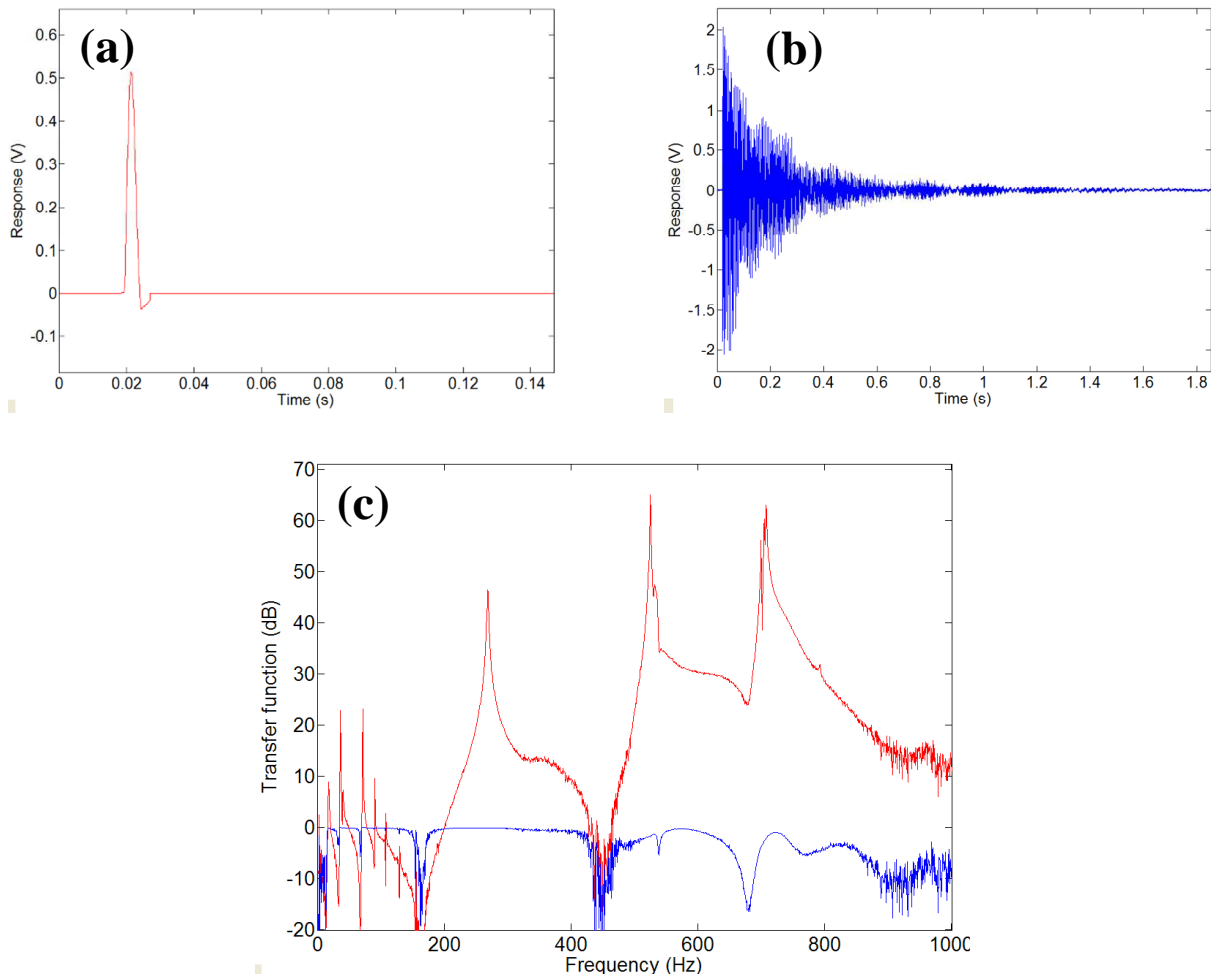
Figure 4.2: (a) Impact spectrum; **(b)** Response spectrum and **(c)** Typical steelpan note Transfer Function with associated coherence (in blue)

A grid of five points as shown in Figure 4.1c was used for the impact test. The accelerometer was positioned such that it was offset from the minor and major axes of the notes. This was done because the nodal lines were highly likely to be located along or in close proximity to these axes. The response of the note was then determined by tapping on the grid with one point being approximately at the centre and the other four impact points were located in the four sectors created by the intersection of the minor and major axes (see Figure 4.1c). Each point was approximately 15mm away from both axes.

Damping measurements throughout this dissertation are reported using the quality factor 'Q' which gives a measure of modal damping. Figure 4.3 illustrates the difference in Q-factors between structures that are heavily and lightly damped. For light damping the Q-factor is related to the loss factor η and the damping ratio ζ by the following expressions:

$$Q = \frac{1}{\eta} = \frac{1}{2\zeta}$$ **4.5**

Damping measurements were extracted using the circle fit of the Nyquist plot. Figure 4.4 shows the use of the circle fitting technique. The Nyquist plot which requires consideration of the frequency range in the immediate vicinity (Figure 4.4b) of the resonance peak is better suited for structures with high damping as a sufficient number of points in the vicinity of the resonance peak can be obtained for the construction of the Nyquist plot. However, there were sufficient data points in the vicinity of the resonance peaks for the response functions of the steelpan notes to enable reliable circle fitting. Further on in this dissertation another curve fitting technique for damping estimation termed Sonogram will be introduced. For structures that are very lightly damped the sonogram analysis offers a better alternative as there is an insufficient number of points in the vicinity of the resonance peak to allow a circle fit to be used that would provide reliable estimation of damping. The sonogram algorithm allowed the damping of several modes in a desired bandwidth to be obtained simultaneously as compared with circle fitting of the Nyquist plot in which the damping can only be determined for one resonant frequency at a time.
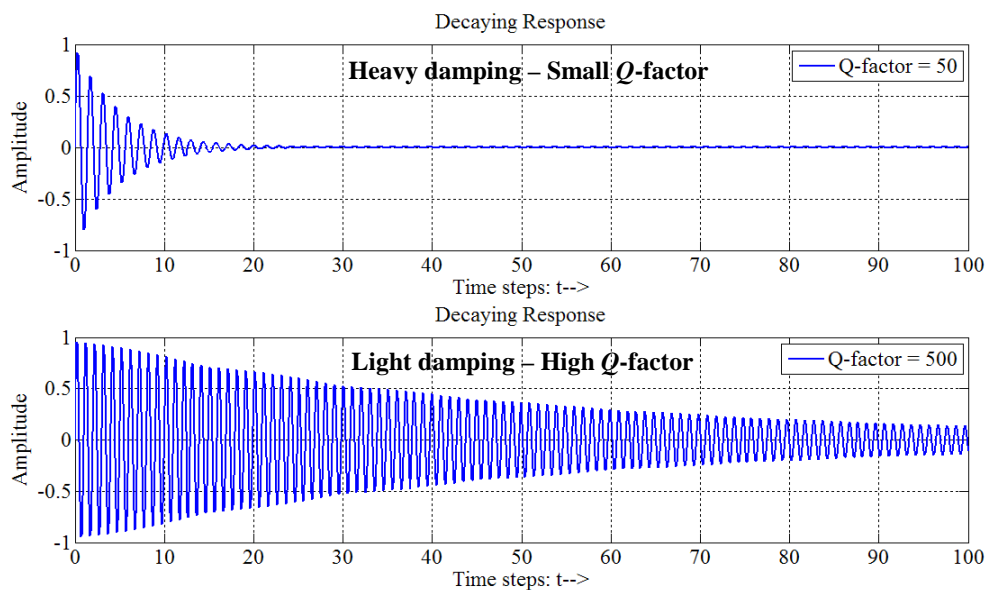
Figure 4.3: Quality factor comparison to illustrate the difference between heavily and lightly damped structures: A high Q-factor means higher quality and lighter damping where vibrations take a longer time to subside.
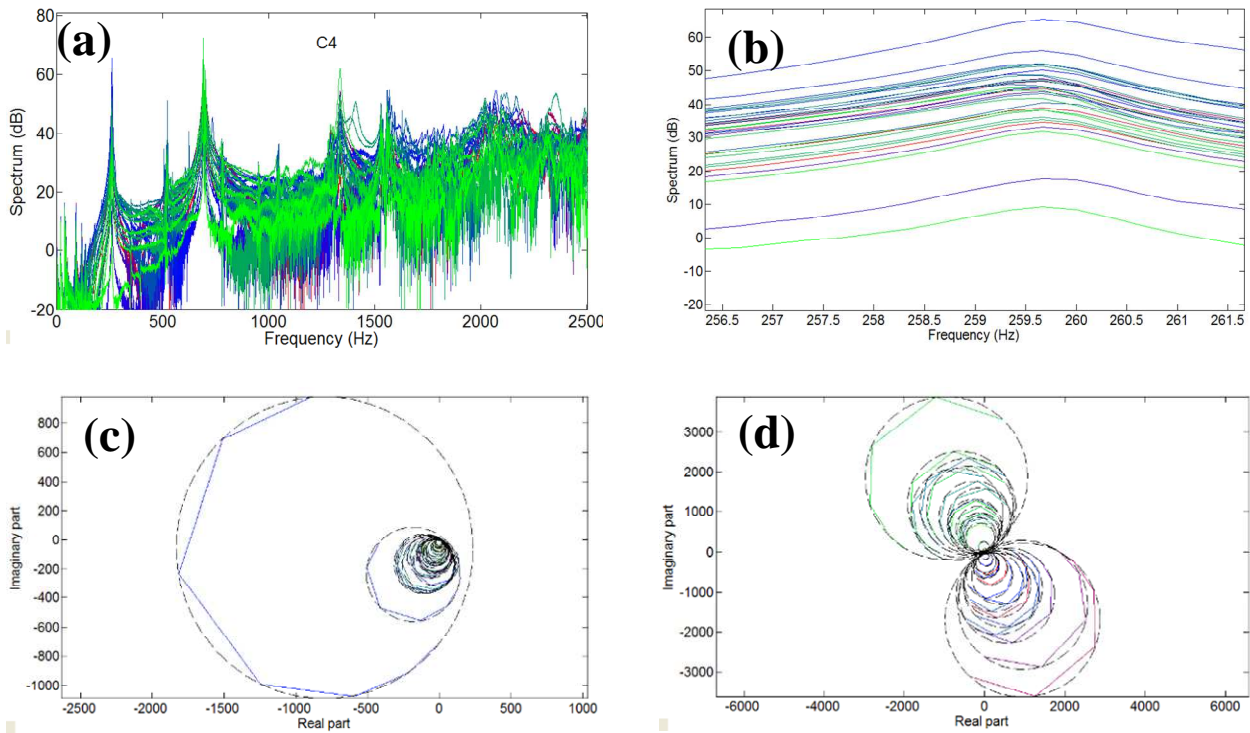
Figure 4.4: **(a)** FRF for the C note on the outer ring **(b)** Bandwidth in the range of the first tuned mode of the C4 note; **(c)** and **(d)** Nyquist plots with circle fits for first and third tuned modes at 260Hz and 691Hz respectively.

4.3.1   Mode frequencies and damping – paint coated pan

The frequency response functions of the C notes on the outer and middle rings on the paint coated pan are used to highlight features which were common among the notes investigated. Figure 4.5a and b show the transfer functions for the C notes on the outer and middle rings respectively (see Figure 4.1d). For the C note on the outer ring (Figure 4.5a) there are at least seven modes and at least three modes in the C note on the middle ring (see Figure 4.5b). Not all of these modes are tuned modes. Typically, the first three modes of the notes on the outer ring are tuned, while only one or two modes in the notes of the middle ring are tuned. Figure 4.5c shows the second and first mode frequencies f_1 and f_2 in the outer notes C_4 to B_4 are tuned in the ratio of approximately 2:1. The third mode frequency f_3 is not an integer multiple of f_1, but the ratio $f_3:f_1$ is approximately twice times a musical fourth 2(4/3). In the notes on the middle ring C_5 to B_5, mode frequencies f_1 and f_2 are not as near to frequencies on the Western musical scale as those on the outer pan ring (see also Table 4.1).
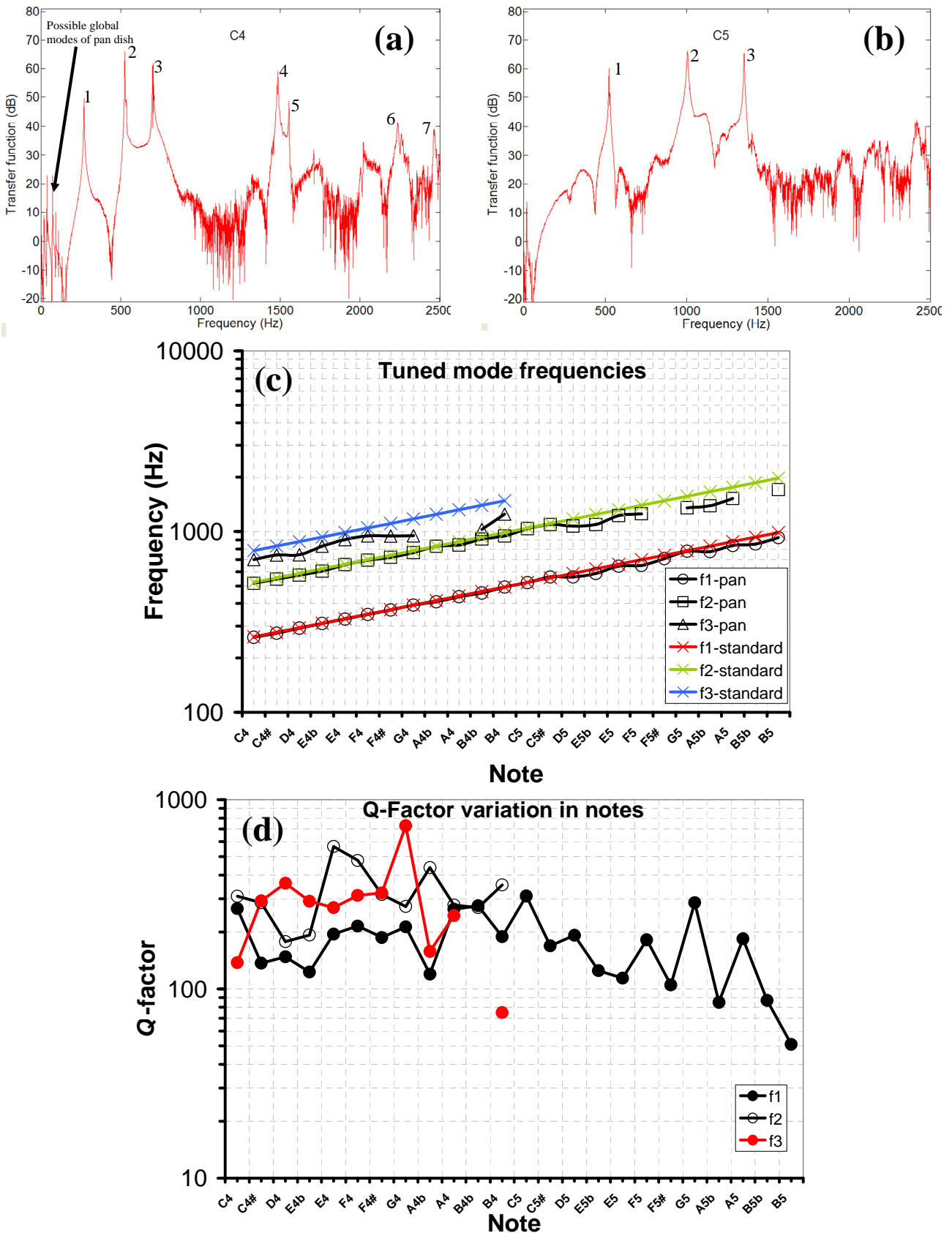
Figure 4.5: Transfer functions for **(a)** C note on outer ring and **(b)** C note on middle ring; **(c)** comparison between tuned frequency and frequencies on the Western Musical Scale and **(d)** *Q*-factors in measured notes for paint coated soprano pan

The modes in Figure 4.5a and b display light damping and this light damping with low modal overlap was common among the 24 notes measured. Figure 4.5d is a plot of the *Q*-factors for the inner and outer notes of the paint coated pan. *Q*-factors were in the range of 50 to 800 with the majority being in the range of 100-300. Another interesting feature of the response function of the steelpan note is highlighted in Figure 4.5a. This feature is indicated by the arrow which points to resonance peaks in the low frequency range of the response. These peaks were particularly predominant in the FRF of the outer notes. Suggestions to what these peaks represent will be highlighted in the discussion.

Table 4.1: Comparison of measured note frequencies on a soprano pan with standard frequencies on the Western musical scale based on A440Hz					
	Outer Notes		**Outer Notes**		**Middle Notes**
Note	**Fundamental**		**Octave**		**Fundamental**
	Standard (Hz)	**Pan (Hz)**	**Standard (Hz)**	**Pan (Hz)**	**Pan (Hz)**
C	**261.7**	259.6	**523.3**	517.9	522.3
C#	**277.2**	273.8	**554.4**	546.3	561.2
D	**293.7**	291.8	**587.4**	574.3	560.6
Eb	**311.2**	309.8	**622.3**	603.8	585.0
E	**329.7**	328.4	**659.3**	655.4	644.1
F	**349.2**	348.3	**698.5**	693.5	650.1
F#	**370.0**	367.6	**740.0**	719.7	709.3
G	**392.0**	391.5	**784.0**	766.2	778.3
Ab	**415.3**	408.7	**830.6**	828.3	774.5
A	**440.0**	436.4	**880.0**	843.0	837.4
Bb	**466.2**	457.7	**932.3**	908.9	853.1
B	**493.9**	493.1	**987.7**	947.1	925.6
Note: mass loading effect of the accelerometer was found to decrease note frequencies by 1 to 3 Hz					

4.3.2 Investigation of mode shapes – chrome plated pan

Mode shape measurements of steelpan notes was done courtesy of Polytec Ltd. The experimental set-up is shown in Figure 4.6a. The chrome plated soprano pan was mounted on an open chassis frame and foam wrapping was used to isolate the pan periphery from the frame surface. The surface of the pan was coated with a thin dusting of chalk powder (developer spray) to reduce light reflection and improve the reflection of the laser beams to the scanning heads.

Excitation was provided from a loudspeaker suspended beneath the pan. A periodic chirp signal was used to provide excitation and the response of the pan was measured using a Polytec 3-Dimensional scanning vibrometer laser system which comprised of three individual lasers or sensor heads that measured the surface velocity from different directions.
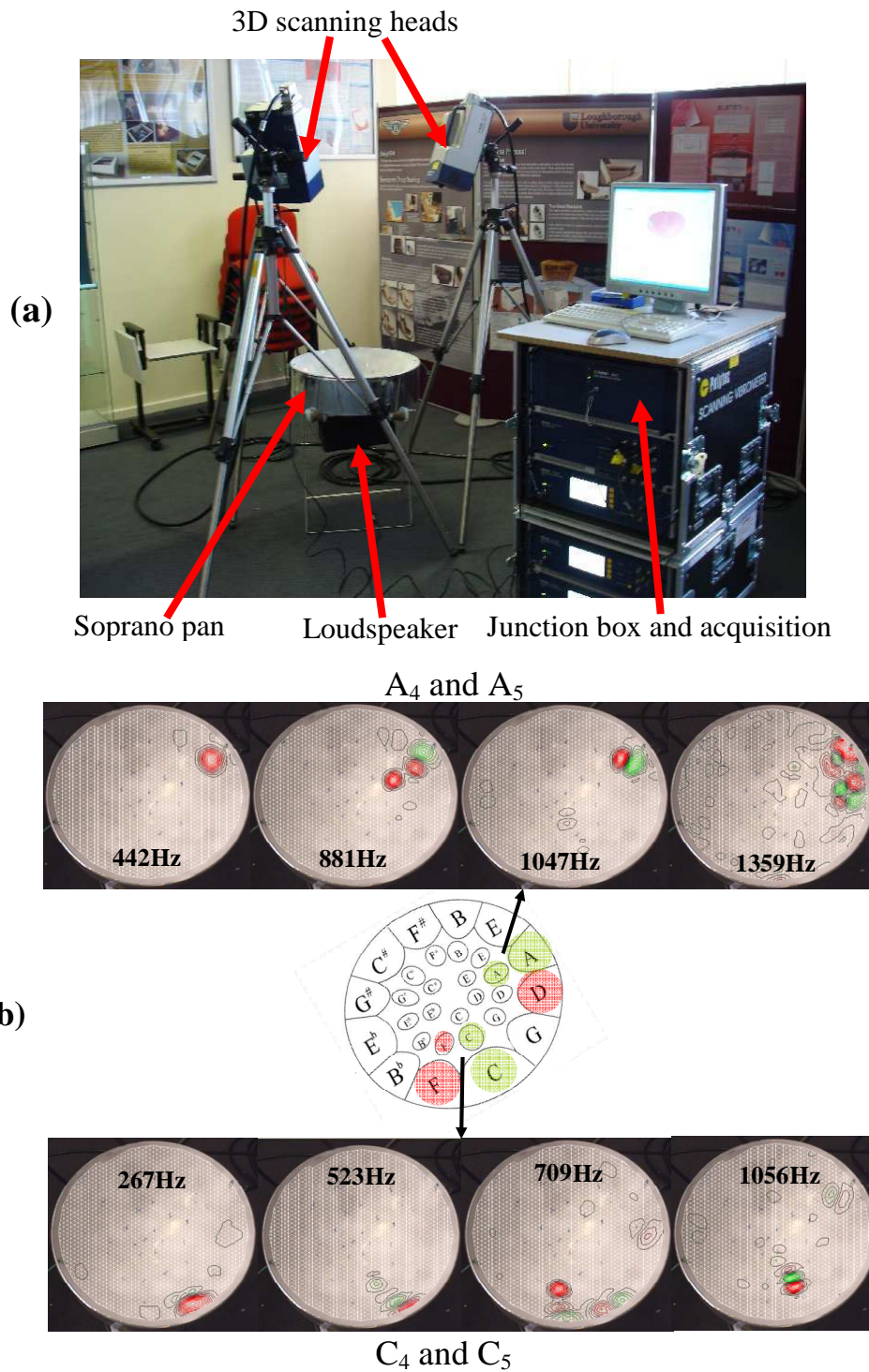
Figure 4.6: (a) Polytec 3D scanning laser vibrometer for mode shape determination and **(b)** operating displacement shapes for A and C notes on chrome plated soprano pan

This allowed extraction of motion components along three perpendicular directions. The settings for the 3-Dimensional scan were for a frequency bandwidth of 5kHz with a resolution of 1.5625Hz (3200 FFT lines), measuring 7420 points with 5 averages. The acquired vibration data was used to prepare animations of operating displacement shapes for each of the note regions on the pan surface. Only mode shapes in the frequency range up to 1400 Hz were provided by Polytec Ltd.

Mode shapes of steelpan notes are widely published and the mode shapes measured were identical to published mode shapes of notes on a soprano pan [139,140]. This can be seen by a sample of the mode shapes from the chrome plated pan in Figure 4.6b for the A and C notes on the outer and middle rings. The first mode of each note involves movement of the entire region whereas the second and third modes have nodal lines that lie along the circumferential and radial directions of the pan dish respectively. Notable is the confinement of the modes to the vicinity of the note. However, in some cases, there is coupling of modes in adjacent notes which have natural frequencies that are near to the main note being excited. For instance at 709Hz (Figure 4.6b), the second and first modes of the F_4 and F_5 notes respectively are excited when the C_4 note resonates at its third natural frequency. Also, at 1359Hz (Figure 4.6b), the A_4 note resonates with a mode that has a pair of circumferential nodal lines while the adjacent D_4 note resonates at a mode which has a circumferential and a radial node line.

4.4　Note Detuning

After measurement of modal parameters on the soprano pan, a pair of notes, the D_4 note on the outer ring and the G_5 note on the middle ring (see Figure 4.1d) of the soprano pan were selected for the detuning investigation. These notes were chosen because their fundamental frequencies were relatively in good tune compared to some of the other notes (see Table 4.1). Detuning in this work was taken to be shifting (increase or decrease) of the fundamental mode frequency from its tuned frequency.

An electromechanical alarm bell was modified for use in this work. Figure 4.7 shows the arrangement in which the round head of a bell clapper is replaced with a hard-rubber tip impact head which is mounted at the end of a threaded shaft and positioned normal to the note surface. The shaft of the impact head is instrumented with a force sensor whose signal was buffered through an appropriate charge amplifier. The frequency of the impacts was controlled using the control box to which the alarm-bell main frame was connected. The alarm-bell main frame was also powered via the control box. The impact force was controlled by adjusting the distance between the impact head and the note surface. In this work, a force level that is comparable to that in normal steelpan playing was used for the detuning tests (see Figure 4.8d).

The impact hammer used for the frequency response measurements had an identical tip as the one to be used in the detuning investigation. Figure 4.8d shows three levels of force that are within the normal playing range. The force level of impact for detuning was adjusted to be within this range. It was found that a distance of approximately 10mm between the impact head and the note surface was sufficient to maintain impact force that was comparable to normal steelpan playing. Figure 4.8a

shows the impact spectrum during the detuning exercise. Here the frequency of the impact was measured as 14Hz. A closer look at one of the peaks (Figure 4.8c) shows what appears to be double peaks. However, the peak labelled 1 represents the impact between the impact head and the note surface while the peak labelled number 2 is the force experienced by the shaft as the impact head overshoots its rest position on rebound from the note surface.
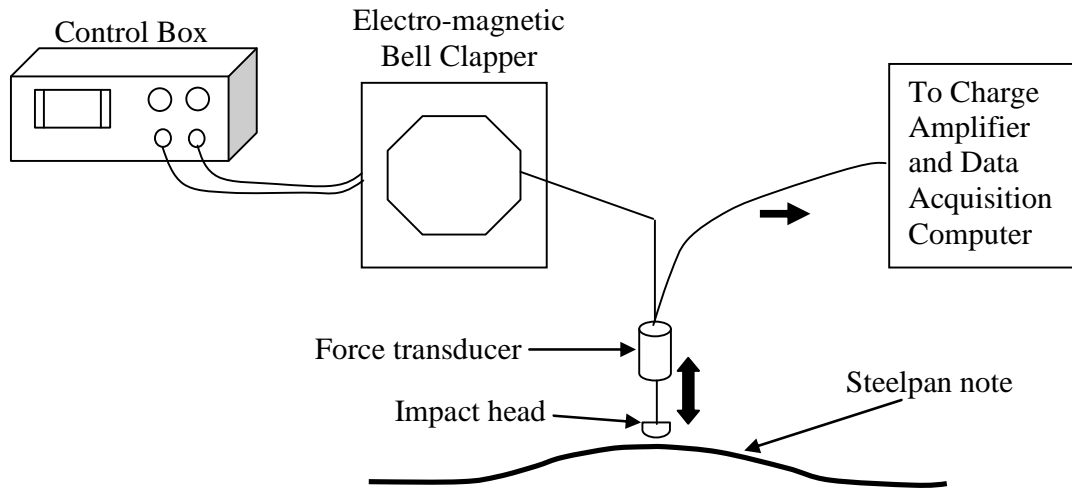
Figure 4.7: De-tuning apparatus arrangement

For both notes used, five regions on their surfaces were chosen for the detuning exercise. One region was at the centre while the other four were located approximately 20mm along the major and minor axes of the note from the centre. Before beginning the detuning impacts, the frequency response function of the note was measured for five averages using a logging frequency and acquisition time of 5 kHz and 2s respectively with a small accelerometer located at position P3 and impact delivered in the vicinity of P1 (see Figure 4.1c). Each region of the note was to be impacted for 360 minutes with the first region of impact being the centre position of the note. Frequency response function measurements were made at intervals of 30 minutes and all tests were conducted at room temperature. The frequency response function of another note on the outer ring – F4 – was measured at the same intervals of 30 minutes when testing each note. This was done to ensure that any changes detected in the note under repeated impact would have been the result of the impacts only. Tests were conducted over several days and to ensure that the same impact positions were maintained, the surfaces of the notes under test were highlighted with a thin film of chalk dust.
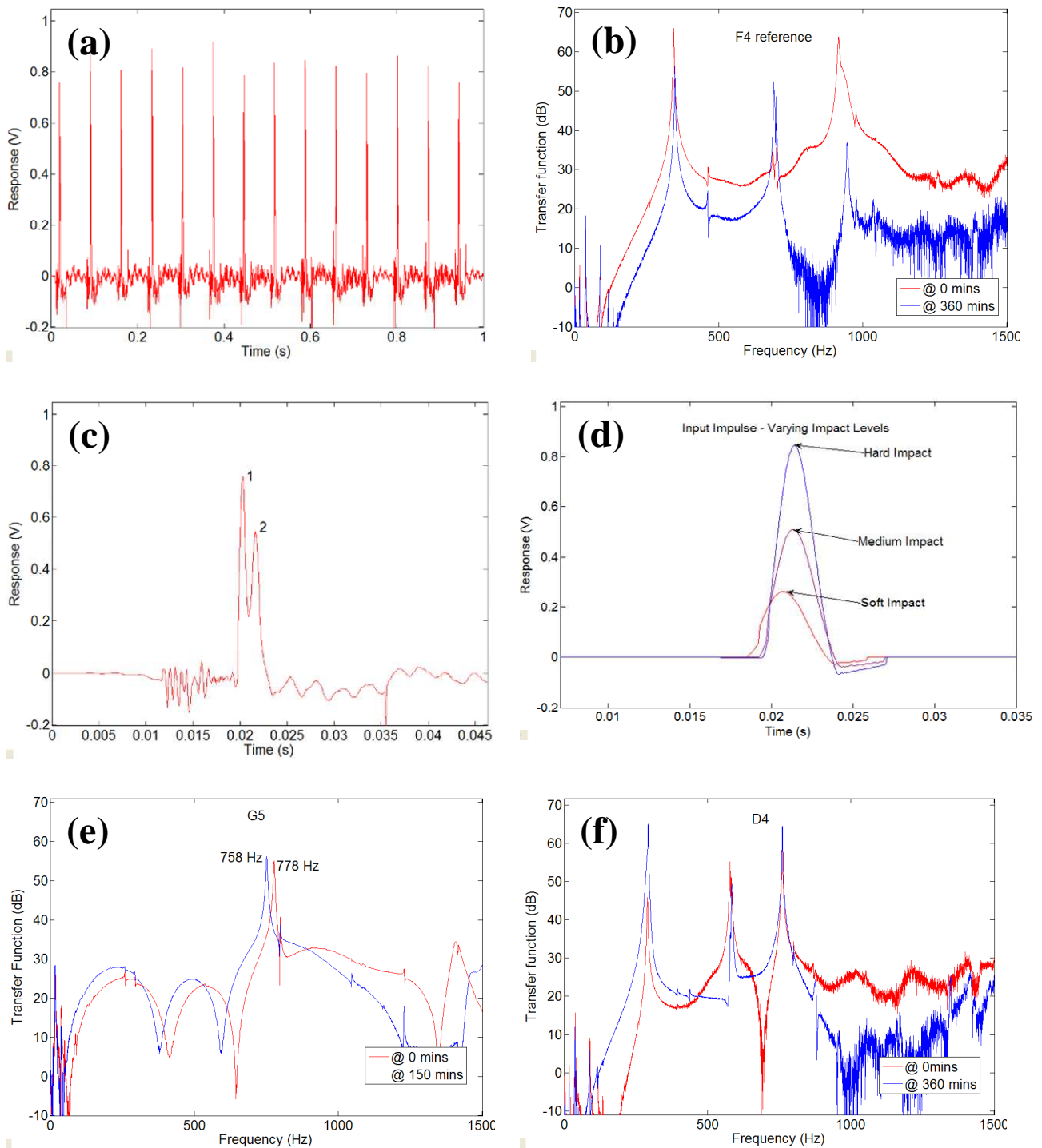
Figure 4.8: (a) Multiple hammer impacts; **(b)** reference note FRF; **(c)** Single impact from (a); **(d)** Varying impact levels for normal playing; **(e)** Middle G note FRF before and after detuning and **(f)** Outer D note FRF

4.4.1   Results: Note detuning

Figure 4.8e and f shows the response spectrum for G5 and D4 respectively. D4 showed no sign of detuning after being subjected to 6 hours of impact in the 5 selected regions. Its fundamental frequency along with its other tuned mode frequencies remained unchanged (see Figure 4.8f). The fundamental mode of G5 was detuned after impacting the centre of the note for 150 minutes (see

Figure 4.8f). Since this detuning was discovered only after 150 minutes of continuous impact, the actual instance of detuning would have occurred between the 120 minute and 150 minute interval. The frequency response of the detuned G5 notes exhibited a frequency decrease of 20Hz (from 778Hz to 758Hz) in the fundamental mode, almost a semi-tone (see Figure 4.8e).

4.5 Discussion

There are numerous works on the investigation of steelpan mode shapes. The majority of these studies predominantly researched the natural frequencies and mode shapes of notes in various steelpan types [139,140,143]. However, although the first section of this chapter was dedicated to the vibration studies of a pair of full size soprano pans, this work was in no way an attempt to merely reproduce mode shapes and natural frequencies. One objective was to focus on details on which little or no attention was directed to in previous studies with the aim of defining a scope for further work in this thesis. One such detail is that of mode confinement. The mode shapes of the chromed soprano pan, provided courtesy of Polytec Ltd, revealed the modes to be mainly confined to the vicinity of the note regions. In Chapter 2, previous studies were identified as mainly focusing on perturbation of note geometry to achieve mode tuning without any consideration of mode confinement in the instrument. Impact tests on a paint coated soprano pan revealed tuned modes to be lightly damped with Q-factors lying mainly in the range of 100 to 300. Further study in this work considered mode confinement and vibration damping in steelpans. Chapter 5 is primarily dedicated to the study of mode confinement. In Chapter 5 the influence of the bowl curvature on mode confinement is investigated in test structures that replicate the geometry of steelpan notes. Chapter 6 is mainly devoted to material damping where the influence of the steelpan making process on material damping is researched.

Other important features of the steelpan are highlighted in Figure 4.5. One feature is highlighted by the arrow in Figure 4.5a which points to resonance peaks in the low frequency range of the C note on the outer ring. These resonance peaks could be a combination of rigid body modes and global modes of the pan dish. Recall the steelpan was supported in its usual playing position i.e. by suspending with elastic cords from its stand. This configuration inevitably approximated a free-free condition of the pan dish. Then the appearance of rigid body mode frequencies in the response function is expected. However, the author is unaware of any previous work that directs attention to this feature of the steelpan note frequency spectrum. The extent to which these rigid body and particularly global modes affect the dynamics of the steelpan may be related to the stiffness of the joint connecting the pan dish to the side or skirt. Pans are predominantly produced from used oil drums in which the top of the drum is connected to the side by means of a seam roll (see Figure

3.13). Only recently, some pan makers are welding the forming blank to the side (Figure 3.13). The effect of the joint type on the dynamics is recommended for further study. Another feature of the response spectrum is highlighted by the numbering of the response peaks in Figure 4.5a. The first three response peaks correspond to the tuned modes of the steelpan note. However, the other peaks numbered 4 to 7 could also be modes that are confined to the note vicinity. These higher frequency modes may also be global modes of the pan dish. Some tuners who claim that they are able to tune more than 3 modes in their pan notes may not be tuning more modes but may be confining more modes which would undoubtedly enhance the tone of their instruments. This claim of being able to tune more than three modes is yet to be proven.

Note detuning was another focus of this work. The effect of impact on tone stability was examined for the G note on the middle ring and the D note on the outer ring of the paint coated pan. Detuning could be defined as a shift (increase or decrease) in the fundamental frequency of a note from its tuned frequency. Although other modes could be detuned, detuning is more likely to be detected when there is a shift in the fundamental frequency. Also, steelpan notes are usually played by impacting close to the centre of the note. Recall in Chapter 2, the fundamental frequency of a note is typically tuned by arching the note at its centre. Therefore any adjustments to the arch height would inevitably result in detuning of the fundamental mode frequency. This is probably why it was relatively easy to detune the G note by continuous impact at its centre. Although measurements of the arch height before and after detuning were not recorded, frequency shifts are highly sensitive to very minute (fraction of a millimeter) changes in the arch height of the note (Chapter 2). Therefore impacting at the note centre may have altered the height of the arch which led to the frequency shift of 20Hz in the G note.

Detuning may be a direct consequence of heavy impact that results in immediate "*de-arching*" or "*flattening*" of the note. However, detuning might also be due to creep or fatigue. Creep is plastic straining that occurs at relatively constant stress while fatigue requires the presence of cyclic stresses. In this work, detuning or alteration in the arch height in the G note on the middle ring might have occurred by creep deformation as relatively constant impact stresses were used. If creep was the mechanism by which detuning occurred then the detuning could be described as time dependent as creep is a time dependent failure mode [48]. The D note on the outer ring showed no sign of detuning which may indicate that the impact stress levels were either too low to cause any creeping or longer exposure to impact may be needed for any detuning to be realized. For further work, it may be useful to compare normal pan playing stresses with stresses used during note tuning. In reality, steelpan notes would be subjected to various levels of impact playing stress over their useful lifetime. These stresses may be cyclic in nature and may also be below the material

yield stress. It may be possible that the mechanism of detuning in this case may be instead due to fatigue degradation of the material. Fatigue is usually accompanied by the presence of micro-cracks [48] which may or may not be visible. It is also likely that detuning may be due to a combination of yield, creep and fatigue degradation.

Steelpans are usually chrome plated to increase corrosion resistance in addition to enhancing the aesthetic appearance. However, electroplating is known to increase tensile residual stresses in addition to the formation of micro-cracks [186]. Both degrade fatigue resistance [186], and steelpans that are chrome plated may be more susceptible to detuning by fatigue. It is also known that during chrome plating, hydrogen may be introduced into the base metal making the material liable to hydrogen embrittlement in addition to increasing residual stresses [186]. While the effects of hydrogen embrittlement and residual stresses are mitigated by post heat treatment of the chromed parts at 400ºC [186], it is not certain whether this post heat treatment of chromed steelpans currently occurs.

In this work, the effect of temperature on tone stability was not considered although it is well known that detuning is a common occurrence in steelpans after airline transportation or playing in extreme temperature conditions. The effect of low temperatures on detuning could be investigated by storing the pan in a temperature controlled refrigerator and measuring the response spectrum of several notes at various time intervals. These measurements could also be taken from a pan that is kept outside on a hot day. Non-contact methods may be used to measure frequency response, surface temperature and surface topography of several notes. Residual stresses might also influence tone stability since each stage of the pan process (sinking, heat treatment, surface peening i.e. tuning and chrome plating) introduces residual stresses [186]. Residual stresses are known to decrease over time [186] and pans may detune slowly at room temperature without being subjected to any impact cycles. A better understanding of the influence of impact, creep, fatigue and residual stresses on detuning is not expected to eliminate detuning. Detuning of the instrument at some stage is inevitable. This knowledge would assist in the making of pans with enhanced tone stability.

4.6 Conclusions

- Mode shapes observed on a soprano pan were consistent with mode shapes published in previous vibration studies on steel pans.
- Modal damping (Q-factors) for the tuned modes of a paint coated soprano pan was in the range of 50 to 800 with the majority of modes having Q-factors in the vicinity of 100 to 300.
- The dynamics of steelpan notes may be influenced by the dynamics of the dish on which they are situated.

- It was possible to detune the G note on the middle ring of a soprano pan after 120 minutes of impact at the centre while no detuning was achieved on the outer ring D note. The G note tuned frequency decreased by 20Hz.

- Note detuning may be more likely to occur by impacting a note at its centre.

- Creep deformation may be responsible for the detuning detected although further work to confirm this is recommended.

Chapter 5   Vibration Studies II: Mode confinement in test pans

5.1 Introduction

An important characteristic of steelpan notes is mode confinement or localisation of modes. This is a crucial element in the development and performance of the instrument. As discussed in Chapter 2, a steelpan note generally has two or three strongly confined modes with resonant frequencies that are coaxed into an approximate harmonic relationship. This is crucial to giving the instrument its pleasant tone. Some pan makers claim to tune more than the usual amount of modes. One such tuner in Dortmund, Germany [17] claims that he is able to tune four modes in the outer notes of his 4ths and 5ths soprano pans and up to three modes in the middle and inner notes.

A few researchers [14,15,150] have investigated the influence of note geometry on mode tuning in steelpan notes. However, Chapter 2 highlighted that the main focus of previous work was mainly on the manipulation of note geometry to achieve modal tuning and not specifically on mode confinement. An outstanding example of mode confinement can be seen by considering the musical saw. Chapter 2 discussed how modes are trapped by alteration of the blade curvature during playing. A similar mechanism of mode entrapment may be operative in steelpan notes since a 2D cross-section of the steelpan note geometry bears resemblance to the bowed musical saw. As discussed is Chapter 2, several steelpan note models do not take into account the bowl geometry or the note-boundary geometry. The work in this chapter primarily focused on the effect of the bowl curvature on mode confinement. This investigation began with the creation of test structures referred to as test-notes. These test-notes formed sections of larger structures referred to as test-bowls or test pans. Steelpan notes are flat or slightly concaved shells embedded in a dish [10]. The test-notes created in this work were an attempt to replicate this important feature of the steelpan note. This was one of the main deciding factors in the choice of geometry.

This study was conducted in two parts. The first part involved a comparison between vibration finite element predictions and modal tests of the test-note structures. The second and final part of this investigation considered the material damping in the test-notes with their test-bowls in free-free and clamped arrangements. Scott and Woodhouse [157] claim that damping in confined modes is governed mainly by acoustic and material damping. This investigation was done to confirm this claim.

5.2 Concept development

The concept behind the development of the test-bowl structure emerged from an analogy to the musical saw. Additionally, the test-bowl geometry had to be simple and the manipulation of the test-bowl curvature had to be conducted in a controlled manner and this is why incremental sheet forming (ISF) was used to manufacture the test structures. The test-bowl geometry is simply a bowl with a flat base (see Figure 5.3a and d). The flat base is referred to as the test-note (Figure 5.3c). Recall in Chapter 3, the use of ISF for the manufacture of minipan dishes. The relationship between the vertical radius R_v and the initial horizontal diameter D of a test-bowl is given by equation 3.1. This shows that the vertical radius of the test-bowl and by extension the curvature of the test-bowl could be manipulated by changing the initial draw angle or wall angle α. The curvature 'κ' of the test-bowl wall surrounding the test-note could be expressed as:

$$\kappa = \frac{1}{R_v} = \frac{2\sin\alpha}{D} \qquad\qquad \textbf{5.1}$$

As the draw angle α of the bowl increases the curvature increases (see Figure 5.1). The influence of increasing the draw angle is seen in **Table 5.1.** Here, the curvature of the bowl surrounding the test-note increases with an increasing draw angle. The influence of increasing bowl-wall curvature on the dynamics of the test-notes was investigated.

Table 5.1: Test-bowl geometrical parameters				
Test-bowl	Draw-angle α (degrees)	Initial Diameter D (mm)	Vertical Radius 'R_v' (mm)	Curvature 'κ' (mm^{-1})
1	20	260	380.1	**0.0026**
2	30	260	260.0	**0.0038**
3	40	260	202.2	**0.0049**
4	50	260	169.7	**0.0059**
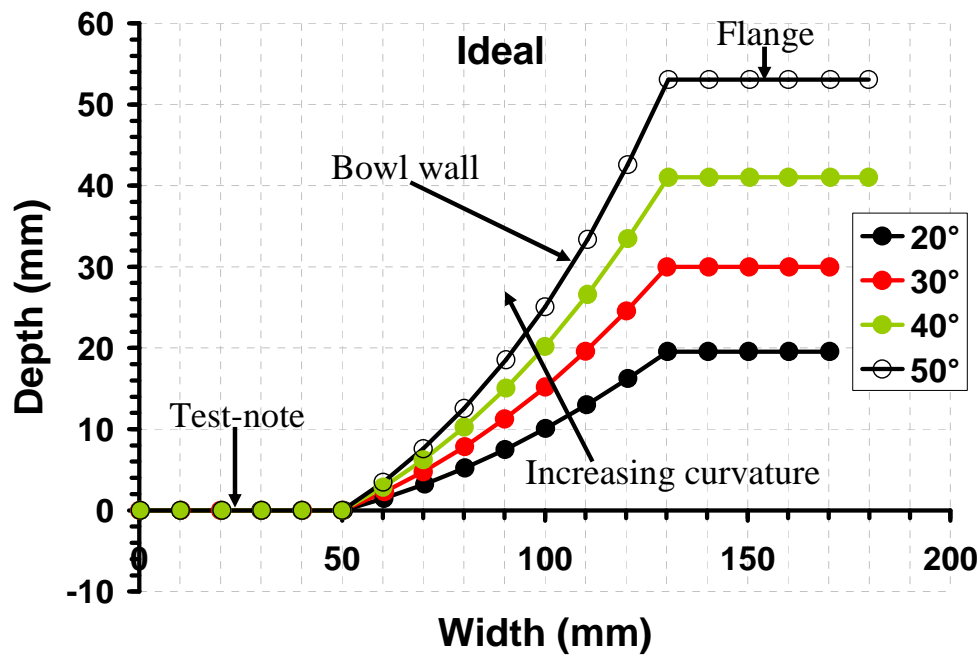
Figure 5.1: Increasing bowl-wall curvature surrounding test-note

5.3 Finite Element Predictions

Before manufacturing the test bowls, finite element models were developed to test the hypothesis of achieving mode confinement with manipulation of bowl curvature. The geometry of the bowls was easily reproduced using the CAD facility in ABAQUS® and an example of the meshed geometry of a test-bowl is provided in Figure 5.2. The FE analysis was conducted on four test-note models as listed in Table 5.1 each having different wall angles *'α'*, but the same initial bowl diameter *D* of 260mm and test-note diameter *d* of 100mm (see Figure 5.1 and Figure 5.3). The finite element mesh was constructed within the FE software package ABAQUS® (ABAQUS/Standard, version 6.7-1, 2007) [187]. The material properties applicable to the steel sections were defined within the model and the value used for low-carbon steel were Young's modulus, E = 200GPa; Poisson's ratio, v = 0.28 and density, ρ = 7800kgm^{-3}. In the model there are two '*fillet*' sections (see Figure 5.2): (1) where the flange meets the bowl and (2) where the bowl meets the test-note region. Constraints and boundary conditions were applied to the edges of the flange so as to suppress linear and rotational movements in this section. This constraint was also chosen as the manufactured test-bowls would also undergo modal testing with their flanges clamped.
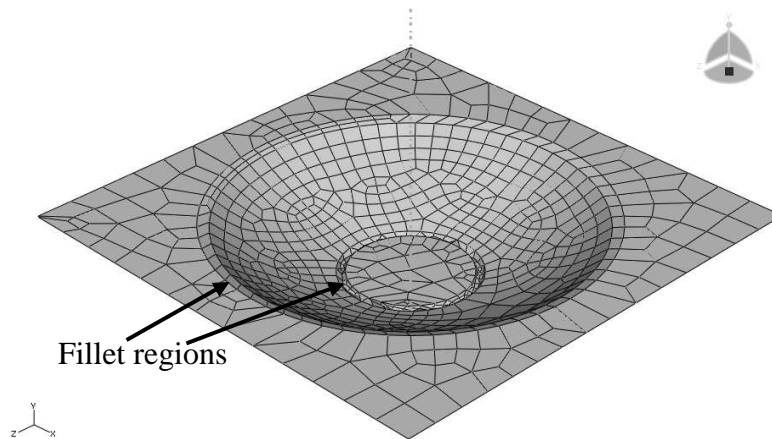
Figure 5.2: Finite element model of the test structure

5.3.1   Shell element selection

The choice of shell elements selected for the FE analysis is critical to obtaining reliable and accurate results. ABAQUS® offers a selection of conventional shell elements for thick and thin shell applications. There are guidelines that are applied when making a choice on shell elements for FE analysis. The use of shell elements is generally decided on by a rule of thumb. If the thickness of the structure to be modeled is less than 1/10 of a global dimension then the structure could be modeled using shell elements. In the case of the test-notes the ratios $t/D = 0.003$; $t/d = 0.009$ and $t/L = 0.002$ where t is the original thickness of the steel sheet used to form the test-bowls; D is the initial horizontal diameter of the test bowl and d is the diameter of the test note. Here all three ratios are < 0.1. The choice now becomes the type of shell element to use: thin shell or thick shell. The fundamental difference between using a thin or thick shell is the effects of transverse shear deformation. For thin shells the effects of transverse deformations are assumed to be small and are therefore neglected while the deformations cannot be ignored in thick shell applications. Another rule of thumb that is applied to assess the significance of transverse shearing in a shell is estimated by again considering the thickness to span ratio. If the thickness to span ratio is greater than 1/15 then the shell is considered thick and vice-versa. For the test structures in this work, the ratio of these dimensions were much less than 1/15 = 0.067 therefore thin shell elements were used to model the test-note structures in ABAQUS®. The thickness of the shells used in the FE study was applied through the section properties. Previous work on ISF [54] shows that the bowl-wall thickness varies with the sine of the draw angle. Therefore it was expected that the upper portion of the test-bowl nearest to the flange would be thinnest. However, since this thinning is about 23% of the original thickness in a small portion of the bowl wall (see Chapter 3), bowl walls were modeled using the original sheet thickness. In the other sections of the bowl – the flange and test-note regions, the original sheet thickness of 0.86mm was also applied.
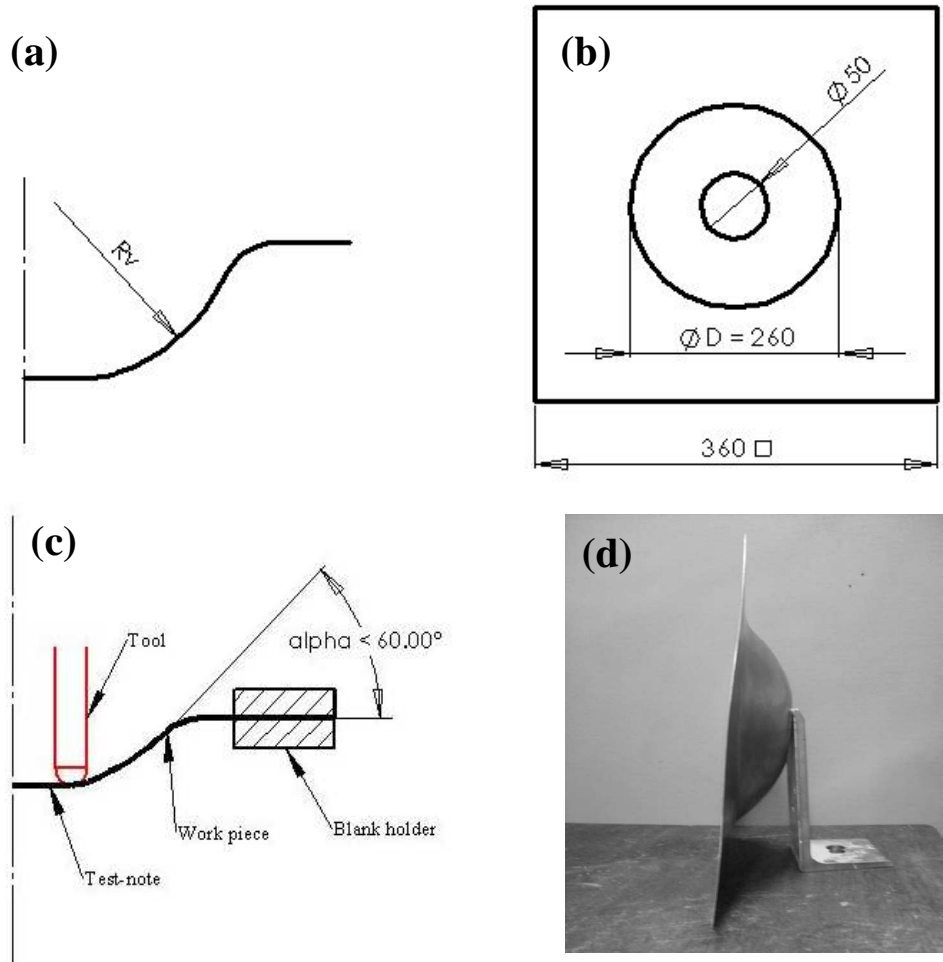
Figure 5.3: (a) Cross-section of test-bowl structure; **(b)** Plan view of test-bowl structure; **(c)** Schematic showing ISF of test-bowls; **(d)** a test-bowl used in the experiments (All dimensions in mm)

In ABAQUS® conventional shells are divided into several categories: small strain thin shells (STRI3, STRI35, S4R5, STRI65, S8R5, and S9R5), thick shells (S8R and S8RT) and general purpose (S3R and S4R). As mentioned previously, thin shells should be used if transverse shear deformation is negligible. However, in this work, in the event that there may be minor effects due to transverse shearing a general purpose shell was selected. Therefore the element S4R (see Figure 5.2) was used. The S4R element uses reduced integration which reduces the amount of time necessary for analyzing the model. Meshing is preceded by the application of local seeds to a selected region of the model. A seed is essentially the width of an element in the mesh grid. In this work, three models were produced for each test-bowl each having local seeds of 5mm, 10mm and 15mm applied to the edge of the flange in order to create the part mesh. This was done to determine the sensitivity of the structural modes to mesh refinement.

5.4 Manufacture of the test-bowls with test-notes

For experimental modal tests, four test-bowls were manufactured using the process of single point ISF – a novel sheet forming process that was used in Chapter 3 to produce mini-pan dishes. A spherical-head tool of radius 7.5mm was used to construct the test-bowls. Axis feeds used were $x = 40\text{mms}^{-1}$, $y = 40\text{mms}^{-1}$ and a z axis acceleration $= 20\text{mms}^{-2}$. The test-bowls were formed in a single pass and had the wall angles $\alpha = 20°$, $30°$, $40°$ and $50°$ respectively. All bowls were manufactured from 360mm x 360mm x 0.86 mm low-carbon steel sheets. The test-note radius of each bowl measures $50\pm1\text{mm}$ (see Figure 5.3b). `

5.5 Experimental Modal Analysis

5.5.1 Measurement set-up

The measurement set-up for experimental modal testing is shown in Figure 5.4a and has three major components which include the supported test-structure, the excitation device and the response measurement device. Prior to any modal testing retro-reflective powder was applied to the test regions of the test-bowl (see Figure 5.4b). This was done by moistening the test surface with a thin film of water and sprinkling the powder on to the surface where the moisture adheres the powder particles to the surface. This procedure increases the reflectivity of the target surface which in turn increases the signal to noise (SNR) by increasing the amount of light returned along the path of the incident beam to the laser vibrometer scanning head.

Each test specimen was supported by clamping at its corners as shown in Figure 5.4b. Clamping the test structure in this manner should not affect the reliability of the frequency response function (FRF) measurements as the confined modes should be unaffected by the boundary conditions at the ends of the sheet which means that damping [157] should be governed solely by internal dissipation in the material and radiation damping [157,188]. However, this finding by Scott and Woodhouse [157] will be tested further on by comparing the material damping measurements in test-bowls supported in free-free and clamped conditions. See Figure 5.4c for the free-free configuration.
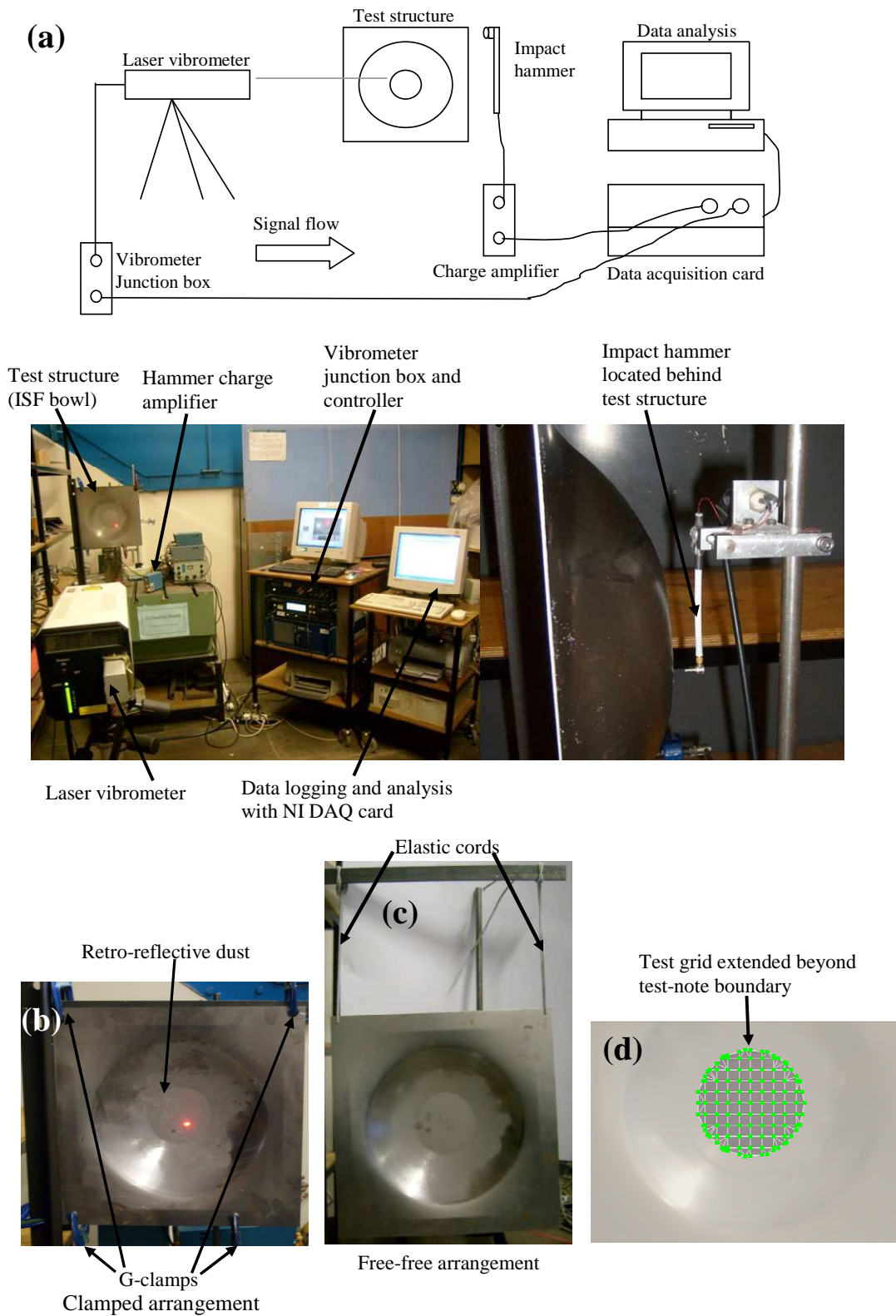
Figure 5.4: (a) Test set-up with laser vibrometer; (b) and (c) clamped and free-free supports and (d) laser vibrometer measurement grid

5.5.2 Excitation and Response Measurement

The impact excitation method is chosen for this test because in comparison to a shaker there is no physical connection between the excitation and the structure. The test-notes were manually excited from behind (or below) at a location approximately at the 10 o'clock position and 20mm away from the centre of the test-note. A grid containing more than 100 points (see Figure 5.4d) was used for each test-note and five measurements were averaged for each point on the grid. This grid was also extended beyond the test-note perimeter to include at least one quarter of the distance along the bowl wall. To obtain an impact signal with a frequency range large enough to excite the frequencies of interest, a small stiff, instrumented, steel-tip hammer is used on a swing and is shown in Figure 5.4a. The miniature impact hammer (PCB 086C80) is instrumented with a force transducer with a sensitivity of 22.5mV/N. The total mass of the hammer is 2.9gm and its handle is made of vinyl tubing. The length of the handle is 9 cm. In this work the hammer distance from the test note was adjusted to ensure that there were no double impacts during the course of the experiment. Typical time series data for the hammer impulse on the test-note region is shown in Figure 5.5a.

Traditionally, modal analysis experiments are conducted by attaching accelerometers to the test structure at locations predicted to yield reliable results. However, the accelerometer mass has the potential to perturb the characteristics of the test structure, especially if the accelerometer is placed close to an anti-nodal point of a vibration mode. A Scanning Laser Doppler Vibrometer (Polytec PSV 300) was used to measure the test-note response to the impact (see Figure 5.5b). The contact-less sensor adds no extra mass to the test-note. The laser vibrometer measures velocity of the vibration at a point in the direction of the laser beam. In the test, the laser beam was focused normally to the test structure. The laser vibrometer was placed on a solid concrete floor which isolated it from the test-note supporting structure so no disturbing vibrations were introduced when performing the measurements. Laser vibrometry applies the Doppler principle which is used to provide a measure of the surface velocity at the point at which the laser beam is incident. The equation below lists the factors which contribute to the Doppler shift measured by the photo-detector inside the vibrometer.

$$f_D = \frac{2v}{\lambda}$$

5.2

where f_D = Doppler shift, Hz

v = vibrational velocity of target surface, ms^{-1}

λ = laser wavelength, m

The wavelength of the laser used in the Laser Doppler Vibrometer (LDV) is constant thereby making the Doppler shift entirely dependent on the surface velocity of the target.

5.5.3   Data acquisition and analysis

The signals from the hammer charge amplifier (PCB 484B11) and the vibrometer scanning head (Polytec OFV 056) were passed onto the Polytec PSV-Z-040 junction box and converted to digital form on the computer. For each test-bowl the data was acquired for a duration of 10 seconds at a 16.38 kHz sampling rate. This time duration was adequate to capture the entire response (see Figure 5.5b). The signal of the force sensor was windowed by a rectangular window and used for triggering (Figure 5.5a). Both signals are transformed to the frequency domain using an FFT. This Fourier transformation is a dedicated algorithm to determine the spectral content of the digitized time signal.
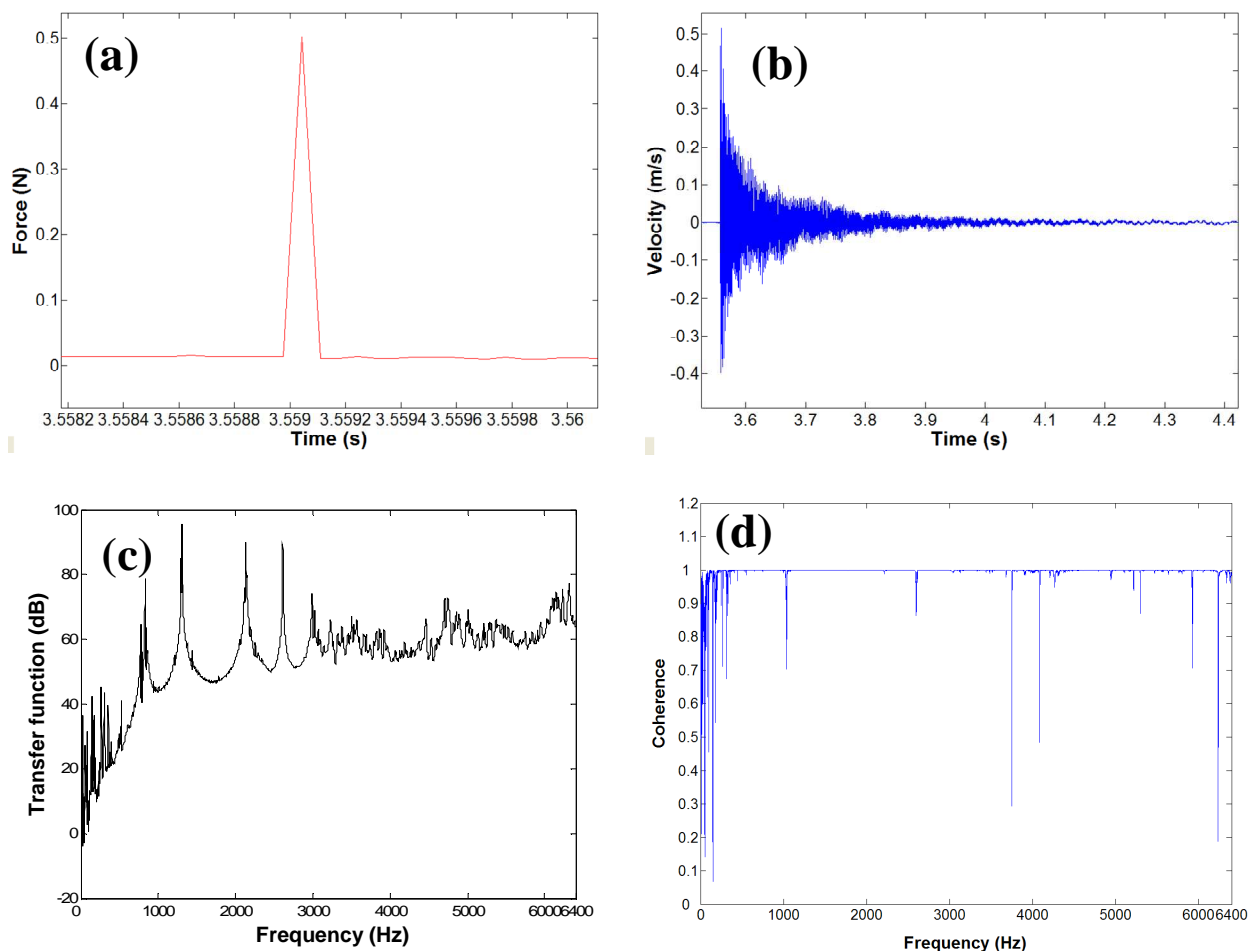
Figure 5.5: Typical time history data for **(a)** input and **(b)** output (velocity) response; **(c)** Averaged transfer function along with **(d)** coherence

The average of the FRF (see Figure 5.5c) was found by repeating the measurement five times for each measuring point so that the coherence function can be calculated which is an indication of the quality of the measured FRF. Note the good coherence shown in Figure 5.5d.

5.6 Results: Finite element predictions and modal tests

A convergence study was conducted in order to ascertain the level of mesh refinement sufficient for reliable prediction of the confined mode natural frequencies and mode shapes. Table 5.2 shows the mode frequencies obtained for various levels of mesh refinement. Reducing the seed size below 5mm resulted in no applicable change in mode frequencies

In this work, confined modes refer specifically to the modes that are localized within the central portion of the test-bowl i.e. the test-note. The interest was in confined modes in the frequency band 0 to 4kHz. The FE analysis for each model gave over 100 modes in this frequency band. Table 5.3 shows the first 100 modes for the ideal 50° test-bowl with modes mainly confined to the test-note region highlighted. The FE predictions shows that (see Table 5.3) the majority of modes in the frequency range are confined to the flange region while in some of the higher frequency modes there is coupling between the bowl-wall and the flange modes (modes 67 and 68); bowl-wall modes and test-note modes (modes 82 and 83) or coupling of modes in all three regions. In the 20° and 30° test-bowls only 3 and 6 confined modes were predicted in the test-note while the 40° and 50° test-bowls had 10 confined modes each in the test-note vicinity.

Table 5.2: Predicted[†] and measured natural frequencies of confined modes

20°

Confined Mode	Mode shape	Predicted Frequency (Hz)			Measured Frequency (Hz)	% Difference
		MS = 15 E = 806	MS = 10 E = 1917	MS = 5 E = 6906		
1	◯	732	690	**658**	**746**	**11.7**
2, 3	◑⊖	1329, 1344	1262, 1267	**1219, 1221**	**1146, 1171**	**-6.3, -4.3**

30°

Confined Mode	Mode shape	Predicted Frequency (Hz)			Measured Frequency (Hz)	% Difference
		MS = 15 E = 877	MS = 10 E = 2048	MS = 5 E = 7321		
1	◯	795	732	**699**	**794**	**12.0**
2, 3	◑⊖	1486, 1513	1390, 1404	**1346, 1353**	**1292, 1305**	**-4.2, -3.7**
4, 5	⊗⊕	2572, 2585	2384, 2387	**2243, 2247**	**2135, 2146**	**-5.1, -4.7**
6	◎	2956	2728	**2638**	**2610**	**-1.1**

40°

Confined Mode	Mode shape	Predicted Frequency (Hz)			Measured Frequency (Hz)	% Difference
		MS = 15mm E = 868	MS = 10mm E = 1915	MS = 5mm E = 7296		
1	◯	853	770	**719**	**854**	**15.8**
2, 3	◑⊖	1640, 1648	1484, 1487	**1401, 1403**	**1441, 1477**	**2.8, 5.0**
4, 5	⊗⊕	2806, 2809	2441, 2464	**2334, 2336**	**2337, 2366**	**0.1, 1.3**
6	◎	3058	2932	**2745**	**2906**	**5.5**
7, 8	⊗⊕	--	3526, 3541	**3334, 3337**	**3313, 3370**	**-0.6, 1.0**
9, 10	⊕⊖	--	--	**3778, 3784**	**3779, 3962**	**0.0, 4.5**

50°

Confined Mode	Mode shape	Predicted Frequency (Hz)			Measured Frequency (Hz)	% Difference
		MS = 15 E = 882	MS = 10 E = 2009	MS = 5 E = 7414		
1	◯	867	767	**733**	**883**	**17.0**
2, 3	◑⊖	1735, 1781	1527, 1530	**1412, 1416**	**1461, 1498**	**3.4, 5.5**
4, 5	⊗⊕	2901, 2970	2520, 2547	**2392, 2402**	**2448, 2466**	**2.3, 2.6**
6	◎	3395	3052	**2828**	**2986**	**5.3**
7, 8	⊗⊕	--	3827, 3830	**3526, 3539**	**3592, 3613**	**1.8, 2.0**
9, 10	⊕⊖	--	--	**4139, 4141**	**4165, 4176**	**0.6, 0.8**

Note: † Predicted natural frequencies calculated using ideal test-bowl geometry; **MS** – mesh size; **E** – Number of shell elements in model
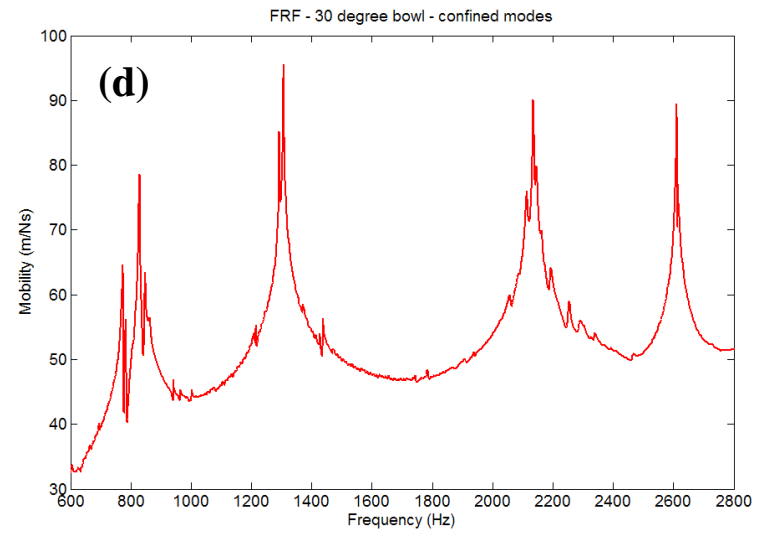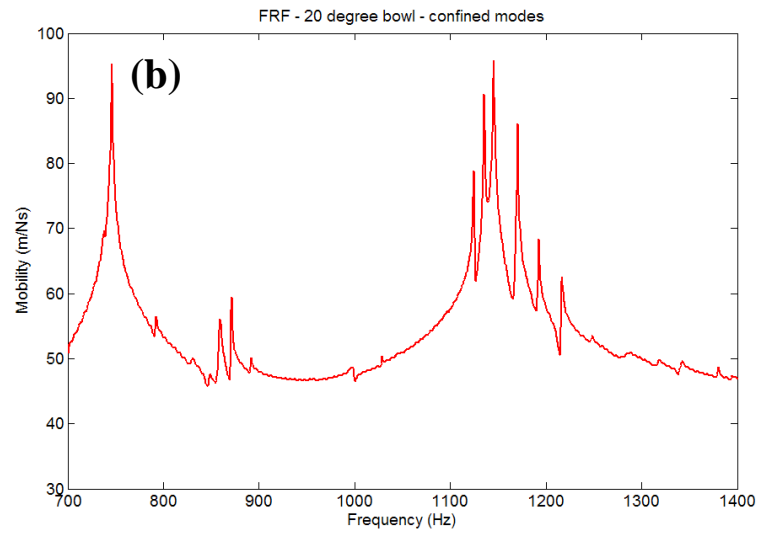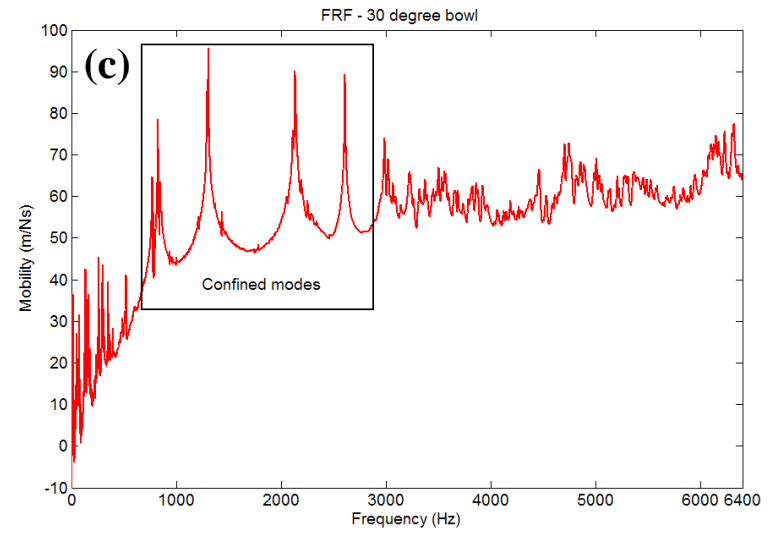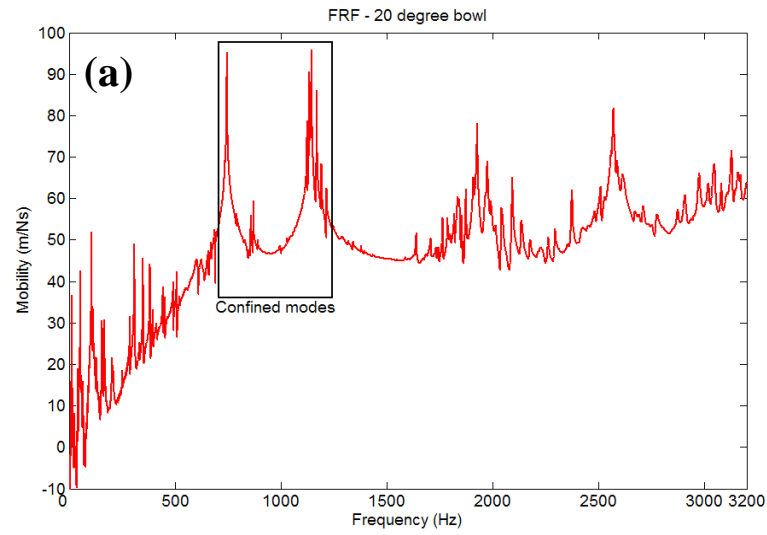
Figure 5.6: Frequency response functions for test bowls: (a)-(b) 20° and (c)-(d) 30°
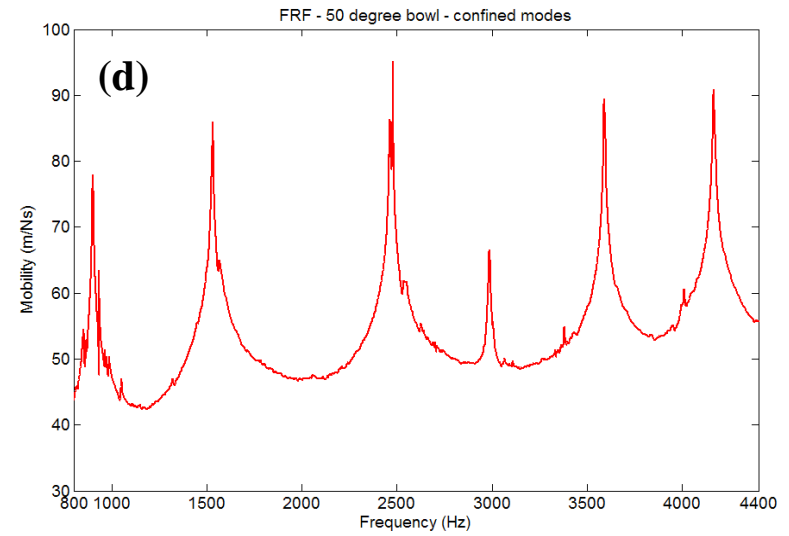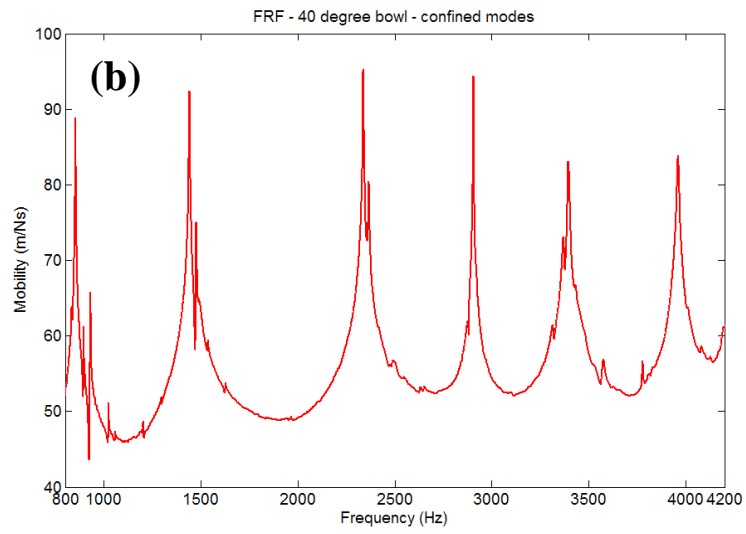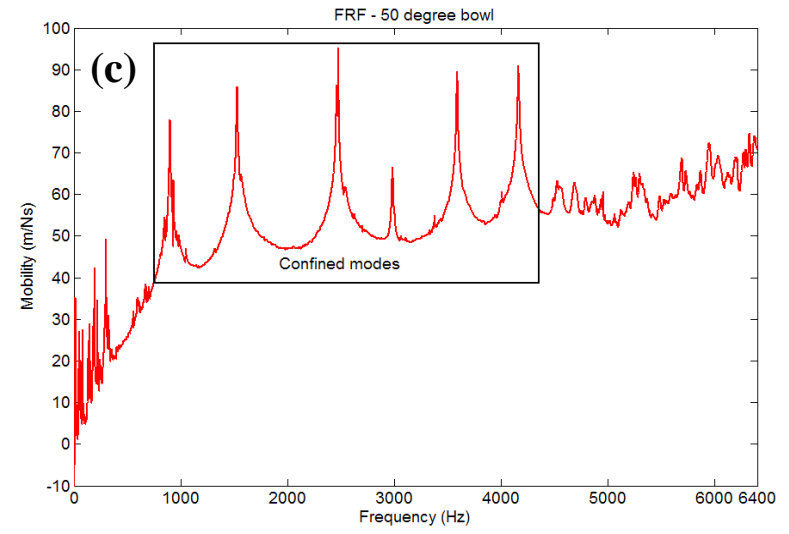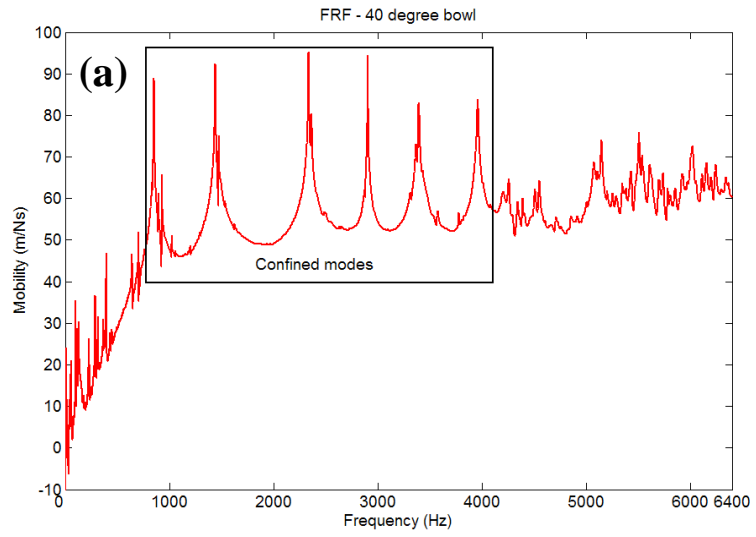
Figure 5.7: Frequency response functions for test bowls: (a)-(b) 40° and (c)-(d) 50°

Table 5.3: First 100 mode shapes for test-note in ideal 50° test-bowl (confined modes highlighted)
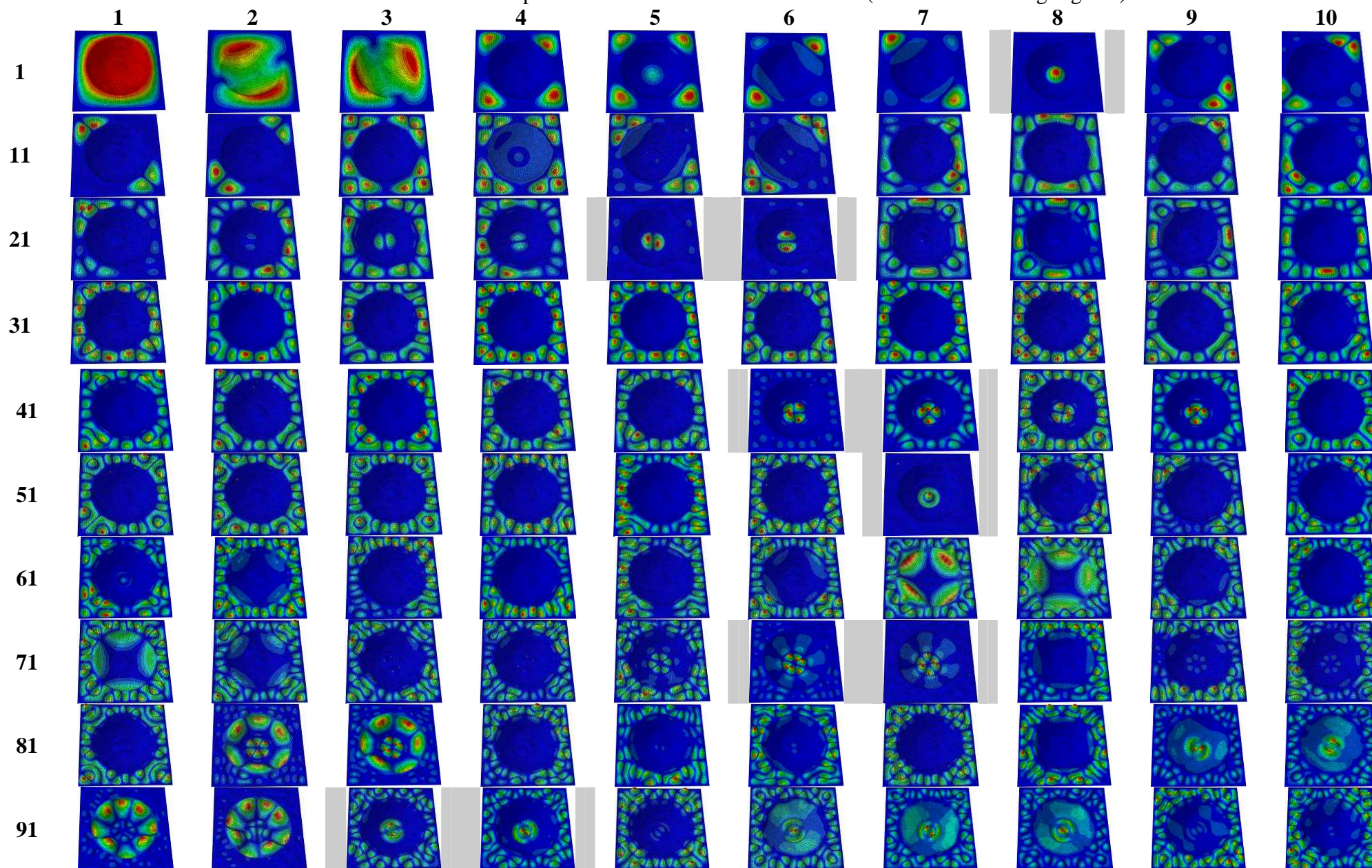
As expected, confined mode shapes for the test-notes bear resemblance to those exhibited in flat circular plates with clamped and simply-supported edges. The FE analysis indicates that the number of confined modes increases as the curvature of the bowl wall is increased.
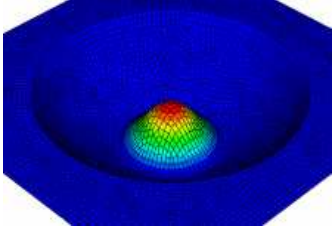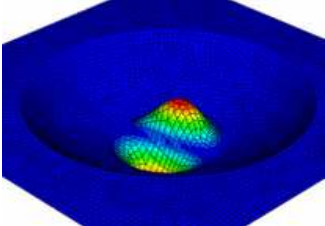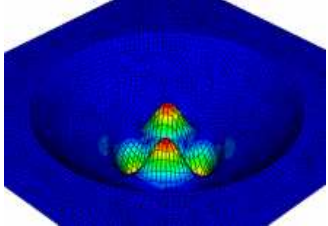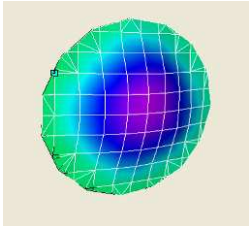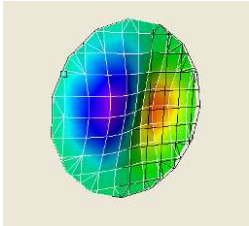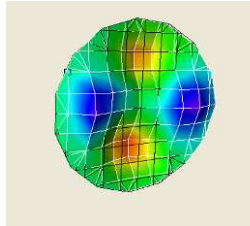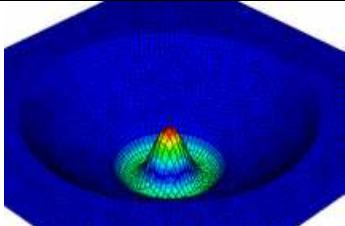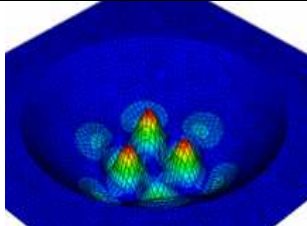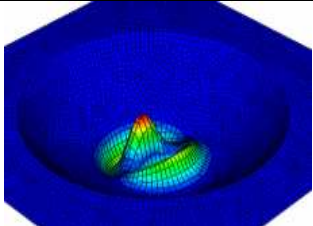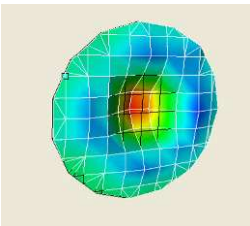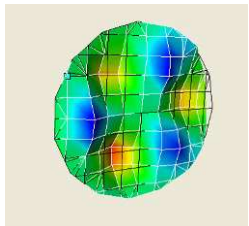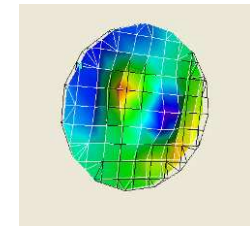
Table 5.4: Predicted and measured confined mode shapes			
Mode shape	1st confined mode	2nd and 3rd confined modes	4th and 5th confined modes
Predicted			
Measured			
Mode shape	6th confined mode	7th and 8th confined modes	9th and 10th confined modes
Predicted			
Measured			

Table 5.2 shows that a 5mm mesh size gave a percentage difference between measured and predicted confined mode frequencies of mostly within 5%. However, this was not seen for the first confined modes in the test-notes of the 20°, 30° and 40° test-bowls in which there were differences to the order of 10% and above between the predicted and measured natural frequencies (see Table 5.2). One possible reason for this discrepancy in the predictions will be discussed in the next section.

Figure 5.6 and Figure 5.7 show the frequency response spectra for the four test-notes. The resonance peaks encased by the rectangular boxes in Figure 5.6a and c and Figure 5.7a and c show the frequency bands of the modes that are localised to the test-note regions. These boxes divide the

response function plots into three regions i.e. the regions to the left and right of the confined mode frequency band and the bandwidth encased by the boxes. The response peaks of the confined modes are clearly identifiable with light damping; well separated peaks and no anti-resonances (see Figure 5.6 and Figure 5.7). The bandwidths containing the confined mode frequencies of the test-notes in the 20°, and 30° test-bowls are 700-1300 Hz, 700-2800Hz respectively (see Figure 5.6b and d) while the bandwidths containing the confined mode frequencies of the test-notes in the 40 and 50 test-bowls are the same at 800-4200Hz (Figure 5.7b and d).

According to Scott and Woodhouse [157], the light damping exhibited by confined modes is mainly governed by radiation and material damping. This will be looked at further on when the material damping in test-notes of test-bowls in clamped and free-free end conditions are compared. The separation and clarity of the response peaks is improved as the bowl wall curvature increases around the test-note. This can be seen by closer examination of the frequency response functions in Figure 5.6 and Figure 5.7. The regions encased by the boxes in Figure 5.6a and c and Figure 5.7a and c are zoomed-in and shown in Figure 5.6b and d and Figure 5.7b and d. Consider the FRF of the test-note of the 20° test-bowl (Figure 5.6b) in the vicinity of 1100-1200Hz. There are at least six peaks (3 pairs) here that could include those of the 2nd and 3rd confined modes. However, the fine-grid used (Table 5.4) during the modal test provided a resolution that made it easy to identify modes which are confined solely to the test-note region. The extra peaks were those of modes which were not confined to the test-note region.

The confinement in the test-note of the 20° test-bowl could be described as relatively weak in comparison to the other test-notes as its confined mode frequencies are in close proximity to those of some of the global modes of the test-bowl structure. For the other test bowls, the natural frequency of the first confined mode of the test-notes tend to be well separated from natural frequencies of other modes of the test-bowl structure. The FE model predicts at least 6 to 7 global structural modes (see Table 5.3) for each test-note in the frequency band to the left of the boxed sections in Figure 5.6a and c and Figure 5.7a and c. These modes tend to involve vibration of the entire structure and are therefore highly damped as their damping will be influenced by the clamping applied to the flange. On the right-hand side of the boxed sections in Figure 5.6a and c and Figure 5.7a and c the FE models predicts the modes in this region to be localised to the bowl wall and/or flange regions (see Table 5.3).

5.7 Updated test-note models

When incremental sheet forming was used to produce minipans in Chapter 3 material springback was identified as a factor which influenced the geometrical accuracy of the formed parts. It is

inevitable that springback would occur in the test-bowls and this could be responsible for the large percentage difference observed between the predicted and measured natural frequencies of the first confined modes in each test note (see Table 5.2). To ascertain whether springback was a contributory factor to the high percentage deviations manifested between the measured and predicted natural frequencies of the first confined modes of the test-notes, one of the test bowls was cut in half using a water-jet cutter to examine its cross-section. Figure 5.8a shows the cross-section of the $50°$ test-bowl. The cut-away immediately reveals the bulging or pillowing of the test-note region (see Figure 5.8a).

The initial FE models treated the test-note region as flat. The next step was to capture the true profile of each of the test-bowls. The average profile of each test-bowl was measured using an OMICRON co-ordinate measuring machine (CMM). Two profiles were measured for each bowl and an average taken. With the centre of the bowl set as the origin, a profile was taken to be a measurement from one flange edge to the opposite flange edge. Figure 5.8b-e compares the ideal test-bowl profiles to their actual profiles. In each case, it is visible that the test-note region is arched as illustrated in Figure 5.8a. There are also deviations in the bowl-walls, particularly in the region between the flange and the beginning of the bowl walls. This is also highlighted in Figure 5.8a.

However, the deviations between the flange and bowl wall regions are not expected to influence the natural frequencies of the test-note. The main concern is the amount of deviation in the test-note region. Figure 5.8f compares the deviation in the test-bowls actual geometry from the ideal shape. The largest degree of pillowing is seen in the test-note of the $20°$ test-bowl. This measures about 2.5mm with the test-note in the $30°$ having a pillow of approximately 2mm while the bulging in the test-notes of the $40°$ and $50°$ test-bowls both measure 1.6mm.

To account for the pillowing effect in the test-bowls, updated models were produced in ABAQUS® using the co-ordinates extracted on the CMM machine. The FE analysis was conducted using the same material and section properties as those used for the initial models. However, the sensitivity to meshing was done using seeds of 10mm and 5mm only. Table 5.5 shows the updated mode frequencies for the confined modes of each test-note. Here, arching raises the confined mode frequencies and better agreement is seen mainly between the measured and predicted frequencies for the first confined mode in each test-note. Compare the values in Table 5.2 and Table 5.5.
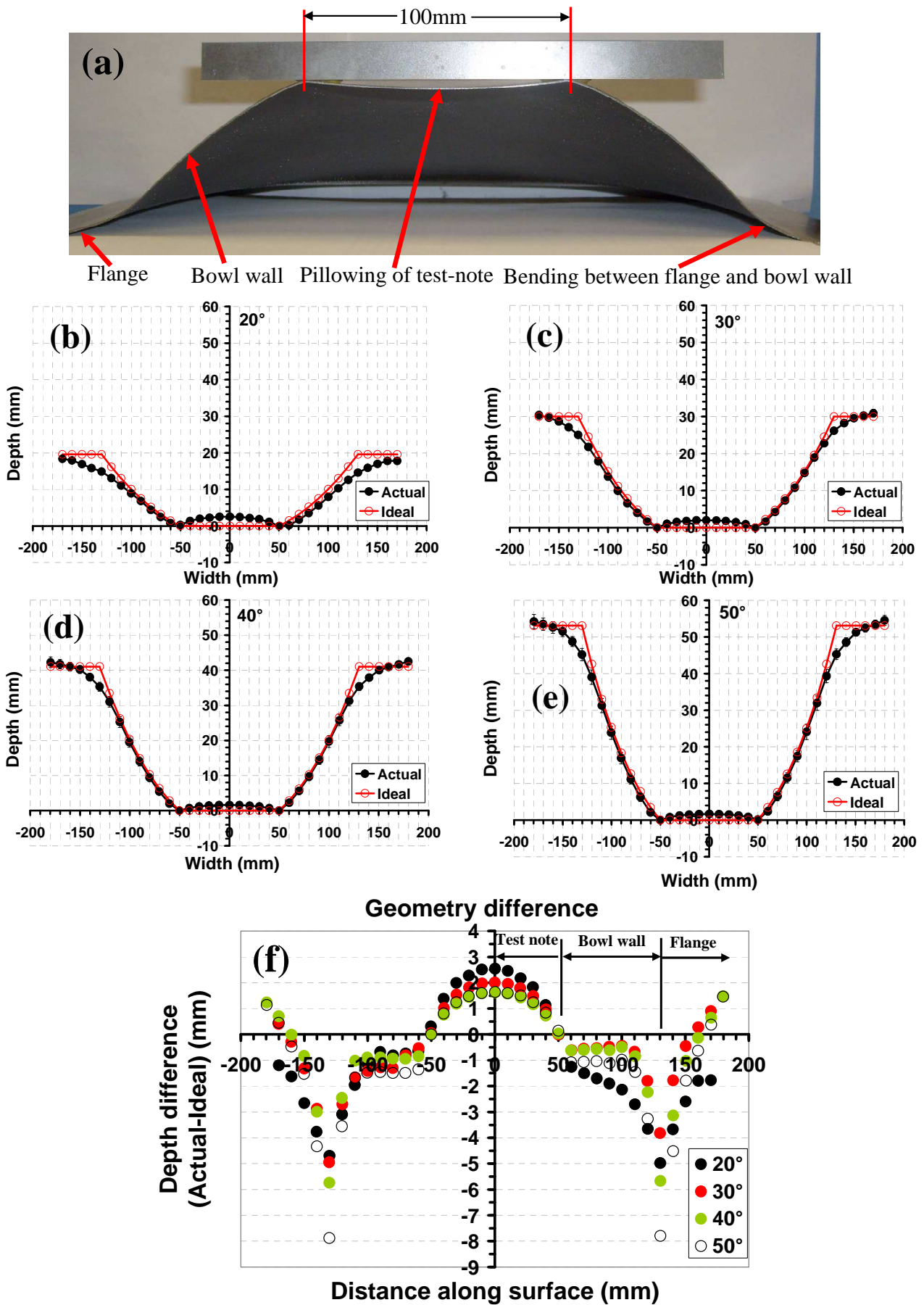
Figure 5.8: (a) cross-section of test-note; **(b)-(e)** Comparison between ideal and actual geometries and **(f)** geometry difference

Table 5.5: Updated predicted[†] and measured natural frequencies of confined modes

20°

Confined Mode	Mode shape	Predicted Frequency (Hz) MS = 10 E = 1854	MS = 5 E = 6827	Measured Frequency (Hz)	% Difference
1		678	**698**	**746**	**6.4**
2, 3		1019, 1020	**1031, 1033**	**1146, 1171**	**10.0, 11.8**

30°

Confined Mode	Mode shape	Predicted Frequency (Hz) MS = 10 E = 1921	MS = 5 E = 6711	Measured Frequency (Hz)	% Difference
1		744	763	**794**	**3.9**
2, 3		1227, 1231	1252, 1255	**1292, 1305**	**3.1, 3.8**
4, 5		2189, 2239	2180, 2232	**2135, 2146**	**-2.1, -4.0**
6		2627	2475	**2610**	**5.2**

40°

Confined Mode	Mode shape	Predicted Frequency (Hz) MS = 10 E = 1804	MS = 5 E = 6728	Measured Frequency (Hz)	% Difference
1		750	761	**854**	**10.9**
2, 3		1332, 1336	1309, 1312	**1441, 1477**	**9.2, 11.2**
4, 5		2424, 2428	2337, 2368	**2337, 2366**	**0.0, - 0.1**
6		2892	2616	**2906**	**10.0**
7, 8		3540, 3573	3306, 3313	**3313, 3370**	**0.2, 1.7**
9, 10		--	3660, 3667	**3779, 3962**	**3.1, 7.4**

50°

Confined Mode	Mode shape	Predicted Frequency (Hz) MS = 10 E = 1956	MS = 5 E = 7193	Measured Frequency (Hz)	% Difference
1		769	759	**883**	**14.0**
2, 3		1349, 1358	1315, 1317	**1461, 1498**	**10.0, 12.1**
4, 5		2275, 2320	2176, 2210	**2448, 2466**	**11.1, 10.4**
6		2783	2556	**2986**	**14.4**
7, 8		3544, 3570	3334, 3342	**3592, 3613**	**7.2, 7.5**
9, 10		--	3661, 3671	**4165, 4176**	**12.1, 12.1**

Note: † Predicted natural frequencies calculated using updated test-bowl geometry; **MS** – mesh size; **E** – Number of shell elements in model

The results suggest that the pillowing of the test-notes may be largely responsible for the large deviations manifested between the predicted and measured frequencies of the first confined modes of the test-notes in the initial models. However, the new percentage difference values for the first confined modes in Table 5.5 are still high in comparison to the percentage difference values of the other confined modes in Table 5.2. This may be due to other factors which will be addressed in the discussion.

5.8 Damping in free-free and clamped test-bowls

In accordance with Scott and Woodhouse the damping in confined modes is independent of boundary conditions and solely influenced by material and acoustic radiation damping [157]. To investigate this, damping was extracted from test-notes of 20°, 30° and 40° test-bowls suspended in two ways: clamped and free-free.
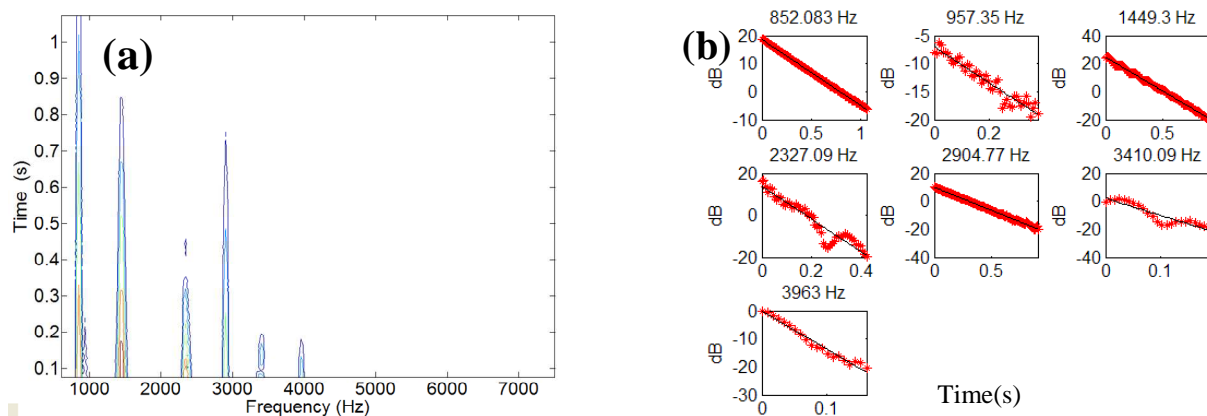
Figure 5.9: (a) and (b) sonogram display for test-note in 40° test-bowl

The free-free arrangement is given in Figure 5.4c and here the bowls were suspended by a pair of elastic bands from holes that were drilled 10mm from each flange. The impact and response locations and the acquisition settings were the same as those used for the clamped test-bowls. However, a grid measurement was not used for the free-free test as only the mode frequencies and damping of the confined modes were required as mode shapes were identified through the test with the clamped arrangement. Modal damping was extracted from time decay rates using the sonogram algorithm which is a curve fitting technique that takes a series of short FFTs of overlapping data segments (see Figure 5.9a).

MODE FREQUENCIES   **DAMPING**
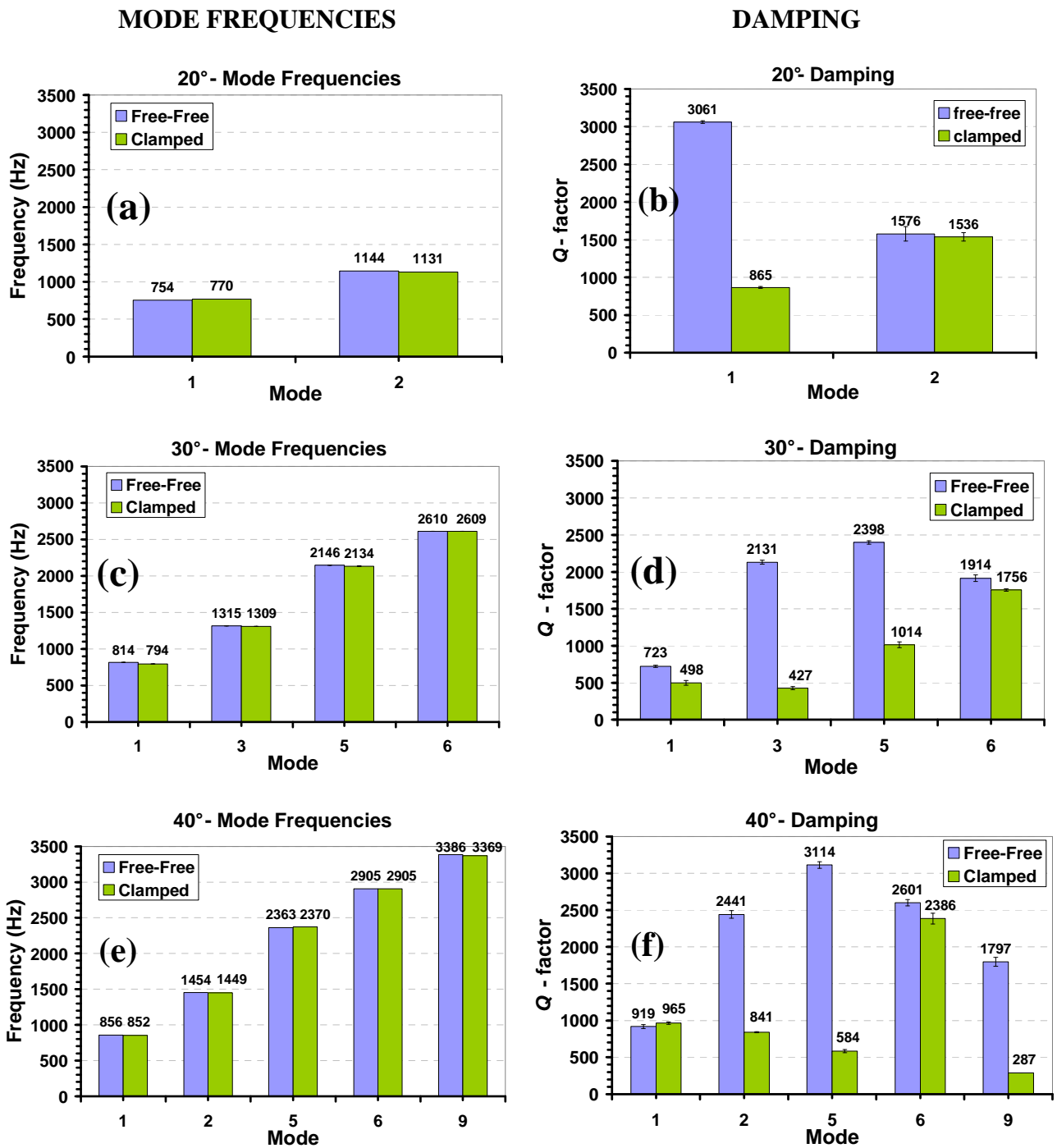
Figure 5.10: Natural frequencies and damping for test-notes of bowls in free-free and clamped conditions: **(a)** and **(b)** 20° test-bowl; **(c)** and **(d)** 30° test-bowl and **(e)** and **(f)** 40° test-bowl

This technique was used because of the light damping exhibited by the confined modes. Resonance peaks are found, and the best fitting exponential decays are calculated on the basis of the variation of each peak height with time. An average of 10 measurements was used when determining the damping of each mode. The analysis also displayed a measure of the fit quality which enabled poor data to be excluded from the measurements (Figure 5.9b). Figure 5.9b shows the damping fits for global and confined modes in the test-note of the 40° test-bowl. The confined modes are at 852Hz, 1449Hz and 2904Hz.

During the tests, it was observed that the sonogram algorithm was not very good at fitting damping for natural frequencies that are close, particularly the paired confined modes i.e. modes 2 and 3, 4 and 5 and so on. Most times the damping of only one mode in the pair would be fitted. It is uncertain how sensitive the sonogram algorithm is to modes whose natural frequencies are in close proximity. One way to overcome this limitation would be to excite the structure at another location so that the damping of both modes in the pair could be computed. However, this was not done and for the test-notes used, the frequency and damping of only one mode in each of the paired modes are reported.

Figure 5.10 compares the natural frequencies and damping for the test-notes in the test-bowls that were supported in free-free and clamped arrangements. For some modes comparable damping is seen but in many cases the free-free configuration gives significantly lower damping (higher Q) Possible reasons for this discrepancy will be elaborated on in the discussion.

There was also a slight variation between the natural frequencies of the test-notes. In some cases the natural frequencies of some of the modes in the test-notes were higher in the free-free condition. This is the case for all the confined modes of the test-note in the 30° test-bowl (Figure 5.10c). However, in this case and for the other test-notes, the difference between the test-notes modal frequencies in the free-free and clamped conditions is negligible and could be ascribed to experimental scatter.

5.9 Discussion

This work has demonstrated that it is possible to achieve mode localisation or mode confinement through manipulation of the bowl-wall curvature surrounding a relatively flat central region. This controlled entrapment of modes to a selected region has implications for the future manufacturing of steelpans. Knowledge of this mechanism of entrapment may also find application in other areas of structural vibrations particularly where the transfer of vibrational energy from one section of a structure to another needs to be minimised. It could be said that there are two facets of steelpan note tuning: 1) mode entrapment and 2) mode tuning. The quality of the instrument may be influenced on how well tuned modes are confined, hence the importance of this work.

It is first important to draw an analogy to the steelpan in order for the findings of this work to be relevant and applicable. Recall, steelpan notes are flat or slightly concave shells embedded in a dish [10]. The test-notes created in this work were an attempt to replicate this important feature of the steelpan note. This was one of the main deciding factors in the choice of geometry. Another important aspect of this work was that the initial horizontal diameter of each test-bowl was fixed at

260mm. Steelpans of all types are usually crafted using oil drums of the same diameter. This also allowed for some comparison between the test-bowls and actual pans. The investigation revealed that the mode confinement was stronger in the test-notes of the test-bowls with the highest curvature (see Figure 5.6c and Figure 5.7a and c). In full size pans, tuners usually tune at most one or two modes in the notes of the low-pitched shallower drums and up to four in the outer notes of the deeper high-pitched pans. It is not certain whether tuning in this way is done deliberately or whether the degree of curvature surrounding the note acts as a constraint.

Some limitations of the findings in this work must also be stated. For instance, the majority of notes in full size steelpans are typically located on the walls of the dish and not at the base. In this work, the test-notes were constructed at the base of the surrounding test-bowl or dish. The influence of note position on mode confinement is yet another topic for consideration and is recommended for future work. It may be difficult to manufacture this geometry in a controlled manner. However, an initial approach would be analysis through finite element studies. Another limitation was that the notes produced in this work were circular mainly because this geometry could be easily reproduced as a CAD model in addition to being easily transformed into a tool-path code for manufacture of the structures. The majority of steelpan notes resemble elliptical or rectangular plates. Further work should also consider mode confinement in rectangular or elliptically shaped notes.

Springback was identified as being a possible contributor to the percentage difference observed between the measured and predicted frequencies of the first confined modes in the test-notes (see Figure 5.8a-f). However, after accounting for this, the percentage difference between the measured and predicted frequencies of the first confined modes of these modes were still relatively high (see Table 5.5). This may indicate that there are other influences besides springback. It is reasonable to assume that the presence of springback may also be a manifestation of the presence of residual stresses in the test-bowl. It is not certain to what extent residual stresses affect the modal properties of the structure but this is another avenue for further investigation. The FE model did not account for the residual stresses that may have been created during the forming of the test-notes. The geometry of the structures was created as CAD profiles for mode studies in ABAQUS®. A better approach might have been to simulate the incremental forming of the test-bowls in ABAQUS® before doing a vibration analysis. This might have helped to provide estimates of material springback.

Since all of the test-notes had the same diameters, it was assumed that as the amount of pillowing increases, the amount of difference between the measured and predicted frequencies would also increase due to an increase in the local stiffening as the height of the pillow increases. However,

this was not realised as the test-notes with the smallest amount of pillowing manifested the largest deviations between the measured and predicted frequencies of their first confined modes (see Figure 5.8f). Although the updated FE results showed improved agreement between measured and predicted natural frequencies for the first confined modes, a similar trend between pillow height and frequency deviation was maintained. The amount of springback may also be influenced by how firmly the structures were clamped within the forming jig. This clamping may have affected the amount of pillowing in each case. There was no means of monitoring or controlling the level of holding force as the forming jig made use of a bolt-and-nut arrangement to secure the plates to be formed.
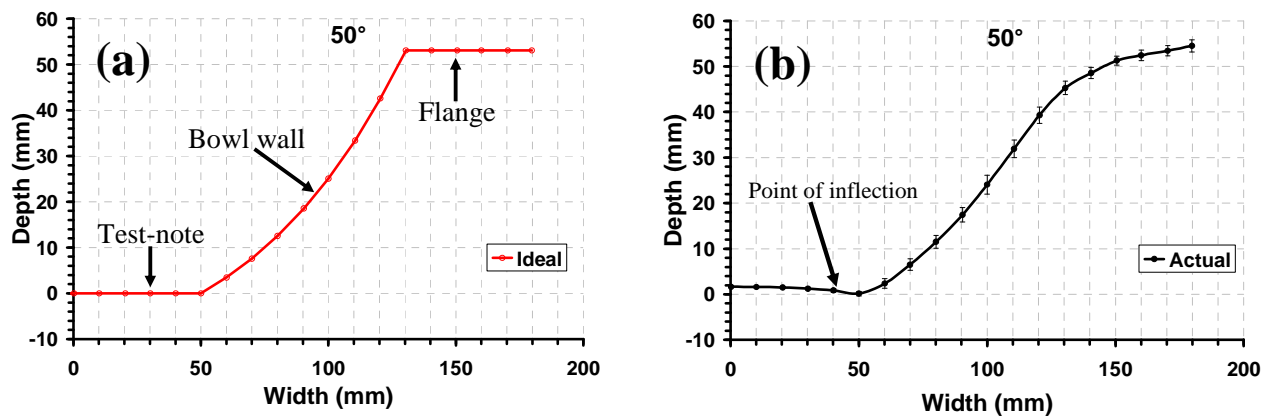
Figure 5.11: 50° test-bowl: **(a)** Ideal bowl with no springback effects and **(b)** Actual bowl with springback effects that creates a point of inflection between the test-note region and the bowl wall

There was also springback in the bowl walls and the flange sections of the test-bowls. While this was not expected to directly influence the behaviour of the test-notes, the springback resulted in the creation of a point of inflection between the test-note region and the bowl wall. This is illustrated in Figure 5.11. Here it is clear that in the ideal geometry (Figure 5.11a) there is no such point of inflection in which there is a change of the curvature in the test-note vicinity from concave to convex. In the actual geometry, this point of inflection may be the main mechanism that is responsible for mode confinement and not the change of curvature that occurs between the test-note and bowl-wall. The level of confinement may depend on the rate of change of bowl depth with respect to the bowl width on either side of the inflection point. This needs to be investigated further.

The level of resolution obtained from the CMM measurements was not sufficient to examine the profile of the note in this region in finer detail. Future work could incorporate the use of a stereovision camera which would capture the entire 3D shape and offer finer resolution. Calculated control in the way in which mode confinement is produced in steelpan might assist in the development of dishes in which the notes require minor adjustment for tuning. To achieve this would also require a close study in conjunction with other geometrical parameters that affect mode

tuning in steelpans. The benefits of this cannot be overlooked. This would reduce the time it takes to tune a steelpan and would also effectively reduce the amount of exposure to high noise levels and hand-arm vibrations currently experienced by pan makers. There would also be some debate on how many modes should be strongly confined in the pan note. The limiting factor would be on how many modes could be practically tuned and therefore a high level of mode confinement may be not be necessary. However, it would be beneficial to determine the effect of strongly entrapping several modes to a single note region while only two or three are tuned.

The light damping displayed by the confined modes, in accordance with Scott and Woodhouse [157] may be an indication that the damping is solely governed by acoustic and material damping. There was good agreement between the *Q*-factor values for some of the corresponding modes in test-bowls supported in free-free and clamped arrangements (see Figure 5.10). However, the damping for some of the confined modes appeared to be affected by the boundary conditions which were not in the immediate vicinity of the test-note. This is probably a result of the coupling to bowl-wall or particularly flange modes close in frequency to the confined modes.

It is also important to indicate that the flange regions, to which clamping was applied, were not perfectly flat. This could be seen in Figure 5.8f. There is between 0.5 and 1.5mm of deviation of the flanges, in the edge region, from its ideal shape (Figure 5.8f). Distortions in the flange may have arisen during the release of the part from the forming jig. During the modal tests, clamping of these uneven flange regions may have resulted in added distortion of the entire structure. These distortions may have altered the boundary conditions in the test-note vicinity and consequently affect the damping properties. It is also seen that in some cases, the mode frequencies of the confined modes were higher than in the clamped condition (see Figure 5.10). The free-free tests were conducted after the tests with the test-bowl in the clamped condition. Any added distortion during the modal test with the test-bowl clamped may have resulted in local stiffening in the test-note region thereby raising the natural frequencies of the confined modes.

5.10 Conclusions

- It is possible to obtain mode confinement in a test-note (flat steelpan note-like region) by varying the curvature of the bowl wall surrounding the region.

- The mechanism of confinement may be a point of curvature change that is created between the test- note region and the bowl wall as a consequence of material springback.

- As the curvature of the bowl wall increases the number of confined modes in the test-note region is increased.

- There appears to be a threshold on the number of modes that could be confined as both 40 and 50 test-bowls contained an identical number of confined modes in the vicinity of the test-note.

- The natural frequency of the first confined mode in each test-note is sensitive to material springback.

- Confined modes in the test-note exhibited light damping, which in agreement with Scott and Woodhouse, may indicate that their damping is solely governed by radiation and material damping.

- The damping of the confined modes of the test-note may be sensitive to distortions in the test-bowl structure.

Chapter 6   Material Studies: Effect of the Manufacturing Regime on Vibration Damping in Steelpans

6.1 Introduction

An important facet of the vibrational behaviour of percussion instruments and by extension any vibrating structure is the effect of damping. Particularly in musical instruments, the level of damping, be it material or non-material, contributes in large part to the quality of the sound produced by the instrument. This work generally considered material damping, and the work reported on in this chapter focused specifically on the effect of the steelpan production regime on material damping in steel sheet that could be used to fabricate steelpans. This was pursued in an attempt to contribute another dimension to the work done in previous research. Previous work, mainly by Murr *et al.* [19] and Ferreyra *et al.* [18] concentrated on how other material properties such as hardness and yield strength were affected by pan production stages and carbon content, with the aim of identifying optimum process parameters that would produce the requisite properties that facilitated the production of high quality pans.

A major portion of this work took the form of an experimental programme in which test structures were put through steps similar to pan production, followed by vibration damping measurements at each step. The overall investigation consisted of three segments. The **first segment** (Figure 6.1) was an experimental simulation that mirrored portions of the pan production process. In this section, test structures were fabricated from low-carbon steel sheet that had comparable chemical composition to steel sheet used in fabricating oil drums. These structures were put through identical stages of the steelpan production process. The test structures herein were rectangular steel strips, and "*test structure*", "*test strip*" and "*rectangular strip*" will be used interchangeably throughout this chapter. Before conducting experiments on these test structures a finite element (FE) vibration analysis was performed to determine mode shapes, natural frequencies and suitable impact locations to be used during experimental modal testing. The **second segment** (Figure 6.1) of this work also involved a simulation of the pan production process but test structures were constructed from bake hardenable (BH) and interstitial free (IF) steel sheets. In this section the damping properties extracted from the BH and IF steel strips were compared with those of the rectangular strips extracted from the low-carbon sheet steel. This was done for two reasons: 1) to ascertain whether the mechanism of strain ageing was connected to the damping behaviour observed in the low-carbon steel sheet and 2) to identify whether such steels could be suitable material alternatives for

pan production. **Segment three** (Figure 6.1) concluded the investigation in which the damping properties of a 4ths and 5ths soprano pan and an Aubrapan were compared with the damping properties extracted from uncoated and coated strips.
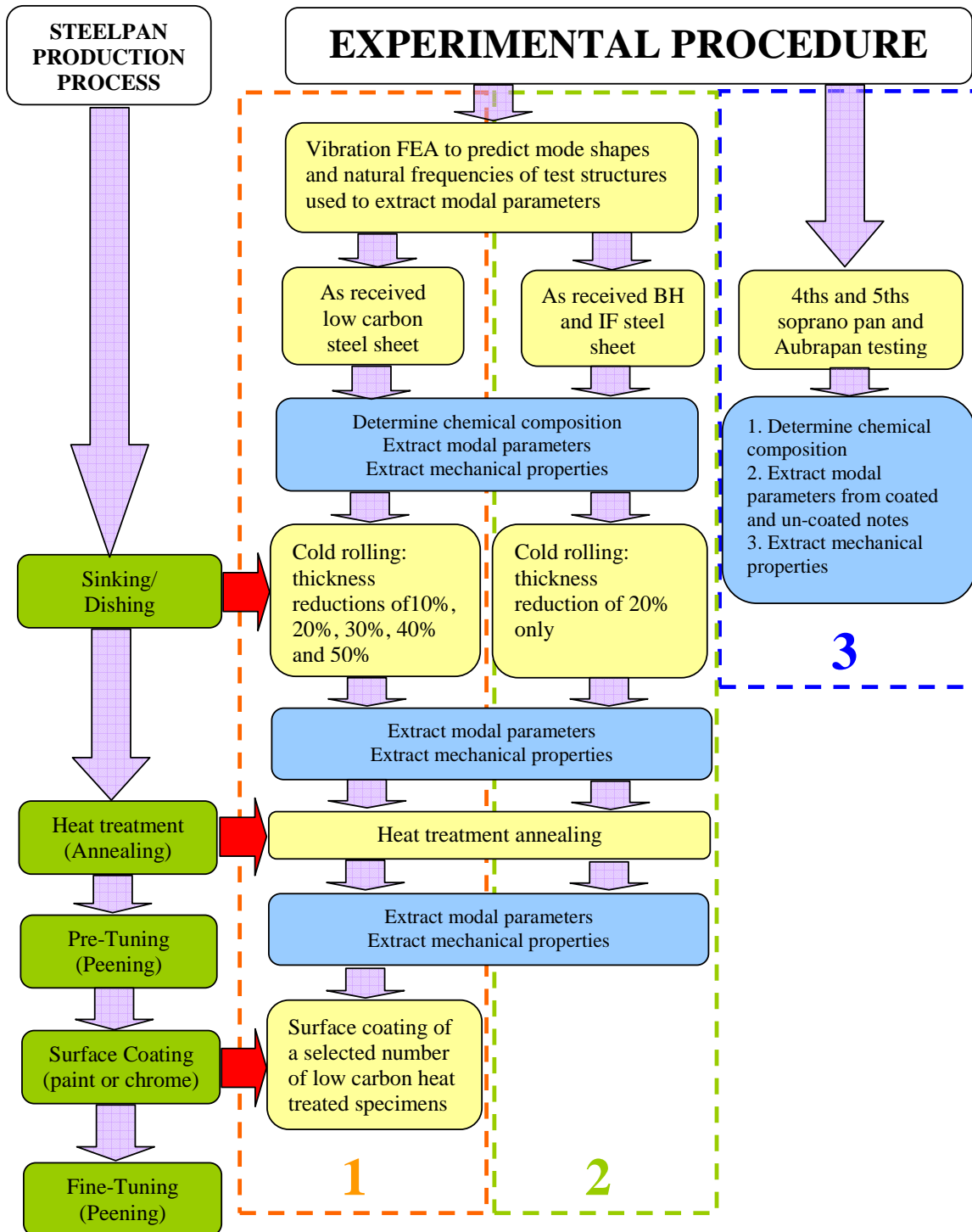
Figure 6.1: Methodology overview: 1) Experiment with low-carbon steel sheet; 2) Experiment with BH and IF steels and 3) Steelpan testing for comparison with low-carbon steel findings.

There are a variety of terms which are used to denote material damping which include: logarithmic decrement (δ), loss factor (η), loss angle (φ), damping ratio (ς), quality factor (Q) and specific damping capacity (ψ). Damping was reported using the quality factor (Q) which was defined in

Chapter 4. Bert [77] gives a comprehensive overview on the mathematical models and the experimental techniques used for measuring some of these damping quantities. The experimental techniques used for the measurement of material damping generally fall into one of the following categories: (a) vibration amplitude decay; use of either frequency domain modal analysis or time domain decay rate methods, (b) steady state measurement of input energy and stored energy; (c) wave propagation methods [74,77,78]. Free-vibration decay methods (time and frequency domain) were employed primarily because they are the most accurate and appropriate for this range of damping i.e. low damping. Another attractive feature of these methods are the relative simplicity with which they could be conducted and the required instrumentation required for conducting these methods were easily accessible.

6.1.1   Objectives

The objectives of this investigation were to: (1) understand how the various manufacturing stages influenced the material damping properties of low-carbon steel sheet used for the production of steelpans; (2) to determine an optimum heat treatment regime for steelpans using material damping measurements; (3) to identify mechanisms responsible for damping changes in the steel used; (4) to determine the effect of carbon content on the damping properties by comparing the material damping and mechanical properties in BH and IF steel grades to the low-carbon steel; (5) to compare the damping properties of a selection of coated and uncoated low-carbon test strips with the material damping in a chrome plated 4ths and 5ths soprano pan and an Aubrapan.

6.1.2   Some Expectations: Effect of cold forming and heat treatment on material damping

Some predictions were made about the expected outcomes of the various tests that were conducted, based on the earlier literature presented in Chapter 2 on damping in metals. In accordance with the literature one might expect the following outcomes:

1. An increase in material damping after cold working

2. A decrease in material damping after heat treatment

3. An increase in material damping after surface coating

4. A permanent decrease in the Young's modulus after cold rolling

5. Recovery of the Young's modulus after the cold rolled material has been heat treated

6. No noticeable change in the hardness after the cold rolled material has been heat treated provided that the recrystallisation temperature is not exceeded

7. An increase in material damping with surface coating

6.2 Experimental Procedure

6.2.1 Materials

Caribbean steelpans are predominantly produced from steel sheets hence the experimental investigations were mainly conducted on low-carbon sheet steels (Table 6.1). The low-C steel which conforms to BS 1449 CR4 was obtained from the material stores at the Cambridge University Engineering Department (CUED). The interstitial free (IF) and bake hardenable (BH) steels were provided by Tata Steel Ltd, Jamshedpur, India under the auspices of Professor Harshad K.D.H. Bhadeshia FREng FRS, Tata Steel Professor of Metallurgy, University of Cambridge. Table 6.1 also lists where the chemical compositions of each steel was obtained.

Table 6.1: Chemical Composition (wt %)										
Material (Steel sheet)	**Original Thickness (mm)**	**C**	**Si**	**Mn**	**P**	**S**	**Al**	**N**	**Ti**	**VHN**[4]
Low-Carbon [1]	0.86	0.061	0.02	0.34	0.019	0.017	0.03	0.0055	-	107
Aubrapan[2]	1.00	0.032	0.02	0.15	0.005	0.017	0.013	0.0023	-	-
IF – HS[3]	1.02	0.0021	0.004	0.05	0.012	0.005	0.035	0.0021	0.062	90
BH[3]	0.82	0.0035	0.04	0.32	0.036	0.005	0.048	0.0018	-	128
Note: 0.061% carbon steel will be referred to as low carbon steel herein										
1) TWI Ltd, Cambridge, UK; **2)** Sheffield Testing Laboratories Ltd, Sheffield, UK; **3)** TATA Steel Ltd, India; **4)** Vicker's Hardness Number in the as-received condition										

6.2.2 Fabrication of test structures

In this section, the fabrication of the test structures is described. The test structures or rectangular strips used in this work were mainly extracted from steel sheet in the as-received and cold-rolled conditions. The initial step in the preparation of these structures required that the mill rolling direction in the as-received steel sheet be identified. Cold rolling of the sheet was done in the same direction as the mill rolling direction (Figure 6.2). Samples of dimensions 180mm x 50mm were cut from the low-carbon steel parent material and rolled to the following thickness reductions: 10%, 20%, 30%, 40% and 50%. These percentages were chosen because recent work by Murr *et al.* [19] has shown the cold reduction in a 570mm diameter soprano pan dish to vary from approximately 10% thickness reduction at the steelpan rim to as much as 50% reduction at the dish base.

Table 6.2: Test strip material and geometric properties					
Strip Properties	**Numerical values**				
Length (L)	*150.0mm (±1)*				
Width (b)	*15.0mm (±1)*				
Density (ρ)	*7800kgm^{-3}*				
Young's modulus (E)	*210GPa*				
Poisson's ratio (v)	*0.28*				
Original thickness (t_0)	*0.86mm (±0.01)*				
	Thickness Reduction (mm) (±0.02)				
Thickness (t)	*10%*	*20%*	*30%*	*40%*	*50%*
	0. 77	*0.69*	*0.60*	*0.52*	*0.43*

A sheet-metal rolling machine was used and the desired cold reduction was achieved by multi-pass rolling and progressive adjustment of the distance between the roller surfaces. Seventy 0.061wt.% carbon-steel rectangular strips of dimensions 150mm x 15mm were extracted, with a guillotine, from the larger cold-rolled samples with a batch of 35 for annealing and air-cooling and the remainder for annealing and water quenching. Each batch was subdivided into 7 groups of 5 – each group having a strip at one of the percentage reductions shown in Table 6.2. Two strips were also extracted from the low-carbon steel sheet in the as-received condition. Test structures extracted in the as-received condition were used to measure the damping of the steel in the as-received state. Samples for tensile and hardness tests were also extracted from sheets cold-rolled in the same manner. However, the use of tensile and hardness testing will be described further on. Although the BH and IF steel test structures were fabricated in an identical manner, detailed description will be given further on when the use of these steels is introduced.

(b)
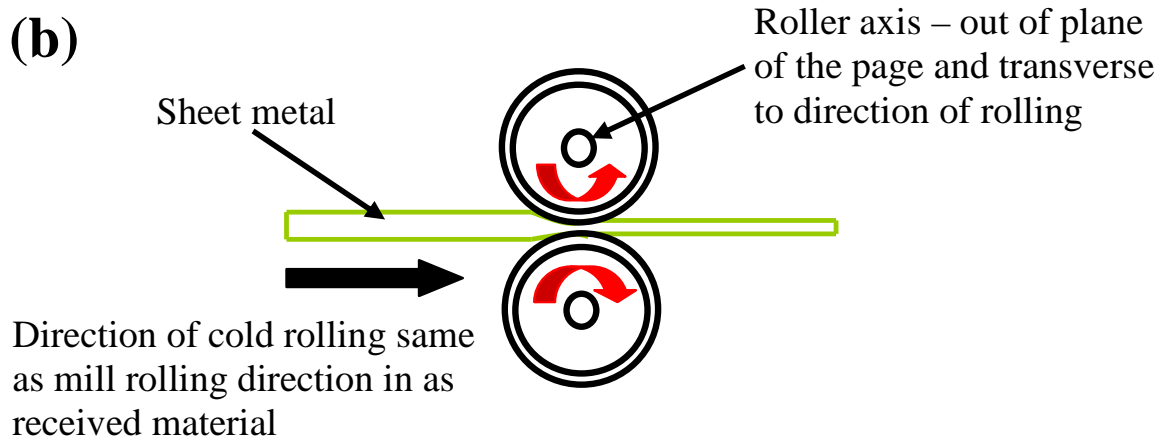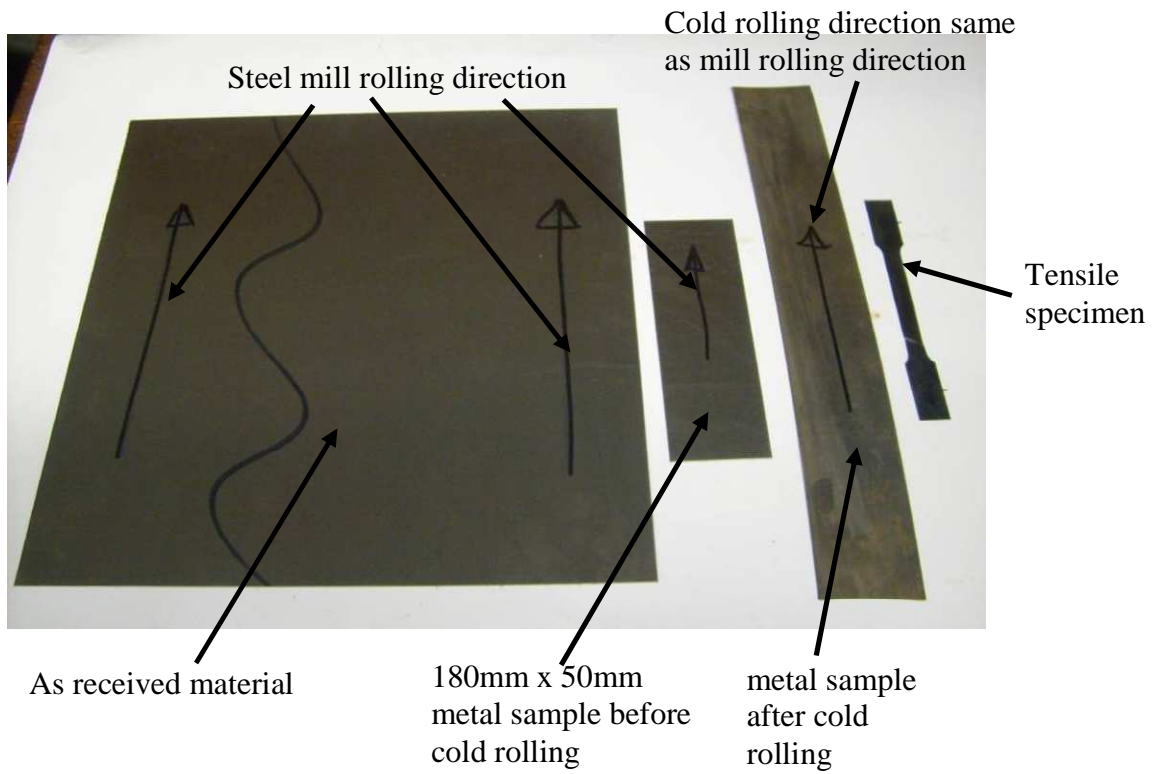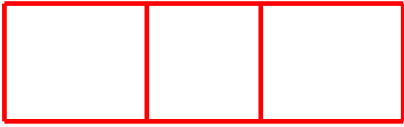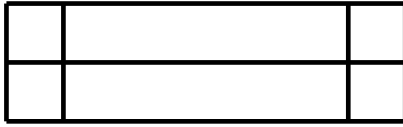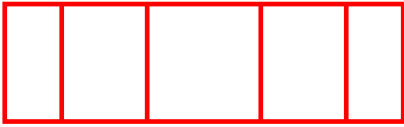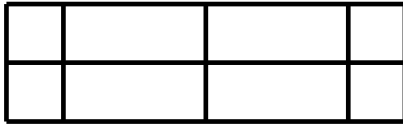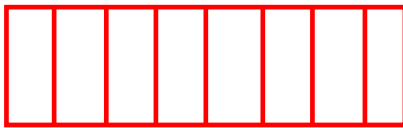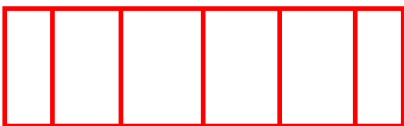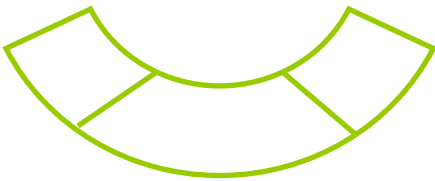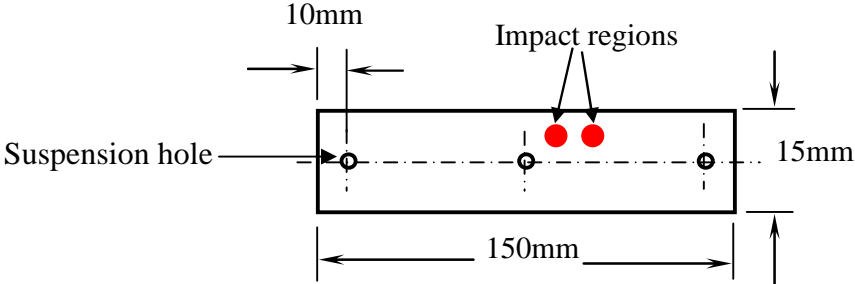
Figure 6.2: (a) As-received and cold-rolled metal samples with mill rolling direction and experimental rolling direction; (b) Experimental rolling direction with reference to roller axes; Rectangular strips, tensile and hardness specimens were extracted from cold-rolled sheet

Mode	Mode shape with node line positions (x, y) mm	Mode	Mode shape with node line positions (x, y) mm

Table 6.3: Mode shapes with node line positions and impact and suspension locations

1) B1

$x = 34; 116$

6) T2

$x = 38; 112\ y = 7.5$

2) B2

$x = 20; 75; 130$

7) B5

$x = 9; 34; 61; 89; 116; 141$

3) B3

$x = 14; 53; 97; 136$

8) T3

$x = 25; 75; 125\ y = 7.5$

4) T1

$x = 75; y = 7.5$

9) B6

$x = 7; 29; 52; 75; 98; 121; 143$

5) B4

$x = 11; 42; 75; 109; 139$

10) T4

$x = 18; 54; 96; 132\ y = 7.5$

P

15

0   150

10mm

Impact regions

Suspension hole

15mm

150mm

Notes: B – bending mode (**Red**); T – torsional mode (**Black**); P – in-plane mode (**Green**); in-plane modes are not used in this work; Impact locations at $x = 83$ or 100 and $y = 10$ – in some instances both positions were used to excite all the modes of interest; **Diagrams are not drawn to scale**

6.2.3 Finite Element Predictions

Before conducting experimental modal tests on the cold-rolled steel strips, approximations of the natural frequencies and mode shapes of the first ten modes of the rectangular strips were predicted using the software ABAQUS [187]. The modal parameters were computed by using the material and geometrical properties listed in Table 6.2. The strips were modeled in ABAQUS® using 4-noded shell elements (S4R) since the ratios $t/L << 1/15$. The resulting mode shapes were used to approximate node line positions (see Table 6.3).

This information was also used to predict suitable impact zones which were set at x=83 and x=100 (see Table 6.3) such that the modes of interest could be easily excited. Locations at which holes could be drilled to facilitate suspension of the strips in a free-free configuration were chosen at 10mm from either side and at the middle of the strips (see Table 6.3). The effect of suspension method on the results will be discussed in section 6.2.7. Table 6.4 lists the frequencies obtained from ABAQUS®. The mode shapes are identical for the first seven modes of all the strips. In-plane modes not considered in this work since the plane of vibration of these modes were in the same plane as the suspension supports. The FE prediction for the BH and IF steel test structures are also included in Table 6.4 for later reference.

6.2.4 Experimental Modal Testing: Low carbon rectangular strips

A schematic of the experimental set-up and hardware used along with the signal flow for experimental modal testing is shown in Figure 6.3. The first modal tests were conducted on the strips in their cold-rolled condition. The strips were supported at both ends in a free-free configuration using nylon thread. Excitation was provided by a miniature impulse hammer on a pendulum fixture and the response was recorded by a laser vibrometer. In this experiment all the strips were excited from behind (Figure 6.3). Impact locations were at 8mm or 25mm (see Table 6.3) from the center of the strip. Sometimes both locations were used in order to obtain all the modes of interest. Only the first ten modes in the frequency range up to 4 kHz were considered. The Logging frequency used was 50 kHz for an acquisition time of 5s and 10 averages were used to produce the coherence.

Material	t (mm)		Predicted natural frequencies 'f' for first 10 modes of rectangular strips									
		Mode	**1**	**2**	**3**	**4**	**5**	**6**	**7**	**8**	**9**	**10**
0.061wt.% C	*0.86**	Mode	**B1**	**B2**	**B3**	**T1**	**B4**	**T2**	**B5**	**P**	**T3**	**B6**
		f (Hz)	204	563	1106	1220	1832	2459	2742	3432	3732	3838
	0.77	Mode	**B1**	**B2**	**B3**	**T1**	**B4**	**T2**	**B5**	**T3**	**P**	**B6**
		f (Hz)	183	504	990	1095	1640	2207	2456	3350	3432	3439
	0.69	Mode	**B1**	**B2**	**B3**	**T1**	**B4**	**T2**	**B5**	**T3**	**B6**	**P**
		f (Hz)	164	452	887	984	1470	1982	2202	3008	3083	3432
	0.60	Mode	**B1**	**B2**	**B3**	**T1**	**B4**	**T2**	**B5**	**T3**	**B6**	**P**
		f (Hz)	142	393	772	857	1279	1727	1915	2622	2682	3432
	0.52	Mode	**B1**	**B2**	**B3**	**T1**	**B4**	**T2**	**B5**	**T3**	**B6**	**T4**
		f (Hz)	123	341	669	745	1109	1500	1660	2277	2325	3086
	0.43	Mode	**B1**	**B2**	**B3**	**T1**	**B4**	**T2**	**B5**	**T3**	**B6**	**T4**
		f (Hz)	102	282	553	617	917	1243	1373	1887	1924	2558
BH steel	*0.84**	Mode	**B1**	**B2**	**B3**	**T1**	**B4**	**T2**	**B5**	**P**	**T3**	**B6**
		f (Hz)	199	550	1080	1193	1789	2403	2679	3432	3647	3749
	0.67†	Mode	**B1**	**B2**	**B3**	**T1**	**B4**	**T2**	**B5**	**T3**	**B6**	**P**
		f (Hz)	159	439	862	956	1428	1925	2138	2923	2994	3432
IF steel	*1.02**	Mode	**B1**	**B2**	**B3**	**T1**	**B4**	**T2**	**B5**	**P**	**T3**	**B6**
		f (Hz)	242	668	1311	1441	2171	2903	3250	3432	4406	4547
	0.82†	Mode	**B1**	**B2**	**B3**	**T1**	**B4**	**T2**	**B5**	**P**	**T3**	**B6**
		f (Hz)	195	539	1054	1165	1747	2347	2615	3432	3562	3661

Table 6.4: Finite element predictions of rectangular strips

Notes: * – as received original thickness; BH – bake hardenable; IF – interstitial free; † 20% thickness reduction; The mode shapes, and the sequence of the mode shapes are identical for the first seven modes of all the strips; **P – in-plane mode**
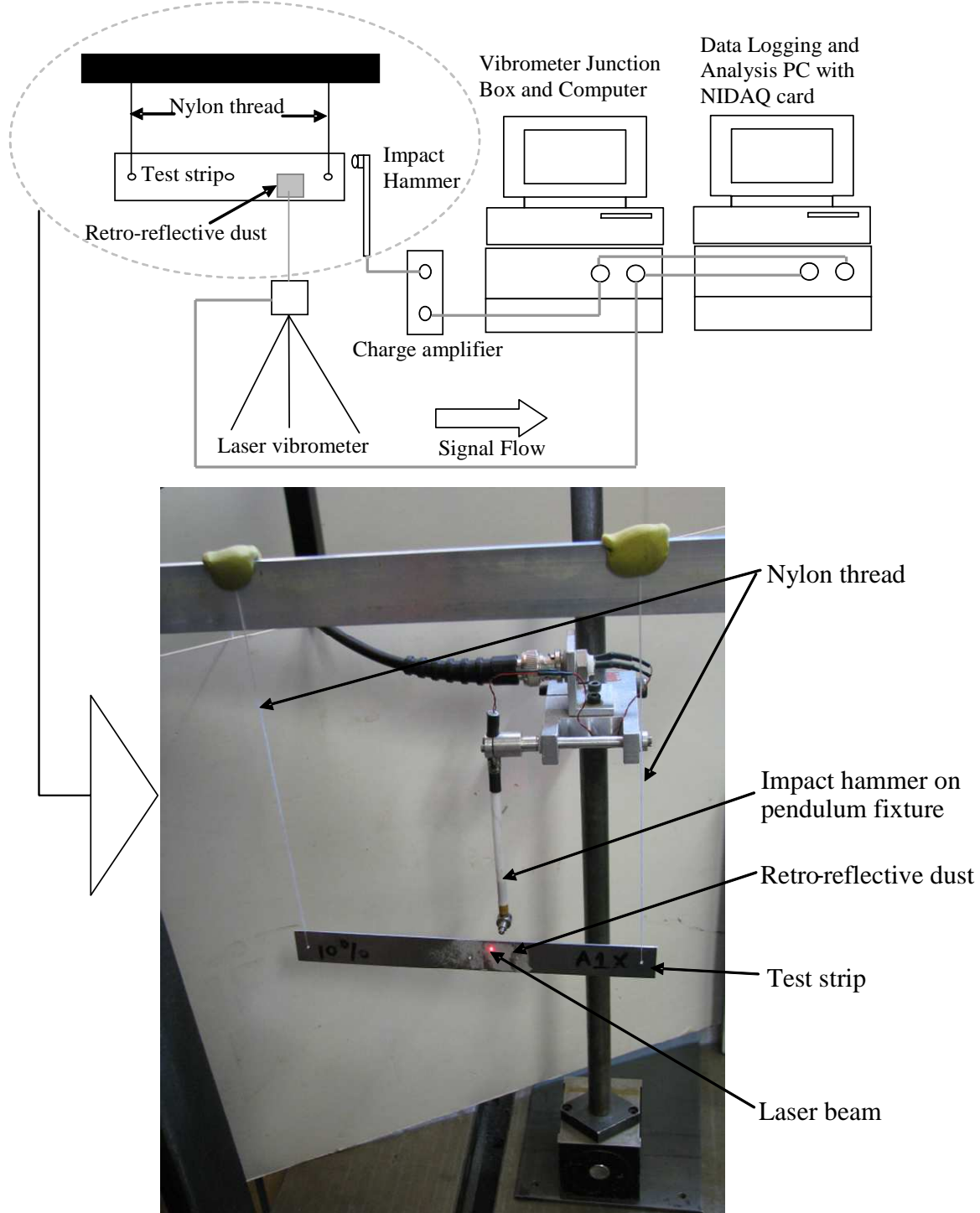
Figure 6.3: Experimental set-up for vibration tests. Strips were tested using two free-free configurations to ascertain the influence of the supports on damping properties: horizontal (shown here) and suspended solely from the center. The impact hammer is located behind the test strip.

Figure 6.4 shows a FRF spectrum for one of the strips up to the Nyquist frequency. Typical time series of the impact impulse and the vibrometer velocity response are shown in Figure 6.5a and b. These signals were checked to insure that there were no clipping and truncated signals were discarded. A typical averaged FRF, and associated coherence, in the frequency range of interest is shown in Figure 6.5c.
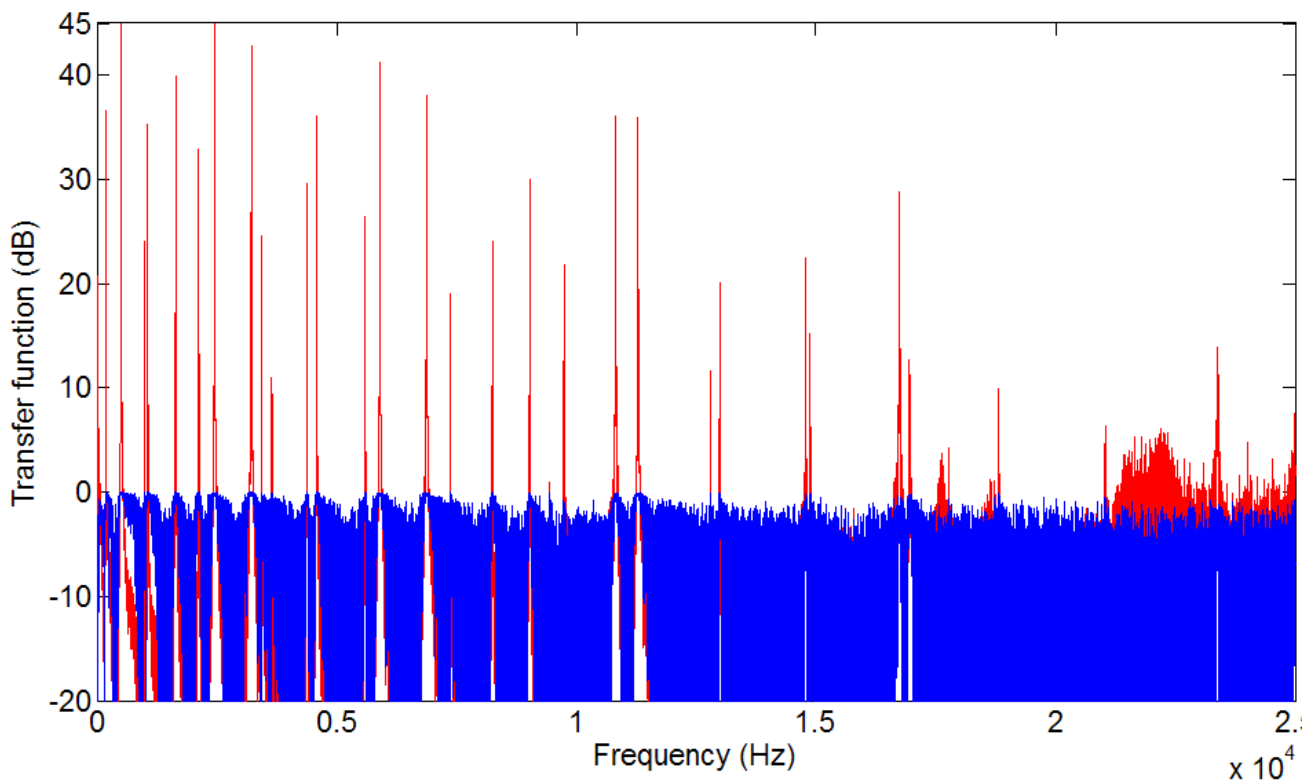
Figure 6.4: Typical averaged frequency response function of a rectangular strip up to the Nyquist frequency. The FRF was checked to ensure that there is no aliasing distortion of the spectrum in the high frequency range. (Logging Frequency = 50kHz for a duration of 5s)

6.2.5 Damping measurements

Damping measurements in this chapter were reported using the quality factor 'Q' which was defined in Chapter 4. Damping measurements were extracted using sonogram analysis. The rectangular strips had very low damping and the sonogram analysis offered a better alternative as there was an insufficient number of points in the vicinity of the resonance peak to allow a circle fit to be used that would provide reliable results. The sonogram algorithm also allowed the damping of several modes in the desired bandwidth to be obtained simultaneously as compared with circle fitting in which the damping can only be determined for one resonant frequency at a time.

The sonogram takes a series of short FFTs of overlapping data segments (Figure 6.6a and b). Peaks were found, and the best fitting exponential decays were calculated on the basis of the variation of each peak height with time. The analysis also displayed a measure of the fit quality which enabled poor data to be excluded from the measurements. Figure 6.6c along with corresponding data in the top section of Table 6.5 is an example of acceptable decay fits. Compare with Figure 6.7 and the bottom section of Table 6.5. When extracting the quality factor, a number of 10 trials were taken and an average rate (Q-factor) was calculated.

6.2.6 Microphone and Laser Vibrometer response measurements

For preliminary vibration tests involving the rectangular strips a small microphone (see Figure 6.8) was used to validate damping measurements collected using the laser vibrometer. In this test the microphone was positioned in the near field (approximately 2cm from strip surface) – just to the front of the impact zone. Figure 6.9 shows a comparison between damping measurements collected using a microphone and a laser vibrometer simultaneously. Both exhibit good agreement. However, the microphone was not used to collect response data throughout the experiment as it regularly recorded unwanted background noise. An accelerometer was also not used to measure the response of the rectangular strips as its mass and damping along with that of its cable would have perturbed the behaviour of the light-weight strips significantly.

Figure 6.9 also highlights the effect of reflective dust and reflective tape on damping measurements. Reflective tape was initially used to improve the reflectivity of the laser-beam on the strip surface. However, the application of a small patch (approx. 5mm x 5mm) of reflective tape was found to significantly increase the damping (lower Q-factors) of the test strips (see Figure 6.9). Reflective dust did not have this effect and was therefore used in all modal tests.

6.2.7 Effect of test structure support on damping measurements

The sensitivity of damping to suspension configuration is crucial particularly in free-free arrangements. To determine the sensitivity of damping to support configuration, test structures in free-free modal tests were suspended in different ways. The configuration that gave the lowest damping (highest Q-factors) was adopted throughout the modal test. To illustrate this, the suspension configurations used for the rectangular strips are shown in Figure 6.10. The configuration with the strip suspended simultaneously from both sides gave the lowest damping and was therefore adopted throughout the experiment. Table 6.6 shows the effect of suspension configuration on damping.
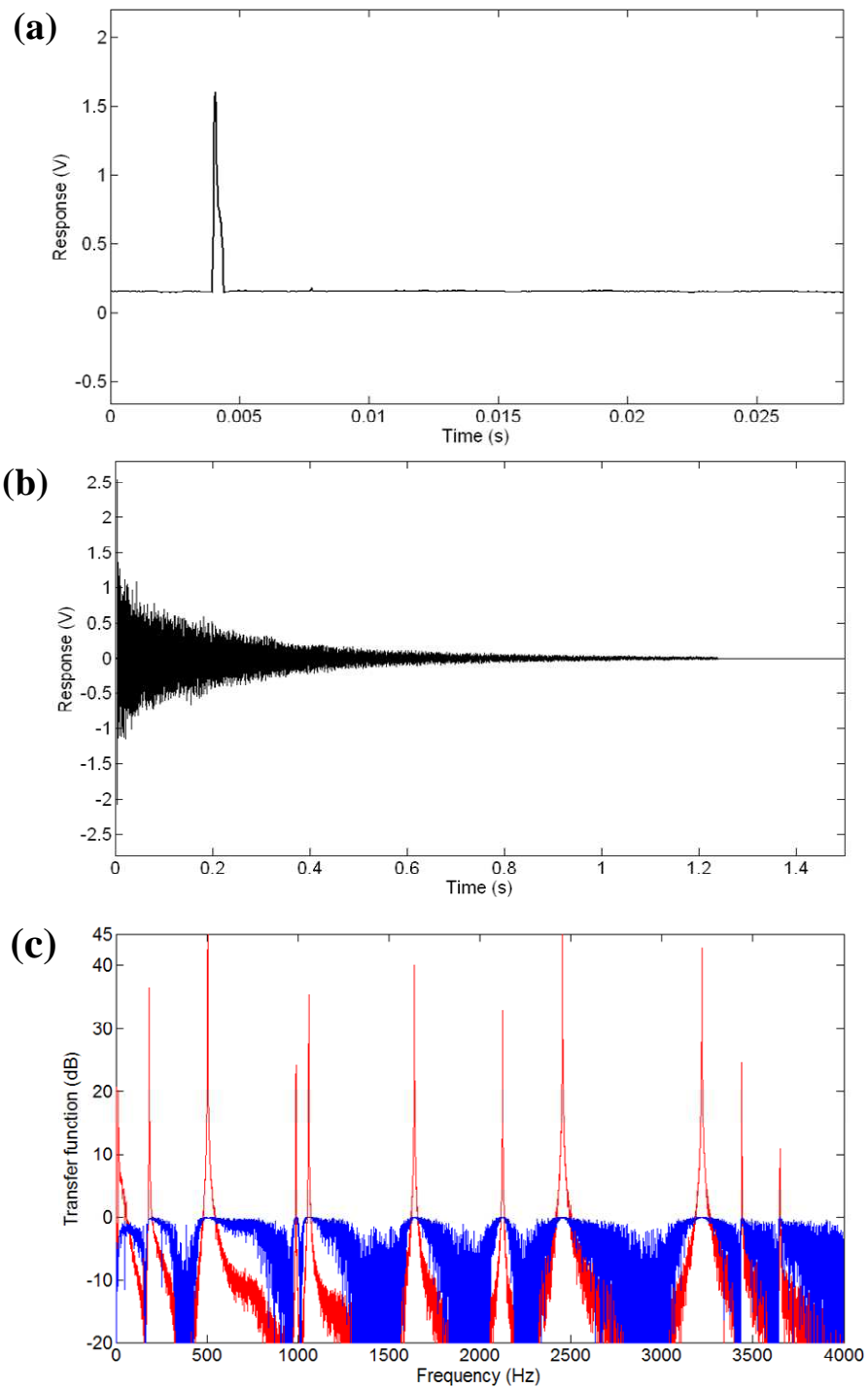
Figure 6.5: Typical time series of the experimental data: (a) input impulse; (b) acceleration response. Note the length of the time window is sufficient to allow all the modes in the frequency range of interest to decay freely; (c) Averaged frequency response function (FRF) of Figure 6.4 (up to 4kHz) and the associated coherence. Note good coherence in the vicinity of resonance peaks.
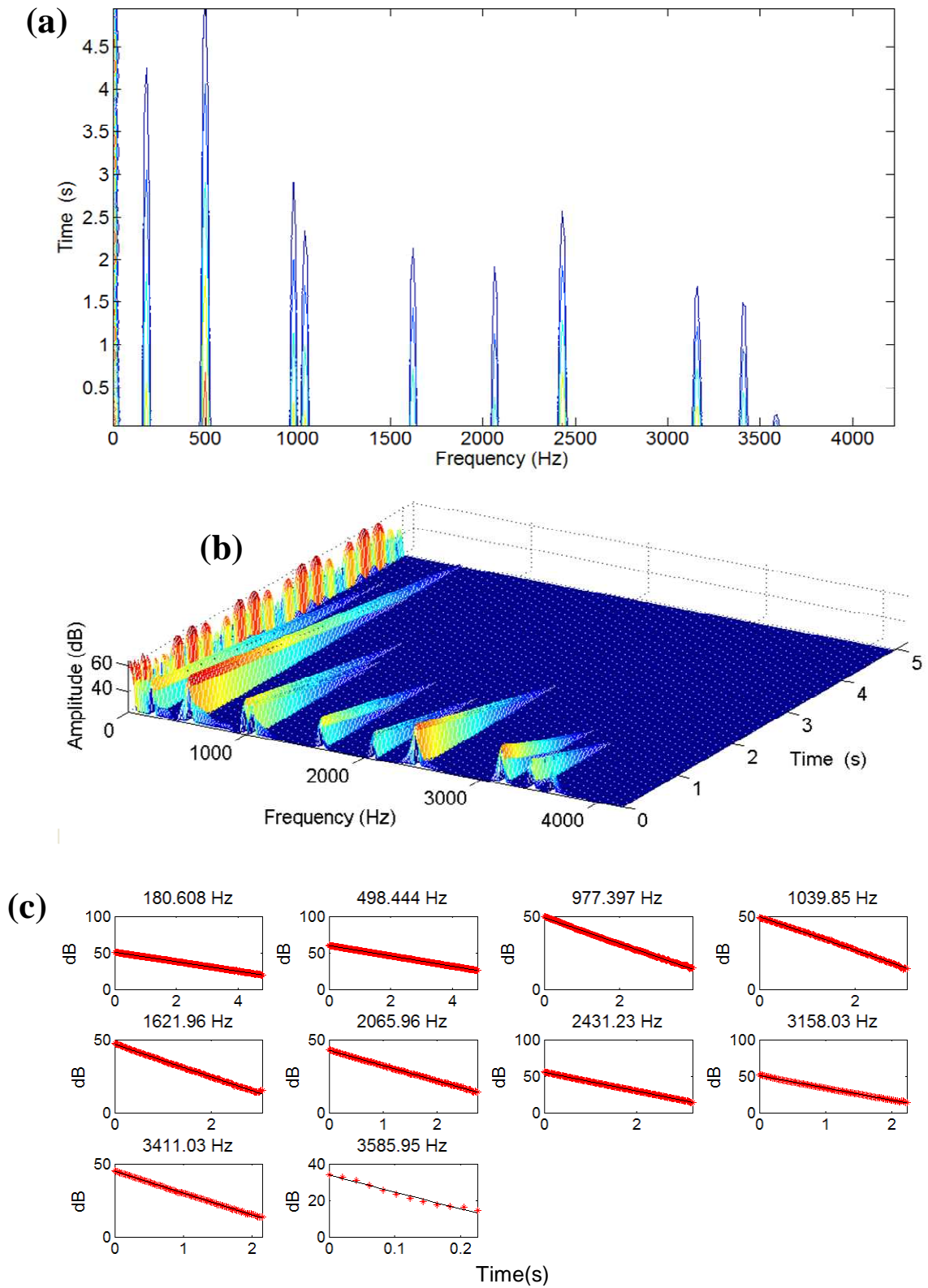
Figure 6.6: Typical sonogram analysis using a Hanning window. This algorithm was used to extract damping properties from test structures. **(a)** Time-frequency sonogram plot **(b)** Time-frequency sonogram plot with amplitude decay **(c)** Decay fits for each natural frequency in (b)
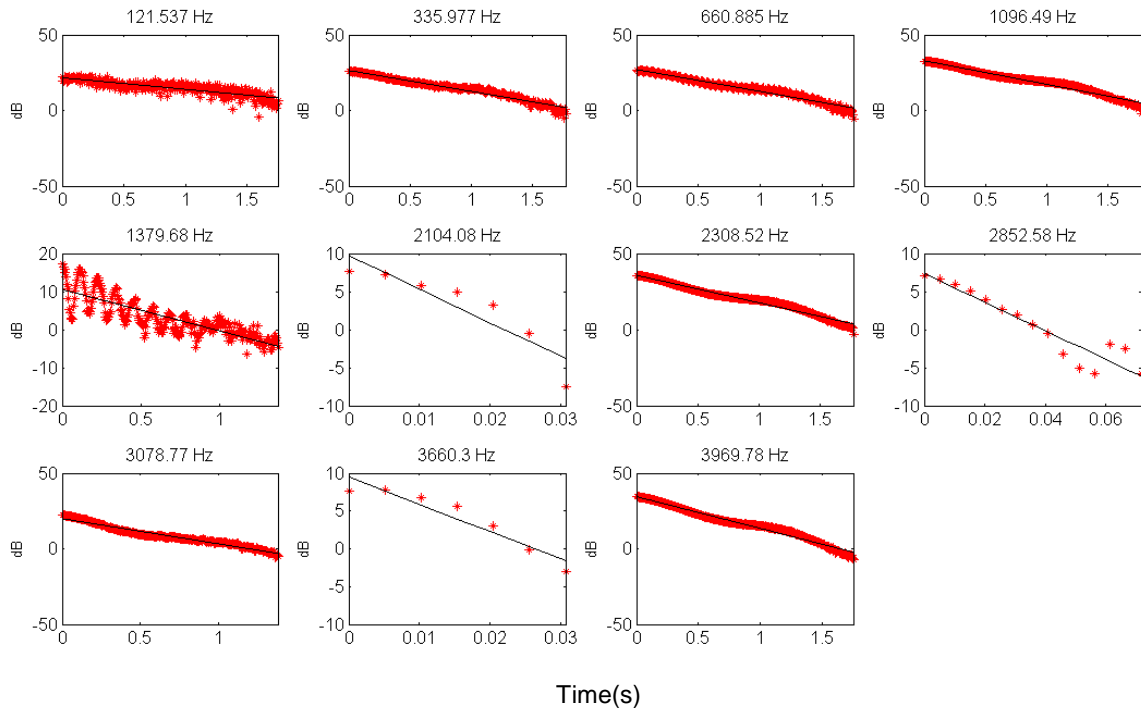
Figure 6.7: A sample of poor decay fits

Table 6.5: *Q*-factors using sonogram algorithm				
Sample of data with good damping fit (corresponding with Figure 6.6c)				
Frequency Hz	**Q-factor**	R^2 **(Q-factor)**	**Points**	R^2 **(Phase)**
180.608	759.2	0.999784	235	1
498.444	1910.2	0.999934	235	1
977.397	2958.3	0.998693	193	1
1039.85	2465.4	0.998745	151	1
1621.96	3960.1	0.998411	150	1
2065.96	5395.1	0.999236	135	1
2431.23	5191.6	0.999821	158	1
3158.03	5125.2	0.998104	110	1
3411.03	6238.3	0.999251	106	0.999998
3585.95	1059.3	0.980583	12	0.999932
Sample of data with poor damping fit (corresponding with Figure 6.7)				
Frequency Hz	**Q-factor**	R^2 **(Q-factor)**	**Points**	R^2 **(Phase)**
121.537	432.8	0.703913	343	0.999999
335.977	663.6	0.958244	347	1
660.885	1240.2	0.958796	343	1
1096.49	1911.7	0.969294	347	1
1379.68	3466.5	0.695843	269	1
2104.08	130.3	0.828889	7	0.999573
2308.52	3497.4	0.972796	347	1
2852.58	415.1	0.890962	15	0.999941
3078.77	5023.6	0.959382	270	1
3660.3	277.8	0.896561	7	0.999983
3969.78	5142.4	0.976856	342	1
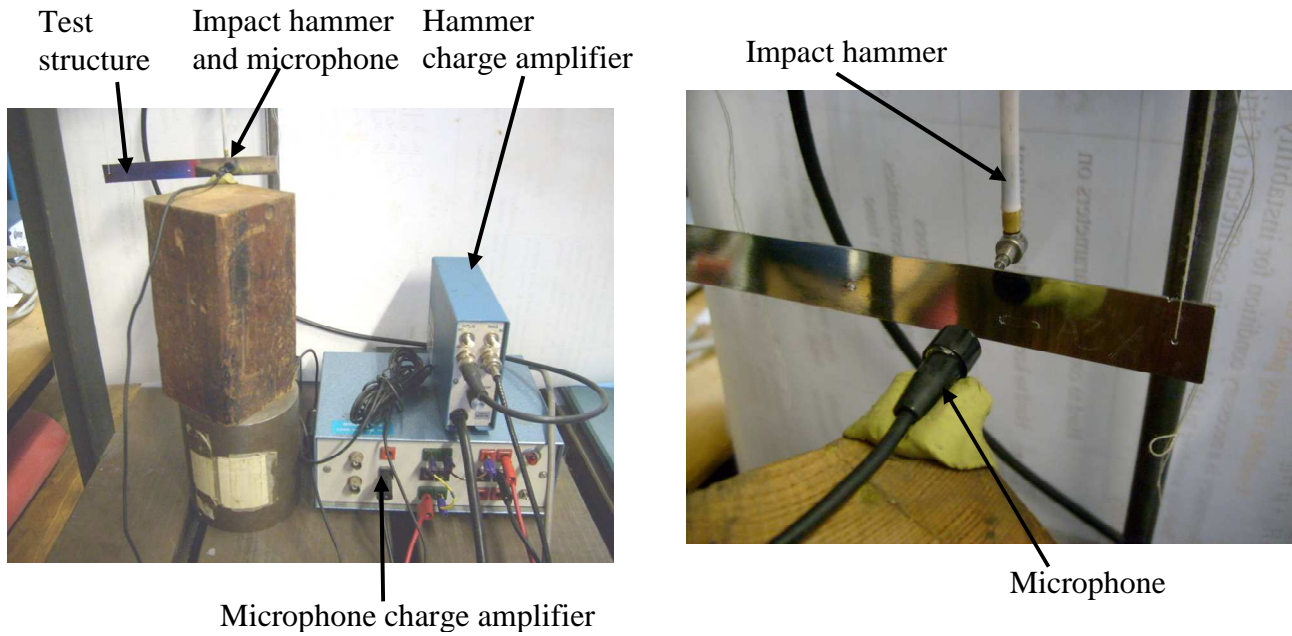
Figure 6.8: Microphone being used as a non-contact sensor; Left: vibration test equipment with microphone; Right: close-up showing microphone position with respect to test structure.
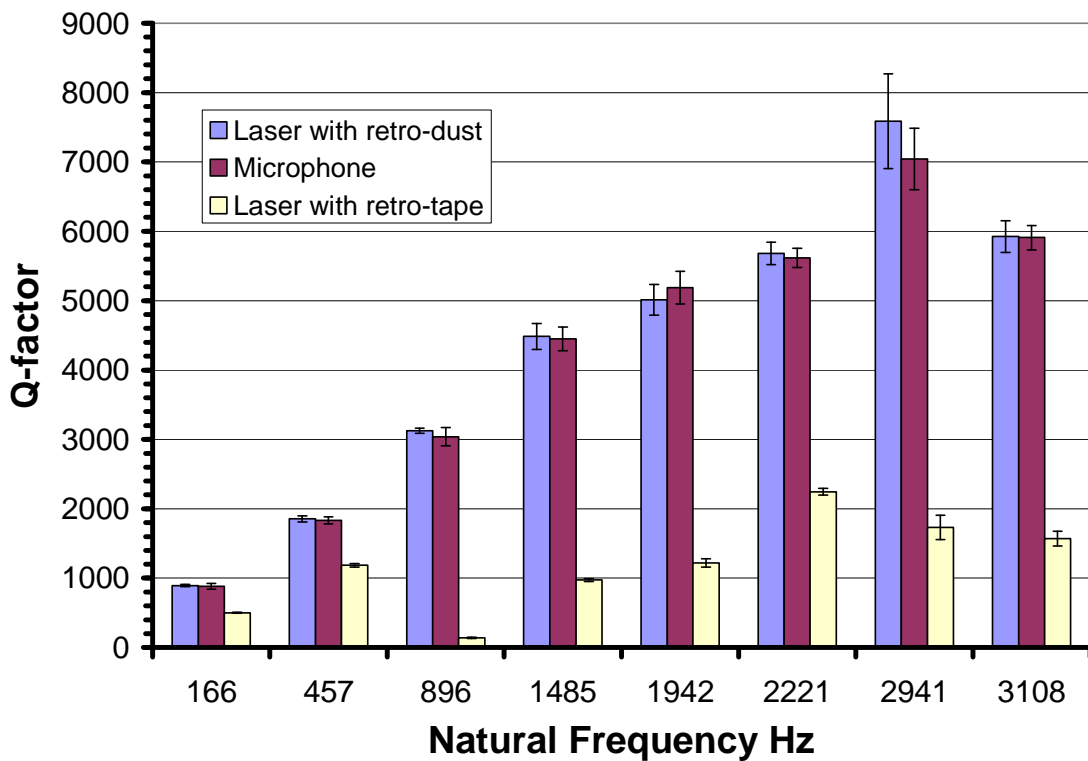
Figure 6.9: Comparison of *Q*-factors for a rectangular test strip using different transducers (laser vibrometer and microphone). The effect of using retro-reflective dust and reflective tape was also compared.
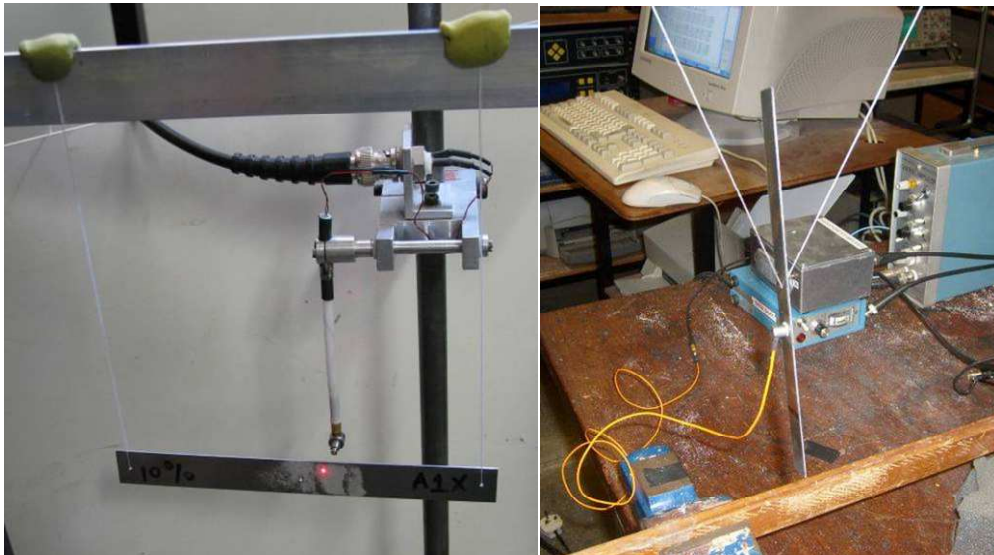
Figure 6.10: Suspension configurations using nylon thread; **Left:** rectangular strip supported at both ends (gave lowest damping) and **Right:** suspended at middle (Note: although an accelerometer is shown attached to strip, it was not used to measure response owing to its relatively heavy weight in comparison to the weight of the strips.)

Table 6.6: Effect of suspension configuration on damping for a rectangular strip like that shown in Figure 6.10			
Suspended from ends		**Suspended from center**	
Frequency (Hz)	Q - **factor**	**Frequency (Hz)**	Q - **factor**
163	217	163	211
449	628	451	455
881	1115	886	568
1461	1500	1468	707
2189	1867	2188	834
3067	2239	3060	945

6.2.8   Rigid body modes

Although rigid body modes were not of interest in the modal tests conducted it is suggested that for an acceptable suspension method, the highest rigid body mode frequency should be less than 10-20% of that of the lowest bending mode [182]. When conducting free-free modal tests this was used as a simple check to provide a measure of how well the supports used approximated that of a free-free condition. Figure 6.11 compares the rigid body mode frequencies with that of the first bending mode for a rectangular test strip whose averaged FRF is shown in Figure 6.4.
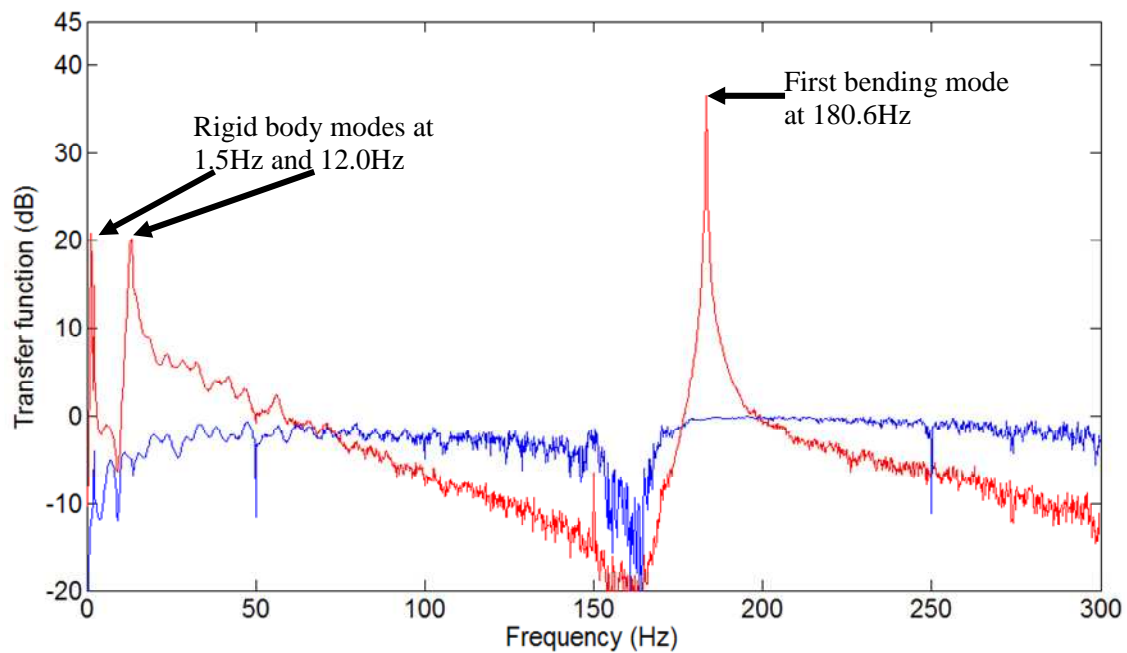
Figure 6.11: Comparison of rigid body mode frequencies with first bending mode in a test strip identical to that shown in figure. Note that the rigid body mode frequencies are less than the recommended 10% of the first bending mode frequency.

6.2.9   Heat treatment - Annealing

After extracting damping measurements from the cold-rolled, low-carbon rectangular strips, all the strips were heat treated. Each group in a batch was annealed using a 3000W furnace and held at one of the following temperatures for 10 minutes: 200°C, 250°C, 300°C, 350°C, 400°C, 450°C and 500°C. Air cooled strips were wrapped in stainless steel foil so as to minimize surface oxidation. Strips to be water quenched were not wrapped but were heated in a metal basket which allowed for quick removal from the furnace for subsequent quenching in a nearby water filled basin. All strips were kept in a desiccator whenever they were not in use so as to minimize surface rusting. After heat treatment, damping measurements were again extracted from the test structures.

6.3 Results: Low-carbon steel

6.3.1   Measured and predicted low-carbon strip frequencies

Before considering and comparing the findings of the IF and BH steels and the soprano pan with the findings of the low-carbon strip experiments, the findings of the low-carbon strip damping experiments would be briefly considered. Firstly, the finite element predictions and the measured frequencies for the majority of the test structures were in good agreement.

Mode No.	Table 6.7: Predicted and measured frequencies (Hz) for cold-rolled low-C steel strips – air cooled														
	Strip thicknesses 't' (±0.01mm) and average mass m(±0.1grams) – original sheet thickness = 0.86mm														
	10% - 0.77mm – 13.8g			20% - 0.69mm – 12.7g			30% - 0.60mm – 11.0g			40% - 0.52mm – 9.8g			50% - 0.43mm – 8.1g		
	Predicted	Measured Before Annealing	Measured After Annealing	Predicted	Measured Before Annealing	Measured After Annealing	Predicted	Measured Before Annealing	Measured After Annealing	Predicted	Measured Before Annealing	Measured After Annealing	Predicted	Measured Before Annealing	Measured After Annealing
1	183	178	179	164	163	164	142	138	140	123	125	125	102	106	105
2	504	492	494	452	451	453	393	391	392	341	344	345	282	289	289
3	990	967	970	887	886	888	772	768	770	669	675	677	553	566	566
4	1095	1042	1043	984	955	964	857	817	825	745	725	730	617	621	622
5	1640	1605	1610	1470	1469	1473	1279	1273	1277	1109	1120	1123	917	936	937
6	2207	2092	2096	1982	1924	1925	1727	1663	1662	1500	1430	1426	1243	1243	1230
7	2456	2402	2410	2202	2198	2204	1915	1903	1909	1660	1674	1678	1373	1398	1400
8	3350	3173	3178	3008	2916	2915	2622	2494	2508	2277	2172	2167	1887	1858	1844
9	3432	-	-	3083	3079	3088	2682	2665	2674	2325	2344	2350	1924	1952	1957
10	3438	3367	3376	3432	-	-	3432	-	-	3086	2906	2902	2558	2524	2511

	10% - 0.77mm – 13.9g			20% - 0.69mm – 12.6g			30% - 0.60mm – 11.0g			40% - 0.52mm – 9.7g			50% - 0.43mm – 8.1g		
Mode No.	Predicted	Measured Before Annealing	Measured After Annealing	Predicted	Measured Before Annealing	Measured After Annealing	Predicted	Measured Before Annealing	Measured After Annealing	Predicted	Measured Before Annealing	Measured After Annealing	Predicted	Measured Before Annealing	Measured After Annealing
1	183	181	181	164	163	163	142	140	141	123	124	124	102	104	104
2	504	499	499	452	450	450	393	395	395	341	342	342	282	285	285
3	990	978	977	887	884	882	772	775	772	669	671	670	553	561	559
4	1095	1052	1045	984	943	931	857	832	829	745	722	721	617	614	614
5	1640	1623	1622	1470	1467	1465	1279	1284	1280	1109	1110	1109	917	927	924
6	2207	2121	2106	1982	1902	1886	1727	1684	1657	1500	1442	1426	1243	1218	1197
7	2456	2436	2432	2202	2195	2192	1915	1919	1915	1660	1659	1659	1373	1384	1381
8	3350	3171	3154	3008	2875	2853	2622	2527	2505	2277	2183	2161	1887	1815	1800
9	3432	-	-	3083	3076	3074	2682	2687	2684	2325	2324	2323	1924	1935	1933
10	3438	3415	3410	3432	-	-	3432	-	-	3086	2950	2927	2558	2514	2469

Table 6.8: Predicted and measured frequencies (Hz) for cold-rolled low-C steel strips – water quenched

Strip thicknesses 't' (±0.01mm) and average mass m(±0.1grams) – original sheet thickness = 0.86mm

Mode No.	LC AR - 0.86mm – 15.3g		BH AR - 0.84mm –14.6g		BH 20% - 0.67mm –11.8g			IF AR - 1.02mm –17.8g		IF 20% - 0.82mm – 14.3g		
	Predicted	Measured	Predicted	Measured	Predicted	Measured Before Annealing	Measured After Annealing	Predicted	Measured	Predicted	Measured Before Annealing	Measured After Annealing
1	204	199	199	196	159	159	160	242	248	195	194	197
2	563	534	550	538	439	439	440	668	684	539	534	541
3	1106	1051	1080	1058	862	862	864	1311	1343	1054	1049	1062
4	1220	1127	1193	1113	956	904	903	1441	1397	1165	1107	1115
5	1832	1741	1789	1753	1428	1429	1431	2171	2225	1747	1739	1760
6	2459	2272	2403	2249	1925	1820	1819	2903	2815	2347	2200	2221
7	2742	2608	2679	2625	2138	2139	2143	3250	3330	2615	2603	2635
8	3432	3420	3432	3376	2923	2756	2757	3432	-	3432	-	-
9	3732	3613	3647	3675	2994	2993	2999	4406	4276	3562	3617	3660
10	3838	3655	3749	3709	3432	-	-	4547	4657	3661	3755	3776

Table 6.9:Predicted and measured frequencies (Hz) for as received low-carbon LC, BH and IF steel strips

Strip thicknesses 't' (±0.01mm) and average mass m(±0.1grams)

This can be seen by examining Table 6.7, Table 6.8 and Table 6.9. Good agreement also existed between natural frequencies that were measured before and after heat treatment. However, for strips that were air cooled, there was generally a small increase in the natural frequencies for most of the strips after heat treatment (see Table 6.7). A similar trend was also observed for the air cooled IF and BH steel strips (see Table 6.9) whereas for the water quenched, low-carbon steel strips the natural frequencies after water quenching were generally lower (see Table 6.8) for the majority of the strips. The case of the IF and BH steels will be highlighted further on when their damping properties are compared with those of the low-carbon steel.

6.3.2 Damping in as received material

A low Q-factor value corresponds to high damping and *vice-versa*. Figure 6.12 shows the material damping in the as-received material for each steel type used in this work. Note that the damping was generally low, with the bulk of the modes having Q-factors greater than 1000. The damping in the 0.061 wt% carbon and IF steel strips were comparable, particularly for frequencies above 1 kHz, whereas damping in the BH as-received condition is lower than that of the low-carbon and IF as-received steel for all modes.
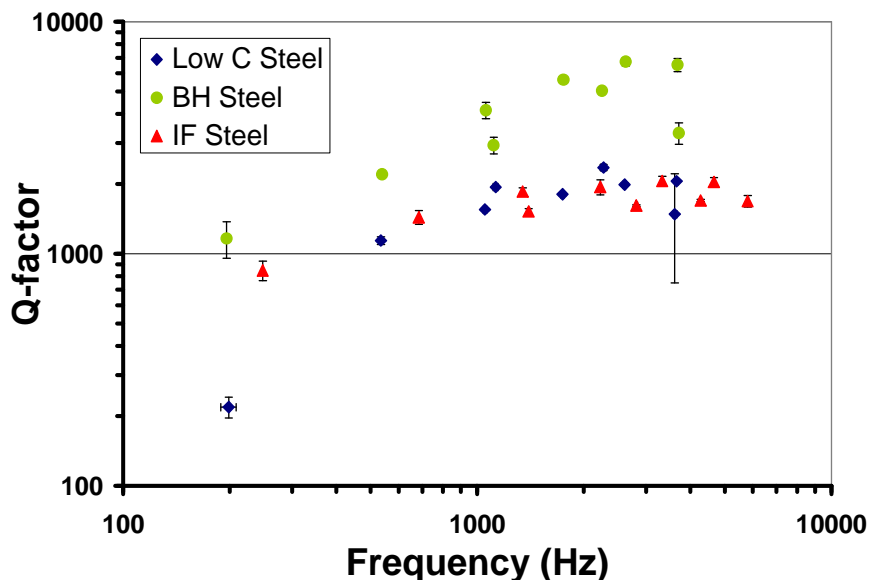
Figure 6.12: Damping for first ten modes in as-received material

6.3.3 Damping variation with cold reduction

Figure 6.13 shows the effect of cold rolling on damping in the first 8 flexural modes of the low-carbon steel strips. Damping for the first 8 modes was shown, as the 9th or 10th modes for some of the strips were in-plane modes. As predicted from the literature, damping increased (lower Q-factor) as the percentage cold reduction (thickness reduction) increased. The largest increase in damping for the majority of the modes was seen for the first 10% of thickness reduction after which

the increase in damping was minimal. The first mode however, did not show such a trend: damping in cold-rolled strips was comparable to damping in the as-received condition.
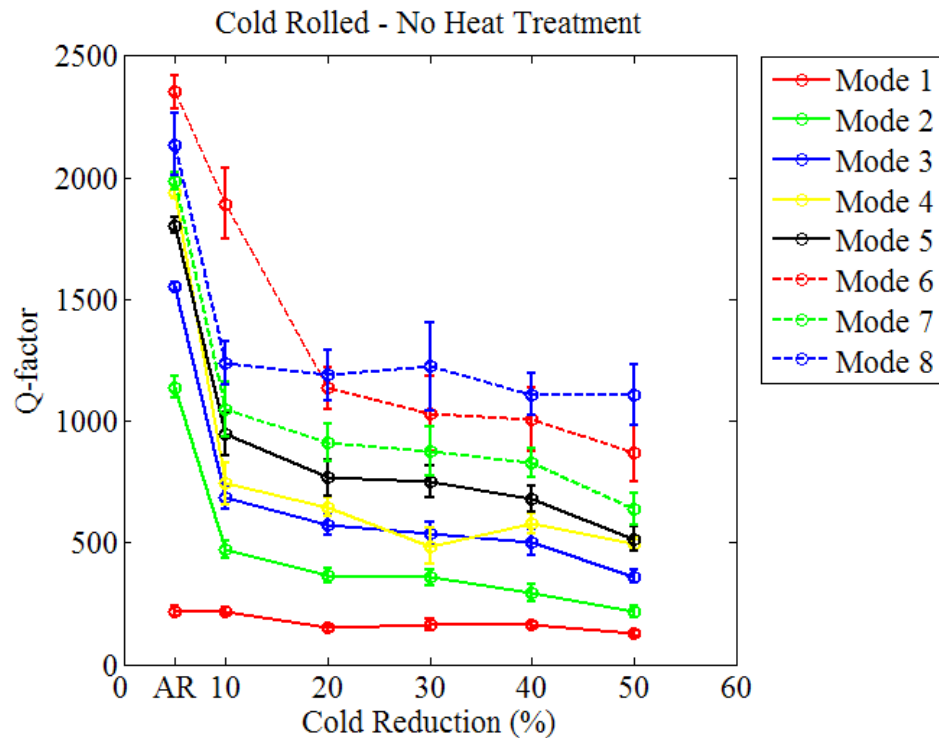
Figure 6.13: Effect of cold rolling on damping in low carbon steel; AR – as received

6.3.4   Damping variation with temperature

Although the natural frequencies of modes up to 4kHz were of interest the experiment provided data for modes up to 25kHz as data logging was conducted at 50KHz. While this data was not essential to the study it provided useful information about the damping properties in the low-carbon strips. For instance, consider non-averaged plots for 10% cold reduced, air-cooled strips up to 16kHz (see Figure 6.14).

The plots shown in Figure 6.14 highlight a number of trends which were seen across all the test structure groups, i.e. both air cooled and water quenched. Before outlining the trends, one of the most notable observations was the audible difference in the duration of the strip vibrations after impact. Strips annealed at much higher temperatures rang for longer indicating a decrease in damping with increase in annealing temperature. This shows that the damping changes being investigated here are of an order to have clearly audible consequences, and to be relevant to musical instruments. The trends were as follows:

- The semi-log plot in Figure 6.14a shows that as annealing temperature was increased damping decreased for each natural frequency.

- The semi-log plot (Figure 6.14a) also shows that at each particular temperature, modal damping became independent of frequency for frequencies beyond approximately 4 kHz
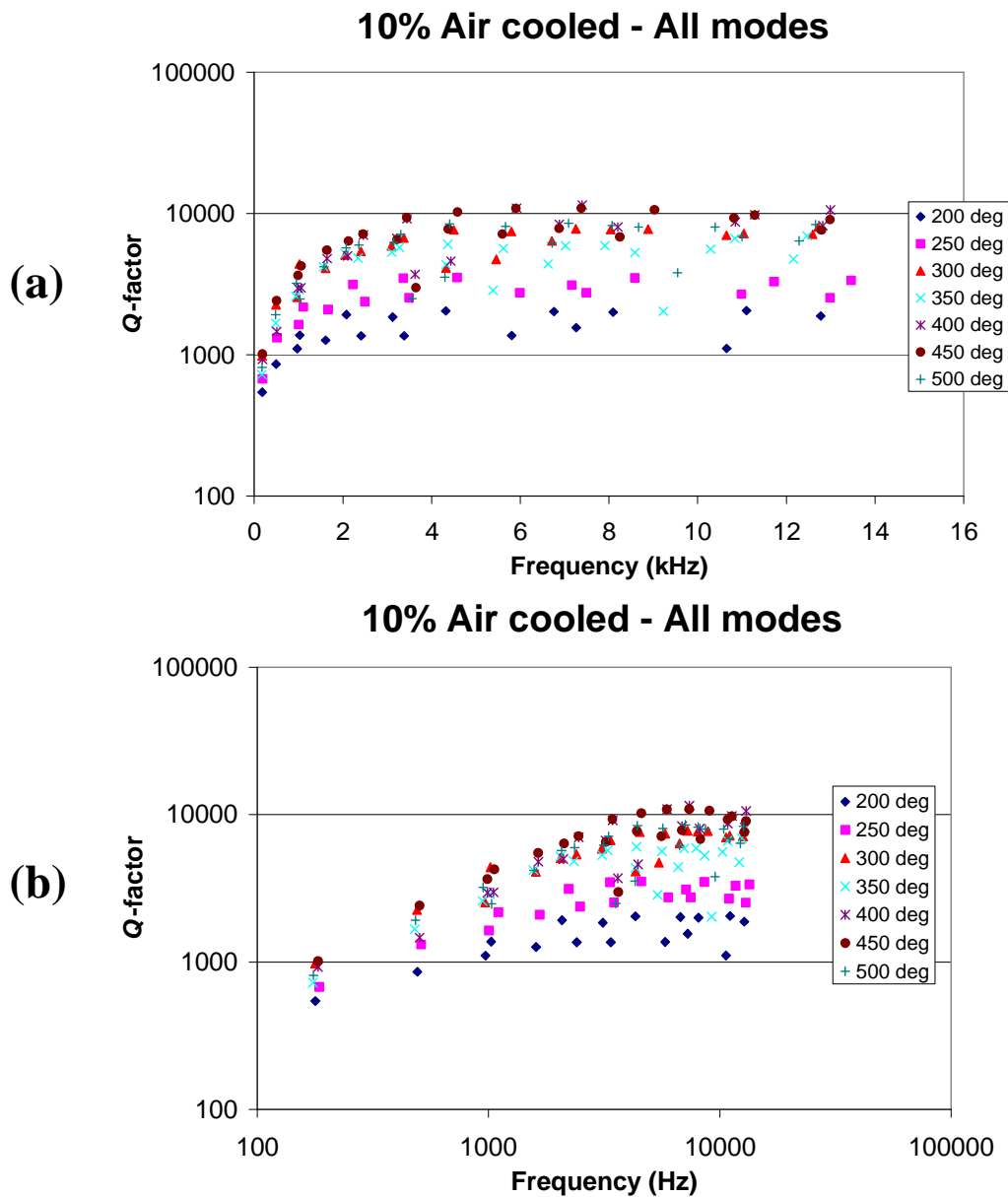
Figure 6.14: (a) semi-log plot and **(b)** log-log plot for 10% cold-rolled and air cooled strips

- The log-log plot in Figure 6.14b shows an approximate linear relationship below approximately 4kHz which indicates a probable power law relationship between frequency and damping.

- Identical trends were observed across all the other low-carbon rectangular strips and non averaged plots for the other low carbon strips are located in Appendix A1.

In this work, the effect of heat treatment on the damping in the first ten modes up to 4 kHz of each test group for the low-carbon test structures were examined. Although modes above 4 kHz were shown in Table 6.9 the majority of modes were below 4 kHz. This bandwidth was selected as it is the frequency range in which the musical notes on the soprano pan are situated. The findings of the damping variation with temperature for the low-carbon strips would be compared with those for the IF and BH steels and that of a soprano steelpan. Before highlighting the findings it is first necessary to state that all tests reported on in this chapter were conducted at room temperature. Temperatures listed on any graphs were temperatures at which annealing was conducted and not temperatures at which experimental measurements were taken.

In the frequency band of major interest, up to 4 kHz, similar trends were observed in the variation of damping with annealing temperature across air-cooled and water quenched test groups for all the low-carbon test strips (Figure 6.15, Figure 6.16a and b and Figure 6.17 to Figure 6.19). It is therefore reasonable to use a single group to highlight these trends. Consider the 10% air cooled test set in Figure 6.15a. The following trends were observed:

- The Q-factor for each mode increased to a maximum value which occurred between 350°C and 400°C before plateauing: There was minimal change in damping beyond 400°C. This is a general trend which was observed with the other test groups. This combination suggests 2 different damping mechanisms added together: one constant, the other with a power law.

- The largest Q-factor (lowest damping) values occurred in 10% reduced strips air cooled and water quenched (Figure 6.15a and b). In these groups the 9th mode Q-factors approached the order of 8000 to 9000 but as percentage reduction increased the maximum levels of damping achieved in corresponding modes decreased. For instance, consider the selection of the 5th mode Q-factors in air cooled groups from 10% to 50% reduction. The maximum Q-factor values for these modes are approximately 5000, 3500, 2800, 2200 and 1400 respectively. This general trend is seen for all air cooled and water quenched strips.
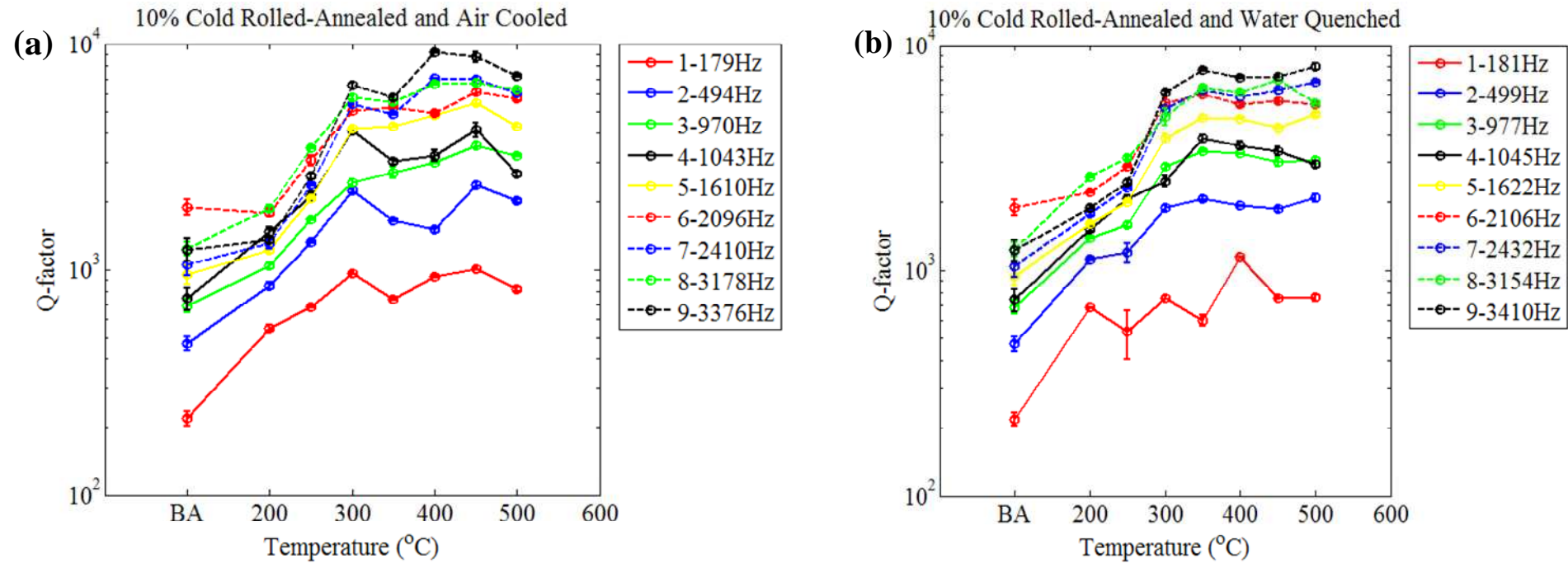
Figure 6.15: **(a)** 10% Air-cooled and **(b)** 10% Water quenched low-carbon steel strips; BA – cold rolled condition at 25°C before being annealed and temperatures on *x*-axis are Annealing temperatures
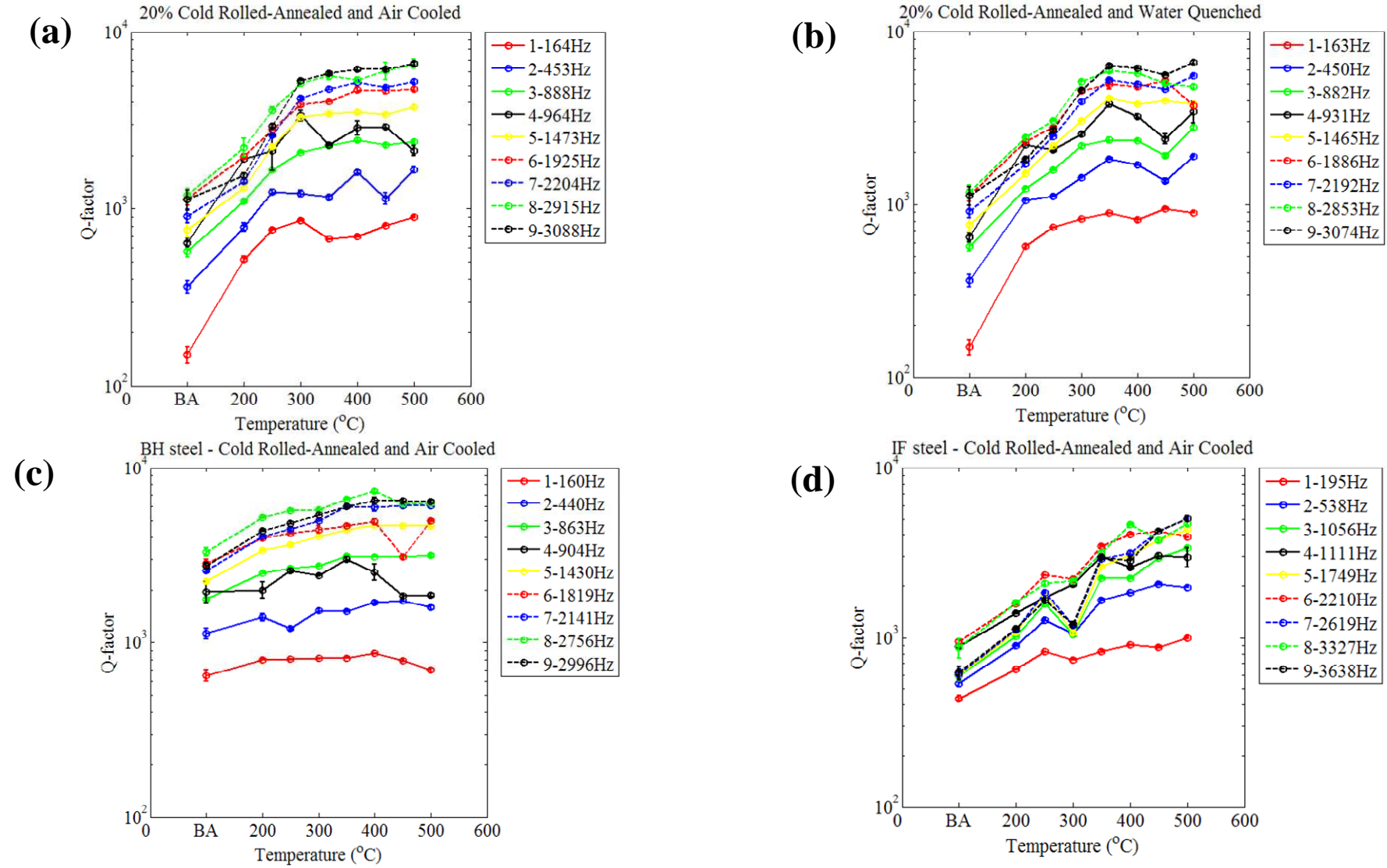
Figure 6.16: 20% Low-carbon steel (0.061wt.%C) **(a)** air cooled **(b)** water quenched, **(c)** 20% BH steel (0.0035 wt.% C) – air cooled, **(d)** 20% IF steel (0.0021 wt.% C) – air cooled; BA – cold-rolled condition at 25°C before being annealed and temperatures on *x*-axis are Annealing temperatures
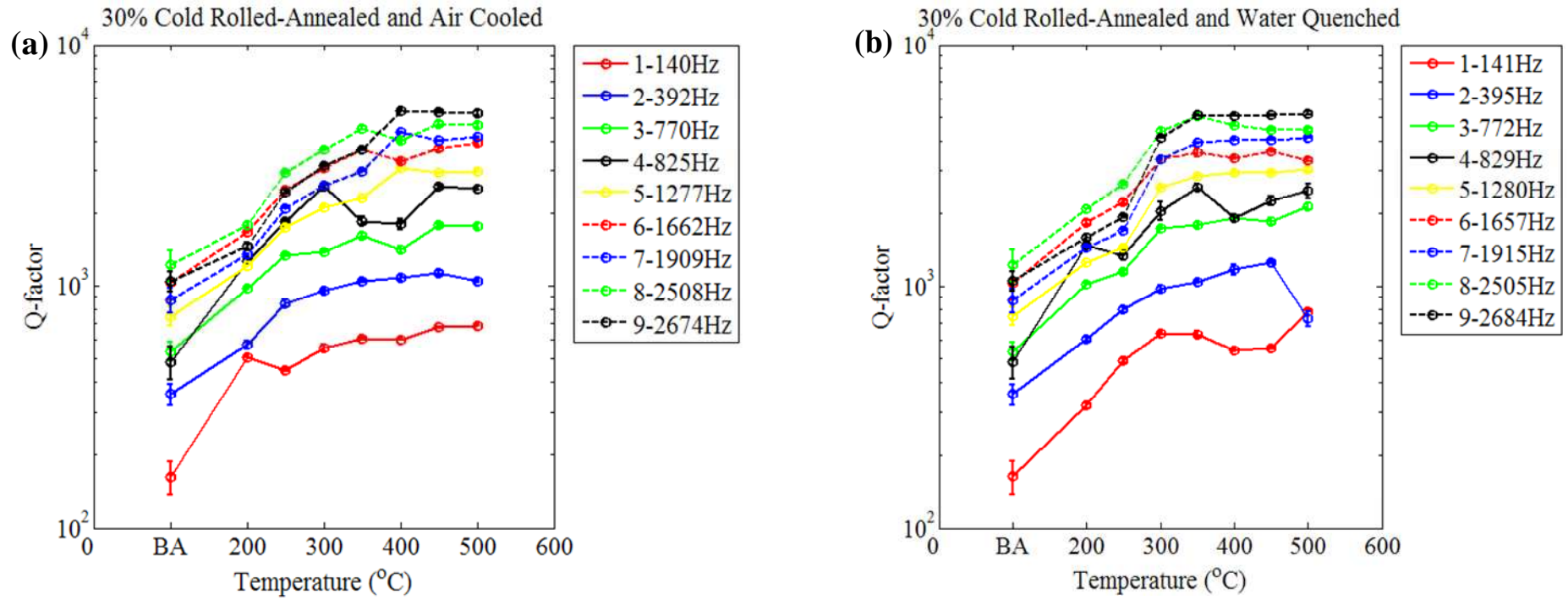
Figure 6.17: **(a)** 30% Air-cooled and **(b)** 30% Water quenched low-carbon steel strips; BA – cold-rolled condition at 25°C before being annealed and temperatures on *x*-axis are Annealing temperatures
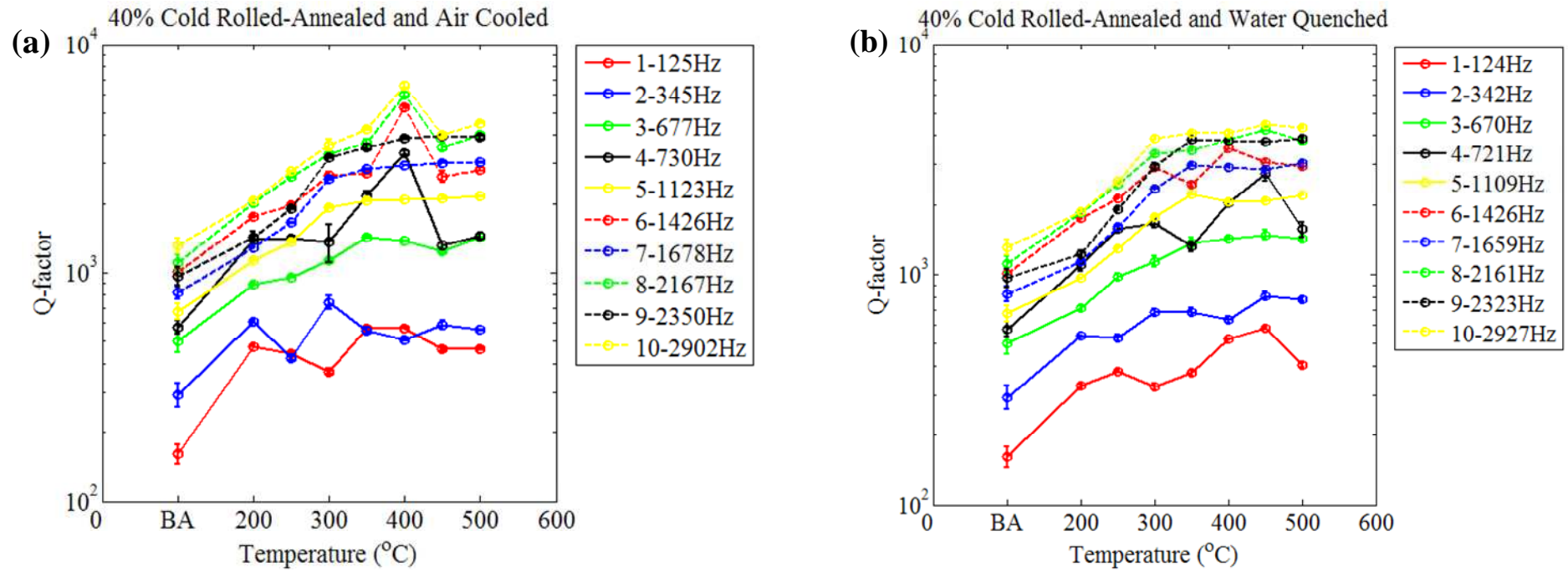
Figure 6.18: (a) 40% Air-cooled and **(b)** 40% Water quenched low carbon steel strips; BA – cold rolled condition at 25°C before being annealed and temperatures on *x*-axis are Annealing temperatures
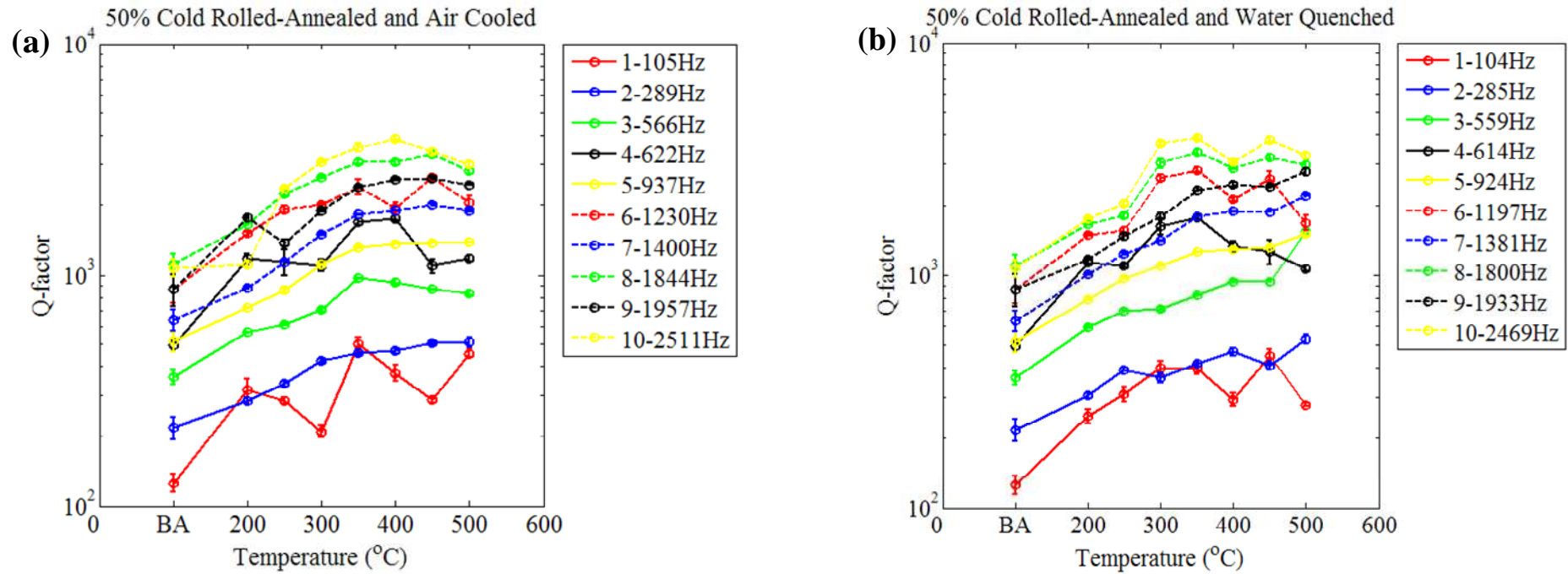
Figure 6.19: **(a)** 50% Air-cooled and **(b)** 50% Water quenched low carbon steel strips; BA – cold-rolled condition at 25°C before being annealed and temperatures on *x*-axis are Annealing temperatures

6.3.5 Air cooling versus water quenching

Consider the *Q*-factors of identical modes of the 10% air cooled and 10% water quenched strips (Figure 6.15a and b). Their values are in close proximity, and this pattern is also generally seen for other air cooled and water quenched test groups. This suggests there is no significant difference in damping between air cooled and water quenched strips.

6.3.6 Damping variation with mode shape and frequency

Another consistent characteristic was found in the *Q*-factor values for bending and torsional modes for the low-carbon steel strips. The modes 1, 2, 3, 5, 7 and 9 for the majority of strips were pure bending modes while modes 4, 6, 8 and 10 were usually torsional with the exception of a few instances where there was an in-plane mode, see Table 6.7 and Table 6.8. With reference to the 10% test group, it was apparent that the *Q*-factor values for the bending modes followed a sequence such that the *Q*-factor of a successive bending mode was higher than the previous bending mode. However, the torsional modes appeared to have a different pattern that did not fit in with the sequence of *Q*-factors for the bending modes. For instance, (see Figure 6.15a and b) the 6th and 8th modes had the highest *Q*-factors in the range BA (before annealing or after cold rolling) to 300°C. In most cases, the highest *Q*-factors were recorded for torsional modes.

To highlight the trends observed with respect to the damping variation with frequency, the low carbon, 10% air cooled and water quenched *Q*-factor versus frequency plots are considered (see Figure 6.20). There are significant differences between strips heated up to 250°C and strips before heat treatment or after cold reduction (designated BA). At 300°C and beyond, however, the log-log fits began to cluster. This general trend was observed across the other air cooled and water quenched low-carbon strips (see Figure 6.21 to Figure 6.24). The temperature at which this clustering begun (i.e. 300°C) corresponded to the temperature beyond which damping plateaued or became independent of annealing temperature. Compare the *Q*-factor versus annealing temperature graphs with their corresponding *Q*-factor versus frequency graph for each thickness reduction group. The same trend was observed. The data can be well fitted by the form $Q = \beta f^{\alpha}$ where *Q* is the material damping, *f* is the natural frequency and β and α are constants. There was reasonably good fit for this power-law relationship as indicated by the R^2 values (see Table 6.10 and Table 6.11). Note that the α values were generally between 0.60 and 0.80. In-plane modes were not used herein but they were easily identified as their *Q*-factor values were much lower than the other modes.
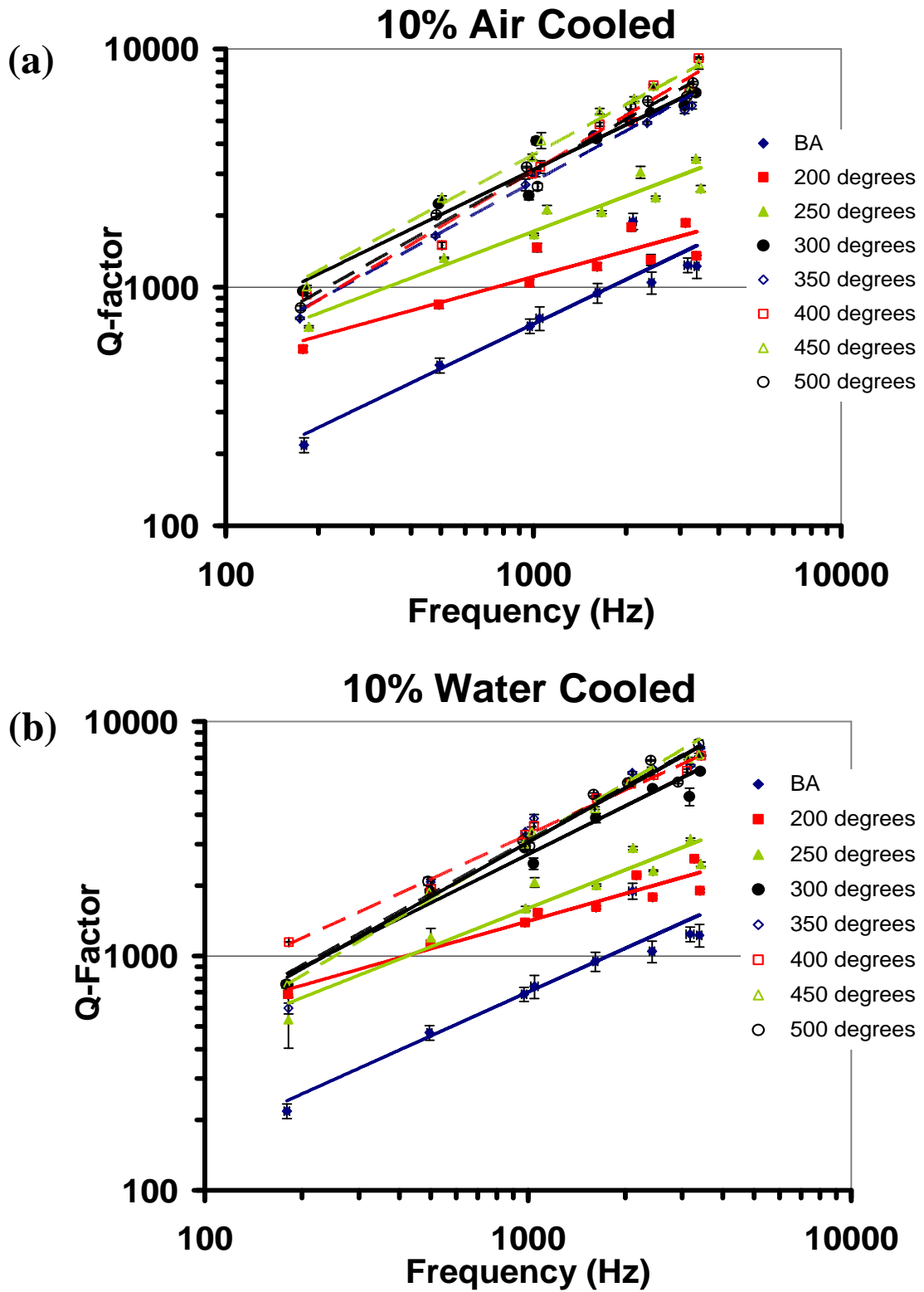
Figure 6.20: Damping-frequency fits for 10% strips (**a**) air cooled and (**b**) water cooled
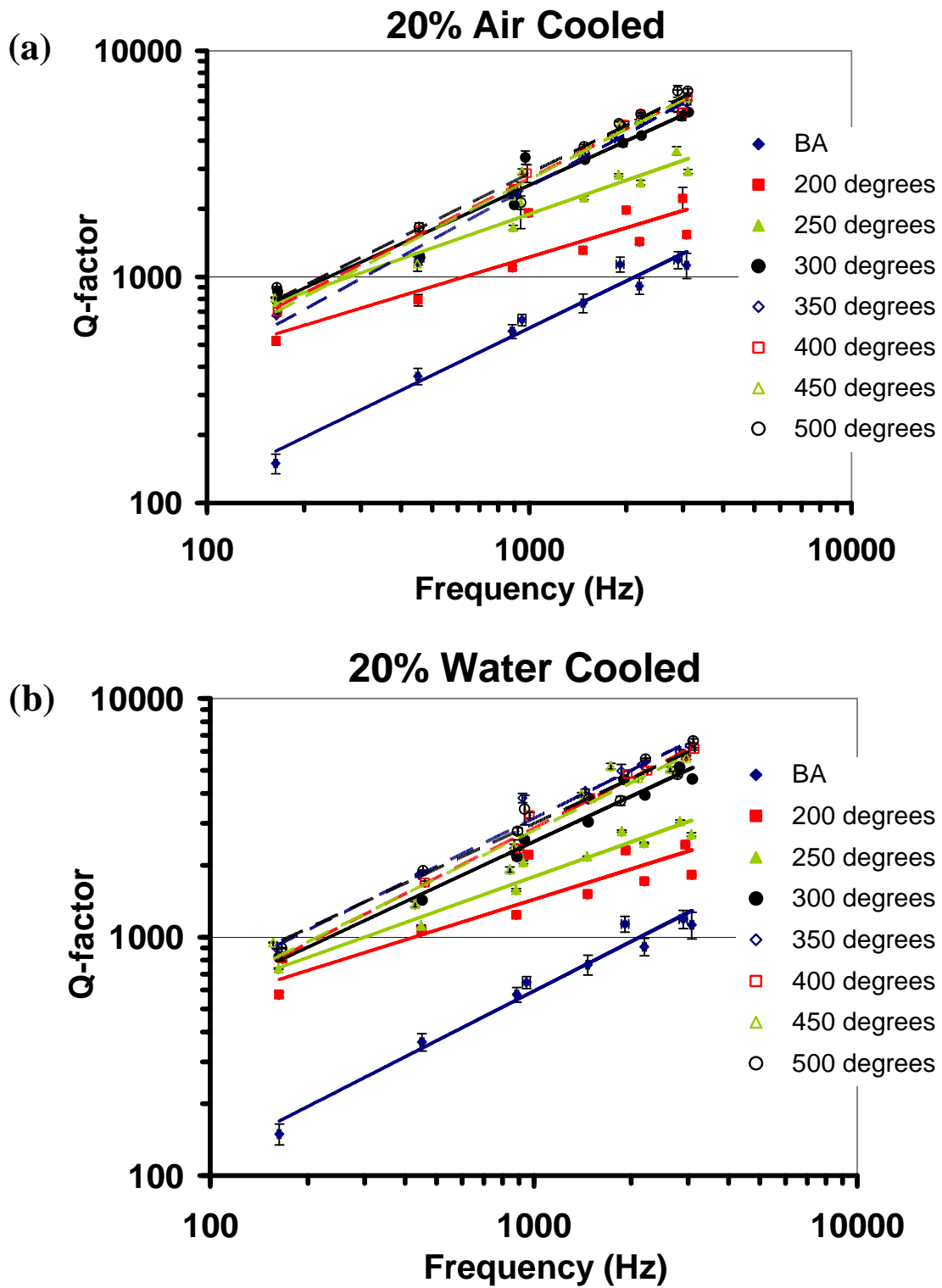
Figure 6.21: Damping-frequency fits for 20% strips (a) air cooled and (b) water cooled
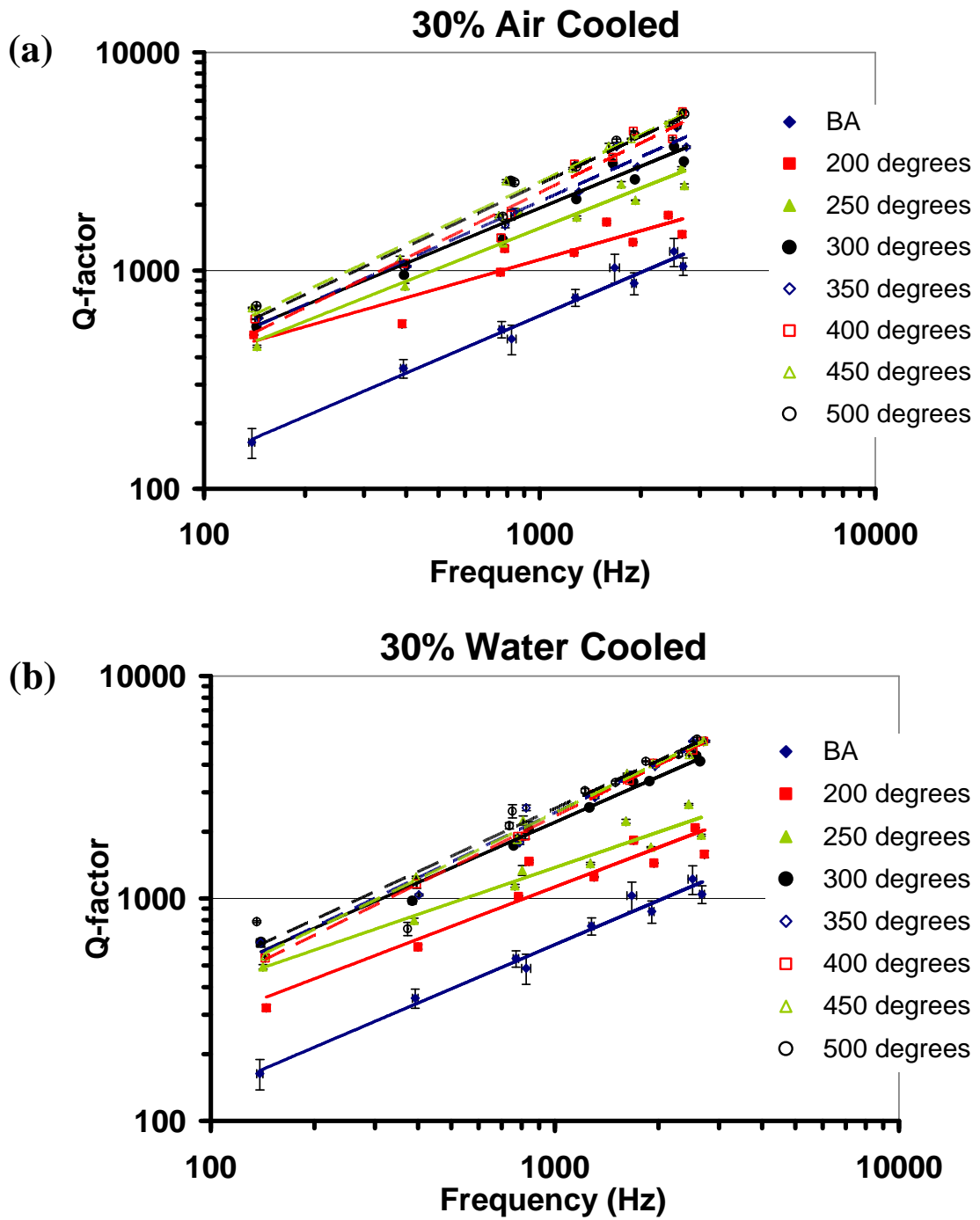
Figure 6.22: Damping-frequency fits for 30% strips **(a)** air cooled and **(b)** water cooled
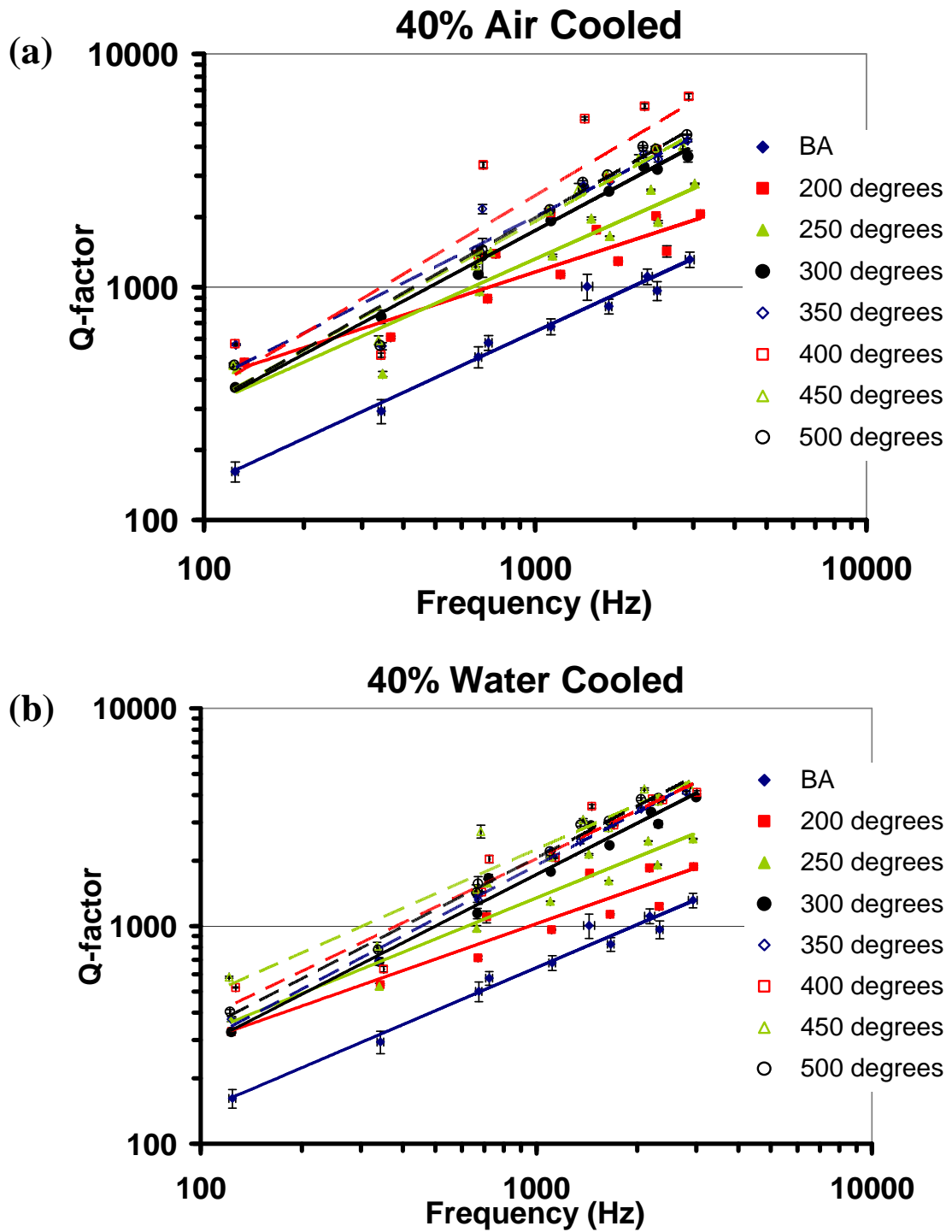
Figure 6.23: Damping-frequency fits for 40% strips **(a)** air cooled and **(b)** water cooled
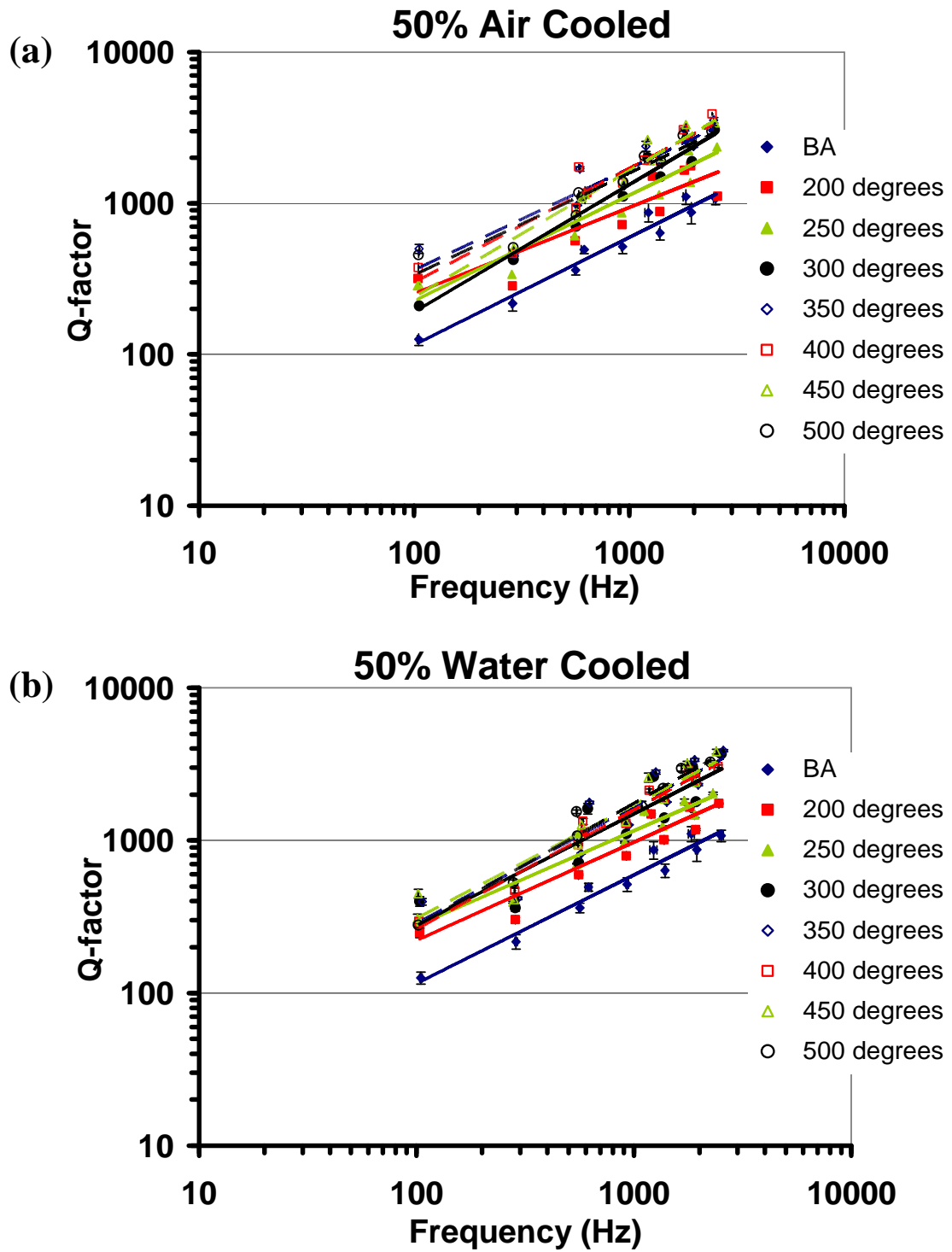
Figure 6.24: Damping-frequency fits for 50% strips **(a)** air cooled and **(b)** water cooled

Strip	10% Air Cooled			10% Water Cooled			20% Air Cooled			20% Water Cooled			BH 20% Air Cooled			IF 20% Air Cooled		
T(°C)	β	α	R^2	β	α	R^2	β	α	R^2	β	α	R^2	β	α	R^2	β	α	R^2
BA	9.6	0.62	**0.88**	9.6	0.62	**0.88**	5.0	0.69	**0.97**	5.0	0.69	**0.97**	45.1	0.54	**0.97**	189.3	0.17	**0.40**
200	94.0	0.35	**0.81**	93.9	0.40	**0.92**	61.9	0.43	**0.79**	76.0	0.43	**0.78**	30.0	0.64	**0.97**	201.2	0.24	**0.64**
250	57.4	0.49	**0.93**	37.0	0.55	**0.92**	60.9	0.50	**0.96**	63.1	0.48	**0.95**	22.9	0.69	**0.97**	203.4	0.29	**0.81**
300	41.1	0.62	**0.95**	23.4	0.69	**0.96**	28.2	0.65	**0.95**	31.7	0.63	**0.98**	24.6	0.69	**0.99**	225.4	0.24	**0.36**
350	20.6	0.71	**0.98**	10.7	0.82	**0.96**	11.7	0.78	**0.99**	30.8	0.69	**0.97**	20.1	0.73	**0.98**	100.7	0.44	**0.85**
400	14.5	0.77	**0.97**	42.0	0.63	**0.99**	18.0	0.72	**0.99**	24.2	0.69	**0.99**	20.0	0.74	**0.98**	86.5	0.47	**0.85**
450	29.2	0.70	**0.98**	14.8	0.77	**0.99**	15.9	0.74	**0.97**	27.7	0.67	**0.94**	21.0	0.71	**0.90**	68.5	0.52	**0.91**
500	20.6	0.72	**0.98**	16.1	0.76	**0.97**	21.3	0.71	**0.97**	38.7	0.63	**0.96**	12.5	0.79	**0.95**	59.9	0.55	**0.95**

Table 6.10: Power law fit values for 10% and 20% low-carbon, BH and IF steel strips

Strip	30% Air Cooled			30% Water Cooled			40% Air Cooled			40% Water Cooled			50% Air Cooled			50% Water Cooled		
T(°C)	β	α	R^2	β	α	R^2	β	α	R^2	β	α	R^2	β	α	R^2	β	α	R^2
BA	6.5	0.66	**0.98**	6.5	0.66	**0.98**	6.8	0.66	**0.98**	6.8	0.66	**0.98**	4.4	0.71	**0.96**	4.4	0.71	**0.96**
200	54.0	0.44	**0.87**	19.1	0.59	**0.90**	46.7	0.47	**0.86**	24.4	0.54	**0.88**	18.3	0.57	**0.74**	11.4	0.64	**0.86**
250	23.0	0.61	**0.96**	35.2	0.53	**0.93**	16.5	0.63	**0.89**	17.7	0.63	**0.91**	9.1	0.70	**0.87**	15.7	0.62	**0.91**
300	23.8	0.64	**0.91**	19.9	0.68	**0.99**	9.2	0.76	**0.99**	7.5	0.79	**0.97**	3.9	0.84	**0.96**	9.5	0.73	**0.80**
350	19.2	0.68	**0.97**	15.1	0.74	**0.97**	14.3	0.72	**0.91**	6.9	0.81	**0.99**	16.4	0.67	**0.85**	8.3	0.77	**0.86**
400	12.4	0.75	**0.96**	11.9	0.77	**0.99**	7.1	0.85	**0.81**	12.4	0.74	**0.93**	9.3	0.75	**0.91**	7.2	0.78	**0.96**
450	18.2	0.71	**0.98**	13.7	0.75	**0.99**	8.2	0.79	**0.96**	20.4	0.68	**0.92**	5.1	0.84	**0.96**	10.0	0.74	**0.88**
500	16.7	0.72	**0.97**	18.1	0.72	**0.90**	7.4	0.81	**0.96**	8.6	0.79	**0.99**	15.0	0.67	**0.92**	6.8	0.80	**0.96**

Table 6.11: Power law fit values for 30%, 40% and 50% low-carbon steel strips

6.4 Low-carbon steel versus ultra-low BH and IF steels

In an effort to understand the damping findings observed with the heat treatment of the low-carbon test structures, two additional investigations were performed on sheet material that had undergone cold forming and heat treatment in the same manner as the low-carbon test structures produced for the vibration tests. The first involved a comparison of the damping properties observed in the low-carbon steel test structures with the damping properties of two ultra-low carbon steels: an IF and BH steel (see Table 6.1). In this investigation only 20% thickness reduced IF and BH test structures were fabricated for comparison with the 20% thickness reduced low-carbon steel test structures. The second investigation consisted of two divisions. The first division considered the mechanical properties extracted from tensile tests for low-carbon specimens. The second division compared the mechanical properties extracted from tensile and hardness tests of the IF and BH steels with those of the low-carbon steel. 20% thickness reduction IF and BH specimens was also used for this comparison.

6.4.1 Vibration testing: IF and BH steels

Rectangular strips of dimensions 150mm x 15mm were extracted from cold-rolled (see Figure 6.2) bake hardenable and interstitial free steels of chemical composition given in Table 6.1. A total of 18 strips were prepared, nine BH and nine IF. In each batch, seven strips (one for each annealing temperature: 200˚C, 250˚C, 300˚C, 350˚C, 400˚C, 450˚C and 500˚C) were extracted along the rolling direction from sheet that had been cold reduced by 20% of the original thickness. The other two strips were extracted from the material in the as-received condition (along rolling and transverse directions). For heat treatment (annealing), the strips were wrapped in stainless steel foil and held in a furnace at the respective temperature for 10 minutes before extracting and cooling normally in air to room temperature. Strips were allowed to cool in wrapping before removing. Material damping (Q-factor) was extracted from the BH and IF strips in the as-received material, after cold reduction, and after annealing using the same equipment and settings (Figure 6.3) as that used for the extraction of damping in the low-carbon strips. Figure 6.25 better illustrates the vibration test procedure sequence adopted for the BH and IF steels.
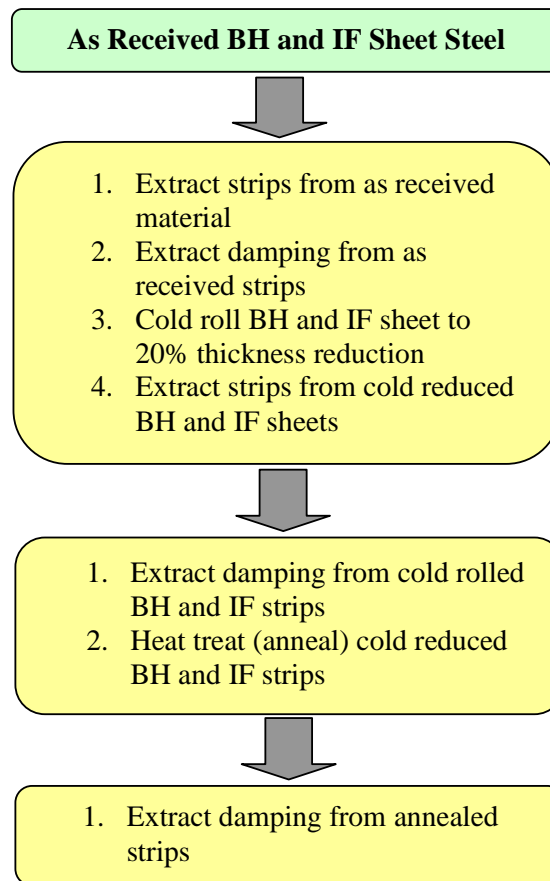
Figure 6.25: Vibration testing procedure sequence for BH and IF rectangular strips

6.4.2 Damping in BH, IF and low-carbon steel compared

Figure 6.16 a, b and c are plots which illustrate the effect of annealing temperature on damping in the 20% cold rolled low-carbon, bake hardenable and interstitial free steels. It was found that:

- Damping in the BH steel could almost be described as independent of annealing temperature, particularly for annealing temperatures beyond 300°C. The majority of the plots in this graph (Figure 6.16c) resemble the plateau region of the low-carbon steel plots in Figure 6.16a. Compare also the rates of increase in Q-factor for annealing temperatures up to 250°C between the low-carbon and BH steels (Figure 6.16a and c). The rate of Q-factor increase in this range was much lower for the BH steel than the earlier results for low-carbon steel (see Figure 6.16a and c).
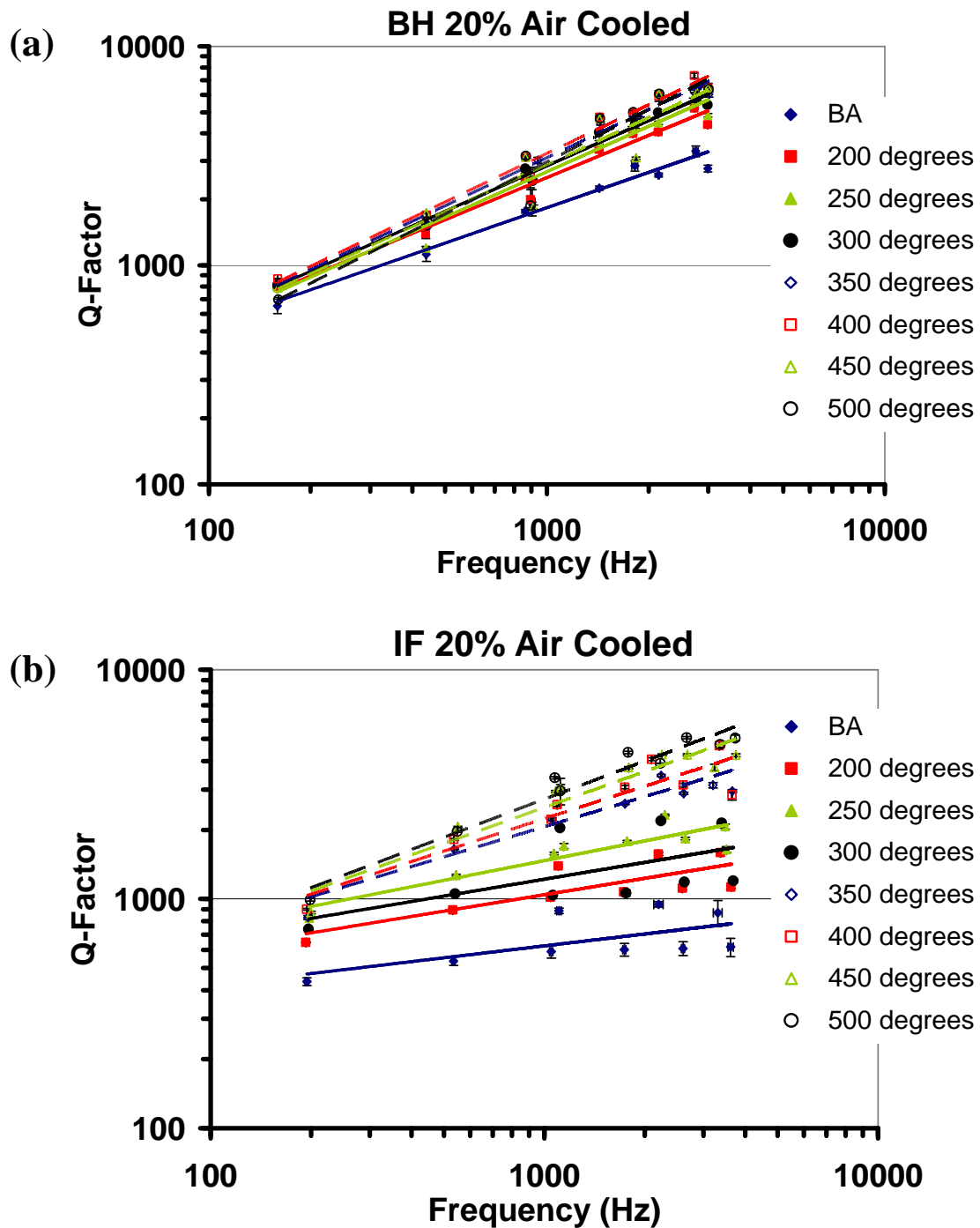
Figure 6.26: Damping-frequency fits for 20% strips **(a)** BH air cooled and **(b)** IF air cooled

- With respect to the IF steel (Figure 6.16d), modal *Q*-factors increased (damping decreased) with minimal indication of plateauing and the damping in this case appeared to be dependent on annealing temperature.

- On comparing the *Q*-factor versus natural frequency plots for the 20% cold-rolled BH, IF (see Figure 6.26a and b) and low-carbon steels (Figure 6.21), it was discovered that: (1) a much better fit was obtained between *Q*-factor and frequency for the BH steel as indicated

by the R^2 values in Table 6.10 and (2) the range of values obtained for the coefficient α was comparable to the range of α values obtained for the low-carbon steels at annealing temperature 300°C and above (see both Table 6.10 and Table 6.11) while this was not the case for the IF steel.

A closer examination of the Q-factor versus annealing temperature plots for the 20% cold-rolled low-carbon, BH and IF steels shown in Figure 6.16a, b and c was made by comparing the damping in each of the nine modes. This is shown in Figure 6.27. The following findings were:

- Overall the modes in the BH steel generally maintained the lowest damping (highest Q's) throughout the range of annealing temperatures. However damping in the low-carbon and BH steels were comparable for annealing temperatures beyond 300°C. It is significant to highlight that the BH steel which has significantly lower carbon content than the low-carbon steel (see Table 6.1) displayed comparable or higher Q's than the low-carbon steel. It was expected that the Q-factors would have been in the following order: low-carbon >BH>IF from highest to lowest. The observed trend will be discussed further on.

- The IF and low-carbon steels had comparable damping at lower annealing temperatures and in the cold rolled state.

- Overall, the highest damping (lowest Q's) were recorded for the IF steels particularly in the higher modes – see modes 5 to 9.
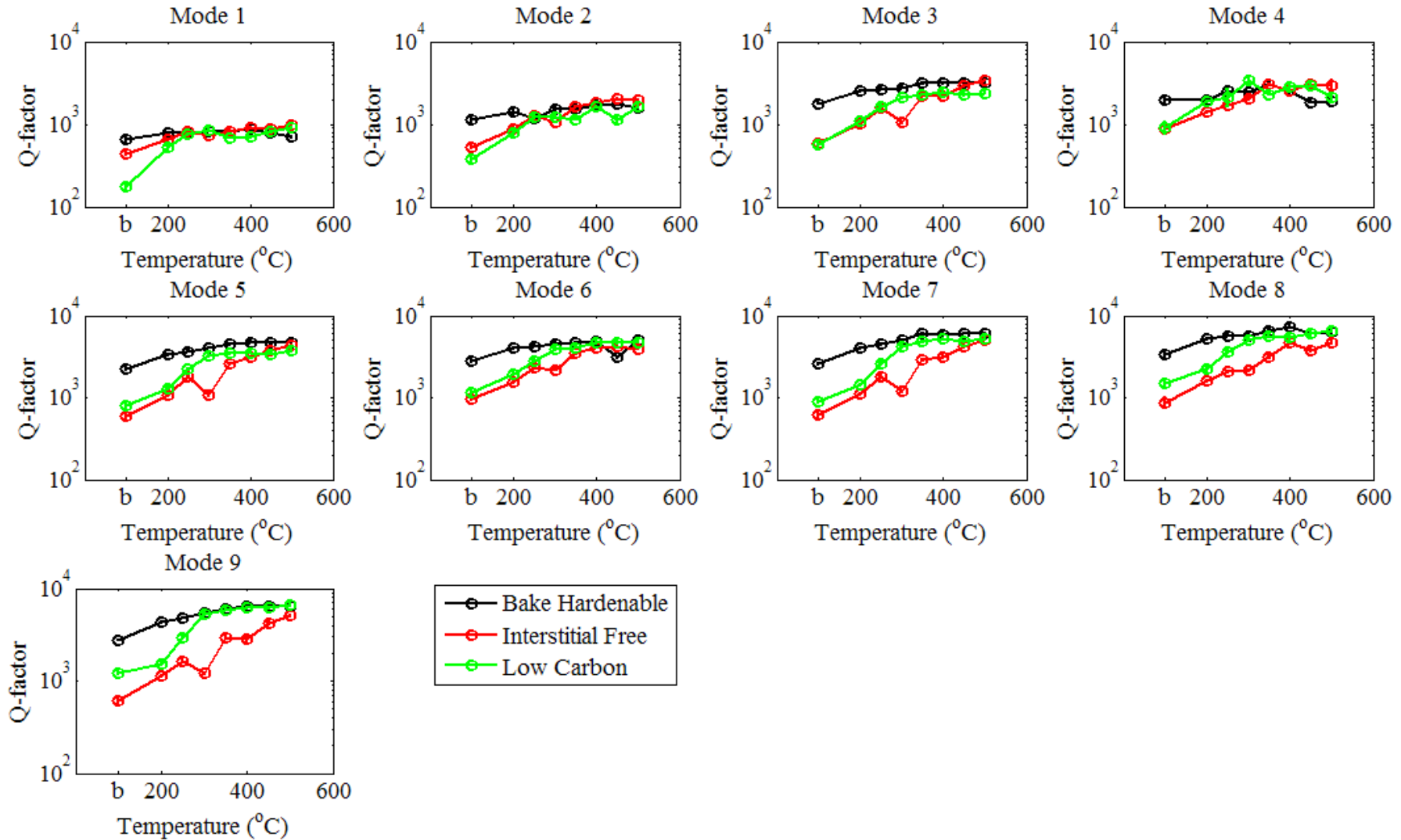
Figure 6.27: Modal damping comparison among 20% cold-rolled carbon strips: The data for these plots were taken from Figure 6.16 (a), (c) and (d)

6.5 Mechanical tests: Mechanical properties in BH, IF and low-carbon steel compared

6.5.1 Tensile tests

The first mechanical tests were room temperature tensile tests on low-carbon, BH and IF steel sheets that had undergone cold forming and heat treatment in the same manner as the low-carbon test structures produced for the vibration tests. Tensile tests were performed on tensile specimens in the following conditions: 1) as-received, 2) cold-rolled and 3) cold-rolled, heat treated and air cooled. Specimens were not made for water quenching as the damping trends observed (see Figure 6.15, Figure 6.16a and b and Figure 6.17 to Figure 6.19) were generally independent of air cooling and water quenching, therefore only one cooling method was chosen when preparing the tensile specimens.

For the low-carbon steel sheet in the as-received condition, tensile samples were extracted along the mill rolling direction and transverse (see Figure 6.2a and b) to this direction. For material in the cold-rolled condition, tensile specimens were extracted only along the rolling direction of strips that were cold-rolled to have the following thickness reductions: 10%, 20%, 30%, 40% and 50%. A total of 42 tensile specimens were prepared, with 2 in the as-received condition (transverse and rolling direction) and the remaining 40 divided into 8 groups, each having a tensile specimen at one of the above thickness reductions. One group was left in the cold-rolled state while each of the remaining groups was wrapped in stainless steel foil and annealed in a furnace at one of the following temperatures for 10 minutes: 200˚C, 250˚C, 300˚C, 350˚C, 400˚C, 450˚C and 500˚C before extracting from the furnace and allowing to cool normally in air to room temperature.

Only 20 samples from BH and IF steels were prepared, ten for each steel type. Two samples for each steel type were extracted in the as-received condition (one along and the other transverse to the rolling direction). The other 8 samples in each group were extracted from 20% thickness reduced sheet. One sample was left in the cold-rolled condition while the other samples were annealed in stainless steel wrapping at one of the following temperatures: 200˚C, 250˚C, 300˚C, 350˚C, 400˚C, 450˚C and 500˚C for 10 minutes before removing from the furnace to cool normally in air to room temperature. The IF and BH samples were extracted from sheet that was cold rolled in the same manner as the low-carbon steel sheet.
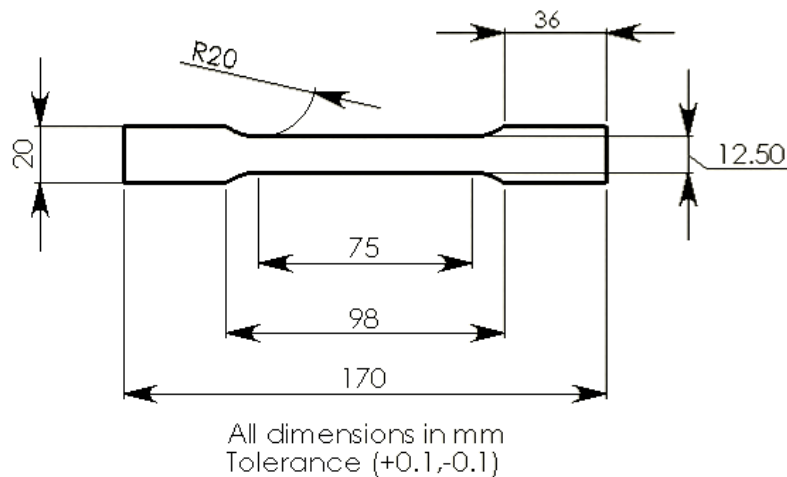
Figure 6.28: Tensile test specimen dimensions in accordance with BS EN 10002 – 1:2001

All tensile samples were extracted from the sheets using a water jet machining center. Tensile samples were made in accordance with specifications given in BS EN 10002 – 1:2001 [189]. Figure 6.28 shows the dimensions of specimens used in the tensile tests. The room temperature tensile tests for the low-carbon steel were conducted using an INSTRON 5584 universal tensile testing machine with a maximum loading capacity of 150kN and a clip gauge was used to measure strain. Tensile tests on the BH and IF steels were conducted on a Tinius Olsen tensile testing machine with a maximum loading capacity of 50kN and the capability to measure the extension without the need of an external gauge. All tensile tests were conducted with a strain rate of 5mms^{-1}.

6.5.2 Hardness and Microscopy Tests

Hardness measurements were also made on polished samples using a HMV Shimadzu Vickers pyramid micro-hardness testing machine with an indentation load of 9.807N (or HV1). A minimum of five readings was taken from each sample and the average value calculated.

Microscopic images were also taken from cold mounted samples that were prepared by grinding on silicon carbide paper to 4000 grit and polished with cloth coated with 1μm diamond paste. In this work, only low-carbon steels were used and therefore the only etchant used was a 2% nital solution (2% nitric acid in ethanol). Optical micrographs were taken with a LEICA microscope with an Altra camera attached.

6.6 Damping trends versus findings from mechanical tests

The results of the mechanical tests will be presented in two parts. The first section looks at the mechanical properties of the low-carbon steel extracted from tensile tests while the second section

compares the mechanical properties of low-carbon, IF and BH steels. Before presenting the findings of the tensile tests it is necessary to highlight the mechanical properties that can be obtained from the stress-strain characteristic provided from the test. Figure 6.29 shows a typical stress-strain graph for mild steel with the respective regions annotated. The region OA is the region in which the steel exhibits elastic behaviour. Beyond point A, the material is said to have undergone plastic strain, thus the portion of the graph from A to E is considered the plastic region of the stress-strain characteristic. An important feature of this work is related to the yield point phenomenon which is represented by the portion AB, sometimes referred to as the '*bat's ear*'. This sharp point is commonly seen in low-carbon steels which are susceptible to strain ageing. Figure 6.29 could be used for reference when considering the stress-strain graphs in Figure 6.30.

A	σ_{UYS}, Upper Yield Strength
B	σ_{LYS}, Lower Yield Strength
B-C	ε_{YPE}, Yield Point Elongation or *Lüder's* strain
C-D	Strain hardening or Work hardening
D	σ_{TS}, Tensile Strength
E	σ_{FS}, Fracture Strength
O-F	Percentage Elongation
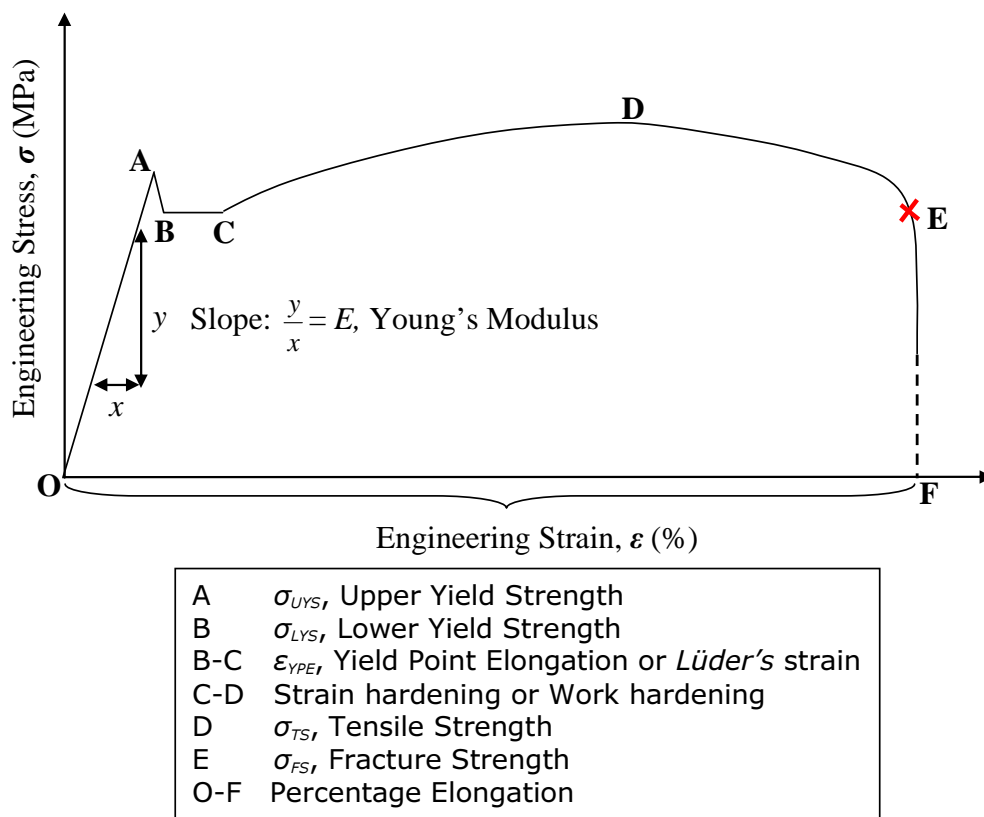
Figure 6.29: Typical stress-strain characteristic of a mild steel

175
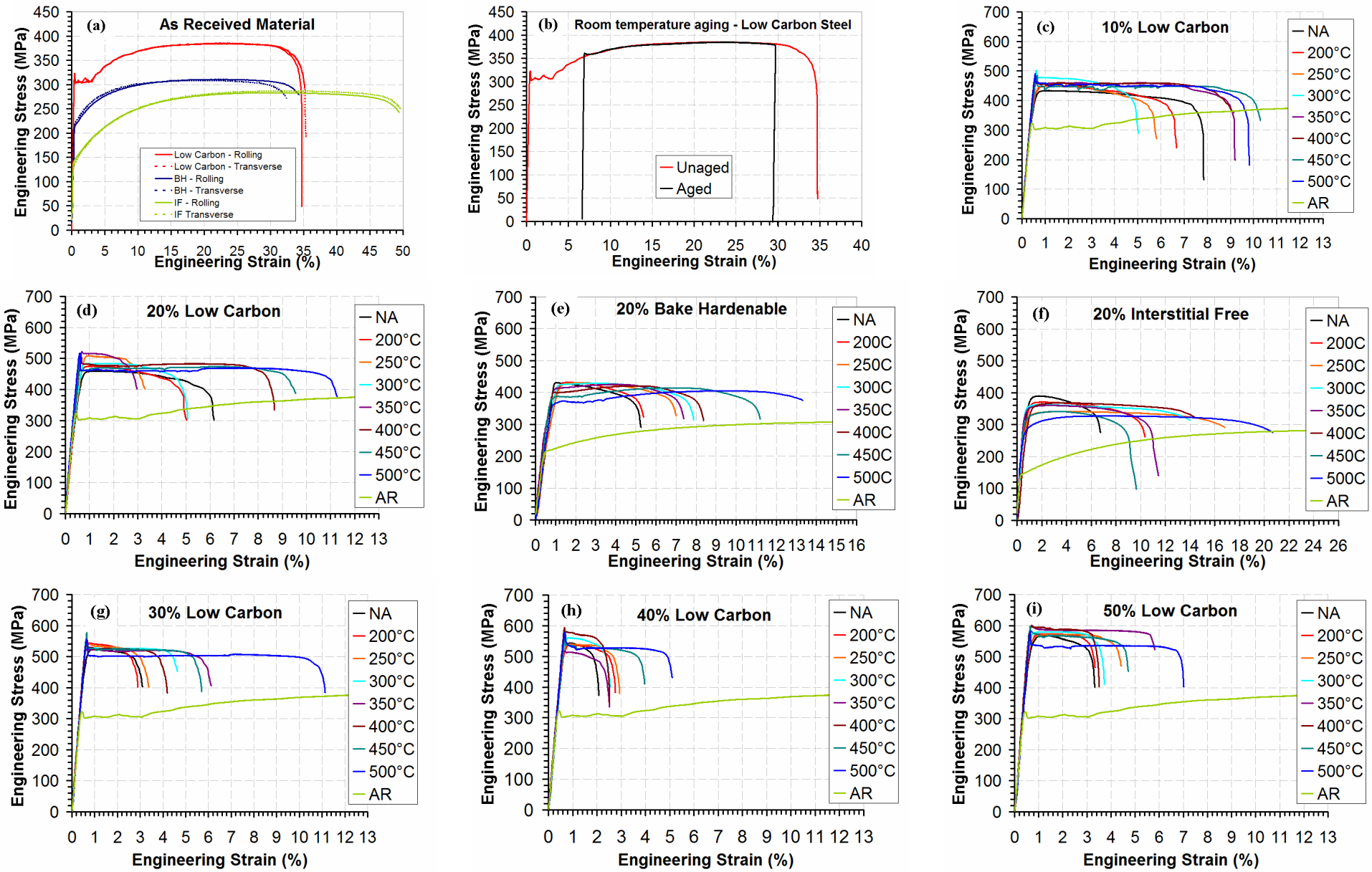
Figure 6.30: (a)-(i) Effect of cold reduction and annealing on low-carbon, bake hardenable and interstitial free tensile testing specimens; AR = as received; NA = not annealed
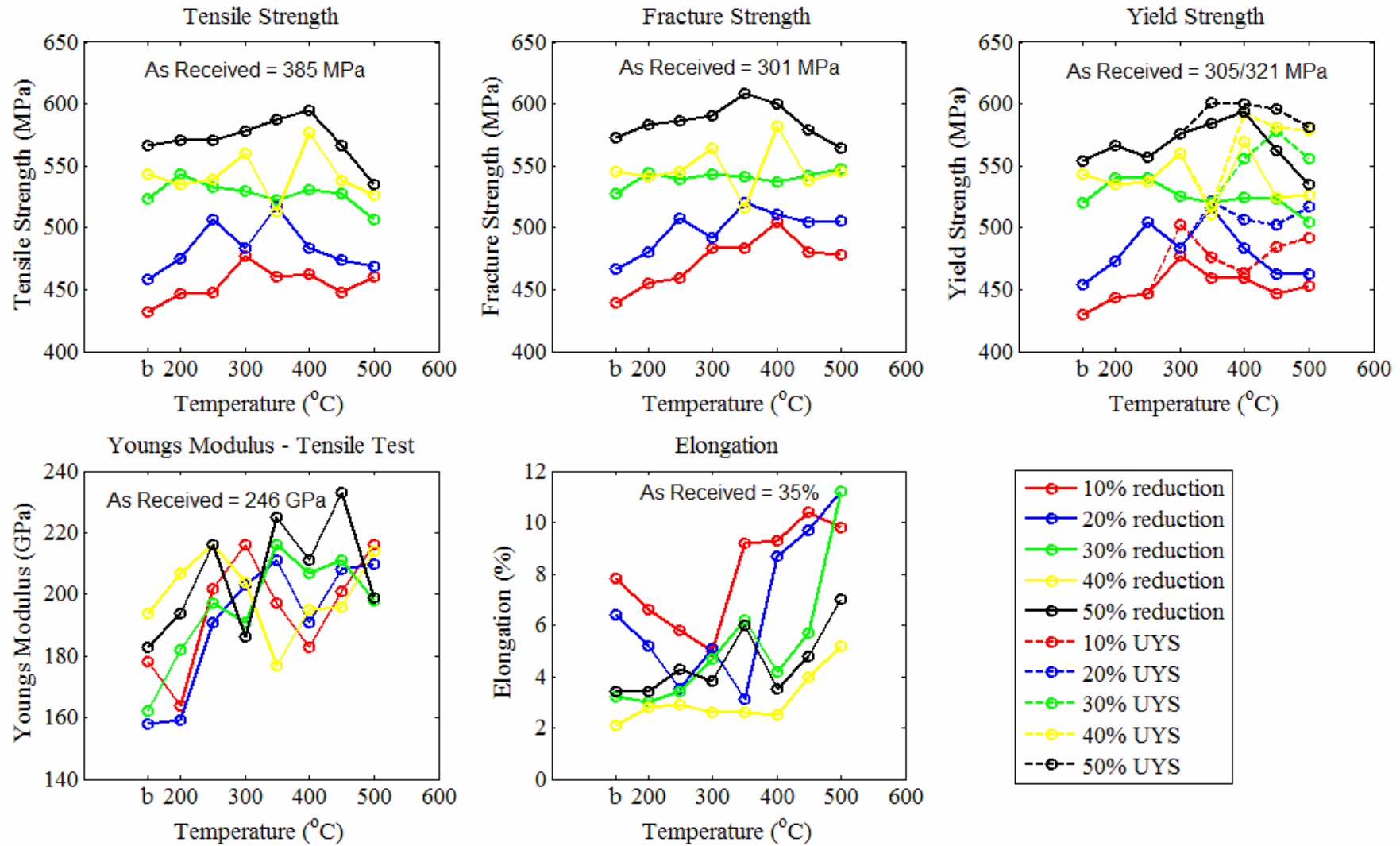
Figure 6.31: Mechanical properties extracted from tensile tests on low-carbon steel (Figure 6.30 a, c, d and g to i); b = before annealing or cold rolled condition
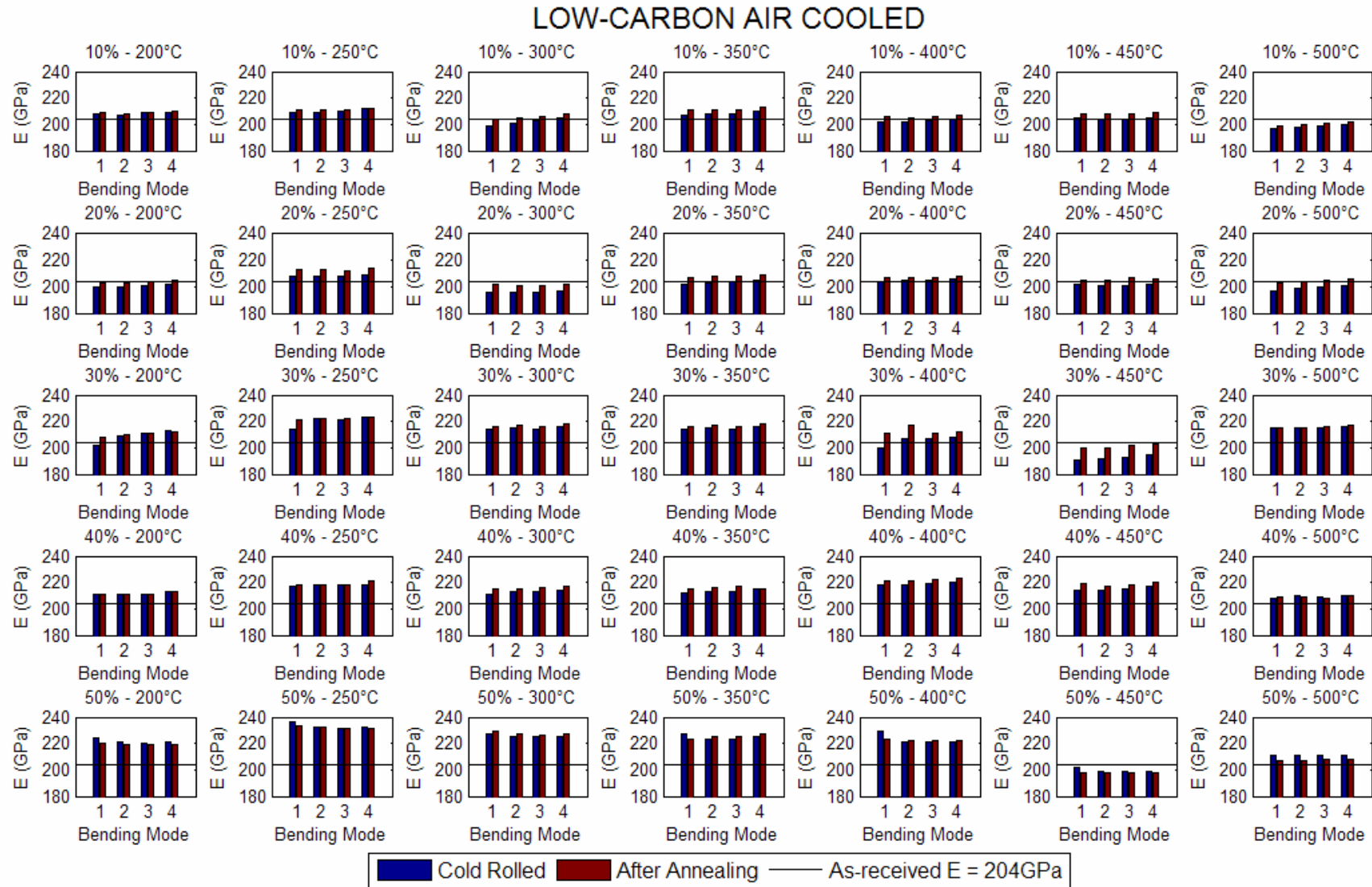
Figure 6.32: Young's Modulus estimates obtained from the first four modes of each air-cooled low-carbon test strip
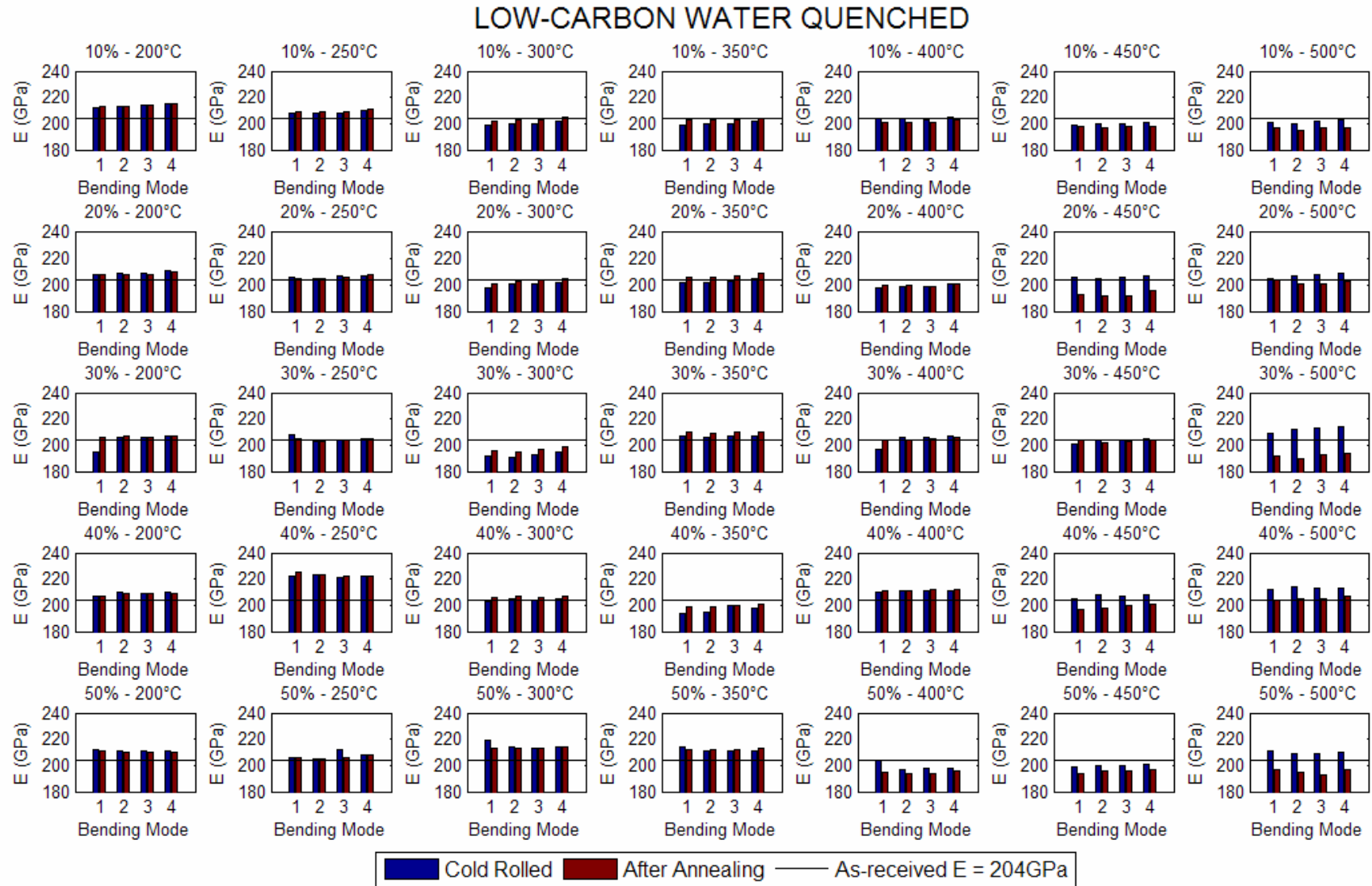
Figure 6.33: Young's Modulus estimates obtained from the first four modes of each water quenched low-carbon test strip
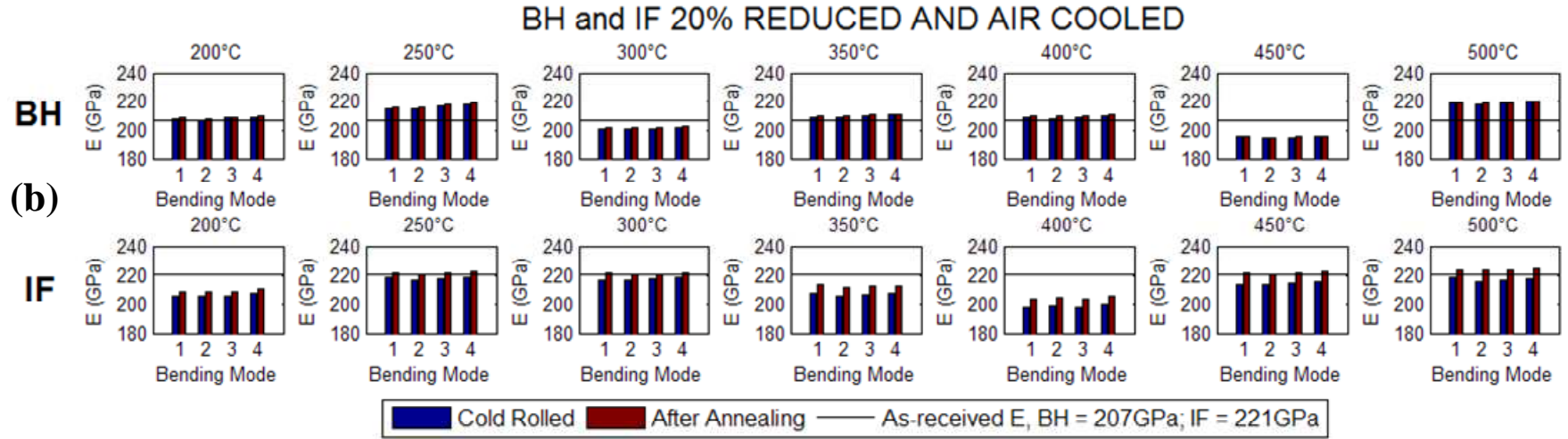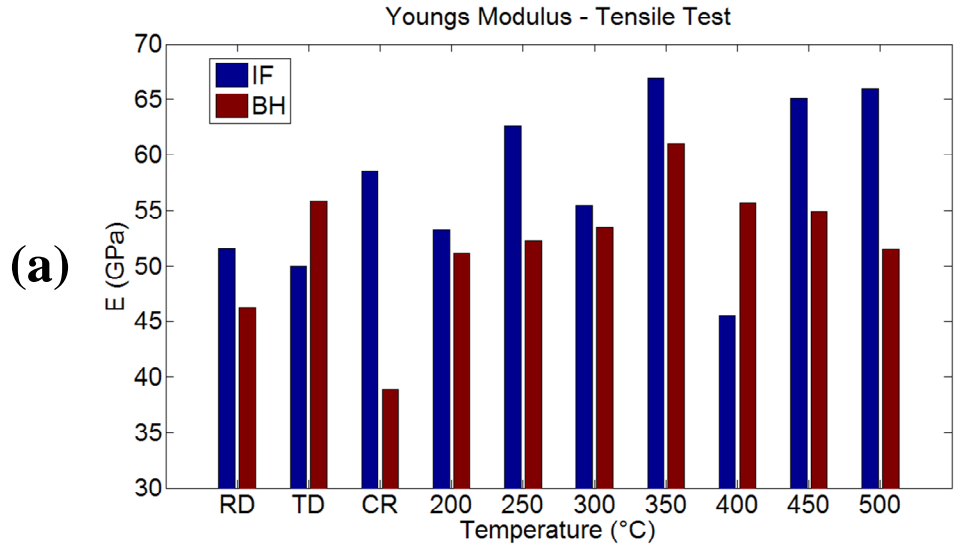
Figure 6.34: Young's Modulus obtained for BH and IF steels: (a) from Tensile Tests and (b) from Vibration Tests; in (a) RD = Rolling Direction; TD = Transverse Direction and CR = cold-rolled in rolling direction and not annealed
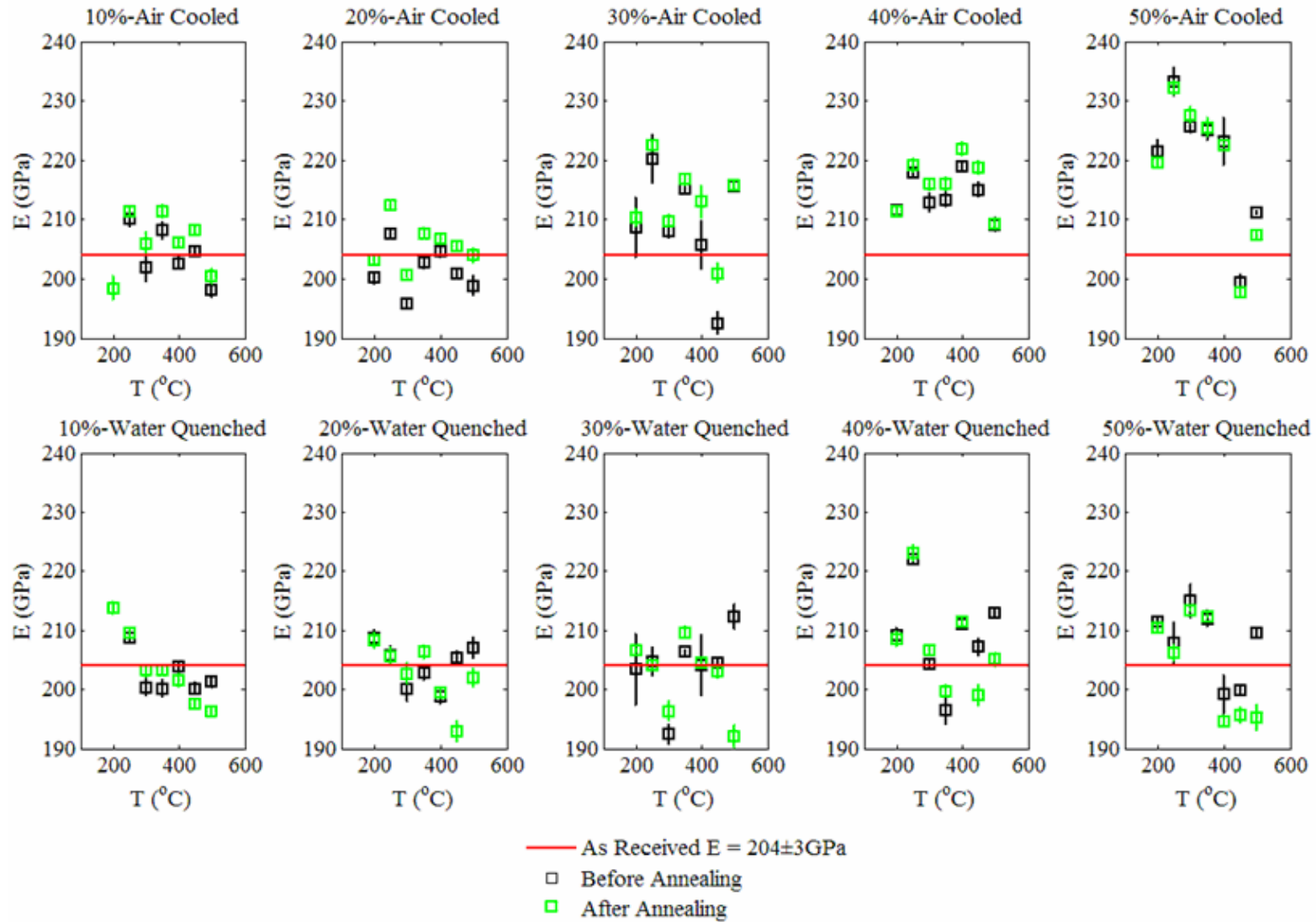
Figure 6.35: Averages for Young's Modulus of low-carbon steel calculated using natural frequencies from vibration tests. These plots are averages of the values shown in **Figure 6.32** and **Figure 6.33**
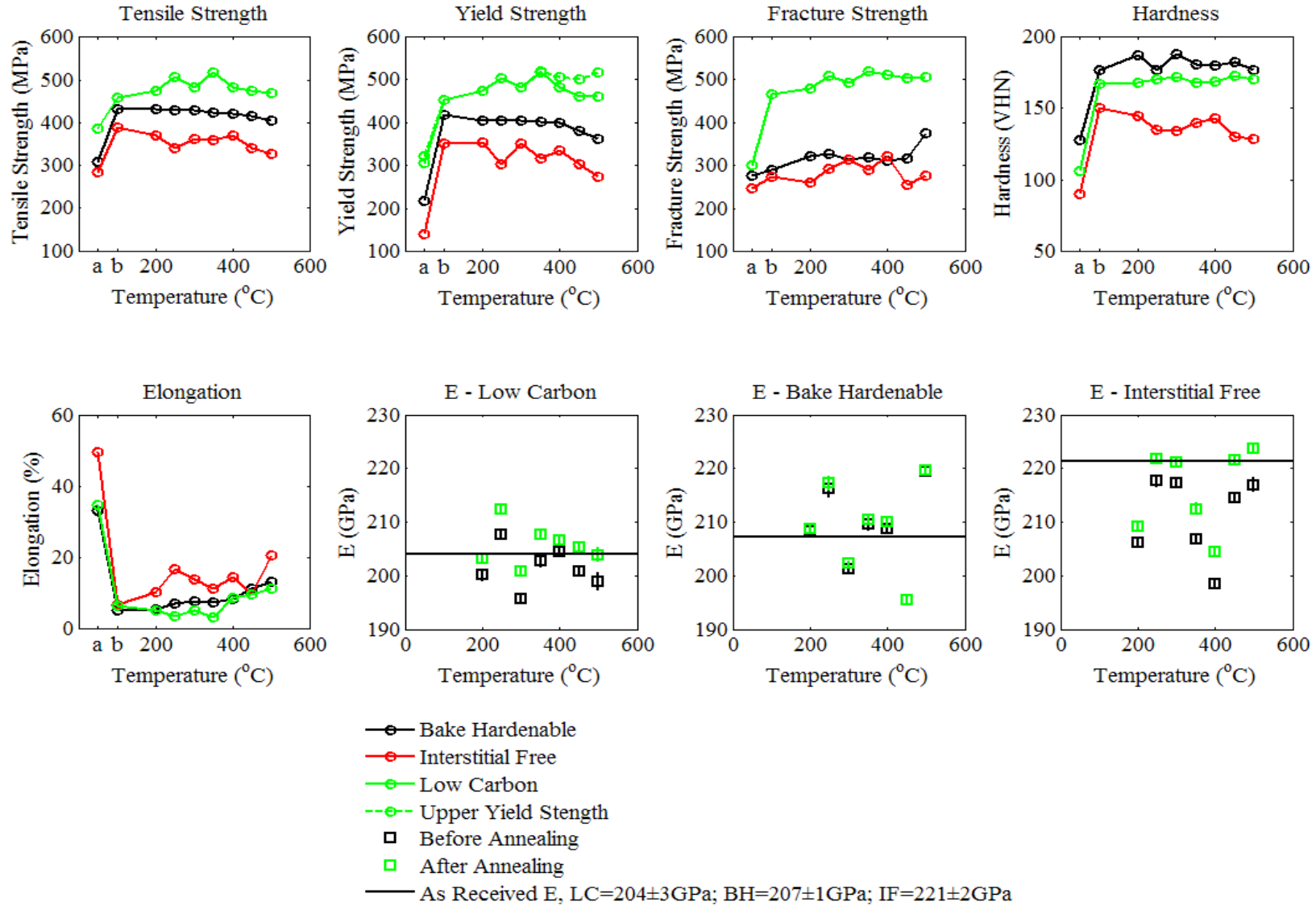
Figure 6.36: Comparison of mechanical properties of 20% Low-Carbon, Bake Hardenable and Interstitial Free steel; a = as-received condition; b = before annealing or cold-rolled condition

The as-received mechanical properties of each of the steels were initially considered. It was found that (see Figure 6.30a):

- Low-carbon steel in the as-received state had the highest yield strength, tensile strength and fracture strength followed by BH and then IF in decreasing order.

- Low-carbon steel in the as-received state exhibited an upper and lower yield point followed by a Lüder's region before strain hardening. This was not observed for the IF and BH steels.

- The low-carbon and BH steels had comparable ductility (elongation) with IF being the most ductile, having almost 50% elongation.

- The stress-strain characteristic is comparable for each of the steels in the transverse and rolling directions which meant that these steels could be described as isotropic.

The trends across the low-carbon steels cold-reduced by 10% to 50% of original thickness were considered. These trends are better highlighted by considering Figure 6.31 which summarizes the respective properties extracted from Figure 6.30c, d and g to i. In each case:

- The tensile strength, yield strength and fracture strength increased with increasing cold reduction

- The tensile strength, yield strength and fracture strength initially increased as annealing temperature was increased, but then decreased again for annealing temperatures of 300°C and above.

- The fall in the tensile strength and yield strengths beyond 300°C was taken to be an indication of the onset of recrystallization and this is reasonable given the high degree of prior deformation experienced by the test-strips. Recrystallization is believed to be accompanied by a fall in tensile strength [27]. To investigate this, coupons were extracted from 20% cold-rolled and air cooled strips for microscopic analysis. Recrystallization would have been manifested in the appearance of an equiaxed grain structure but examination revealed elongated microstructures of comparable grain size with no indication or sign of nucleation or grain growth (see Appendix A2). The micro-hardness values for these specimens are stable across the range of annealing temperatures (see Figure 6.36). Figure 6.36 also shows that the hardness of the un-annealed (after cold rolling) sample is comparable to the annealed samples.

- There was a return of the upper-yield-point for annealing temperatures of 300°C and above (see the yield strength plots in Figure 6.31). This corresponded to the annealing temperatures at which damping in the low-carbon rectangular strips began to plateau. Compare Figure 6.15a, Figure 6.16a, Figure 6.17a, Figure 6.18a, and Figure 6.19a with the yield strength plot in Figure 6.31. The return of the upper-yield-strength was an indication of strain ageing in the tensile samples.

- The strain aged specimens showed an increased capacity for further cold work. Consider the elongation plot in Figure 6.31. Note the decrease in elongation prior to 300°C or before the return of the yield point. After 300°C the percentage elongation in the samples generally increased.

6.6.1 Effect of cold rolling and heat treatment on Young's Modulus

Young's modulus was determined using two methods. The first method used the gradient of the straight portion of the stress-strain characteristic and the second method used the vibration frequencies of the first four pure bending modes of the free-free strips obtained from the vibration tests. This method required the measurement of the geometric dimensions and the mass of each strip. The theoretical natural frequencies f_n of a free-free beam are calculated from [190]:

$$f_n = (\beta_n l)^2 \frac{1}{2\pi} \sqrt{\frac{EI}{\rho A l^4}} \qquad\qquad\qquad \textbf{6.1}$$

where ρ is the density of the beam material and this was estimated by using the mass and the dimensions of the beam where l is its length and b and t are the width and thickness of the beam respectively. EI is its bending stiffness, A is its cross-sectional area (b x t), and $\beta_n l$ are the eigenvalues of the beam. The eigenvalues corresponding to the first four pure bending modes used to estimate the Young's Modulus E were 4.730041, 7.853205, 10.995608 and 14.137165 [191]. The area moment of inertia, I is calculated $bt^3/12$. Using the values measured, the equation 5.1 above could be rearranged and the Young's Modulus could be expressed as:

$$E = \frac{\rho A}{I} \left[\frac{2\pi f_n l^2}{(\beta_n l)^2} \right]^2 \qquad\qquad\qquad \textbf{6.2}$$

The majority of the Young's modulus estimates obtained from the tensile tests laid well outside published values for steel which is typically between 190-210 GPa (see Figure 6.31 and Figure 6.34a). This could be due to a number of factors which will be highlighted in the discussion.

However, better estimates for Young's modulus were obtained using the bending modes. Note the following in Figure 6.32, Figure 6.33 and Figure 6.34b:

- It is practical to consider the Young's modulus values of a single test strip to highlight the major trends. For instance, consider the 10% reduced, low-carbon test strip, annealed at 200°C and air cooled (Figure 6.32). The Young's modulus values in the cold rolled condition are comparable. This is also true for the Young's modulus values after annealing – their values are comparable. This was expected and this trend is visible throughout the low-carbon, BH and IF strips (see Figure 6.32, Figure 6.33 and Figure 6.34b).

- The horizontal line on each bar-chart represents the averaged Young's modulus of each of the steels in their as-received condition. For the low-carbon steel, the as-received Young's modulus is 204±3GPa. In some cases, particularly for the 10% and 20% reduced air-cooled strips, the Young's modulus in the cold-rolled state is lower than the as-received Young's Modulus. However, in the majority of cases for the air-cooled strips the Young's modulus values had increased after annealing the cold-rolled test strips (see Figure 6.32 and Figure 6.35).

- With respect to the water quenched strips, unlike the air-cooled strips, the majority of Young's modulus estimates were within the range of published values of Young's modulus for steel (190-210GPa) (see Figure 6.35). In some instances the cold-rolled Young's modulus was not lower than the as-received Young's modulus. However, the Young's Modulus values of the strips annealed at higher temperatures (at 450°C and above) were lower than the Young's Modulus values in the-cold rolled state (see Figure 6.33 and Figure 6.35).

6.6.2 Comparison across Low-carbon BH and IF steels

Figure 6.36 compares the mechanical properties of the three steels extracted from mechanical and vibration tests. The following was noted:

- The low-carbon steel exhibited the highest strengths across the group in the order Low-carbon > BH > IF from the highest to lowest. As annealing temperature was increased a gradual decrease in the yield strengths and tensile strengths of the BH and IF steels was seen although the strengths could be described as relatively stable over the range of annealing temperatures. BH and IF exhibited much lower fracture strengths when compared to the low-carbon steel, with IF having fracture strengths at approximately half the fracture strengths of low-carbon.

- A similar trend was expected for the hardness in that the low-carbon steel was expected to show the highest hardness values. However, the bake hardenable steel exhibited the highest hardness values across all annealing temperatures. Hardness values of the low-carbon and BH steels remained relatively stable across the range of annealing temperatures while the hardness in the IF steel decreased steadily as the annealing temperature was increased.

- There was no yield point effect in any of the annealed IF and BH steels.

- Ductility recovery in the annealed BH and low-carbon steels were comparable as indicated by the elongation plot in Figure 6.36. The IF steel showed the greatest recovery and ability for further cold forming with an elongation of almost 20% after annealing at 500°C.

- Better estimates of the Young's modulus were obtained for the BH and IF steels using the natural frequencies of the first four bending modes for each strip (Figure 6.34b). Consider also the Young's modulus plots for the steels in Figure 6.36. Note that the average Young's modulus is indicated by the solid horizontal line on each graph. The average values of 'E' for the BH and low-carbon steels were in agreement with the published range of 'E' for steels while the IF steel had an average 'E' of about 10GPa above the upper limit of this range. Also, like the low-carbon steel strips, the 'E' values for both the BH and IF steels, after annealing, were higher than the 'E' values in the cold rolled state (see Figure 6.34b and Figure 6.36). Nevertheless, the majority of values across all the steels were within the published range of 'E' for steel.

- It was observed that the Young's modulus across all the steels had generally decreased on cold reduction and increased with annealing. In some cases the Young's modulus after cold reduction was higher than in the as-received state.

6.6.3   Strain ageing at room temperature

Further confirmation of strain ageing of the low-carbon steel was manifested after straining a tensile sample by 7% and setting aside at room temperature for one week before completing the tensile test. Figure 6.30b shows the occurrence of strain ageing with the return of a very small yield point and decreased ductility.

6.7   Comparison with steelpans: Low-carbon steel strips versus soprano pans

The third and final segment of the work in this chapter involved a comparison of the findings of the vibration and mechanical tests conducted on the low-carbon steel structures with the vibration and

mechanical properties extracted from two soprano pans: a chrome plated 4ths and 5ths soprano pan and a paint coated Aubrapan (see Figure 6.37a and d). These comparisons were made primarily in an effort to validate the findings of the simulation of the pan making process. The comparisons were as follows:

1. The first comparison involved an investigation which extracted mode frequencies and damping from the notes on both pans for comparison with the frequency and damping trends obtained from uncoated, chrome-plated and paint-coated low carbon test structures.

2. The second investigation was done by comparing the vibration properties (natural frequencies and damping) of rectangular strips extracted from the uncoated Aubrapan with the vibration properties obtained from the cold-rolled low-carbon test structures.

3. The third and final comparison examined the hardness of coupons extracted from four regions of the Aubrapan and compared these with the hardness values obtained from the low-carbon steel.

The investigation began by determining the chemical composition of the Aubrapan since rectangular strips were extracted from the Aubrapan for comparison with the cold rolled low-carbon steel test structures. This data is provided alongside the chemical compositions of the other materials used in this work (see Table 6.1). Note that the carbon and nitrogen content in the Aubrapan steel was approximately 50% of that of the C and N content in the low-carbon steel. The same could be said when comparing the content of Al and Mn for both the Aubrapan steel and the low-carbon steel.

6.7.1   Modal testing of the soprano pans

Impact modal testing was used to extract mode frequencies and damping from the notes of both pans. A small lightweight Brüel and Kjær accelerometer (type 4516) was used to measure response. The apparatus arrangement used in these tests could be found in Chapter 4. The accelerometer was fixed to the note surface with a thin film of beeswax. The sampling frequency and logging time were 10kHz and 2s respectively. The accelerometer was positioned such that it was offset from the minor and major axes of the notes. This was done because the nodal lines were highly likely to be located along or in close proximity to these axes. The response of the note was then determined by tapping on a grid of five points (see Figure 6.37c). One point was approximately at the center and the other four impact points were located in the four sectors created by the intersection of the minor and major axes (Figure 6.37c), each point being approximately 15 mm away from both axes. The modal frequencies and damping were extracted using a sonogram.

The pans used in this investigation are shown in Figure 6.37a and d. Some of the notes in each pan were not used in the modal tests: the inner notes of the 4ths and 5ths soprano pan (see Figure 6.37b) were not used as they were damaged, while the 4 smallest notes closest to the rim of the Aubrapan (see Figure 6.37f) were not used as they were not tuned. In this work, two sets of vibration tests were performed on the Aubrapan, one in which the protective surface coating of the pan was intact and the other vibration test was conducted after removal the coating. The coating of the Aubrapan was removed by applying a paint remover (see Figure 6.37d and e), commercially sold under the name Nitromors (an all purpose paint and varnish remover). The stripped coating was removed by washing the Aubrapan surface under running water.

6.7.2 Surface Treatments – spray painting and chrome plating

Steel pans are primarily coated for protection against corrosion. At this stage of the production process, pan makers add a thin layer of paint or chrome onto the pan surface. To understand the effect of coating on the vibration properties of the steelpan a number of samples from the heat treated batches of strips were selected for spray painting or chrome plating. The strips selected for each coating type are listed in Table 6.12. Acetone was used to remove any dirt and grease from the strips to be painted. Halfords matt-grey primer was applied by spraying a single pass of paint onto each side of the strips. An approximate nozzle distance of 200mm was maintained during spray painting. All strips were allowed to dry for one day before conducting vibration tests.

Chrome plating was conducted by Cambridge Electroplating Ltd. Although the company was unwilling to provide the details of their electroplating process, it is believed they subscribed to a typical procedure for electroplating that comprises the following steps:

1. Degreasing and polishing
2. Cold water rinse
3. Electroplate copper
4. Cold water rinse
5. Electroplate nickel
6. Cold water rinse
7. Electroplate chrome
8. Cold water rinse
9. Hot water rinse
10. Dry

Table 6.12: Strips chosen for spray painting and chrome plating															
Chrome Plated								**Spray Painted**							
T°C	200	250	300	350	400	450	500	**T°C**	200	250	300	350	400	450	500
10%	X							10%							
20%	X							20%	X						
30%	X	X	X	X	X	X	X	30%	X						
40%	X							40%		X	X	X	X	X	X
50%	X							50%	X						
Note: Only air cooled strips were used for chrome plating and only water quenched for spray painting															

6.7.3   Extraction of rectangular strips and coupons from the Aubrapan

Six rectangular strips, each of length approximately 150mm x 15mm were extracted from the uncoated Aubrapan (see Figure 6.37g-k) for vibration tests. The strips were extracted using a FANUC ROBOCUT wire cutting EDM (Electric Discharge Machine). The strips were labeled A to F (Figure 6.37h-k) and the respective average thicknesses in mm of the strips obtained from measuring at five locations were (0.64±0.03), (0.79±0.12), (0.81±0.12), (0.85±0.01), (0.60±0.02) and (0.87±0.02). Note the strips with the largest deviations in thickness (strips B and C) were the strips that were extracted along the radial direction of the Aubrapan. Note that this pan would have been formed by hammering which stretches the surface of the drum head. Recall also the Aubrapan bowl wall thickness variation presented for this pan in Figure 3.12a. Suspension holes were also drilled at 10mm from either side of each strip to enable suspension during modal testing.

Five coupons, for hardness measurements, labeled A to E, each approximately 15mm x 15mm were taken from the uncoated Aubrapan. Four coupons (A to D) were taken from the pan surface (see Figure 6.37l) and one from the skirt (coupon E). The four coupons (A to D) were extracted at approximately 45mm, 110mm, 165mm and 260mm from the rim and had thicknesses of 0.89mm, 0.75mm, 0.60mm and 0.54mm. The coupon extracted from the pan side was 1.10mm thick. Hardness was measured along the through-thickness radial direction of the coupons.

6.7.4   Modal testing of extracted and coated test structures

Impact modal testing was used to extract the natural frequencies and modal damping from these strips. A Polytec OVF 302 scanning laser vibrometer head was used to measure response and a miniature PCB hammer on a pendulum was used to provide controlled impacts. The same experimental arrangement (see Figure 6.3), impact and response detecting positions, suspension configuration and surface preparation were employed as in the modal tests for the low-carbon test structures. A logging frequency and logging time of 50 kHz and 5s was also used.
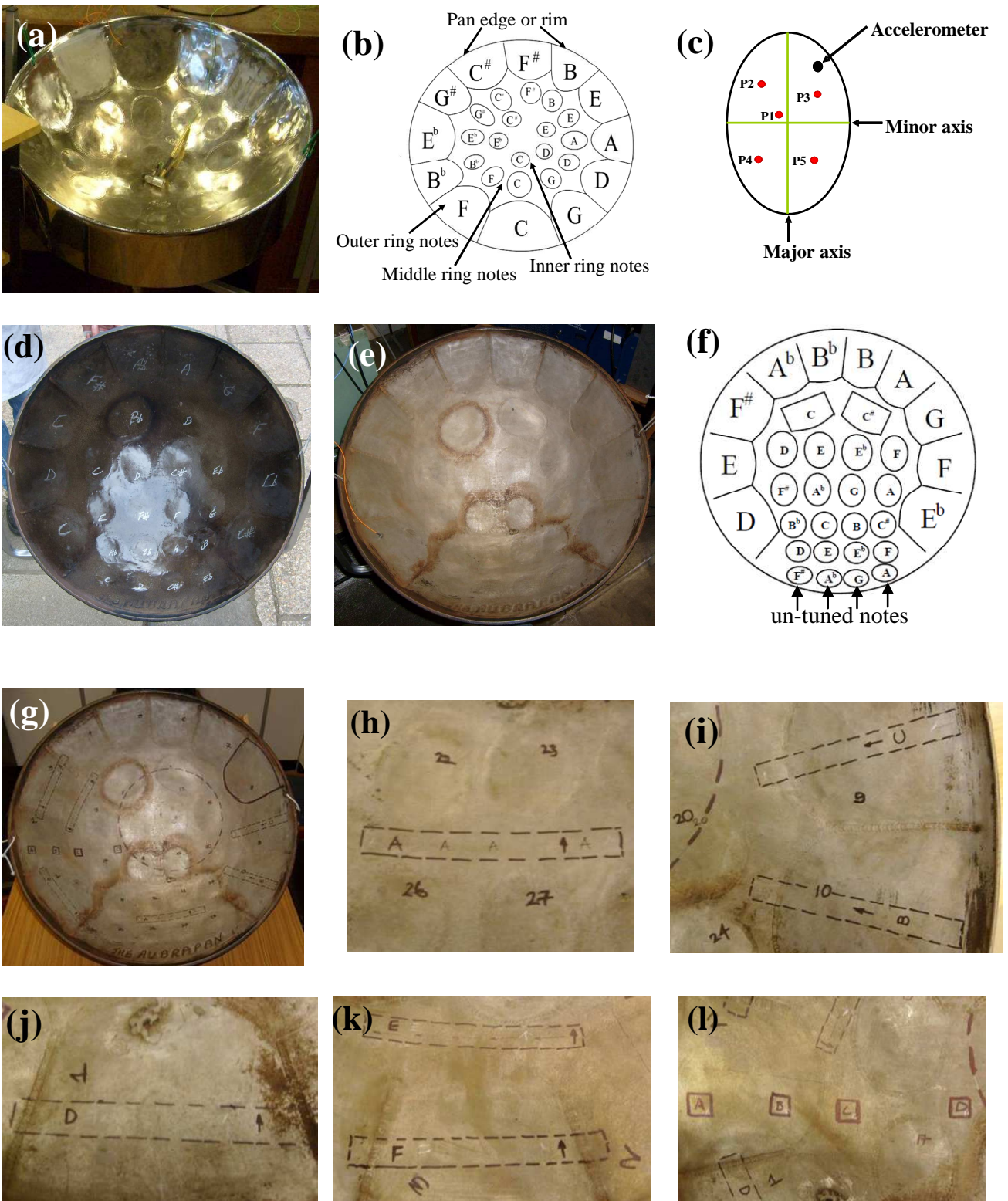
Figure 6.37: **(a)** chrome plated 4ths and 5ths soprano pan; **(b)** 4ths and 5ths soprano pan note arrangement; **(c)** Impact and response locations on pan notes; **(d)** coated Aubrapan; **(e)** uncoated Aubrapan; **(f)** Aubrapan note arrangement; **(g)** Regions for extraction on Aubrapan; **(h)-(k)** Locations of rectangular strips extracted from Aubrapan and **(l)** Locations for coupon extraction for hardness measurement

The quality factor was extracted using a sonogram algorithm. Ten impact trials were taken for each strip and an average rate (Q-factor) was calculated for each mode in the bandwidth of interest.

6.8 Results: Comparison with steelpans: Low-carbon steel strips versus soprano pans

Consider the plots for the chrome plated 4th's and 5th's soprano pan and the Aubrapan (Figure 6.38a and b). What is immediately apparent is that the range of Q-factors for all the notes considered on both pans was similar, with values ranging between 100 and 1000. Additionally, Q-factors of the fundamental modes of the notes in both pans were towards the lower end of this range (100-500). The second and third mode Q-factors were typically higher than the fundamental mode Q-factors in both pans (see Figure 6.38a and b). Here only the fundamental and second modes were shown for the Aubrapan since these were the only two modes in each of the measured notes that gave good sonogram fits whereas at least the first three modes in the chrome plated 4ths and 5ths soprano pan gave acceptable fits. In the case of the Aubrapan, the Q-factors for all modes of the measured notes on the coated Aubrapan were lower (see Figure 6.38b), in all cases, than the corresponding Q-factors in its uncoated condition. This trend was expected.

The main aim of this exercise was to compare the damping obtained from the uncoated and coated (chrome-plated and spray-painted) rectangular strips to damping of the modes in the steelpan notes and identical strips extracted from the Aubrapan. Firstly, note the damping trend with annealing temperature for both chrome plated and spray painted strips (see Figure 6.39). This trend is shown before and after the coating process. Note that the coated strips were not annealed. The graphs illustrate the damping change on coating. The following was noted:

- There was a compression of the Q-factor ranges in both cases. On chrome plating the upper limit Q-factor was reduced from approximately 6000 to 2000 (compare Figure 6.39a and b) whereas for spray coating the upper limit Q-factor was reduced from 5000 to 1500 (compare Figure 6.39c and d). The range of Q's for the chromed and sprayed strips were 400-2000 (Figure 6.39b) and 300-1500 (Figure 6.39d) respectively. This reduction in Q-factor was expected with surface coating.
- An increase in the natural frequencies of the chromed strips whereas a small decrease was observed in the natural frequencies of the sprayed strips.
- In both cases there was an initial increase in Q-factor, up to 300°C for chromed plated and up to 350°C for the sprayed strips before there was either a plateauting of the Q-factor (in the case of the chromed strips) or a small decrease in the Q-factor as in the case of the paint sprayed strips.
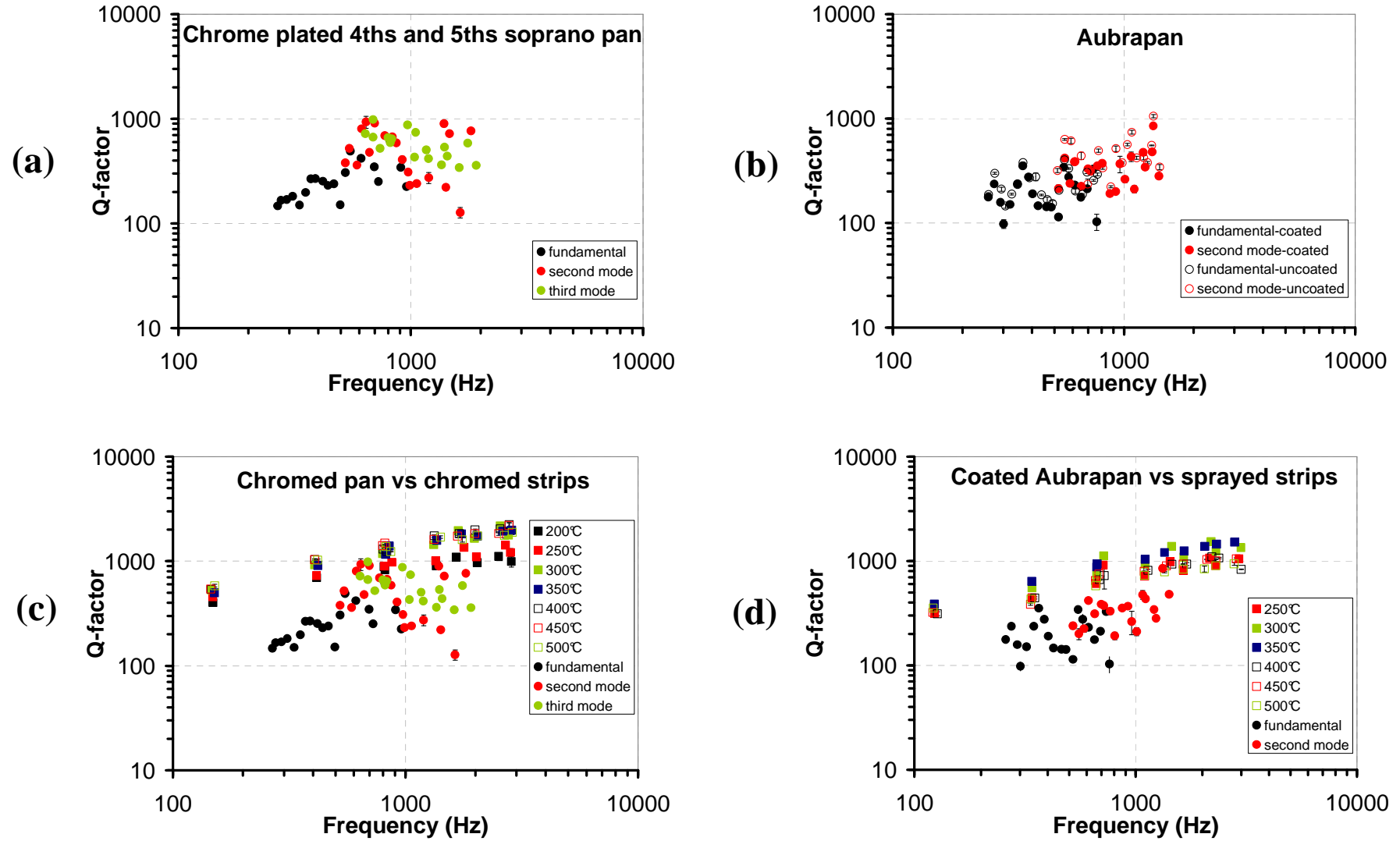
Figure 6.38: (a) Damping in chrome plated 4ths and 5ths soprano pan; **(b)** Damping in coated and uncoated Aubrapan; **(c)** Damping comparison with chromed pan and chromed strips and **(d)** Damping comparison with coated Aubrapan and spray painted strips
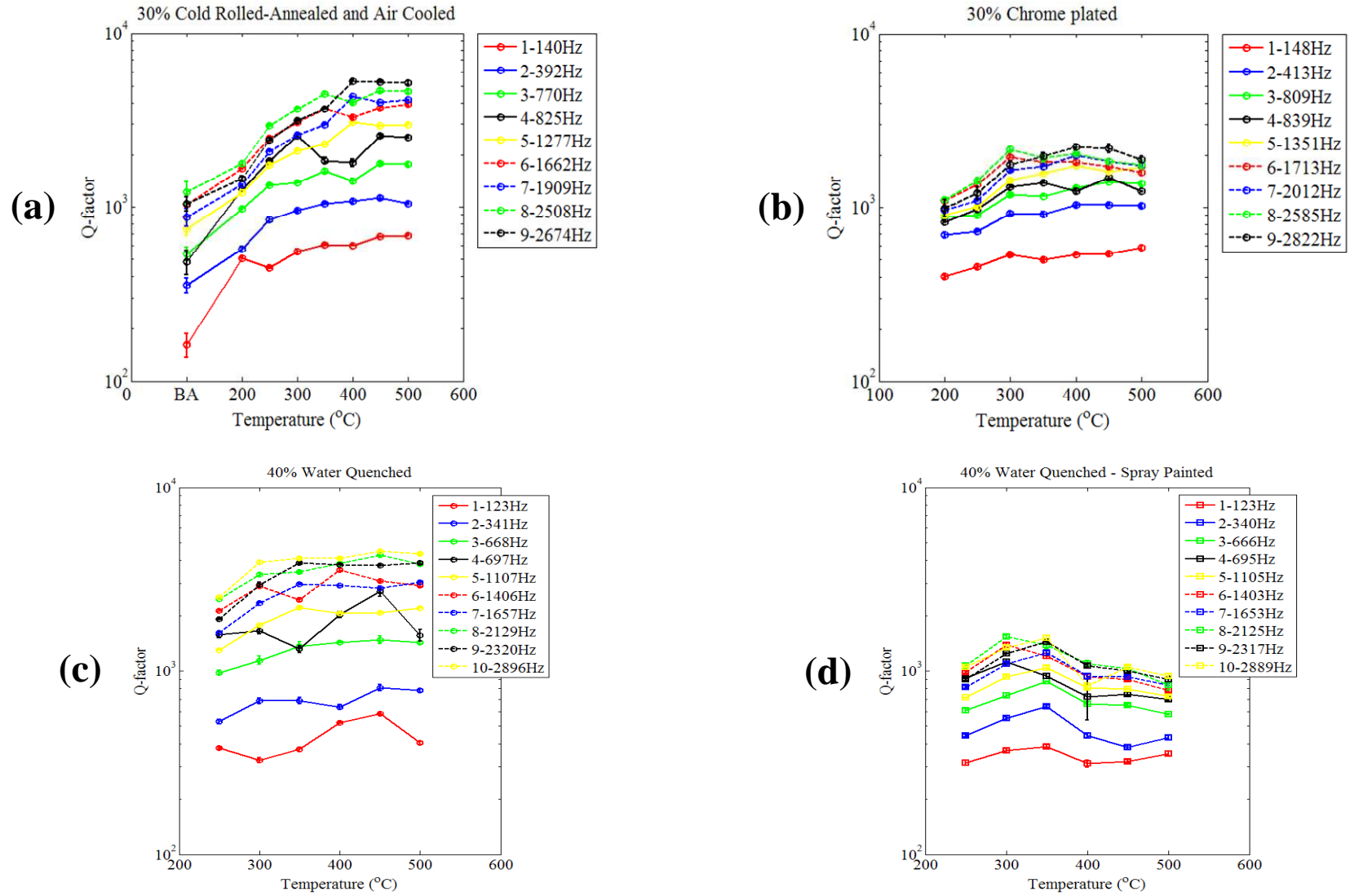
Figure 6.39: **(a)** and **(b)** Damping before and after chrome plating respectively; **(c)** and **(d)** Damping before and after spray painting respectively

The next investigation was to determine if the damping factors of the chromed and sprayed strips would be comparable to Q-factors extracted from the chromed and spray painted pans respectively. Figure 6.38c compares the damping in the chromed pan with the chrome plated strips while Figure 6.38d compared the damping in the coated Aubrapan with the sprayed strips. There are two aspects of these plots that must be highlighted.

- Firstly, in both cases the Q-factors of the notes in the chromed 4ths and 5ths soprano pan and the Aubrapan were lower that those exhibited by the chrome and spray coated strips respectively (see Figure 6.38c and d).
- Secondly, the damping in the pans does not show the same linear trend (power law fit) with frequency as the chrome and spray coated strips exhibited. These findings will be elaborated on in the discussion (see Figure 6.38c and d).

Another important facet of this work was to compare the damping of strips extracted from the uncoated Aubrapan with the cold-rolled and annealed low-carbon strips. The damping across all the extracted strips was compared to the damping in the notes of the uncoated Aubrapan and the following findings were made:

- Although some of the strips were extracted from within note regions (see Figure 6.37i, j and k), Figure 6.40a shows that the extracted strips exhibited lighter damping (higher Q-factors) than the notes of the uncoated Aubrapan.
- However, on comparing the damping across the extracted Aubrapan strips with the 10% and 50% cold rolled strips, that were air cooled after annealing, better agreement was seen. Figure 6.40b shows the Q-factors of the extracted strips overlaying those of the 10% cold rolled strips. Note that the majority of the extracted strips had comparable thickness to the 20% rolled strips. However, the damping values of the 10% and 50% strips were used as they represented the upper and lower limits of the Q-factors exhibited by the cold-rolled and annealed low-carbon strips. The Q-factors of the extracted Aubrapan strips were well within this range.
- The amount of interstitial elements, particularly C and N, is known to have an influence on the damping properties of steel [85,88]. Although comparable damping was observed for the extracted Aubrapan and rolled strips, note that the content of C and N in the Aubrapan material is almost half of that of the steel sheet used to produce the rolled strips (see Table 6.1).
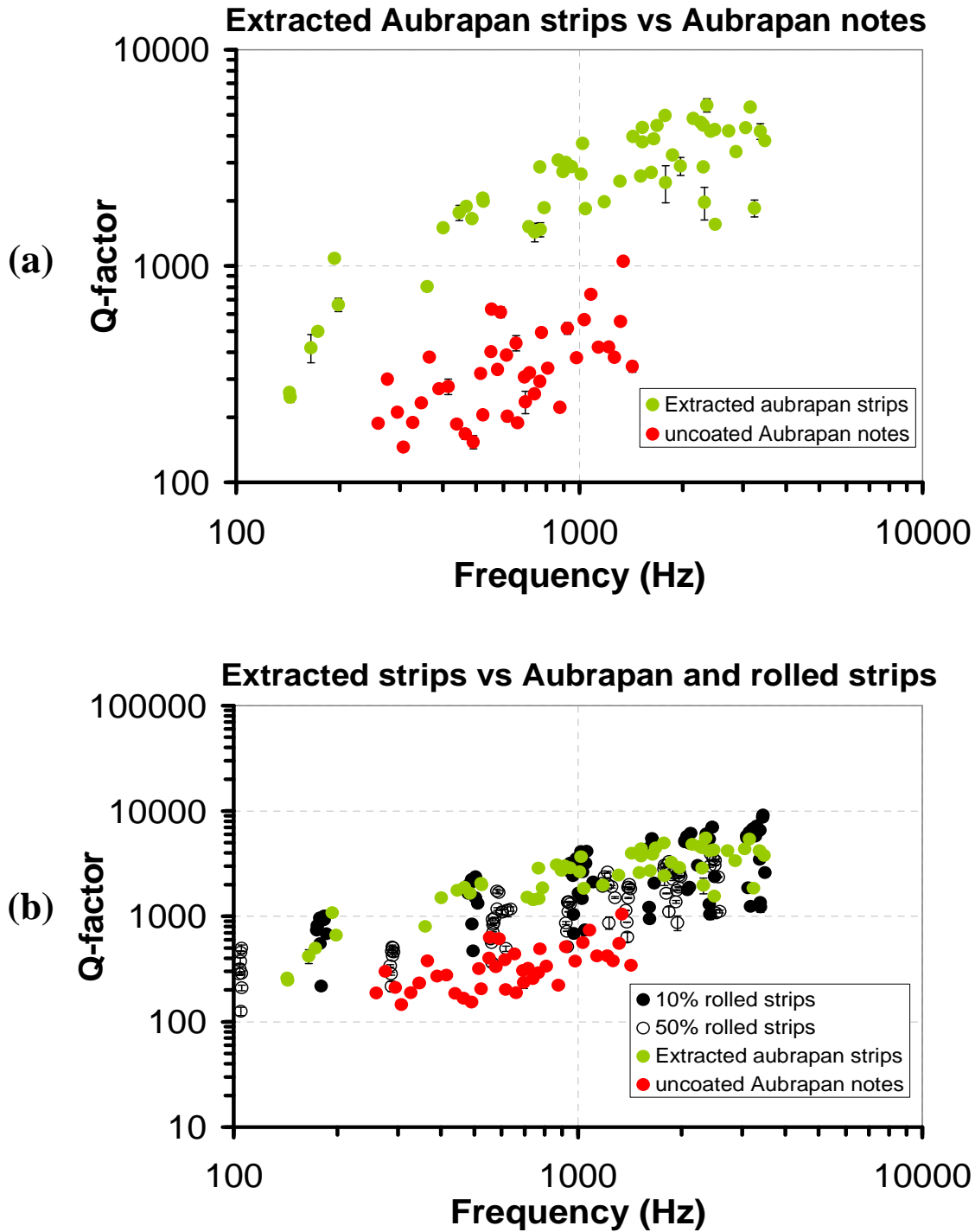
Figure 6.40: (a) Damping of extracted Aubrapan strips and uncoated Aubrapan notes compared; **(b)** Damping of extracted Aubrapan strips and uncoated Aubrapan notes compared to 10% and 50% cold-rolled and air-cooled low-carbon steel strips

6.8.1 Hardness from extracted Coupons

Table 6.13 lists the hardness of the coupons extracted from the Aubrapan. The hardness increases as the bowl depth increases and this was expected as the thickness strain in the stretched Aubrapan increases from the rim of the pan to its base. Although the Aubrapan had a original thickness that was slightly greater than the original thickness of the low-carbon strips, it was discovered that

Aubrapan strips extracted from regions having comparable thickness strains to the low-carbon strips were not as hard. Compare the hardness of coupon B in Table 6.13 with the hardness of the 20% low-carbon strips in Figure 6.36. This development may be due to the lower carbon content of the Aubrapan (see Table 6.1). However, it was also observed that these softer Aubrapan extracted strips manifested Q-factors that were comparable to the harder low-carbon steel strips (see Figure 6.40b).

Table 6.13: Hardness of coupons extracted from Aubrapan			
Coupon	**Vickers Hardness (HV1-9.807N)**	**Thickness (mm)**	**Thickness reduction* (%)**	**Radial position from rim in mm**
A	135	0.89	5.3	45
B	**159**	**0.75**	**20.2**	**110**
C	171	0.60	36.2	165
D	168	0.54	42.6	260
E (Skirt)	136	1.02	-	-
Original dish thickness = 0.94mm				

6.9   DISCUSSION

The findings of this chapter will be discussed in three main sections. The first section considers the observed trends in the material damping and mechanical properties of the tested steels (Low-carbon, BH and IF). The second section discusses the findings of the comparison of the material damping in the tested steelpans and the rolled low-carbon test structures. The third and final section recommends a methodology for further work on material studies, particularly the application of low-carbon steels to steelpan production.

6.9.1   Prelude to Discussion

It is first important to highlight that the material damping trends observed in each part of the experimental simulation with the low-carbon steel test-structures were in good agreement with the expectations at the onset of this investigation. These expected outcomes were listed at the beginning of this chapter. Two important outcomes in this list were: (1) that material damping would increase with cold rolling but (2) would recover (or revert to levels comparable to damping in the as-received material condition) on subsequent heat treatment of the cold rolled test structures. These and other deductions were realised and will be discussed in more detail in subsequent sections.

There is currently no material specification for steelpans. The need for a material standard was alluded to in the Trinidad and Tobago Bureau of Standards 1992 conference paper on standardization of the steelpan by Roach [12], in which a list of work to be done on the steelpan included the purchase, testing and analysing of sample steels. To date, there is no evidence that any work on this initiative was conducted. Standardization of the steelpan in Roach's paper mainly

referred to standardization of the note arrangement or note placement (see Chapter 1), note size and note shape in steelpans. Other work by Copeland [192] also focused on the standardization of note placement.

More recently, work by Murr *et al.*[19] and Ferreyra *et al.*[18,20] focused on the effect of the steelpan making process on the metallurgical and acoustic properties of several drum steels which had different carbon and residual element contents. While these studies recommend a range for carbon content and an optimum heat treatment temperature, the acoustic analysis did not consider the damping properties of the steels tested but instead focused on the effect of the pan making process on the frequency spectra of replica steelpan notes. Unarguably, the works of Murr *et al.* [19] and Ferreyra *et al.*[18] have contributed significantly to a better understanding of the behaviour of low-carbon steels in the pan making process but the intent of these works were not towards the development of a specification in any form. The work in this thesis aimed to build on the contributions by Murr and Ferreyra but with the intent of specifically making a few recommendations for the development of a material specification in addition to proposing a methodology for doing so. In the following discussion, some of the findings in this thesis will also be compared to some of the findings of Murr *et al.*[19] and Ferreyra *et al.*[18].

The development of specifications for the standardization of materials for the steelpan should initially consider low-carbon steels. Low carbon steel has long been the *de-facto* material for pan making, primarily through the use of oil barrels which are primarily constructed from low-carbon steel. However, the manufacture of tight-head barrels is regulated by standards [70,71] which specify the grade of low-carbon steel sheet to be used for their construction. These grades of steels were not specified with the intention that the containers would be used primarily or subsequently for musical instruments and may or may not be suitable for pan making. One manner of dealing with this is highlighted further on in the discussion.

Low-carbon steel continues to be relatively cheap, highly available, and tuning methods over the past 70 years have evolved and fixated around its usage. The development of a specification should not only consider mechanical material properties but should also incorporate guidance on material vibration properties that would facilitate the production of high quality steelpans. This is the reason why this work considered the vibration and mechanical properties of the steels used.

6.9.2 Trends in vibration and mechanical properties

- **Predicted and measured natural frequencies**

Measured and predicted natural frequencies of the fabricated test strips were in good agreement and this can be seen by considering Table 6.7, Table 6.8 and Table 6.9. The exercise of conducting a finite element prediction was primarily to be able to easily identify vibration frequencies during modal testing and to locate the best locations so that the modes of interest could be easily excited. However, in a majority of instances, the natural frequencies after heat treatment and cooling had either increased or decreased. An increase in the natural frequencies after heat treatment was more typical for the air cooled strips (see Table 6.7) whereas the water cooled strips predominantly registered a decreased natural frequency after annealing and quenching. These changes in natural frequencies may be related to a change in the Young's Modulus which will be discussed further on. The natural frequency may also be affected by expansion and contraction experienced by the test strips during heat and cooling and this factor may be of greater significance particularly in the water quenched strips which would have experienced rapid contraction on quenching in water. Another important aspect is in connection with local stiffening at the supports during modal testing. Local stiffening [182] results in increased natural frequencies but sufficient care was taken to avoid this problem during modal testing. In-plane modes were not used in this work since the plane of vibration of these modes was in the same plane as the suspension supports. These modes were also easily identified as their Q-factors were significantly lower than the Q-factors of the flexural modes.

- **As-received material properties**

Consider Figure 6.30a. On the basis of ductility, all three steels would be suitable for dishing. As expected the BH and IF steels were characterised by low yield strengths which also contributed to their superior stretch-ability. In the case of the IF steel it is well known that the addition of elements such as Nb, Ti or aluminium contribute to the formation of textures that enable superior stretching and drawing characteristics (see Table 6.1). Table 6.1 lists the chemical composition of each steel with the IF steel sheet having the lowest carbon content and the low-carbon steel having the highest. The mechanical properties of yield strength, tensile strength and fracture strength also followed the same sequence with the IF steel having the lowest values for these properties and the low carbon steel having the highest.

The absence of the yield point phenomenon and a Lüder's region in the BH and IF stress-strain characteristic was also an indication of the superior formability of these steels meaning that such steels could be formed without the appearance of stretcher strains. However the as-received Vicker's hardness numbers (VHN) of the BH, IF and low carbon steels were 128, 90 and 107 respectively. It was expected that the hardness would also follow the same sequence as the carbon content with the IF steel having the lowest hardness value and the low carbon steel having the highest. However, the BH steel was the hardest.

Note also the trend with the as-received vibration damping properties (see Figure 6.12). The vibration damping properties could be described as independent of carbon content with the IF and low-carbon steels having comparable damping values while the BH steel displayed the lightest damping (Highest Q-factor values). The literature indicates [85,88] that damping increases with increasing carbon content and in light of this it was expected that the low-carbon would have exhibited the lowest Q-factors (highest damping) while the BH and IF steels would have had the highest Q-factors. However, it seemed as though the IF steel was an exception to this rule. Recall that IF steels contain small amounts of alloying element additions, in this case, Titanium (see Table 6.1). This acts to reduce the amount of carbon and nitrogen in solution by forming stable carbides and nitrides thereby leaving very little carbon available in solution for engagement in dislocation-interstitial atom interactions. This may explain why the as-received damping in the IF steel was comparable to that of the low-carbon steel. The assumption is also being made that dislocation-interstitial interaction is majorly responsible for the damping properties exhibited by the steels investigated.

- **Vibration and mechanical property trends with cold forming and heat treatment**

The increase in damping with cold reduction was primarily attributed to the increase in dislocation density. This is widely reported on in the literature [80-82]. The increased strength and reduced ductility were also expected with increasing cold reduction. The high sensitivity to cold reduction in the first 10% of cold rolling will be used further on to explain the difference between the material damping in the experimental test strips and material damping in the tested steelpans. In respect of the hardness, only hardness measurements for 20% cold-rolled and air cooled low-carbon strips were compared with the IF and BH steels and this will be discussed shortly. However, if hardness measurements were taken across all the low-carbon steels it was expected that hardness would increase with increasing cold reduction.

One highlight of this work was the vibration damping and mechanical property trends exhibited by the low-carbon, IF and BH steels with annealing heat treatment. With regard to the low-carbon steel, the first trend was the expected increase and plateauing of the Q-factors values among water quenched and air cooled test specimens. This plateauing of Q-factor values typically began between the annealing temperatures of 300°C and 400°C. This temperature range also corresponded to the temperature range (300°C and 400°C) between which the return of the yield point effect was manifested in the tensile specimens, as indicated by a very sharp upper yield point. The onset of the return of the yield point was also accompanied by increased yield strength and decreased ductility (elongation) which are both indicators of strain ageing. This development indicated that strain

ageing may be in part or majorly responsible for the damping trends (the plateauing) observed in the low-carbon steel test structures.

Figure 6.41 lists a range of internal damping mechanisms in metals. This table could be used to help isolate probable mechanisms that could be responsible for the damping trend in the low-carbon and BH steels which appeared to suggest the combination of two damping mechanisms. A process of elimination would be used to isolate likely damping mechanisms. The elimination criteria would be mechanisms that occur at room temperature in the frequency range of 0 to 4kHz. Room temperature is taken to be 25°C. On the basis of room temperature, Figure 6.41 indicates that mechanisms numbered 1, 3, 5, 10, 11, 13 and 18 are likely candidates. Magnetic and electromagnetic mechanisms 1 and 3 respectively could be eliminated leaving mechanisms 5, 10, 11, 13 and 18. After applying the frequency constraint of 0 to 4kHz, mechanisms 5, 10 and 13 which are thermoelastic damping (5), relaxation of dislocations in the high temperature range (10) and damping depending on the history of deformation (13) remain possible candidates. Mechanism 5 and 10 can be eliminated because a temperature difference across the strips would be necessary for thermal currents to be operative; also mechanism 10 only spans the frequency range between 10 and 1000Hz. Therefore mechanism 13 which is dependent on frequency, strain and temperature is a likely candidate over the entire frequency range of interest. However, the temperature in this case maybe temperatures at which damping measurements are recorded and not annealing temperatures. In this work it is evident that the relatively constant damping values that were obtained for annealing temperatures beyond 400°C were dependent on the degree of prior deformation since this damping threshold decreased with increasing thickness strain. This table also does not account for the changes in damping which may occur by the pinning of dislocations by interstitials (strain ageing). It is likely that this dislocation-interstitial interaction may be the dominant mechanism in the region below 400°C.

Another trend was found with the relationships obtained by considering the plots between the natural frequencies and the damping of the low-carbon test strips where $Q = \beta f^{\alpha}$. The values for the coefficient of α for test strips heated beyond 300°C were typically between 0.60 and 0.80. It is not certain whether this relationship is a characteristic of the strain ageing phenomenon in low-carbon steels. Efforts to locate comparable information were difficult: data for a range of low-carbon steels need to be gathered and analysed before any conclusions can be made. It may be that this information may be useful for the development of a quality control criterion for ensuring that selected low-carbon steels meet the vibration damping requirements for steelpan making. However, the application of this relationship to steelpan production is not immediately apparent and further research is therefore recommended.

Type of damping / Type of internal structure reorganization	LINEAR		NONLINEAR	
	Relaxation $f(\omega,T)$	Resonant $f(\omega)$	Hysteretic $f(\varepsilon)$	Viscous $f(\omega,\varepsilon,T)$
Magnetic	1 Magnetoelastic relaxation 2 Eddy currents	2 Magnetoelastic resonance	3 Ferromagnetic hysteresis	
Thermal	5 Thermoelastic damping (thermal diffusion, thermal currents)		6 Thermal hysteresis	
Damping from dislocations	9 Relaxation of dislocations-low temperature range 10 Relaxation of dislocations-high temperature range	11 Dislocation resonance	12 Dislocation hysteresis 14 Deformation Hysteresis	13 Damping depending on history of deformation
Damping depending not only on dislocations	15 Relaxation on grain boundaries			16 Viscoelastic delay microcreep
Point defects	17 Relaxation on point defects			
ATOMIC — Damping depending on solvent atoms	18 SNOECK'S damping 19 Ordering in solid solutions 20 KOESTER'S damping 21 Damping caused by phase processed in solid solutions			
Electronic Mechanisms	7 Electronic absorption of ultra-sounds 8 Phonon and phono-electronic mechanisms			

Figure 6.41: Damping Mechanisms after A. Muszynska, "Tlumienie wewnetrzne w ukladach mechanicznych (Internal damping in mechanical systems)," Dynamika Maszyn, Polish Academy of Science, Ossolineum, Warsaw, pp. 164-212, 1974 (in Polish) in Nashif *et al.* [78] p. 62

In order to substantiate the deduction that strain ageing was primarily or at least in part responsible for the damping trends observed with annealing heat treatment, the material damping in 20% cold reduced and annealed BH and IF steels were compared to the 20% cold reduced air cooled low carbon steel strips. The concept behind using these steels (BH and IF) was that they possess very minute quantities of interstitial atoms (carbon and nitrogen) (see Table 6.1) and therefore the degree of strain ageing which accompanied the heat treatment of cold-rolled samples of these steels would be modest or almost negligible in comparison to the strain ageing that may occur in the low-carbon steel. The IF steel sheet used in this work contained Titanium (Table 6.1) which further reduced the carbon and nitrogen in solution through the formation of stable carbides and nitrides. On this

premise, it was therefore reasonable to expect that the highest damping (lowest Q-factor values) would be manifested by the BH and IF steels. This expectation was not entirely realised but in most cases (see Figure 6.27) the IF steel displayed the lowest Q-factors. This finding could be accepted as a confirmation of the deduction. Although the BH steel was also expected to exhibit comparable damping to the IF steel but instead manifested the lightest damping among the group of steels, was an indication that very minute contents of interstitial atoms could have major effects on damping properties and that vibration damping in low and ultra-low carbon steels may not be very sensitive to carbon content. Further work needs to be conducted in order to establish how sensitive material damping is to carbon content in low and ultra-low carbon steels.

There were also comparable findings between the low-carbon and BH steel Q-factor-natural frequency plots. For the fit $Q = \beta f^{\alpha}$, the coefficient α for the BH strips also fell between the values 0f 0.60 and 0.80 while this was not the case for the IF steel (see Table 6.10 and Table 6.11). In the case of the IF steel the deviation from this trend might be due to the presence of Ti which reduces the amount of C and N in solution.

Another unexpected trend was in connection with the hardness values in the three steels. The low-carbon steel was expected to display the highest hardness values but this was instead manifested by the BH steel. This could be explained by the fact that the BH steel had a higher hardness value in the as-received condition and thus for the same degree of cold reduction would have achieved a higher VHN value. It was also noted that the VHN values of all the steels were relatively stable across the range of annealing temperatures and this was expected as these steels do not contain the minimum amount of carbon (0.3 wt%) required to achieve any hardening (through martensite formation) by heat treatment and therefore microscopic examination would have revealed a predominantly ferritic microstructure.

It is also important to indicate that although strain ageing appeared to have taken place in the BH steel there was no indication of this in the stress-strain characteristics in that no yield point phenomenon was observed, neither was there any marked increase in yield strength or decrease in ductility. Instead, the yield strength in the BH steel decreased gradually over the range of annealing temperatures. It is useful to recall that BH steels were primarily designed for light press work (especially for the automobile manufacture industry) which normally would not exceed a few percent [193] after which the maximum bake hardening effect (40-50MPa increase in yield strength [193]) is achieved by baking the formed part (heat treatment) at 170/180°C for 20 minutes [106,193,194]. In this work, the samples had a thickness strain of 20% which is far greater than that of light presswork in addition to being annealed at temperatures which far exceed the recommended

range for the heat treatment of bake hardenable steels. The heavy cold reduction experienced by the BH steel in this work might have impaired its ability to benefit from the bake hardening effect or it could be said that the large deformation resulted in a weakened bake hardening response [106,194].

6.9.3   Effect of cold forming and heat treatment on Young's Modulus

The Young's Modulus estimates obtained using the vibration test was consistent with published values for '*E*'. For future work it is recommended that two or more techniques be used to estimate the Young's Modulus and this may include a tensile test, a free-free vibration test or a three point bending test. The poor estimates (reduced values) of '*E*' from the tensile test may be due to several reasons which include slippage in the grips, sample misalignment due to worn components, machine stiffness or worn clip gauge surfaces. Moreover the expected trends were generally in agreement with the literature mentioned earlier in the introduction to this chapter, for instance, in that the Young's Modulus was expected to show an increase with heat treatment annealing and this was generally observed. However, these changes were small and may not affect the overall performance of the steelpan in any form.

6.9.4   Comparison to previous work on the material aspects of the steelpan

This work was in no way a repeat of the work conducted by Ferreyra *et al.*[18] but there were some aspects of this work that were in good agreement with their work and they were as follows:

- The present work discovered that the temperature range at which the plateauing of material damping and the onset of strain ageing begun where identical i.e. between 300°C and 400°C. Ferreyra *et al.*[18] also concluded that the optimum strain ageing conditions to achieve appropriate hardness to facilitate tuning in the low carbon steels they tested appeared to be about 350°C for 10 minutes.

- The present work discovered that there was no apparent difference in the vibration damping of water quenched or air cooled strips. An identical conclusion was made by Ferreyra *et al.* [18] with respect to air cooled and water quenched strain aged samples.

However, there were some differences in both studies. For instance, in this study, the effect of varying time on material damping properties was not considered. A fixed time of 10 minutes was used, whereas in the work of Ferreyra *et al.* [18] annealing times of 1 minute and 10 minutes were used. Further research could consider the effect of annealing heating times in intervals of 5 minutes up to 30 minutes. Although, there was agreement with respect to hardness measurements made in this work and the work done by Ferreyra *et al.* [18] there was an anomaly. For instance, in one case

the VHN of the upper portion (where outer notes are located) of a sunken drum head with a chemical composition (0.062% C, 0.017% P, 0.41%Mn, 0.02%Cr, balance Fe) comparable to the low-carbon steel used in this work was 171. Compare this value with those of the 20% cold rolled samples in this work in which the VHN across all annealing temperatures averaged 170. The difference was that Ferreyra *et al.* [18] reported increases in the hardness after heat treatment of 10% and 50% cold reduced samples at 370°C for 1 minute and 10 minutes. They attributed this increase in hardness to strain ageing. In this work, the hardness increase achieved in the test structures may be attributed mainly to strain hardening while the material damping changes manifested with heat treatment could be mainly attributed to the phenomenon of strain ageing.

At this stage it is important to draw attention to the fact that the bake hardenable steel used in this work manifested comparable material damping characteristics (see Figure 6.16c) in addition to achieving hardness values (Figure 6.36) that were comparable to its low-carbon steel counterpart. The only difference with these steels was the chemical composition and the mechanical properties such as yield, tensile and fracture strengths. On the basis of hardness, BH steel would be a prime candidate for pan manufacture. With yield strength approximately 100MPa lower (see Figure 6.30a) and comparable elongation (see Figure 6.36) the BH steel becomes an increasingly attractive candidate. It is also uncertain whether pans require steels that have yield strengths that fall within a certain range. If the BH steel used in this work does not meet the strength requirements, it is important to point out that these ferritic steels can be strengthened through the mechanism of solid solution strengthening but such steel will inevitably be more expensive than a plain low-carbon steel. This draws deeper attention to the need for further research to be conducted in order to specify ranges of mechanical properties (yield strength, tensile strength, fracture strength, ductility, impact toughness, strain hardening exponent, grain size, strain ratio and fracture toughness) for a wide range of low-carbon steels. The output would be to provide a guideline for suitable steels for pan making. This could be approached by first identifying steel drums which experienced and internationally renowned tuners would classify as exceptional material for pan making. This could be done for at least 10 to 20 tuners in 5 countries (Trinidad, USA, UK, Switzerland and Germany) where the steelpan is popular. The intent here would be to examine the chemical composition and mechanical properties of specimens extracted from these drums in an effort to establish any similarities. This information may be useful in forming the basis for the development of a material specification for pans.

6.9.5   Comparison to Aubrapan and 4ths and 5ths Soprano pan

The foremost intent of this part of the investigation was to examine the effect of surface coating on the material damping from a selection of the annealed low carbon strips. It is important to highlight

that there were some limitations in this examination, which were as follows: (1) the same chrome plating regime applied to the chrome plated steel pan may not be the same regime followed when the strips were chrome plated. This was the case as both test structures were chrome plated at different locations. Additionally, the surface coating applied to the Aubrapan was not of the same constituents as that of the paint applied to the low-carbon steel strips. A better approach would allow these parameters to be identical in both instances but it was not possible in this case. Nevertheless, the damping in the chromed and painted strips were lower (higher Q-factor) than the damping in the chromed and painted pans respectively (see Figure 6.38c and d). It is useful to remember that steelpan notes are usually pre-tuned before coating and fine-tuned after coating. The peening action during tuning may cold work the surface of the notes by a few percent. A small amount of cold work could contribute to a significant amount of damping increase (lower Q-factor) as seen in Figure 6.13 and this may explain why the damping in the pans were slightly higher than the damping in the strips.. This finding also presents an opportunity for further investigation where the damping in pans notes could be measured at four stages: (1) before pre-tuning, (2) after pre-tuning/coating, (3) after coating/before fine-tuning and (4) after fine tuning. Though a light-weight accelerometer was used, the mass would have decreased the Q-factors slightly

Secondly, the coated strips did not exhibit the same trend with frequency as did the steelpan notes and this may be in part due to the difference in geometry (shape) of the notes and the strips. The notes resemble flat circular and elliptical shells while the test strips were rectangular beams. A better approach might have been to construct identically shaped test structures for comparison with the steelpan notes.

Another crucial development was with the damping exhibited by the extracted Aubrapan strips. Good agreement was found to exist between the damping in the extracted strips and the low-carbon strips (Figure 6.40). This may be taken as a validation of the use of rolling to simulate the cold working of the steel sheet by hammering during the dishing process.

The material damping in the extracted Aubrapan strips did not show good agreement with the material damping in the Aubrapan notes (see Figure 6.39). Similar damping values were expected in the extracted Aubrapan strips and the Aubrapan notes as the material damping of confined modes (i.e. of the tuned modes in the Aubrapan notes) are primarily due to material damping [157]. However, this discrepancy may be due to the peening of the notes during tuning which would have some influence on the stress state of the instrument. The residual stresses in the pan dish might influence the damping and this is also another matter for further work.

Although the Aubrapan had half the amount of C and N as the low-carbon steel strips (see Table 6.1), the *Q*-factors of the extracted Aubrapan strips were well within the upper and lower bounds of the *Q*-factors extracted for the low-carbon strips (Figure 6.40). This was not expected but in the case of the BH steel this may indicate that material damping in low-carbon steels may not be very sensitive to interstitial atom content and that low-carbon steels with carbon contents that differ widely may demonstrate material damping characteristics that are identical.

6.9.6   Recommendations for future work

Apart from some of the other recommendations for further work that were made earlier in the body of this discussion there are a few more recommendations that should be considered for extension of this initiative and include:

- Other techniques for the measurement of material damping should be used and the findings compared to the findings obtained from the free-free damping method used herein.

- The development of a vacuum chamber in which the experiment could be conducted. Here the hammer impacts could be automatically controlled by a cam arrangement and the response could be measured by a microphone or a laser vibrometer. Conducting the experiment in a vacuum chamber would mitigate the effects of air resistance.

- Another way of investigating the effect of carbon on the damping behaviour seen in steels would be to introduce the use of a Snoek test where carbon is removed from solution and the damping is measured after each instance.

- The point above could be reinforced by the computation of activation energies as it is known that there is good agreement between activation energy required for the return of the yield point and the diffusion of carbon in ferrite [27].

- In this work rectangular beam like test strips were used. A better alternative would have been to use structures that were geometrically identical. For instance, the thickness reduction required could have been achieved by rolling or preferably by using a power hammer after which the shapes could have been extracted from the cold worked material using a water-jet cutting machine.

- The recommendation in the previous point should also be accompanied by the measurement of damping at each stage of the production of a pan. In this work the damping was only extracted from pans that had undergone all the production stages.

6.10 Conclusions

- As expected and in agreement with earlier literature on damping, cold rolling resulted in a decrease in material damping; annealing heat treatment resulted in damping recovery while surface coating lead to a material damping decrease.

- There was no apparent difference in the damping trends in test structures that were air cooled or water quenched.

- The coinciding of the temperature ranges at which the stabilisation (plateauing) of material damping occurred and at which there was an onset of strain ageing suggested that an annealing temperature between 300°C and 400°C would be appropriate for the heat treatment of pans.

- Strain ageing may be largely responsible for the stabilisation (plateauing) of the material damping in the annealing temperature range 300°C to 400°C.

- There was no apparent change in hardness with the onset of strain ageing and hardness remained generally stable over the range of annealing temperatures.

- Cold rolled and heat treated samples manifested comparable hardness indicating that strain hardening was primarily responsible for the hardness increase.

- Ultra-low carbon BH steel and the low carbon steel exhibited comparable hardness and material damping values over the range of annealing temperatures indicating that material damping may not be very sensitive to interstitial atom content in low carbon steels and that a much wider range of low-carbon steels may be acceptable for pan making but further investigation was recommended.

Chapter 7   Summary and Outlook

7.1   Summary

The thesis has provided new insights into the production and acoustics of pans. The findings are summarized below:

7.1.1   Production studies

- Multi-pass incremental sheet forming results in minimal extension of the stretched zone in the dish walls formed.

- A break even analysis shows that the pan making process could be profitable if incremental sheet forming is used in the dishing stage. However, this profitability could be jeopardized by the tuning stage.

7.1.2   Vibration studies

- A steelpan note is more likely to be detuned by repeated impacts at its centre.

- It is possible to confine modes to the vicinity of a flat region by variation of the bowl-wall curvature surrounding the region.

- The number of confined modes increases with increasing bowl-wall curvature.

- The mechanism of confinement appears to be due to the point of curvature change between the flat region and the bowl wall.

- Confined modes display light damping suggesting that the damping is mainly due to material and acoustic radiation damping.

7.1.3   Material studies

- Damping trends in cold-rolled and annealed low carbon steel specimens indicates that an annealing temperature between 300°C and 400°C would be appropriate for the heat treatment of pans.

- Damping trends suggest that a combination of at least two mechanisms is operative in the range of annealing temperatures used.

- Strain hardening was primarily responsible for the hardness increases displayed by the low-carbon steels.

- Ultra-low carbon bake hardenable and the low-carbon steel used exhibited comparable hardness and material damping values over the range of annealing temperatures indicating

that material damping may not be very sensitive to interstitial atom content in low-carbon steels and that a much wider range of low-carbon steels may be acceptable for pan making.

7.2 Outlook

7.2.1 Further research on low-carbon steels for pan making

Low-carbon steel will remain the material of choice for pan production for many years, mainly because it is cheap, abundantly available and tuning methods have evolved around its usage. Although it was shown in Chapter 6 that a wide range of low-carbon steels may be suitable for pan production, there still needs to be a definitive specification for low-carbon steels that lends to the production of high quality steelpans. Steelpans are still widely produced from oil containers that were once used to store toxic or hazardous chemicals. The material issue needs to be addressed before any other stage of the pan making process. Since the quantity of steel consumed for pan production is a minute fraction of the world steel consumption, it would be difficult to persuade a steel mill to produce a low-carbon steel with specific properties for pan making. However, there are other industries that have developed a wide range of low-carbon steels, particularly the automobile and piping industry. Future work could involve a matching of the mechanical property requirements for the production of high quality pans with the mechanical properties of a few of the steels used in automotive or piping applications. The steelpan industry will not only benefit from the regulations applied to these steels but pan makers will also have readily access to commercially available steel with consistent properties.

7.2.2 Considerations for future production studies

In Chapter 3 it was shown that the application of incremental sheet forming to the production of miniature and full size pans is commercially viable. However, the ISF machine at the CUED was only capable of producing miniature pan dishes due to size constraints. Further study should be extended to include the production of full size pan dishes by ISF. None of the minipans produced in this worked were tuned. Future work should also incorporate a study that compares the tuning in dishes made by three forming processes: ISF, a method, such as spinning, which produces a dish with relatively constant wall thickness and a traditionally hammer formed dish. Although tuners tend to prefer stretched dishes, there is no evidence to suggest that stretched dishes are the only dishes that are suitable for pan making. This investigation could be done by means of a blind study whereby selected pan makers are provided with dishes in which the method of dish forming would not be declared to the pan makers.

Multi-pass forming was used to extend the stretched zone in the miniature dishes formed in Chapter 3 and only minimal extension was achieved. Although ISF may be commercially viable its acceptance as an alternative forming method for pan dishes may depend on the thickness distribution. An alterative approach to multi-pass forming may be the trial of different tool paths. Future use of ISF should not be limited to dish forming but extended to the forming of the note boundaries and possibly the creation of notes whose geometry will require minimum adjustment afterwards to achieve modal tuning.

7.2.3   Vibration modeling of pans

The art of steelpan tuning has been perfected by trial and error over several decades, yet despite advances in computational capabilities, the modeling of steelpan vibration behaviour remains a challenge. The work in Chapter 5 of this thesis was able to provide some insight on a single aspect of the vibrational behaviour of the instrument i.e. mode confinement. Future mode studies should not only incorporate the aspect of mode confinement but should also take into account the effect that departure from symmetry and varying thickness has on the vibration behaviour of steelpan notes. Reliable note models might assist in the improvement of current tuning methods and may also help to reduce the time it takes to master the craft of tuning. Furthermore, reliable note models might provide insight towards the partial or complete tuning of pans. Reliable models may also aid in the design and tuning of pans of different metals such as aluminum, α-brass and stainless steel.

Appendix

Appendix A1: Non-averaged plots for air cooled and water quenched test strips
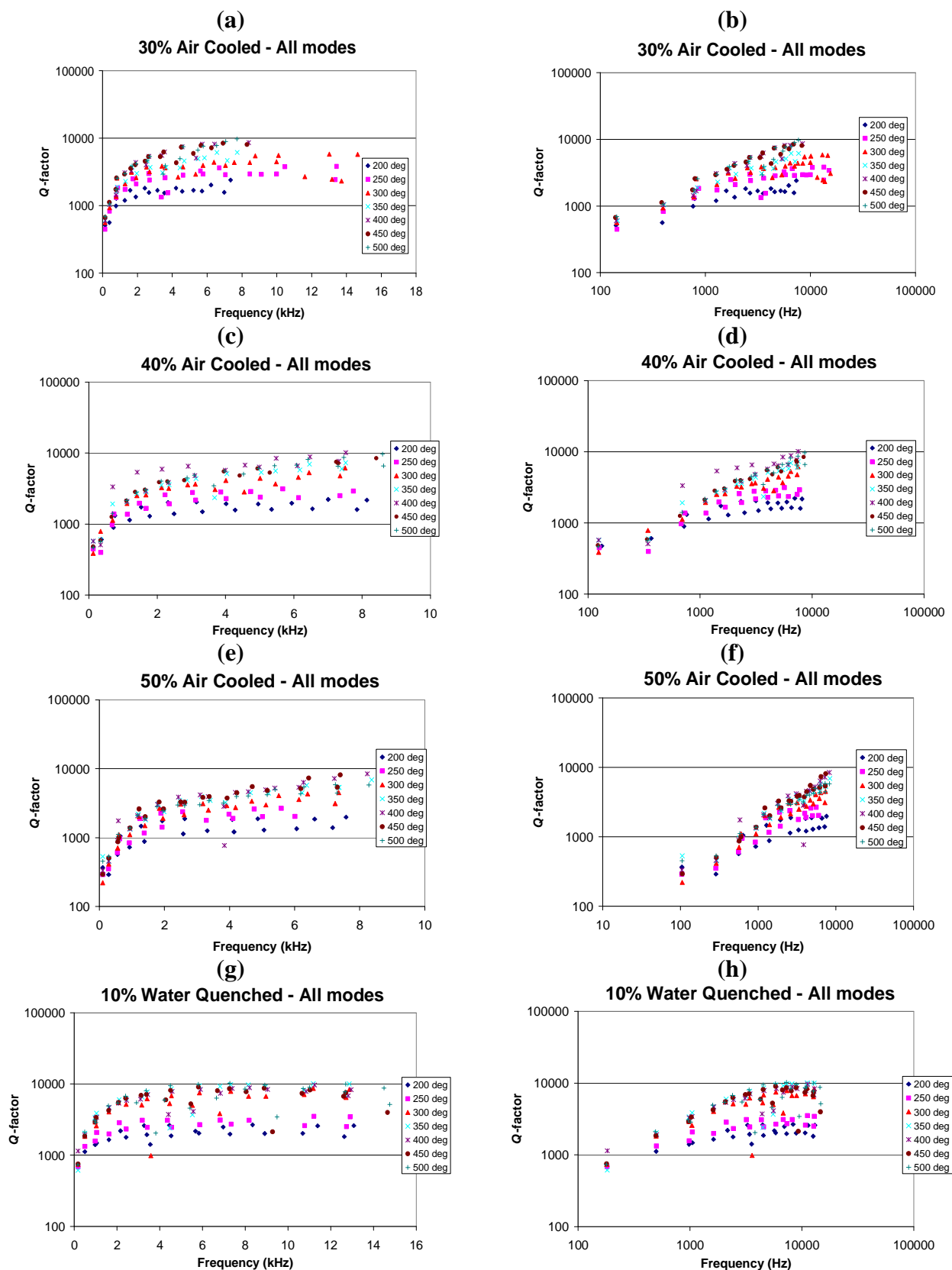
Figure A1-1: (a)-(f) semi-log and log-log plot for 30-50% cold reduced and air cooled strips and (g)-(h) semi-log and log-log plot for 30-50% cold reduced and water quenched strips

211
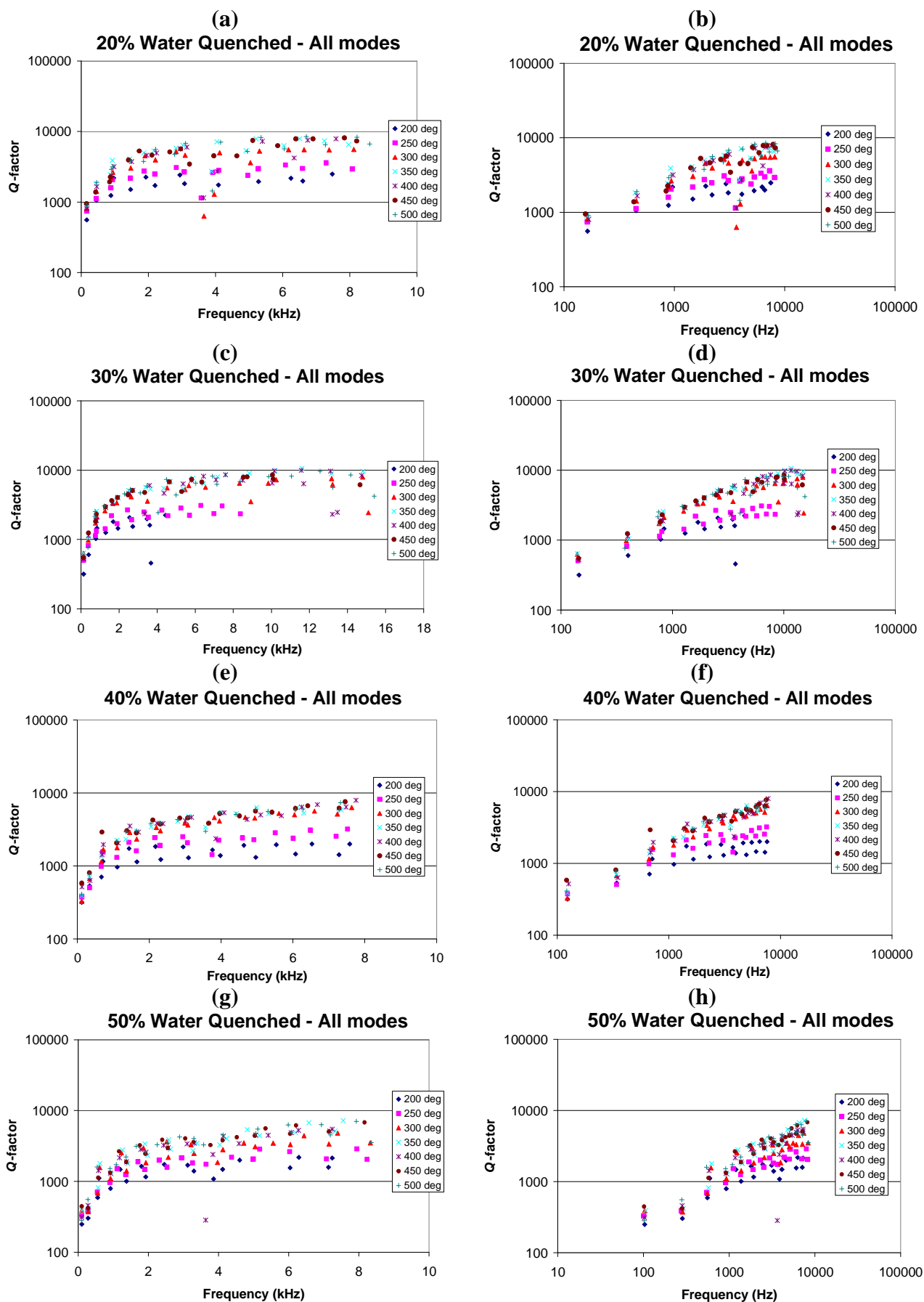
Figure A1-2: (a)-(g) semi-log and log-log plot for 20-50% cold reduced and water quenched strips

Appendix A2: Microstructures for low-carbon steel samples
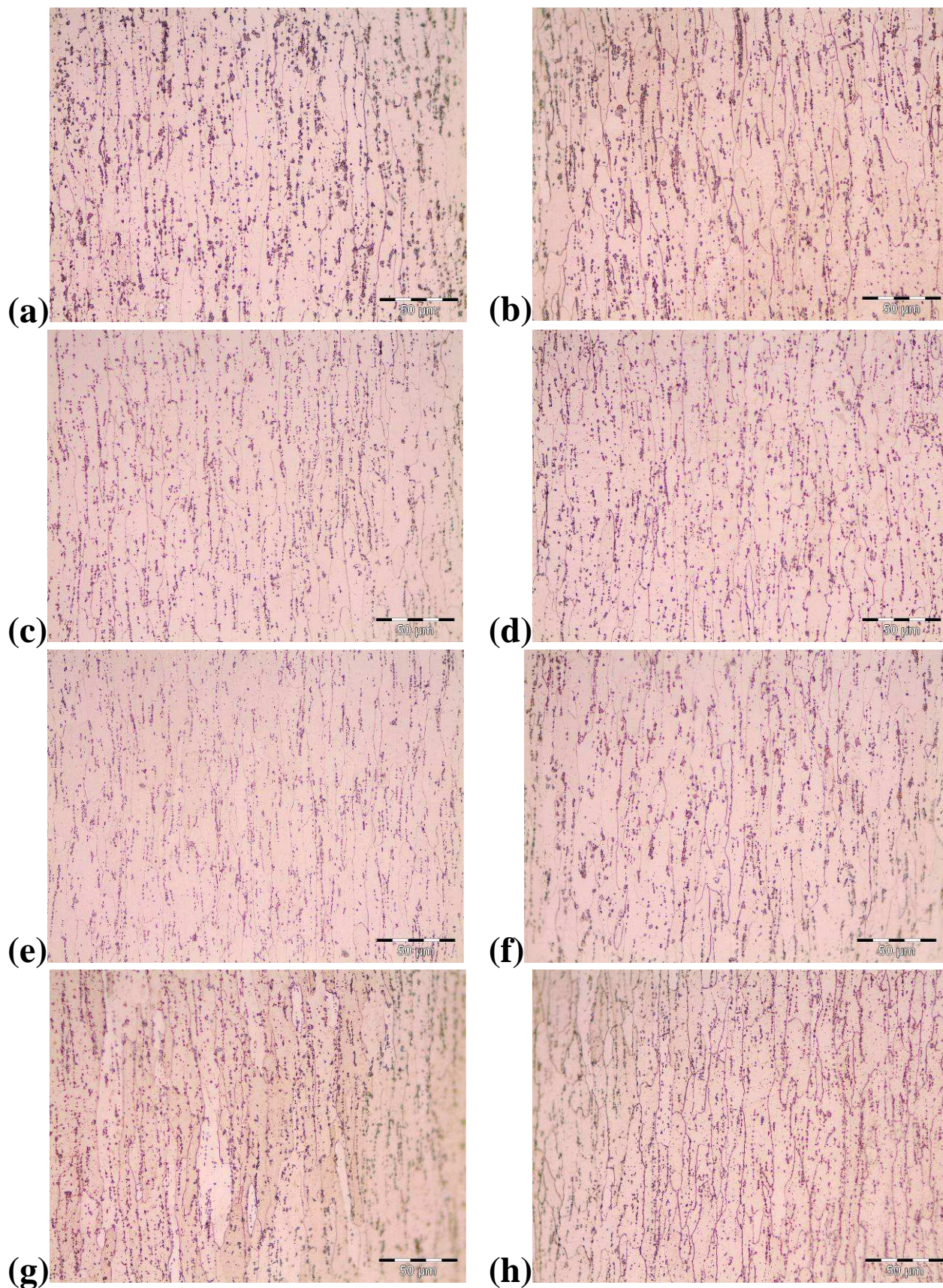
Figure A2-1: Microstructures corresponding to approximately 20% cold reduction and annealing for 10 minutes of 0.061%C steel: (a) not annealed (b)-(h) annealed at 200˚C, 250˚C, 300˚C, 350˚C, 400˚C, 450˚C and 500˚C respectively and air cooled. Etchant: 2% Nital

References

[1]   Joseph, T., *Squabbles over standardisation*, in *Trinidad Express, November 2*. 2000: Port-of-Spain. p. 9.

[2]   O'Connor, A.G., *Steel Drums; PAN: Heartbeat of a nation.* Percussive Notes, 1981. **19**(3): p. 54-55.

[3]   Aho, W., *Steel Band Music in Trinidad and Tobago: The Creation of a People's Music.* Latin American Music Review, 1987. **8**(1): p. 26-58.

[4]   Blake, F.I.R., *The Trinidad and Tobago Steel Pan: History and Evolution*. 1st ed. 1995, Port of Spain: Speeds Printery.

[5]   Cowley, J., *Carnival, Canboulay and Calypso: Traditions in the making*. 1998, Cambridge: Cambridge University Press.

[6]   Gibson, G., *Ellie Mannette on the Beginnings of Pan in Trinidad.* Percussive Notes, 1986. **34**: p. 34-37.

[7]   Wilkings, V. and M. La Rose, *The History of the Steel Band*. 2006, Singapore: Tamarind.

[8]   Pichary, L., *Results of the Steel Pan Survey 90*. 1990, Tunapuna: Trinidad and Tobago Bureau of Standards.

[9]   *Steel Drums: <http://www.kmm.info/Steel%20Drums.htm>*.   [cited 15 October 2007].

[10]   Kronman, U., *Steelpan Tuning: A handbook for steelpan making and tuning*. 1991, Stockholm, Sweden: Musikmuseet.

[11]   *Steelpan regions: http://210.136.151.134/00_diary/cubismo/archives/images/steelpan.gif* [cited 5 September 2007].

[12]   Roach, K., *The Imperatives for Standardization*. 1992, Tunapuna: Trinidad and Tobago Bureau of Standards.

[13]   *Sound Pressure Level Table: <http://www.sengpielaudio.com/TableOfSoundPressureLevels.htm>*.   [cited 19 September 2007.

[14]   Bridge, J. *The Vibrational Modes of the Notes of the Tenor Steelpan: A Finite Element Study*. in *Proceedings of the Thirteenth International Congress on Sound and Vibration (ICSV13)*. July 2-6, 2006. Vienna, Austria.

[15]   Rossing, T.D., D.S. Hampton, and U.J. Hansen, *Music from oil drums: The acoustics of the steel pan.* Physics Today, 1996. **49**(3): p. 24-29.

[16]   Muthukumaran, P., R.B. Bhat, and I. Stiharu, *Boundary Conditioning Technique for structural tuning.* Journal of Sound and Vibration, 1999. **220**(5): p. 847-859.

[17]   Schulz, E., *Personal Communication.* 15-18 December 2006: E.C.S. Steel drums, Dortmund, Germany.

[18]   Ferreyra, E., J.G. Maldonado, L.E. Murr, S. Pappu, E.A. Trillo, C. Kennedy, M. Posada, J. de Alba, R. Chitre, and D.P. Russell, *Materials science and metallurgy of the Caribbean steel drum. Part II. Heat treatment, microstructures, hardness profiles and tuning effects.* Journal of Materials Science, 1999. **34**(5): p. 981-996.

[19]   Murr, L.E., E. Ferreyra, J.G. Maldonado, E.A. Trillo, S. Pappu, C. Kennedy, J. de Alba, M. Posada, D.P. Russell, and J.L. White, *Materials science and metallurgy of the Caribbean steel drum. Part I. Fabrication, deformation phenomena and acoustic fundamentals.* Journal of Materials Science, 1999. **34**(5): p. 967-979.

[20]   Ferreyra, E., L.E. Murr, D.P. Russell, and J.F. Bingert, *Elastic interactions and the metallurgical and acoustic effects of carbon in the Caribbean steel drum.* Materials Characterization, 2001. **47**(5): p. 325-363.

[21]   *David sinking <http://www.steelpan-steeldrums-information.com/images/David-sinking.jpg>.*   [cited 13 July 2009].

[22]   *Mark-Michael sinking <http://www.jumbierecords.com/journal_images/pan_Mark_Michael.jpg>.*   [cited 13 July 2009].

[23]   Poon Chong, P., *Personal Communication.* June 2009: Metal Industries Company Limited.

[24]   Ilmorinne, T. and L. Lamminen, *Numeerista painomuovausta robotilla*, in *OHUTLEVY.* 2004. p. 10-12.

[25]   Schäfer, T. and R.D. Schraft, *Incremental sheet metal forming by industrial robots using a hammering tool*, in *10^{émes} Assises Européennes de Prototypage Rapide.* 14-15 September, 2004: Paris, France.

[26]   Allwood, J.M., N.E. Houghton, and K.P. Jackson, *The Design of an Incremental Sheet Forming Machine*, in *11th Conference on Sheet Metal.* 2005: Erlangen.

[27]   Dieter, G.E., *Mechanical Metallurgy.* S.I. Metric ed. 1988, Singapore: McGraw-Hill.

[28]   Jeswiet, J. and E. Hagan, *A review of conventional and modern single-point sheet metal forming methods.* Proceedings of the Institution of Mechanical Engineers, 2003. **217**(Part B: Journal of Engineering Manufacture): p. 213-225.

[29]   Wong, C.C., T.A. Dean, and J. Lin, *A review of spinning, shear forming and flow forming processes.* International Journal of Machine Tools and Manufacture, 2003. **43**(14): p. 1419-1435.

[30]   Fletter, R.P. *Metal Spinning Tutorial. <http://prl.stanford.edu/documents/pdf/spinning.pdf>*.
1995 [cited 13 January 2007].

[31]   Portavecchia, D., *Steel bands are big business*, in *The Advertiser, December 7*. 1973:
Croydon, London.

[32]   Ramsundar, P., *Personal Communication*. June 2009: University of Trinidad and Tobago.

[33]   Cooper, M., *Personal Communication*. 18 May 2009: panland Trinidad Ltd.

[34]   Rohner, F. and S. Schärer. *A new material leads to another sound*. in *Proceedings of the 1st
International Conference on the Science and Technology of the Steelpan*. 2000. Port-of-
Spain, Trinidad: 157-162.

[35]   *Conventional spin forming: < www.custompartnet.com/wu/sheet-metal-forming >*.   [cited
22 September 2009].

[36]   Griffin, M.J., H.V.C. Howarth, P.M. Pitts, S. Fischer, U. Kaulbars, P.M. Donati, and P.F.
Bereton, *Guide to good practice on hand-arm vibration. Non binding guide to good practice
with a view to implementation of Directive 2002/44/EC on the minimum health and safety
requirements regarding the exposure of workers to the risks arising from physical agents
(vibrations)*. EU Good Practice Guide HAV, V7.7 ed. 2006, Luxembourg: European
commission.

[37]   HSE, *Hand-arm vibration: The Control of Vibration at Work Regulations 2005*. 2008, The
Office of Public Sector Information, Surrey, UK: HSE Books.

[38]   Agate, J.N., *Some aspects of injuries resulting from the use of vibratory tools.*

[39]   Taylor, W., D. Wasserman, V. Behrens, D. Reynolds, and S. Samueloff, *Effect of air
hammer on the hands of stonecutters. The limestone quarries of Bedford, Indiana, revisited.*
British Journal of Industrial Medicine, 1984. **41**: p. 289-295.

[40]   Weir, E. and L. Lander, *Hand-arm vibration syndrome.* Canadian Medical Journal
Association, 2005. **172**(8): p. 1001-1002.

[41]   Telford, E.D., M.B. McCann, and D.H. MacCormack, *"Dead Hand" in users of vibrating
tools.* The Lancet, Sept. 22, 1945: p. 359-360.

[42]   Altan, T. *Processes for hydroforming sheet metal - Part II: Sheet hydroforming with a
punch:< http://nsmwww.eng.ohio-state.edu/March06R_DUpdate.pdf >*. 2006 [cited 12
January 2007
].

[43]   Altan, T. *Processes for hydroforming sheet metal - Part I: Sheet hydroforming with a die:<
http://nsmwww.eng.ohio-state.edu/Feb06R_DUpdate.pdf >*. 2006 [cited 12 January 2007].

[44]   Joseph, T., *Williams axed local pan press research*, in *Trinidad Express, April 19*. 2002: Port-of-Spain.

[45]   Whitmyre, G. and H.J. Price, *Production of a Caribbean Steel Pan - United States Patent: 6,212,772 B1*. 2001.

[46]   Schärer, S., F. Rohner, and P. Schober. *The technology of a new rawform*. in *International conference on the science and technology of the steelpan*. 16-18 Oct, 2001. Port of Spain, Trinidad: 189-196.

[47]   Altan, T. *Processes for hydroforming sheet metal - Part III: SHF-P and SHF-D case studies:< http://nsmwww.eng.ohio-state.edu/April06R_DUpdate.pdf >*. 2006 [cited 12 January 2007].

[48]   Hosford, W.F., *Mechanical Behaviour of Materials*. 2005, New York: Cambridge University Press.

[49]   Murr, L.E., S.M. Gaytan, M.I. Lopez, D.E. Bujanda, E.Y. Martinez, G. Whitmyre, and H. Price, *Metallurgical and acoustical characterization of a hydroformed, 304 stainless steel, Caribbean-style musical pan*. Materials Characterization, 2008. **59**(3): p. 321-328.

[50]   Allwood, J.M., *Future developments in incremental sheet frming*. 2007, University of Cambridge.

[51]   Cerro, I., E. Maidagan, J. Arana, A. Rivero, and P.P. Rodríguez, *Theoretical and experimental analysis of the dieless incremental sheet forming process*. Journal of Materials Processing Technology, 2006. **177**(1-3): p. 404-408.

[52]   Allwood, J.M., A.N. Bramley, T.W. Ridgman, and A.R. Mileham, *A novel method for the rapid production of inexpensive dies and moulds with surfaces made by incremental sheet forming*. Proceedings of the IMechE Part B: Journal of Engineering Manufacture, 2006. **220**: p. 323-327.

[53]   Allwood, J.M., *Future developments in incremental sheet forming*, in *4th Chemnitz Car Body Colloquium*. 8-9 November, 2005: Chemnitz, Germany.

[54]   Jeswiet, J., F. Micari, G. Hirt, A. Bramley, J. Duflou, and J. Allwood, *Asymmetric Single Point Incremental Forming of Sheet Metal*. CIRP Annals - Manufacturing Technology, 2005. **54**(2): p. 88-114.

[55]   Kim, T.J. and D.Y. Yang, *Improvement of formability for the incremental sheet metal forming process*. International Journal of Mechanical Sciences, 2000. **42**(7): p. 1271-1286.

[56]   Micari, F., G. Ambrogio, and L. Filice, *Shape and dimensional accuracy in Single Point Incremental Forming: State of the art and future trends*. Journal of Materials Processing Technology, 2007. **191**(1-3): p. 390-395.

[57]   Ambrogio, G., I. Costantino, L. De Napoli, L. Filice, L. Fratini, and M. Muzzupappa, *Influence of some relevant process parameters on the dimensional accuracy in incremental forming: a numerical and experimental investigation.* Journal of Materials Processing Technology, 2004. **153-154**: p. 501-507.

[58]   Ambrogio, G., V. Cozza, L. Filice, and F. Micari, *An analytical model for improving precision in single point incremental forming.* Journal of Materials Processing Technology, 2007. **191**(1-3): p. 92-95.

[59]   Hussain, G. and L. Gao, *A novel method to test the thinning limits of sheet metals in negative incremental forming.* International Journal of Machine Tools and Manufacture, 2007. **47**(3-4): p. 419-435.

[60]   Kopac, J. and Z. Kampus, *Incremental sheet metal forming on CNC milling machine-tool.* Journal of Materials Processing Technology, 2005. **162-163**: p. 622-628.

[61]   Dai, K., Z.R. Wang, and Y. Fang, *CNC incremental sheet forming of an axially symmetric specimen and the locus of optimization.* Journal of Materials Processing Technology, 2000. **102**(1-3): p. 164-167.

[62]   Kim, Y.H. and J.J. Park, *Effect of process parameters on formability in incremental forming of sheet metal.* Journal of Materials Processing Technology, 2002. **130-131**: p. 42-46.

[63]   *DIN 8580 Manufacturing processes - terms and definitions (German National Standard).* 2003, Deutsches Institut Fur Normung E.V.

[64]   Siegert, K. and S. Wagner. *TALAT lecture on stretch forming 3703 <http://www.eaa.net/eaa/education/TALAT/lectures/3703.pdf>.* 1994 [cited 8 September 2009].

[65]   *StateMaster - Encyclopedia: English wheel <http://www.statemaster.com/encyclopedia/English-Wheel >.* [cited 6 September 2009].

[66]   *Mittler English Wheel <http://www.vansantent.com/images/Mittler_English_Wheel.gif>.* [cited 8 September 2009].

[67]   *The English Wheel <http://www.hotrodders.com/gallery/data/500/english_wheel_-_2_002.jpg>.* [cited 8 September 2009].

[68]   *250 ton drawing press:< http://www.bikudo.com/buy/details/491794/250_90_ton_capacity_h_type_deep_drawing_press.html#desc >.* [cited 21 September 2009].

[69]   Gay, D. *Steel drums to steelpans.* in *Proceedings of the 1st International Conference on the Science and Technology of the Steelpan.* 2000. Port-of-Spain, Trinidad: 163-178.

[70]   *ASTM International A366/A 366M - 97$^{\varepsilon 1}$: Standard specification for commercial steel (CS) sheet, Carbon (0.15 Maximum Percent) Cold Rolled.* 1998.

[71] *United Nations Designation UN1A1-101-01: Carbon steel tight head 55-gallon drum specification.* 2001.

[72] Murr, L.E., C.A.C. Imbert, E.V. Esquivel, A.A. Bujanda, N.E. Martinez, K.F. Soto, A.S. Tapia, S. Lair, A.C. Somasekharan, R. Kerns, S. Irvine, and S. Lawrie, *Metallurgical and acoustical comparisons for a brass pan with a Caribbean steel pan standard.* Journal of Materials Science, 2004. **39**: p. 4139-4155.

[73] Murr, L.E., E.V. Esquivel, S.C. Lawrie, M.I. Lopez, S.L. Lair, K.F. Soto, S.M. Gaytan, D. Bujanda, R.G. Kerns, P.A. Guerrero, and J.A. Flores, *Fabrication of an aluminum, Caribbean-style, musical pan: Metallurgical and acoustical characterization.* Materials Characterization, 2006. **57**(4-5): p. 232-243.

[74] Bloss, B. and M.D. Rao, *Measurement of damping in structures by the power input method.* Experimental Techniques, 2002. **26**(3): p. 30-32.

[75] Marin, J., *Mechanical Behaviour of Engineering Materials.* 1962, London: Prentice-Hall International. 272-289.

[76] Adams, R.D., *The damping characteristics of certain steels, cast irons and other metals.* Journal of Sound and Vibration, 1972. **23**(2): p. 199-216.

[77] Bert, C.W., *Material damping: An introductory review of mathematic measures and experimental technique.* Journal of Sound and Vibration, 1973. **29**(2): p. 129-153.

[78] Nashif, A.D., D.I.G. Jones, and J.P. Henderson, *Vibration Damping.* 1985, New York: John Wiley & Sons, Inc.

[79] Brinkman, J.A., C.E. Dixon, and C.J. Meechan, *Interstitial and vacancy migration in Cu_3Au and copper.* Acta Metallurgica, 1954. **2**(1): p. 38-48.

[80] Eshelby, J.D., *Dislocations as a Cause of Mechanical Damping in Metals.* Proceedings of the Royal Society of London. Series A, Mathematical and Physical Sciences, 1949. **197**(1050): p. 396-416.

[81] Johnson, W., *Dislocation damping after plastic deformation in interstitial-free and carbon steels.* Journal of Alloys and Compounds, 2000. **310**(1-2): p. 423-426.

[82] Wilks, J., *Dislocation damping in metals.* British Journal of Applied Physics, 1965. **16**(5): p. 587-603.

[83] Nowick, A.S., *On the interpretation of "low-temperature" recovery phenomena in cold-worked metals.* Acta Metallurgica, 1955. **3**(4): p. 312-321.

[84] Allgeier, T., R. Adams, and W. Evans, *Vibrational measurement of the specific damping capacity of 15–5 ph stainless steel.* Proceedings of the Institution of Mechanical Engineers, Part C: Journal of Mechanical Engineering Science, 1997. **211**(1): p. 49-53.

[85]   Baik, S.B., J.C. Kim, K.K. Jee, M.C. Shin, and C.S. Choi, *Effects of Carbon Content and Cold Working on Damping Capacity and Mechanical Property of Fe-17wt.%Mn Martensitic Alloy.* J. Phys. IV France, 1995. **05**(C8): p. 391-396.

[86]   Golovin, S.A. and S.I. Arkhangel'skii, *Damping of oscillations in different metals.* Metal Science and Heat Treatment, 1966. **8**(5): p. 348-351.

[87]   Granato, A., A. Hikata, and K. Lücke, *Recovery of damping and modulus changes following plastic deformation.* Acta Metallurgica, 1958. **6**(7): p. 470-480.

[88]   Potekhin, B. and A. Potekhin, *Effect of the heat-treatment regime and carbon content on the damping properties of steel 01Kh6F2.* Metal Science and Heat Treatment, 1997. **39**(12): p. 504-507.

[89]   Zener, C., *Internal Friction in Solids IV. Relation Between Cold Work and Internal Friction.* Physical Review, 1938. **53**(7): p. 582-586.

[90]   McClintock, F.A., S. Backer, A.S. Argon, G.S. Reichenbach, E. Orowan, M.C. Shaw, and E. Rabinowicz, *Mechanical Behaviour of Materials*. Addison-Wesley Series in Metallurgy and Materials, ed. M. Cohen, F.A. McClintock, and A.S. Argon. 1966, Reading, Massachusetts, U.S.A.: Addison-Wesley Publishing Co. Inc. 471-487.

[91]   Ashby, M.F., *Materials selection in mechanical design*. 3rd ed. 2005, Amsterdam; Boston: Butterworth-Heinemann.

[92]   *Substech:< http://www.substech.com >*.   [cited 10 July 2009].

[93]   Schärer, S. and F. Rohner. *Hardening steel by nitriding*. in *Proceedings of the 1st International Conference on the Science and Technology of the Steelpan*. 16-18 Oct, 2000. Port-of-Spain, Trinidad: 179-188.

[94]   Hikata, A., R. Truell, A. Granato, B. Chick, and K. Lucke, *Sensitivity of Ultrasonic Attenuation and Velocity Changes to Plastic Deformation and Recovery in Aluminum.* Journal of Applied Physics, 1956. **27**(4): p. 396-404.

[95]   Zener, C., *Internal friction in solids.* Proceedings of the Physical Society, 1940(1): p. 152-166.

[96]   Cottrell, A.H. and B.A. Bilby, *Dislocation Theory of Yielding and Strain Ageing of Iron.* Proceedings of the Physical Society. Section A, 1949(1): p. 49-62.

[97]   Higgins, R.A., *Properties of Engineering Materials*. 2nd ed. 1998, New Delhi: Viva Books Private Limited.

[98]   Higgins, R.A., *Engineering metallurgy: applied physical metallurgy*. First south Asian edition ed. 1998, Delhi: VIVA

[99]   Granzow, W.G., *Fabrication characteristics of carbon and low-alloy steels*. Vol. 1 ASM Handbook, Properties and Selection: Irons, Steels and High Performance Alloys. 2005: ASM International.

[100]   Callister, W.D., *Materials science and engineering: an introduction*. 7th ed. 2007, New York: John Wiley and Sons, Inc.

[101]   Llewellyn, D.T., *Steels: Metallurgy and Applications*. 2nd ed. 1994, Oxford: Butterworth-Heinemann Ltd.

[102]   Llewellyn, D.T. and R.C. Hudd, *Steels: Metallurgy and Applications*. 3rd ed. 2000, Oxford: Butterworth-Heinemann.

[103]   *Strain rate sensitivity* <*http://aluminium.matter.org.uk/content/html/ENG/default.asp?catid=208&pageid=21444 16609>*.   [cited 21 December 2009].

[104]   Totten, G.E., *Steel heat treatment handbook: metallurgy and technologies*. 2nd ed. 2006, Boca Raton: Taylor and Francis Group, LLC.

[105]   Hosford, W.F. and R.M. Caddell, *Metal forming: mechanics and metallurgy*. 3rd ed. 2007, Cambridge: Cambridge University Press.

[106]   Davies, G., *Materials for automobile bodies*. 2003, Oxford: Butterworth-Heinemann.

[107]   Vander Voort, G.F., *Service characteristics of carbon and low alloy steels*. Vol. 1 ASM Handbook, Properties and Selection: Irons, Steels and High Performance Alloys. 2005: ASM International.

[108]   Honeycombe, R.W.K., *Steels: microstructure and properties*. 1981, London: Edward Arnold.

[109]   Smallman, R.E. and R.J. Bishop, *Modern physical metallurgy and materials engineering*. 6th ed. 1999, Oxford: Butterworth-Heinemann.

[110]   Ferreyra, E. and L.E. Murr, *Metallography in music: Microstructures in the Caribbean steel drum.* Materials Characterization, 2000. **45**(4-5): p. 341-351.

[111]   Davis, J.R., ed. *Surface hardening of steels: understanding the basics*. 2002, ASM International: Ohio, USA.

[112]   Rossing, T.D., *Science of Percussion Instruments*. Series in Popular Science, ed. R.J. Weiss. Vol. 3. 2000, Singapore: World Scientific.

[113]   Rossing, T.D., C.A. Anderson, and R.I. Mills, *Acoustics of Timpani.* Percussive Notes, 1982: p. 18-30.

[114] Ramakrishna, B.S. and M. Sondhi, *Vibrations of Indian Musical Drums Regarded as Compostite Membranes.* The Journal of the Acoustical Society of America, 1954. **26**(4): p. 523-529.

[115] Raman, C.V. and S. Kumar, *Musical drums with harmonic overtones.* Nature, 1920. **2620**(104): p. 500.

[116] Raman, C.V., *The Indian Musical drums.* Proceedings of the Indian Academy of Science, 1935. **A1**: p. 179-188.

[117] Deutsch, B.M., C.L. Ramirez, and T.R. Moore, *The dynamics and tuning of orchestral crotales.* Journal of the Acoustical Society of America, 2004. **116**(4): p. 2427-2433.

[118] Bork, I., *Practical tuning of xylophone bars and resonators.* Applied Acoustics, 1995. **46**(1): p. 103-127.

[119] Bretos, J., C. Santamaría, and J.A. Moral, *Frequencies, input admittances and bandwidths of the natural bending eigenmodes in xylophone bars.* Journal of Sound and Vibration, 1997. **203**(1): p. 1-9.

[120] Bretos, J., C. Santamaría, and J.A. Moral, *Tuning process of xylophone and marimba bars analysed by the finite element modelling and experimental measurements.* Journal of the Acoustical Society of America: Technical Notes and Research Briefs, 1997. **102**(6): p. 3815-3816.

[121] Suits, B.H., *Basic physics of xylophone and marimba bars.* American Journal of Physics, 2001. **69**(7): p. 743-750.

[122] Bretos, J., C. Santamaría, and J. Alonso Moral, *Finite element analysis and experimental measurements of natural eigenmodes and random responses of wooden bars used in musical instruments.* Applied Acoustics, 1999. **56**(3): p. 141-156.

[123] Rossing, T.D., *Acoustics of percussion instruments: Recent progress.* Acoustical Science and Technology, 2001. **22**(3): p. 177-188.

[124] Bork, I., A. Chaigne, L.-C. Trebuchet, M. Kosfelder, and D. Pillot, *Comparison between Modal Analysis and Finite Element Modelling of a Marimba bar.* ACUSTICA.acta acustica, 1999. **85**: p. 258-266.

[125] Rossing, T.D., J. Yoo, and A. Morrison, *Acoustics of percussion instruments: An update.* Acoustical Science and Technology, 2004. **25**(6): p. 406-412.

[126] McLachlan, N., B.K. Nigjeh, and A. Hasell, *The design of bells with harmonic overtones.* Journal of the Acoustical Society of America, 2003. **114**(1): p. 505-511.

[127] Mills, R.G.J., *Tuning of bells by a linear programming method.* Journal of the Acoustical Society of America, 1989. **85**(6): p. 2630-2633.

[128] Perrin, R., T. Charnley, and J. dePont, *Normal modes of the modern English church bell.* Journal of Sound and Vibration, 1983. **90**(1): p. 29-49.

[129] Perrin, R., G.M. Swallowe, T. Charnley, and C. Marshall, *On the debossing, annealing and mounting of church bells.* Journal of Sound and Vibration, 1999. **227**(2): p. 409-425.

[130] Rossing, T.D., *Chimes and Bells.* Percussive Notes, 1982. **19**(3): p. 42-57.

[131] Rohner, F. and S. Schärer. *History, Development and Tuning of the Hang.* in *Proceedings of the International Symposium on Musical Acoustics (ISMA 2007).* September 9-12, 2007. Barcelona, Spain.

[132] Rossing, T.D., A. Morrison, U.J. Hansen, F. Rohner, and S. Schärer. *Acoustics of the Hang: A hand-played steel instrument.* in *Proceedings of the International Symposium on Musical Acoustics (ISMA 2007).* September 9-12, 2007. Barcelona, Spain.

[133] Copeland, B., A. Morrison, and T.D. Rossing, *Sound Radiation from Caribbean steelpans.* Journal of the Acoustical Society of America, 2005. **117**(1): p. 375-383.

[134] Hansen, U.J. and T.D. Rossing, *Modal studies in a double second Caribbean steel drum.* The Journal of the Acoustical Society of America, 1989. **85**(S1): p. S32-S32.

[135] Hansen, U.J. and T.D. Rossing, *Modal analysis of a Caribbean steel drum.* The Journal of the Acoustical Society of America, 1987. **82**(S1): p. S68-S68.

[136] Hansen, U.J. and T.D. Rossing. *The Caribbean Steelpan, and some offsprings.* in *Forum Acusticum.* 2005. Budapest.

[137] Hansen, U.J., T.D. Rossing, E. Mannette, and K. George, *The Caribbean Steel Pan: Tuning and Mode Studies.* MRS Bulletin, 1995. **20**(3): p. 44-46.

[138] Rossing, T.D. and U.J. Hansen. *Science of the Steelpan: What is known and what is not.* in *Proceedings of the 1st International Conference on the Science and Technology of the Steelpan.* 2000. Port-of-Spain, Trinidad: 17-31.

[139] Rossing, T.D. and U.J. Hansen, *Vibrational mode shapes in Caribbean steelpans Part II: cello and bass.* Applied Acoustics, 2004. **65**: p. 1233-1247.

[140] Rossing, T.D., U.J. Hansen, and D.S. Hampton, *Vibrational mode shapes in Caribbean steelpans. I. Tenor and double second.* Journal of the Acoustical Society of America, 2000. **108**(2): p. 803-812.

[141] Rossing, T.D., U.J. Hansen, E. Manette, and K. George, *The Caribbean Steelpan: Tuning and Mode Studies.* MRS Bulletin, 1995. **20**(3): p. 44-46.

[142] Rossing, T.D., U.J. Hansen, and D. Scott Hampton. *Modal analysis of steelpans: holographic, computer, sand patterns, and microphone scanning.* in *Proceedings of the 1st*

International Conference on the Science and Technology of the Steelpan. 2000. Port-of-Spain, Trinidad: 73-82.

[143] Barlow, C.Y., B.E. Richardson, J. Woodhouse, and J. Zarek, *The Caribbean Steel Drum.* Proceedings of the Institute of Acoustics, 1988: p. 193-198.

[144] Dennis, R.A., *A preliminary investigation of the manufacture and performance of a tenor steelpan.* West Indian Journal of Engineering, 1971. **3**(1): p. 32-71.

[145] Olson, H.F., *Music, Physics and Engineering, 2nd edition.* 1967, New York: Dover. 80.

[146] Soedel, W., *Vibrations of shells and plates.* 3rd, revised and expanded ed. 2004, New York: Marcel Dekker Inc.

[147] Achong, A., *Steelpan as a system of non-linear mode-localized oscillators, I: Theory, simulations, experiments and bifurcations.* Journal of Sound and Vibration, 1996. **197**(4): p. 471-487.

[148] Achong, A., *The steelpan as a system of non-linear mode-localized oscillators, Part III: The inverse problem - Parameter estimation.* Journal of Sound and Vibration, 1998. **212**(4): p. 623-635.

[149] Achong, A. *The theory of the steelpan.* in *Proceedings of the 1st International Conference on the Science and Technology of the Steelpan.* 2000. Port-of-Spain, Trinidad: 1-16.

[150] Achong, A. and K.A. Sinanan-Singh, *Steelpan as a system of non-linear mode-localized oscillators, Part II: Coupled sub-systems, simulations and experiments.* Journal of Sound and Vibration, 1997. **203**(4): p. 547-561.

[151] Achong, A., *Non-linear analysis of compressively/thermally stressed elastic shell structures on the steelpan and the underlying theory of the tuning process.* Journal of Sound and Vibration, 1999. **222**(4): p. 597-620.

[152] Achong, A., *Vibrational Analysis of Circular and Elliptic Plates Carrying Point and Ring Masses and with Edges Elastically Restrained.* Journal of Sound and Vibration, 1995. **183**(1): p. 157-168.

[153] Achong, A., *Vibrational analysis of mass loaded plates and shallow shells by the receptance method with application to the steelpan.* Journal of Sound and Vibration, 1996. **191**(2): p. 207-217.

[154] Rossing, T.D. and N.H. Fletcher, *The Physics of Musical Instruments: 2 Rev Ed edition.* 2 Rev Ed edition ed. 1999, New York: Springer-Verlag.

[155] Rossing, T.D., F.R. Moore, and P.A. Wesley, *The science of sound, 3rd edition.* 2002, San Francisco: Addison Wesley.

[156] Gay, D. *Finite Element Modelling of Steelpan Vibrational Modes*. in *Proceedings of the 1st International Conference on the Science and Technology of the Steelpan (ICSTS)*. October 16-18, 2000. Port-of-Spain, Trinidad: p. 53-71.

[157] Scott, J.F.M. and J. Woodhouse, *Vibration of an Elastic Strip with Varying Curvature*. Philosophical Transactions: Physical Sciences and Engineering, 1992. **339**(1655): p. 587-625.

[158] *The Musical Saw: http://www.earthlingsmusic.net/images/SawMan2.jpg* [cited 14 November 2007].

[159] Nurse, K., *GLOBALIZATION AND TRINIDAD CARNIVAL: DIASPORA, HYBRIDITY AND IDENTITY IN GLOBAL CULTURE*. Cultural Studies, 1999. **13**: p. 661-690.

[160] Verbert, J., B. Belkassem, C. Henrard, A. Habraken, J. Gu, H. Sol, B. Lauwers, and J. Duflou, *Multi-Step toolpath approach to overcome forming limitations in single point incremental forming*. International Journal of Material Forming, 2008. **1**(0): p. 1203-1206.

[161] Young, D. and J. Jeswiet, *Wall thickness variations in single-point incremental forming*. Proceedings of the IMechE Part B: Journal of Engineering Manufacture, 2004. **218**: p. 1453-1459.

[162] Kerns, R.G., S.C. Lawrie, A. Lawrie, R.J. Drouin, and D.R. Gettes, *Pan musical instruments and methods for making same: United States Patent - US 7,745,711 B2*. 2010.

[163] Payne, A.C., J.V. Chelsom, and L.R.P. Reavill, *Management for Engineers*. 1995, Chichester: John Wiley & Sons.

[164] Davies, D.B., *The art of managing finance: A guide for non-financial managers*. 1985, London: McGraw-Hill.

[165] Gutierrez, P.H. and N.L. Dalsted. *Break even method of investment analysis no. 3.759:< http://agecon.uwyo.edu/riskmgt/financialrisk/Break-even%20method%20of%20investment%20analysis.pdf>*. 2008 [cited 12 May 2010].

[166] *Panyard Jumbie Jam minipan<http://www.amazon.co.uk/Panyard-Jumbie-Jam-Steel-Pan/dp/B002EIOK34/ref=sr_1_2?ie=UTF8&s=officeproduct&qid=1281452068&sr=8-2>*. [cited 8 August 2010].

[167] *New Castle drum centre <http://www.newcastledrum.co.uk/Home-SubSection.aspx?SubCategoryId=208&CategoryId=13&SubCategorySection=S&PageId=209>*. [cited 8 August 2010].

[168] *Panyard Lead soprano pans<http://www.panyard.com/pans/pans.php?view=LEADS>*. [cited 8 August 2010].

[169] *E.C.S. steel drums, Dortmund, Germany <http://www.ecs-steeldrums.de/index_13_64.html>*. [cited 8 August 2010].

[170]   *Sheet metal guillotine <http://www.machinetoolsupplier.com/>*.   [cited 22 May 2010].

[171]   *SR-5016M Manual Slip Roll <http://www.toolsplus1.com/srslip.htm>*.   [cited 22 May 2010].

[172]   *Smarty TX160 ALU 160amp AC/DC TIG Welder <http://www.welding-supplies-online.co.uk/merchant-4-7-143.ihtml>*.   [cited 23 May 2010].

[173]   *CNC Water jet cutting machine <http://www.iwmwaterjet.com/>*.   [cited 15 June 2010].

[174]   *Fluke 63 Infrared thermometer <http://isswww.co.uk/Infrared-Thermometer/Fluke/Fluke-63-Infrared-Thermometer/>*.   [cited 22 May 2010].

[175]   *Oxyacetylene welding torch <http://www.shopwiki.co.uk/acetylene+torches>*.   [cited 15 June 2010].

[176]   *Clarke CBG6SB 6" Bench Grinder with Sander <http://www.machinemart.co.uk/shop/product/details/cbg6sb-6in-bench-grinder-with-sander/path/bench-grinders-grinding-wheels>*.   [cited 22 May 2010].

[177]   *Makita Angle Grinder 9557NB/1 840W <http://www.diy.com/diy/jsp/index.jsp?linktype=topnav_BandQLogo&ts=1274621563788>*.   [cited 23 May 2010].

[178]   *Salvage value and depreciation of capital equipment <http://www.assetaide.com/depreciation/sl-sv.html>*.   [cited 23 May 2010].

[179]   *Electricity rates: Europe's Energy Portal <http://www.energy.eu/#domestic>*.   [cited 15 June 2010].

[180]   *Water jet machining subcontract cost:< http://www.machinery-market.co.uk/documents/pdf/242.pdf>*.   [cited 15 July 2010].

[181]   Joseph, T., *Pan Shocker: Americans patent pan plan*, in *Trinidad Guardian, April 16*. 2002: Port-of-Spain.

[182]   Ewins, D.J., *Modal Testing: Theory, Practice and Application* 2nd ed. 2000, Baldock: Research Studies Press Ltd.

[183]   Heylen, W., S. Lammens, and P. Sas, *Modal Analysis Theory and Testing*. 2003, Leuven: Katholieke Universiteit Leuven.

[184]   He, J. and Z.-F. Fu, *Modal Analysis*. 2001, Oxford: Butterworth-Heinemann.

[185]   Maia, N.M.M., J.M.M. e Silva, J. He, N.A.J. Lieven, R.M. Lin, G.W. Skingle, W.-M. To, and A.P.V. Urgueira, *Theoretical and Experimental Modal Analysis*, ed. N.M.M. Maia and J.M.M. e Silva. 1997, Somerset, UK: Research studies press Ltd.

[186]   Stephens, R.I., A. Fatemi, R.R. Stephens, and H.O. Fuchs, *Metal fatigue in engineering*. 2nd ed. 1980, New York: John Wiley and Sons Inc.

[187]   SIMULIA, *Abaqus, Getting started with Abaqus, Version 6.7*. Interactive ed. 2007.

[188]   Barlow, C.Y., J.F.M. Scott, and J. Woodhouse, *The Musical Saw.* Proceedings of the Institute of Acoustics, 1988: p. 187-192.

[189]   *Metallic materials - Tensile testing Part 1: Method of test at ambient temperature*. British Standard (BS EN 10002-1:2001).

[190]   McConnell, K.G., *Vibration Testing: theory and practice*. 1995, New York: John Wiley & Sons, Inc.

[191]   Rao, S.S., *Mechanical Vibrations*. 3rd ed. 1995, New York: Addison-Wesley Publishing Company.

[192]   Copeland, B., *Note on the standardization of the steelpan.* West Indian Journal of Engineering, 1988. **13**(1): p. 89-92.

[193]   Kishida, K., *Nippon Steel Technical Report No. 81: High Strength Steels for Light Weight Vehicle*. 2000.

[194]   Das, S., S.B. Singh, O.N. Mohanty, and H.K.D.H. Bhadeshia, *Understanding the complexities of bake hardening.* Materials Science and Technology, 2008. **24**(1): p. 107-111.